The Institute of Paper Science and Technology

Atlanta, Georgia

Doctor's Dissertation

An Investigation of Z-direction Density Profile Development During Wet Pressing

James Robert Burns

April, 1992

An Investigation of Z-direction Density Profile Development During Wet Pressing

A Thesis Submitted by

James Robert Burns

B. S. 1975, University of South Carolina

M. S. 1979, University of South Carolina

B. S. 1982, University of South Carolina

in partial fulfillment of the requirements
for the degree of Doctor of Philosophy
from the
Institute of Paper Science and Technology
Atlanta, Georgia

April, 1992

ABSTRACT

The dynamic compression and expansion behavior of the wet fiber mat is a key factor in understanding the mechanisms of wet pressing and density development. At present, this behavior is poorly understood. This thesis presents the results of an experimental program which clarifies the complex process of unidirectional, pressure-driven fluid flow through a highly deformable porous web. The objectives are 1) to develop a technique for illustration of dynamic density gradient development in handsheets pressed in a platen press, 2) to apply the technique to measurement of the influence of process variables on density development, and 3) to develop a density profile database for future wet pressing model development.

The major experiment carried out in this research was the careful investigation of the rapid stress-deformation characteristics (wet pressing) of 150 g/m^2 mats of softwood and hardwood pulp fibers. This included investigation of the deformation and recovery behavior of three zones within handsheets under the influence of several process variables (nip residence time, moisture ratio, freeness, and furnish). A laboratory press simulator, built by Burton at IPST, was modified to supply the applied pressure profile using a "rock dropper" and a servo-hydraulic press. This modified simulator permits controlled pressing within the wide speed ranges encountered in paper machine press sections. The simulator is instrumented to measure the applied mechanical load, the height of the moving platen above the stationary platen, and the height of copper targets embedded in the sheet at various levels during the forming process. In simulated wet pressing, these targets move with the fibers as the sheet is compressed indicating both web

and zonal thicknesses. The instantaneous apparent density of the zones within the web is calculated from the target separation distances and the known zonal basis weights.

From the measurements described above and others, the indications are that increasing moisture ratios in high freeness softwood handsheets produce no significant increase in the densification gradient development. In addition, increasing the moisture level in the same softwood furnish at a lower freeness still appears to have no significant effect on density gradient development. However, the net effect of lowering the freeness appears to be an overall decrease in the rate of densification of the zones. This indicates that as freeness decreases the fiber network resistance to fluid flow increases.

INTRODUCTION

During the pressing operation on a paper machine, water removal is brought about by mechanically squeezing the water from the sheet. Thus, water removal is accomplished simply by reducing the sheet volume. It is the primary purpose of the press section to maximize water removal while simultaneously creating the density potential required for developing desirable sheet properties. Over the years, press designs have been altered in efforts to improve the performance of the operation. These improvements have included better felt designs, higher press loads, increased sheet temperatures, and extended nip presses. Despite these improvements, the dryness level exiting the modern press section rarely exceeds 55% dryness due to fundamental limitations of the process. In contrast, a study by Heller and Tewksbury (1972) indicates that dryness levels of 70% are attainable by mechanical water removal.

The behavior of a wet pulp sheet in a dynamic press nip is defined by several important mechanisms which have been described by Ceckler and Thompson (1982). These mechanisms include the flow and compression characteristics of the wet pulp sheet and the dependence of fluid flow on the degree of sheet compaction. In order to analyze the behavior of these wet sheets in a quantitative manner, the compression-expansion behavior and the flow resistance of the sheet under different stages of compression must be known or approximated. Analysis of the wet sheet behavior is complicated by the potential development of both hydraulic and structural pressure gradients across the sheet thickness which can produce a nonuniform compression profile and density gradient.

Evidence of density gradient development comes from a variety of processes which involve fluid flow through highly compressible porous materials. Fluid flow through these compressible porous materials forms the basis for many diversified fields of research such as soil mechanics, ground water hydrology, water purification, and such industrial processes as filter cake formation, fluid extraction by compression, and the wet pressing of paper. The most important aspects of flow through a saturated compressible porous material are its deformation from mechanical compression, forces associated with fluid flow, and the effect of deformation of the medium on its permeability, porosity, and compressibility (Biot, 1941). The existence of a density gradient inside the sheet in the wet press nip can also be inferred from the development of mathematical models for the wet pressing of paper and the consolidation of other compressible porous materials. These models typically require the simultaneous solution of equations describing both fluid flow and material deformation.

Physical measurement of the compression and expansion behavior of pulp fiber sheets is needed to verify both previous and future mathematical models of wet pressing. As future models are developed it will become necessary to describe the dependency of the sheet's permeability on the level of sheet compaction as has been attempted by Kerekes and McDonald (1990, 1991). At present, little work has been done on measurement of dynamic density gradient development during the wet pressing of pulp fiber sheets. Therefore, development of suitable equipment for observation of the compression and expansion behavior of wet pulp fiber handsheets is required for demonstration of dynamic density gradient development. Also, observation of density gradient development under the influence of several

process variables would contribute significantly to our understanding of the mechanism(s) of sheet densification inside the wet press nip and perhaps lead to development of better water removal methods and more desirable dry sheet properties.

The dynamic compression and expansion behavior of wet fiber sheets is a key factor in understanding the mechanisms of wet pressing and density development. Therefore, the objectives of this work were 1) to develop a technique (including the necessary equipment) for illustration and measurement of dynamic z-directional displacement of targets embedded (density gradient development) in handsheets pressed between parallel platens, 2) to apply the technique to measurement of the influence of process variables on density development, and 3) to develop a density profile database for future wet pressing model development.

LITERATURE REVIEW

FLUID FLOW-INDUCED DENSITY DEVELOPMENT IN HIGHLY COMPRESSIBLE POROUS MATERIALS

The bulk of the literature describing density gradient development resulting from fluid flow through a compressible porous material can be divided into two categories based on the state of fluid flow. The first category is steady-state fluid flow under a constant pressure driving force. The second category is unsteady-state fluid flow resulting from a dynamic pressure driving force. In these processes the permeability changes rapidly with deformation of the medium.

Steady-state Fluid Flow-induced Density Gradient Development

The first work describing fluid flow within a deformable permeable (porous) material was probably that of Biot (1941, 1955). Biot considered the deformation of liquid-saturated materials within the scope of "infinitesimal" elastic strain theory (defined as less than 2% strain). Parker, *et al.* (1987) extended Biot's theories beyond infinitesimal elastic strains to larger "finite" strains. Parker, *et al.* considered the case of steady, one-dimensional flow through a slab of porous deformable material (polyurethane foam) restrained at the downstream end by a freely draining rigid support. They showed that the strain distribution was uniform under steady mechanical compression without fluid flow. If the strain was produced by fluid flow, however, the strain distribution became highly nonuniform in the direction of fluid flow and was similar to that described by Caro, *et al.* (1984) and Lanir, *et al.* (1990).

Parker, *et al.* (1987) studied the one-dimensional flow of an incompressible fluid through a deformable porous material both theoretically and experimentally. Their theoretical model is essentially that of Biot (1955) with the assumption that the stiffness and permeability of the matrix are functions of the local strain gradient. The stiffness and permeability properties of a polyurethane foam material were measured. These properties were then used to predict the rate of fluid flow and the distortion of the matrix as a function of the applied pressure difference across the material. Comparison of the predictions of the model with experimental observations indicated good qualitative agreement.

In a separate set of permeability versus strain experiments, Parker, *et al.* also observed that the fluid flow induced a nonuniform distribution of local strain within the foam matrix even at small pressure drops. To obtain the strain distribution in the foam matrix, required measurements at several different pressure drops and calculation of the permeability from the initial slope of the measured flow rate versus pressure drop curve.

In flow experiments similar to those of Parker, *et al.*, Caro, *et al.* (1984) examined the effects of solvent drag on a different polyurethane foam matrix by measuring the pressure drop-flow rate relationship. Deformation of the foam matrix resulting from steady-state fluid flow was nonlinear with all fluids, with the deformation increasing with increasing flow rate. Transverse calibration marks on the foam showed compaction which in the steady-state (or at a constant flow rate) was nonuniform and increasing in the direction of flow. The nonuniformity of the strain gradient was attributed to the cumulative effect of fluid drag on the foam matrix. Upon application of a

step increase of the applied stress (a step increase in fluid flow), the deformation propagated through the foam in a manner similar to the prediction (a parabolic displacement field) of Lai and Mow (1980) for cartilage. The combined effects of mechanical loading and fluid drag were also examined in experiments in which foam blocks were compressed between grids upstream and downstream of the foam samples. As the flow rate increased, the level of compaction decreased upstream and increased downstream indicating an increase in the drag-induced density gradient downstream. Caro, *et al.*'s strain gradient is consistent with the gradient observed by Parker, *et al.* (1987). In general, the nature of the flow and the resultant strain distribution are dependent upon the properties of the porous matrix, the fluid, and their interaction. Boundary conditions such as geometry, applied pressure, and compression history of the porous matrix have also been shown to affect the strain distribution.

Lanir, *et al.* (1990) studied the nonlinear finite strain deformation response of an open-celled polyurethane foam in response to fluid filtration both theoretically and experimentally at steady-state flow rates. They measured the influence of different fluid pressures on the uniaxial strain distribution along a foam cylinder supported at the downstream surface by a rigid but highly permeable filter. The flow-induced strain along the foam cylinder was found to be highly nonuniform. The strain gradient was flat near both ends of the sample but steep in the middle as shown in Figures 1 and 2. The equilibrium strain distributions resulting from glycerol filtration at low pressures are shown in Figure 1. The equilibrium strain distributions at higher pressures using water are shown in Figure 2. The predicted response from their model for each of the fluid pressures used is also shown.

They concluded that the distributions of stress and strain along the foam indicated that the flow limitation was associated mainly with the downstream portions of the matrix. These flow limitations were due to the high level of compression and the lower strain-dependent permeability in the downstream portions of the foam.

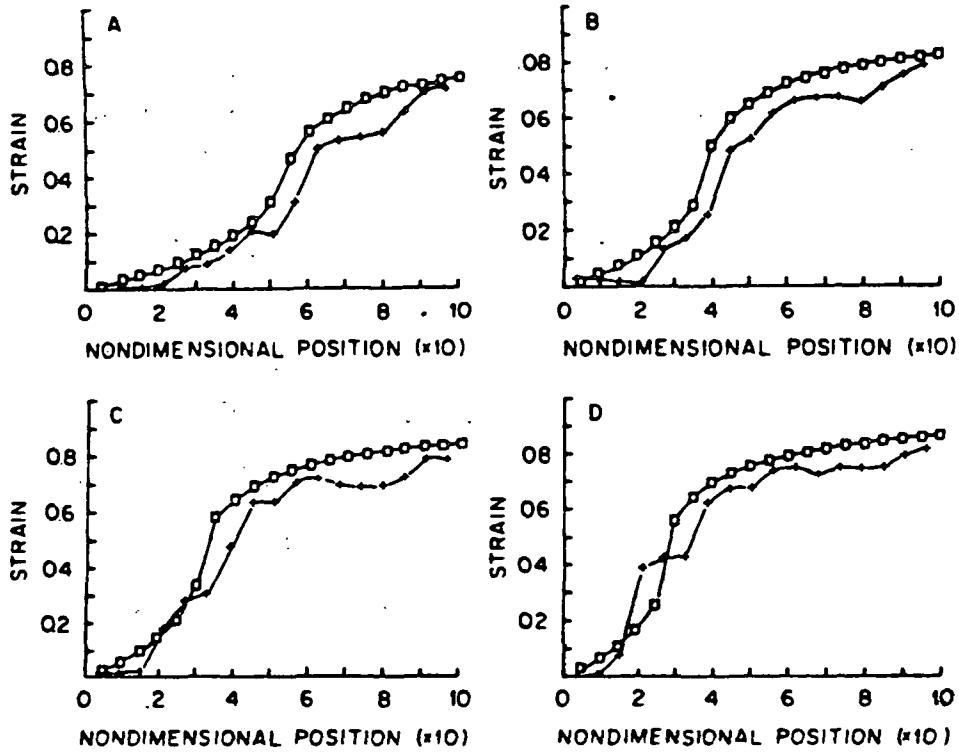

Figure 1. Equilibrium strain distribution in a polyurethane foam resulting from glycerol filtration. The fluid pressures are: A - 2.5 kPa; B - 5.0 kPa; C - 7.5 kPa; D - 10.0 kPa. Results are for both (❑) - theoretical and (+) - experimental cases. Positions 0 and 1.0 represent the fluid-foam matrix and the foam matrix-filter interfaces, respectively. (After Lanir, *et al.*, 1990)

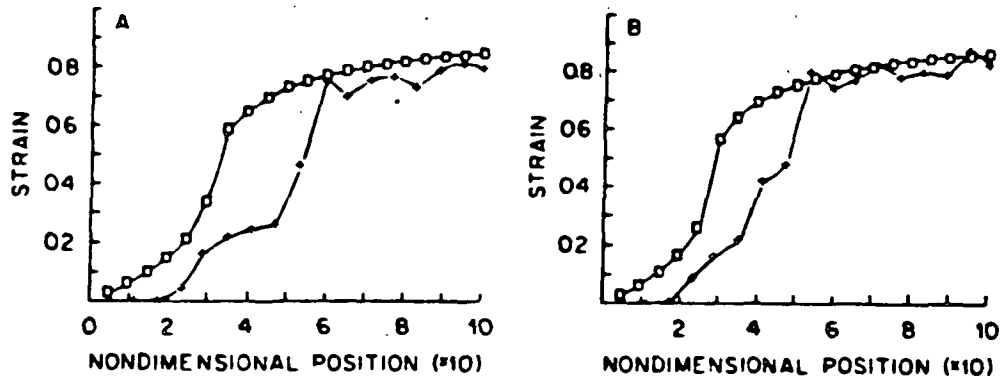

Figure 2. Equilibrium strain distribution as in Figure 1 but under higher water pressures: A - 7.5 kPa and B - 10.0 kPa. Results for both (❑) - theoretical and (+) - experimental cases. (After Lanir, *et al.*, 1990)

Unsteady-state Fluid Flow-induced Density Gradient Development

The literature describing density gradient development resulting from unsteady-state fluid flow through compressible porous media is limited. The literature can be divided into two categories based on the level of strain in the medium. The first category involves infinitesimal strains and the second category finite strains. Infinitesimal strain theory is used to describe consolidation of porous media when the deformations are small compared to the thickness of the consolidating layer (less than 2%). This restriction is well suited to the study of soil consolidation when dealing with soil layer thicknesses from a few meters to several kilometers. To handle larger deformations of a thin (much less than 1 meter thick) compressible layer, a finite strain theory was developed. Application of these two theories to the consolidation of soils and other materials has yielded results that indicate the

potential for development of a density gradient in a porous material undergoing compression.

Gibson, *et al.* (1967) developed a theory for finite strain nonlinear consolidation of thin layers which avoided the limitations of small strains. Variation of soil compressibility and permeability during consolidation were taken into account. Their theory was applied to the one-dimensional consolidation of thin layers in which the influence of the self-weight of solids and pore fluid on the consolidation process was unimportant relative to the applied stresses.

The model results are presented in terms of a "local degree of consolidation" of each layer as a function of time. At short times the local degree of consolidation varies sharply as a function of position in the layer, with the most rapid change in the gradient (or degree of consolidation) occurring at the flow-exiting surface. At longer times the slope of the curve approaches a more horizontal level which indicates that the sample was approaching complete consolidation.

Manins and Roberts (1975) applied infinitesimal strain theory to the initial deformation of a liquid-filled poroelastic material subjected to a variable pressure. The material permeability was described as a function of the local deformation of the material. The deformation of the porous material was regarded as quasi-static, which allowed them to neglect inertia effects in comparison to the effects of the fluid pressure (Cribb, 1964). By considering the deformation gradients to be small (1 to 2%), they were also able to consider the material as deforming elastically and, therefore, obeying Hooke's law. The displacement field for the material was a two-dimensional

rectangular block in plane strain. The block was constrained all around and compressed on one side only. The compression velocity was a function of time only (after Challen, 1966). Their experimental and model setups allowed fluid to freely escape only in the transverse direction. This displacement field was considered because of its similarity to rolling processes generally employed in industrial fluid expression equipment. The equations describing infinitesimal strains were applied to two two-dimensional models in plain strain to obtain the pressure and displacement fields resulting from dynamic loading. The first model allowed slip to occur on all boundaries and consisted of a rectangular section of material. The material was constrained by two impermeable frictionless walls, one of which was approaching the other at a constant velocity. The medium was constrained transversely by two perfectly permeable frictionless walls. The whole system was immersed in a bath of fluid with a reference pressure of zero such that the medium was completely saturated. The second model was the same as the first except that the moving boundary was considered perfectly rough so that no slip occurred on this surface.

Model results indicated that under certain conditions the restrictions of infinitesimal strain theory would be violated for small elapsed times or if the permeability varied significantly. It was seen that even with proper consideration of local material variations and the medium permeability the pressures predicted from the constant permeability model were off by as much as 100 percent from the measured values. Therefore, the requirement of small displacement gradients (small strains) limits the applicability of their results to the initial stages of such processes. This limitation was severe and

indicates that the infinitesimal strain approach should not be used for strains greater than 1-2%.

Summary

Considerable evidence has been presented from the literature to show that steady- and unsteady-state fluid flow through a compressible porous medium result in deformation of the medium due to drag or shear forces associated with the flow. There is also evidence that the combination of mechanical and flow-induced compression affects material properties such as permeability and compressibility. This establishes the importance of developing a detailed knowledge of the strain and density distribution in compressible porous materials which undergo rapid compression such as wet paper webs.

Most of these authors have used visual methods to observe the nonuniform strain distribution in these materials due to the large z-dimension of their sample. In effect, the authors have simply drawn lines on the sides of the blocks of material and measured the change in distance separating the lines under different flow situations. Unfortunately, given the small z-direction thickness for wet paper webs and the short duration of the wet pressing event, it is difficult to use visual methods of this type to observe the development of a nonuniform z-direction density profile. Since no suitable visual methods had been developed for use in the study of thin (1-2 mm thick) compressible fiber mats before this work was begun, an alternative method was developed.

MEASUREMENT OF Z-DIRECTION DENSITY GRADIENT DEVELOPMENT

Flow-controlled Versus Compression-controlled Pressing

An important concept in wet pressing which has its origin in the field of soil mechanics is the distribution of the applied load between the fiber network and the surrounding fluid. The degree to which the fluid phase carries the total applied load depends, to a great extent, on the flow resistance of the fiber network and the flow receiver supporting the fiber network. Wahlstrom (1969, 1979), Chang and Han (1976), and Ceckler and Thompson (1982) have observed two modes of press behavior arising from this dependence on sheet flow resistance. In the first mode (typical of high moisture ratio and high flow resistance sheets), a flow-controlled situation exists. For flow-controlled wet pressing, the primary impedance to water removal is the flow resistance of the fiber network. The amount of water removal in this mode depends on the press impulse, with pressure and time being interchanged freely to achieve a given level of dewatering. The press impulse (I) is defined as follows:

$$I = \int_0^t P(t)\, dt \tag{1}$$

where P = pressure as a function of time

t = time

In the second mode, typical of low moisture ratio and low flow resistance sheets, removal of the free water between the individual fibers becomes the dominant factor. Press impulse is still important in this situation, but pressure now exhibits a more independent effect.

To study the flow-controlled and compression-controlled behavior of wet fiber sheets, Chang and Han (1976), Carlsson (1983), Ceckler, *et al.* (1982), Jantunen (1985), Burton (1987), Jaavidaan (1987), and Szikla and Paulapuro (1989 a, b) have relied on the platen press nip geometry to simulate wet pressing. The advantages of the platen press over the roll press geometry are the simplicity of instrumentation of the nip and the ability to control the shape and duration of the applied pressure curve. Data obtained from platen presses have been shown by Ceckler, *et al.* (1982) to be a reliable predictor of the results obtainable from the roll geometry.

Web Compression and Thickness Measurements

Carlsson (1983) clarified how water was removed from the wet paper web by making direct measurements of sheet thickness change in a laboratory platen press. He described the effects of applied pressure, pressure pulse time (analogous to nip residence time, NRT), refining (beating), and basis weight on the compression and expansion behavior of the wet web.

He found that by increasing the applied pressure while keeping other factors constant the maximum solids content of the web could be increased. As a consequence of the increased solids content, the flow resistance in the web increased, resulting in an even higher hydrodynamic pressure in the sheet.

Variation of the pressure pulse time indicated that the time-dependent flow phenomena in the sheet became less important than the elastic modulus of the fibers as the pressure pulse time was increased. At longer press times (greater than 25 msec), the wet sheets exhibited a more compression-

controlled behavior in which the hydrodynamic pressure decreased, and the point of maximum dryness moved closer to the point of maximum pressure. The observed sheet expansion increased for longer pressure unloading times which were on the order of 10-15 msec.

Carlsson also showed that beaten chemical pulps exhibited a more flow-controlled behavior in which the maximum solids content occurred beyond the midpoint of the pressure pulse. In these handsheets the sheet expansion was only 5 to 10%. The unbeaten pulp was more compression-controlled. It had a maximum solids content near midnip and exhibited a relatively strong expansion upon release of the applied load.

Carlsson also examined the effect of increasing sheet basis weight (thickness) on the compression and expansion behavior of the wet web. He reasoned that by increasing the sheet basis weight the distance the water must travel in the z-direction to exit the sheet would be increased and therefore would have a significant effect on the compression and expansion behavior. He concluded that "as a consequence of the increased basis weight the total flow resistance increased due to the longer flow path length, which in turn led to generation of a higher hydrodynamic pressure in the sheet structure." Web dewatering became more flow-controlled with increased basis weight. Carlsson also found that the point of maximum solids content moved toward the end of the applied pressure pulse at higher basis weights.

Jantunen (1985) developed an apparatus, similar to that of Carlsson (1983), to study the z-direction dynamic compression behavior of wet webs during simulated wet pressing. He measured the z-direction web compressibility with the intent of studying dynamic "viscoelastic and plastic"

web properties under conditions corresponding to the wet pressing process in papermaking. Figure 3 (from Jantunen) shows the relative compressibility of several groundwood (mechanical) pulps and chemical pulps when the press impulse was a rising-ramp with a peak applied pressure of 7.1 MPa. The compression increase was rapid when the risetimes were from 1.5 to 5 msec and tended to slow down in the 5 to 10 msec range in the case of the 206 CSF groundwood (pulp number 5). The relative compressibility of the chemical pulps and the low freeness mechanical pulps was markedly less than that of the "high" freeness mechanical pulp (pulp number 5). The speed of compression was shown to increase with the rise time of the press impulse. The strong effect of freeness on compressibility indicated that the dewatering process of these samples was partly flow-controlled.

The effect of pressing time on the maximum dry solids content of the low freeness mechanical and chemical pulps can be seen in Figure 4. In high-freeness pulps the rate of increase in dry solids content was very rapid in the time range of 1.5 to 5 msec, indicating that freeness level affects the maximum solids level achievable.

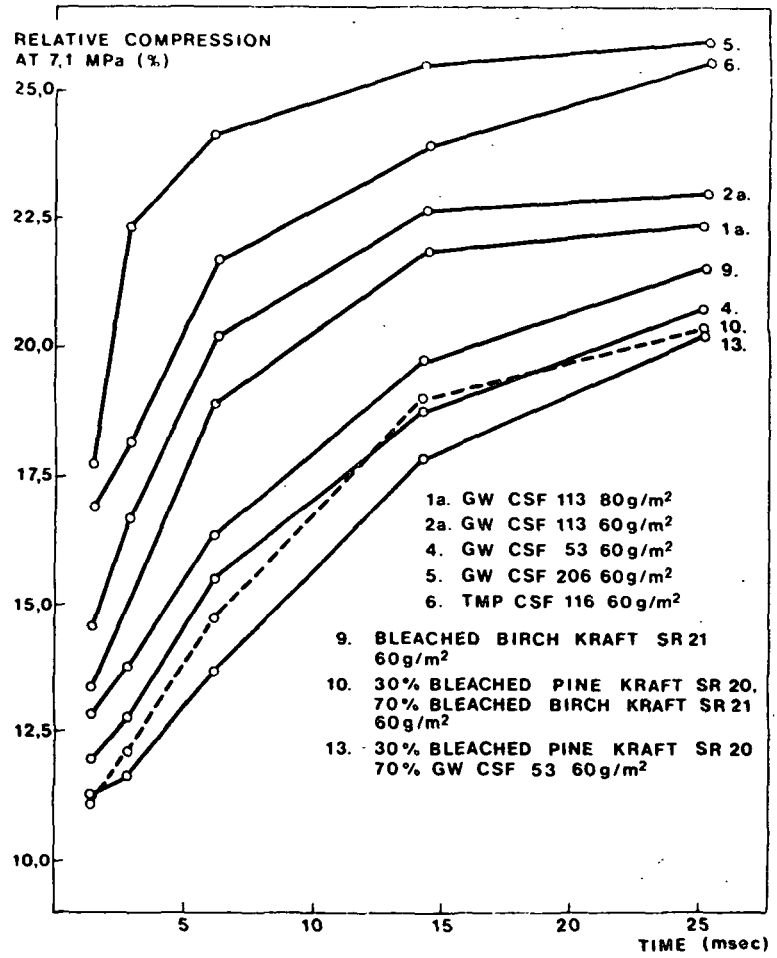

Figure 3. The relative compression of different pulps as a function of press impulse duration. (After Jantunen, 1985)

El-Hosseiny (1990) has recently shown that the stress-strain curves for the compression and expansion of 100 g/m^2 bleached softwood kraft sheets tested at high strain rates superimpose well on those obtained at very low strain rates. These sheets were prepressed using a bench-scale roll press to a predetermined moisture content before testing in a manner similar to that used by Burton (1987). El-Hosseiny's wet sheet loading conditions and compression results are shown in Table 1. The average deformation rate for

the first three handsheets ranged from 38.11 mm/sec to 42.27 mm/sec. The original thickness and the percent of maximum compression of these three handsheets ranged from .463 to .497 mm or 56 to 60%, respectively.

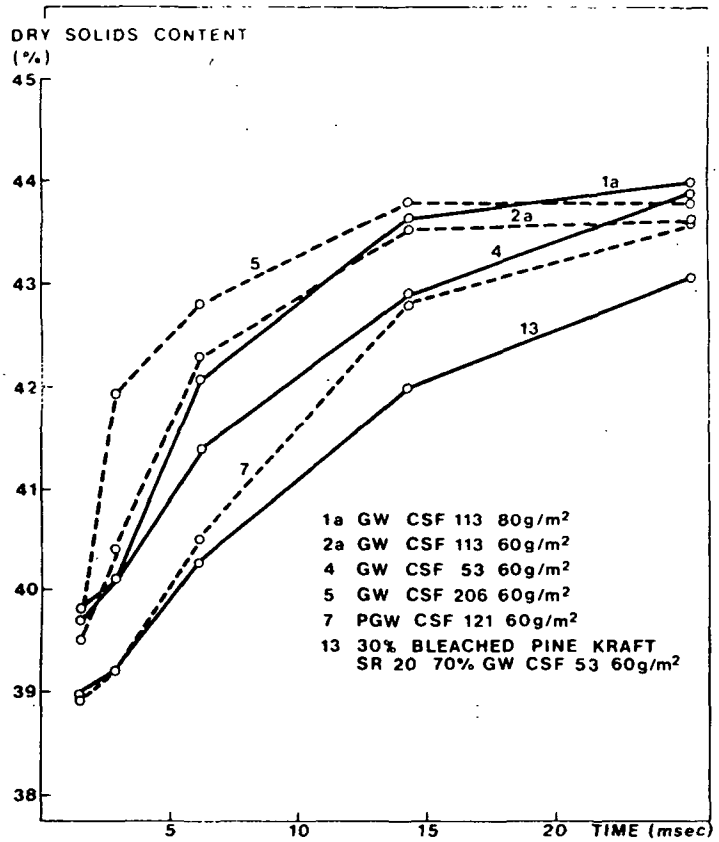

Figure 4. Effect of press impulse duration on the maximum dry solids content of different pulps. (After Jantunen, 1985)

Table 1. El-Hosseiny's wet sheet loading conditions.

Dry basis weight (g/m^2)	Moisture ratio	Average deformation rate (mm/sec)	Maximum pressure (kPa)	Original thickness (mm)	Final thick-ness (mm)	Recovered thickness (mm)
108	3.67	42.27	4540	.497	.218	.457
103	3.74	39.14	4915	.463	.189	.454
101	3.83	38.11	4840	.475	.193	.430
100	3.63	0.085	6985	.452	.150	.447
103	3.5	0.085	6985	.460	.145	.460

In Figure 5 El-Hosseiny shows the relationship between the structural pressure applied to a sheet (during loading and unloading) and the corresponding thickness. The curve is quite different during loading and unloading. The sheet thickness during unloading remains essentially constant until the applied pressure reaches a small value. El-Hosseiny states that "after reaching the small applied pressure the sheet thickness increases to almost its original value." Figure 5 does not support this claim, but it does show that the sheet expansion is equal to the final thickness as shown in column 6 of Table 1. After an unspecified amount of time has passed, the sheets do recover to approximately their original thickness as shown in Table 1.

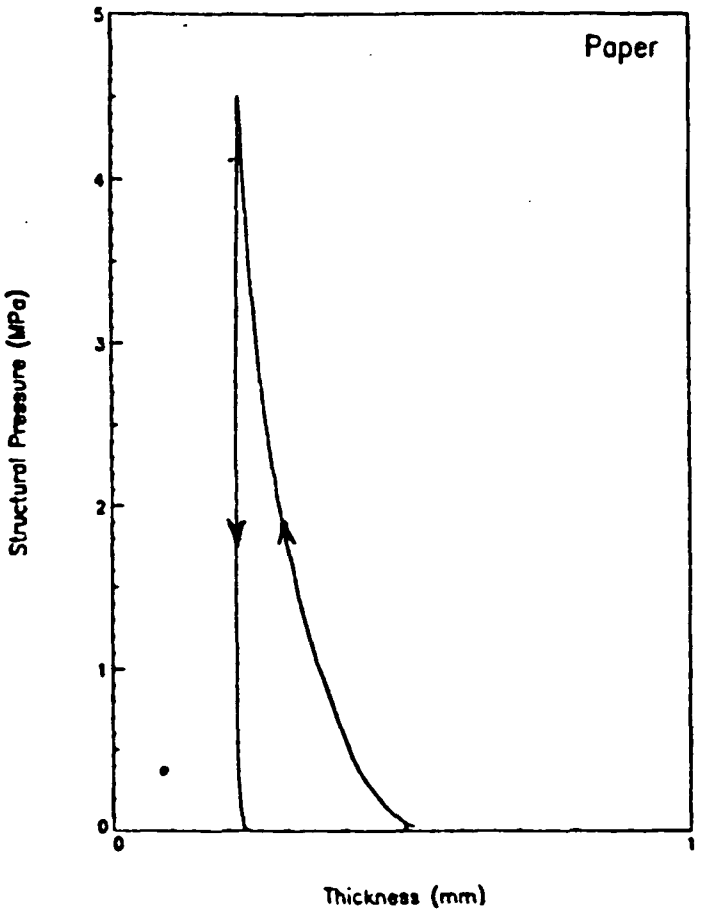

Figure 5. Typical compression curve for wet sheets. (After El-Hosseiny, 1990)

Summary

Evidence has been presented from the literature describing the effects of freeness, basis weight, and nip residence time on the compression and expansion behavior of saturated pulp sheets. Decreasing freeness tends to drive the compression behavior of the sheet toward what has been described as flow-controlled pressing. Freeness levels typical of unbeaten pulps tended to behave in a more compression-controlled manner. At low freenesses mechanical and chemical pulps tended to compress rapidly if the rise time of the applied pressure pulse was on the order of 1.5 to 5 msec. On the other hand, if the rise time was on the order of 5 to 10 msec, the compression rate was slowed considerably. Also the compression of low freeness mechanical and chemical pulps was much less than that of higher freeness mechanical pulps which implies that the dewatering and compression behavior was more flow-controlled. It has also been show that increasing sheet basis weight increases the flow resistance and the hydraulic pressure generated in the sheet. Therefore, the compression behavior as a result of increasing the basis weight was more flow-controlled.

SHEET STRATIFICATION

MacGregor (1983) was one of the first to characterize an effect of wet pressing he termed "sheet stratification." He defined stratification as "the change in vertical distribution of fiber and filler caused by fluid shear forces during the dynamic wet pressing process." This definition has been adopted here to describe the development of a z-direction density gradient due to fluid flow through a compressible porous fiber mat (a handsheet).

MacGregor has also suggested that "the degree of sheet stratification depends a great deal on the rate of compression and the completeness of the pressing process." He believed that the amount of stratification was highly dependent on the flow resistance of the fiber network, the amount of water present, and the physical characteristics of the fibers themselves. Illustration of the dependence of sheet stratification on these variables has awaited the ability to directly measure the spatial relationships among strata during compression and expansion of the sheet inside the nip.

MacGregor illustrated the stratification effect by visualizing two situations in which sheets were compressed to the same thickness, but at different compression rates as shown in Figures 6a and 6b. These sheets were arbitrarily divided into 10 equal strata prior to compression. If compression was controlled such that a very small hydraulic pressure gradient was produced, the 10 stratum lines remained essentially equidistant through the compression (Figure 6a) of the sheet. Additional requirements for the sheet to compress at a uniform z-direction deformation rate were 1) the sheet must have a small z-direction thickness; 2) the sheet must possess a high z-direction permeability; and 3) the load must be applied slowly. These factors would prevent development of a hydraulic pressure gradient which would accelerate densification or development of a density gradient at the flow-exiting surface of the sheet. At the end of compression, both of these sheets contained the same amount of water because they were compressed to the same thickness. However, the sheet that was compressed more rapidly exhibited more fiber compaction at the flow-exiting surface.

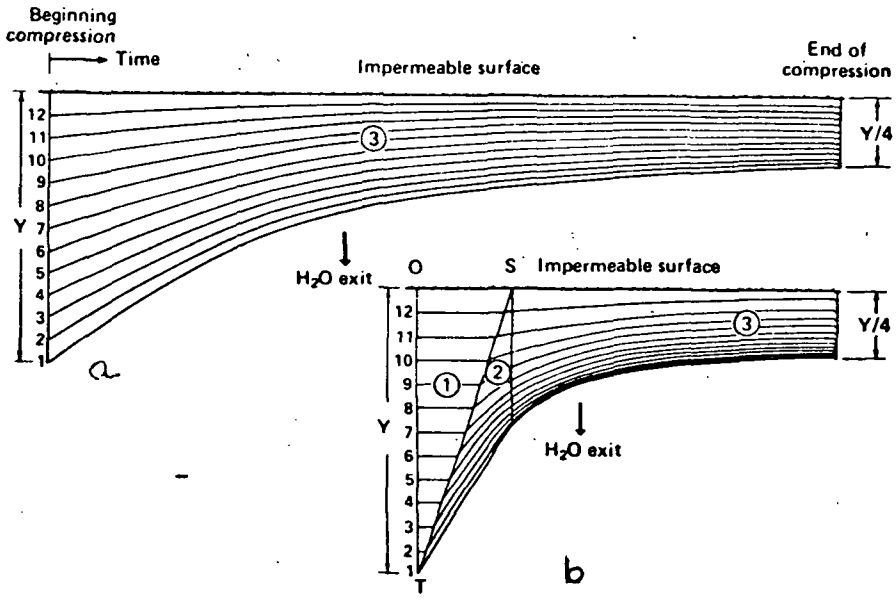

Figure 6. Illustration of stratification wavefront. (After MacGregor, 1983)

MacGregor has described the concept of coupling of the material deformation and the fluid flow processes. How this coupling results in development of a z-direction density gradient is a complex interaction of many variables. The variables which affect density gradient development can be divided into two major groups based on their effect on flow resistance and compression rate. Variables which affect flow resistance are web temperature, level of refining, fiber type, sheet basis weight, filler content, sheet formation, and fiber compressibility. The variables which affect compression rate are machine speed, roll hardness, roll diameter, felt compressibility, and press load. Significant changes in any one or a combination of these variables (for example, increased compression rate) can create a change in the density gradient in the direction of fluid flow as shown in Figure 6b.

Quantitative analysis of the dynamic internal behavior of the sheet requires knowledge of the flow resistance (dynamic permeability) of the fiber

mat and its dependence on the degree of compaction, as well as a detailed knowledge of the level of compaction (or density) in the direction of fluid flow (Jantunen, 1985). Such an analysis is complicated by the development of both hydraulic and structural pressure gradients across the sheet which can produce a nonuniform compression profile (or z-direction density gradient). Figure 7 from Nilsson and Larsson (1968) illustrates the concept of distribution of the total applied pressure (PT) in terms of hydraulic pressure (PH) and structural pressure (PC) components inside the web. The hydraulic pressure (PH) increases from its lowest value at the felt side of the paper web to its highest value at the roll side of the sheet where the load is applied.

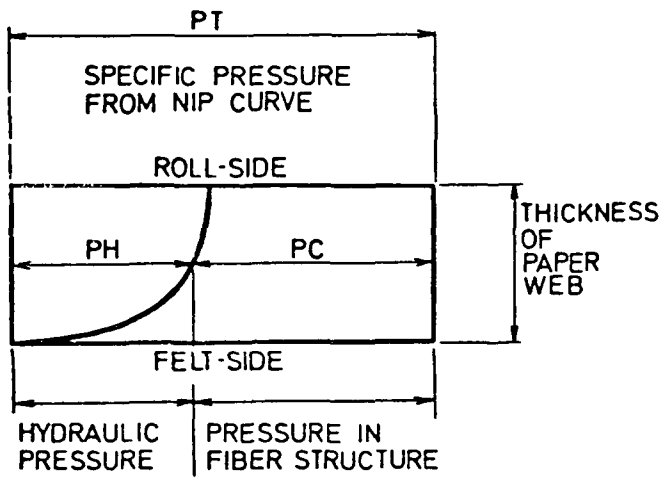

Figure 7. Pressure distribution in the paper web. (After Nilsson and Larsson, 1968)

Figure 8 shows MacGregor's (1983) measurements of the total applied pressure (P_A) and the hydraulic pressure (P_H) at the roll-sheet interface inside a press nip as a function of the machine direction position. The structural

pressure (P_M) is taken as the difference between the total applied pressure and the hydraulic pressure. These curves indicate the presence of low pressure tails at the beginning and end of the nip. The hydraulic pressure peaks well before the peak applied pressure and the middle of the nip.

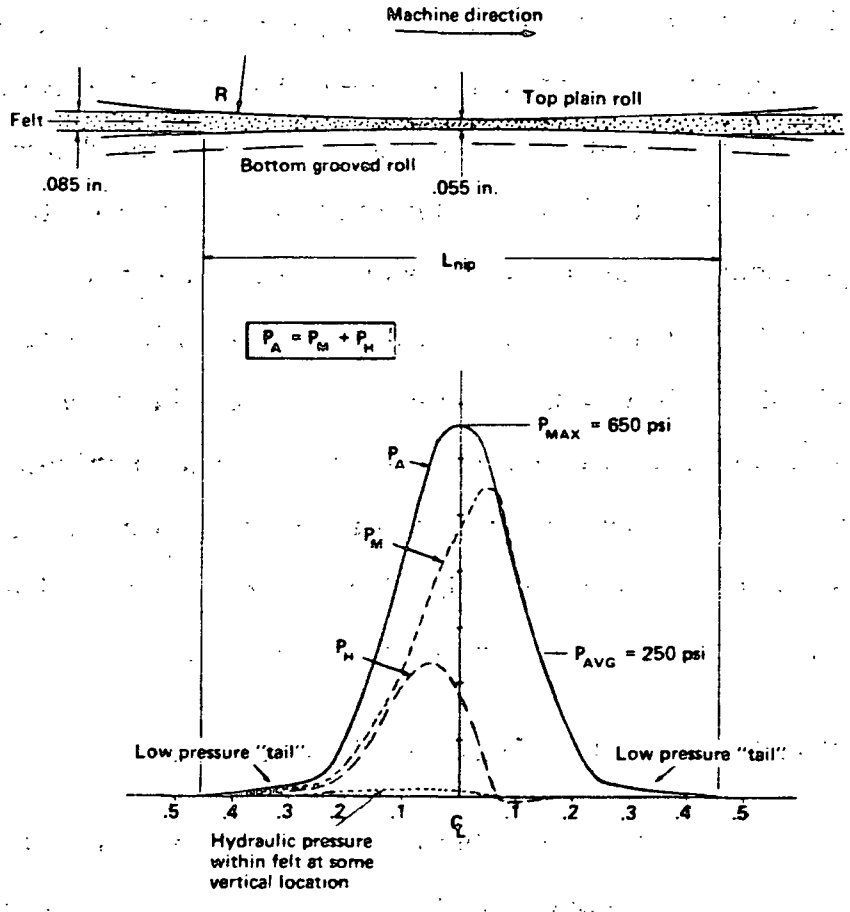

Figure 8. Pressure profiles in a felted nip. P_A = total applied pressure, P_H = hydraulic pressure at the roll-sheet interface, and P_M = structural pressure measured as a function of machine direction position inside the wet press nip. (After MacGregor, 1983)

EXPERIMENTAL EVIDENCE OF Z-DIRECTION DENSITY GRADIENT DEVELOPMENT

Having reviewed the theoretical models describing density gradient development, our attention is now focused on experimental evidence of density gradient development. When work began on this thesis, only limited experimental evidence of nonuniform density profile development (during the platen pressing of paper) had been published Wicks (1982), Davis *et al.* (1983), Jantunen (1985), and Burton (1987), and after beginning this thesis, two additional papers were published by Szikla and Paulapuro (1989 a, b). The available experimental evidence is provided by three different types of experiments. In the first type of experiment, layered handsheets were pressed, and the density of each layer was measured. In the second type of experiment, handsheets were pressed, dried, and the z-direction density distribution was determined using image analysis. In the third type of experiment, density gradient development was measured directly by instrumenting a platen press nip. The results from these experiments are summarized below.

Density Gradient Determination with Layered Handsheets

The first experiments to indicate the development of density gradients during wet pressing were conducted by Wicks (1982). Wicks was primarily interested in the effects of press design configuration on the development of sheet two-sidedness and its effect on sheet quality.

Wicks examined the distribution of water inside the sheet after passing through a press nip and its effect on sheet two-sidedness by pressing layered 300 g/m^2 (five 60 g/m^2 layers) handsheets. These handsheets were separated

after pressing, and the weight of each layer was measured to determine its dryness. The sheets were pressed between a solid press roll and a blotter with different directions of water removal. He determined the density distribution of the composite sheets by measuring the densities (weights) of each 60 g/m^2 layer. The density differences measured between layers were relatively small, with a maximum difference of 60 kg/m^3 between adjacent layers; the average sheet density was 530 kg/m^3. His results indicated that sheet dryness was highest in the layer adjacent to the blotter (felt), and therefore, the highest sheet density occurred in this layer. The layers farther away from the blotter had successively lower densities. Additional evidence of density gradient development was found by pressing multilayer sheets between two felts to simulate a double-felted press nip. The layers at the felt surfaces always showed significantly greater densities than the layers at the center of the sheet.

Density Gradient Determination with Image Analysis

Szikla and Paulapuro (1989 a) believed that a key factor in understanding the mechanisms of wet pressing was examination of the dynamic compression behavior of wet fiber mats. To study the effects of dynamic compression on z-direction density distribution, Szikla and Paulapuro developed a new technique based on image analysis. In this method an image of the paper cross section is formed in such a way that the fiber wall area is a number of grey-levels darker than the void area. The cross section image is divided into several vertical planes for analysis, and the fiber wall area in each plane is determined. The density of each plane is assumed to be proportional to the measured fiber wall area. The average density of the sheet was measured in a conventional way (such as sheet grinding) to

validate the method and to convert the measured wall area into density. The repeatability of the density distribution measurement was examined and found to be acceptable. Some scatter was observed in the data when samples were taken from different parts of the sheet.

In their experimental work, Szikla and Paulapuro placed wet-pressed sheets with a solids content of 30% between blotters and then dried them on a drying drum with a surface temperature of 65 °C. Some handsheets were frozen in liquid nitrogen immediately after pressing and freeze-dried in an attempt to preserve the internal structure of the sheet. These sheets were then examined with the image analysis technique described above. The z-direction density distribution of paper made without wet pressing was almost uniform. The density of these sheets was slightly higher (475-500 kg/m^3) on the wire side of the sheet (flow-exiting side) than on the top side of the sheet (425-450 kg/m^3) and was attributed to formation effects. When the sheet was pressed with a rapid, strong pressure pulse and dried at 65 °C, a marked density gradient was observed in the paper. The direction of the density gradient in the handsheets depended upon the direction in which water removal had occurred. The density increase was always largest on the felt side (flow-exiting side) and smallest on the solid platen side. Comparison of the changes in density indicated that density development was independent of whether water was removed through the wire side or the top side of the sheet (see Figure 9). When Szikla and Paulapuro removed water from the sheet so slowly that no significant hydraulic pressure was formed in the sheet, essentially no Z-direction density gradient was observed as shown in Figure 10.

It is worthwhile noting that the freeze-dried sheets (shown in Figure 11) did not display the same Z-direction density gradient as the sheets dried at 65 °C (shown in Figure 10). The outer layers of the freeze-dried sheets remained bulkier than the inner parts (lower in density), and their density seemed to be independent of the direction of water removal. This could be an indication that crystallization of the water when the sheets were frozen and freeze dried may have affected any gradient present from either formation or wet pressing of the sheets.

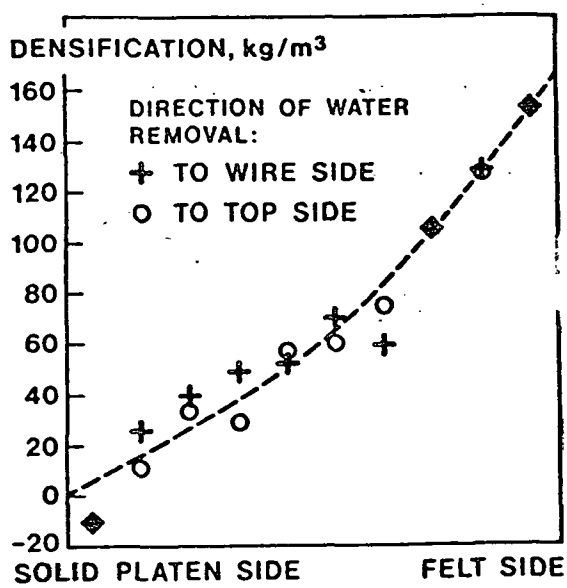

Figure 9. Densification of paper as a consequence of wet pressing. (After Szikla and Paulapuro, 1989 a)

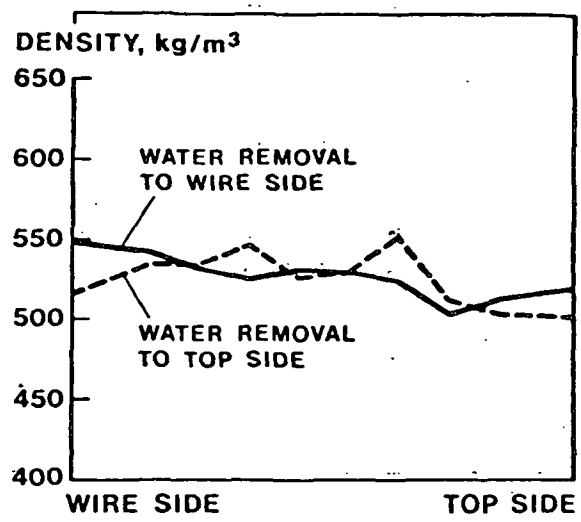

Figure 10. Z-direction density distribution of paper wet pressed with a slow, low-pressure pulse. (After Szikla and Paulapuro, 1989 a)

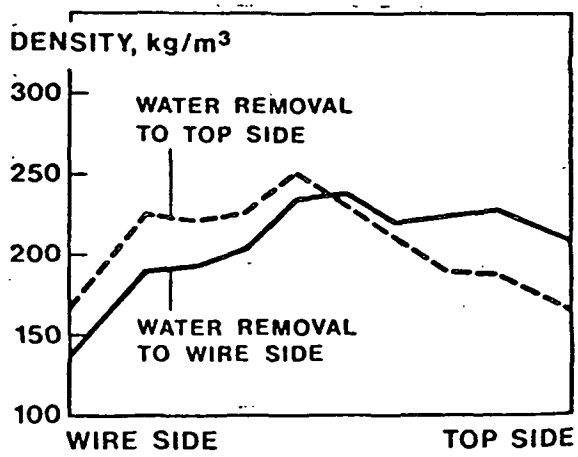

Figure 11. Z-direction distribution of paper wet pressed with a fast, high-pressure pulse and freeze-dried. (After Szikla and Paulapuro, 1989 a)

Szikla and Paulapuro (1989 b) also stated that "rapid pressing may produce quite a steep z-direction gradient in the structural pressure." To get a

rough idea of the structural pressure (or pressure carried only by the fiber structure) in the sheet, they measured the applied pressure and deformation of a sheet with an initial solids content of 60% as shown in Figure 12. In this case the compression speed was about the same as that used to determine the density distributions (the compressive pressure increased from 0 to 10 MPa in 1.5 msec). The high solids content was chosen to minimize the buildup of hydraulic pressure in the sheet. They concluded that in the density distribution tests the structural pressure of the web was probably lower than the curve in Figure 12 indicates because the solids content was much lower. However, on the basis of the pressure-deformation curve in Figure 12 and hydraulic pressure measurements, Szikla and Paulapuro have concluded that "only a small structural pressure was generated in the web and most of the compressive pressure was balanced by the hydraulic pressure" due to their measurement of a small hydraulic pressure.

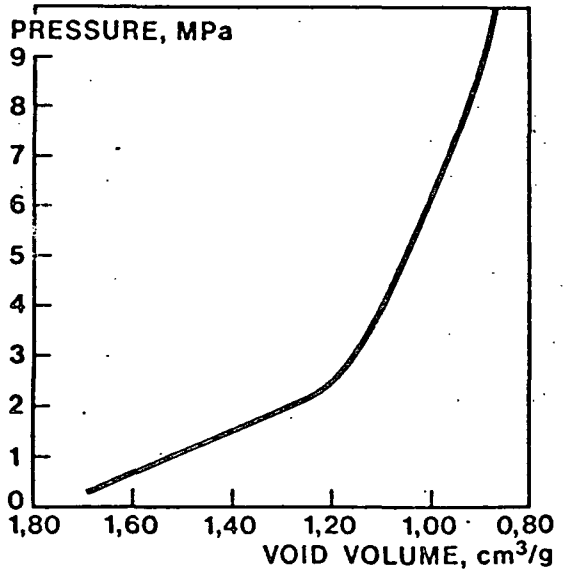

Figure 12. Pressure versus deformation curve for wet paper web, initial dryness 60%. Total compression time from 0 to 10 MPa was 1.5 msec. (After Szikla and Paulapuro, 1989 b)

Finally, they concluded that wet pressing can considerably change the z-direction density distribution of even low basis weight sheets. As an example, the density of a 100 g/m^2 sheet made from chemical pulp was shown to increase by one-third on the flow-exiting side and yet remain unchanged on the solid platen side if the water removal was fast and one-sided. They theorized that "the z-direction change in paper density seems to be a consequence of different compression states in different layers in the z-direction during wet pressing, and increased fiber bonding during evaporative drying seems to be the dominating mechanism for the final densifying effect of wet pressing."

Density Gradient Development by Direct Measurement

At the beginning of this thesis, only two attempts had been made to measure dynamic z-direction density gradient development (Davis *et al.* (1983) and Burton (1987)). Davis *et al.* used a Wahren-Zotterman (1978) (falling weight) parallel platen type of wet press nip to develop a displacement measurement system using eddy current proximity detectors to measure the overall thickness change of both the felt and the sheet inside the press nip. The system was also used to measure the displacement (position change) of thin (25.4 μm thick) open mesh copper targets placed at the felt-sheet interface and the solid platen-sheet interface. The thickness change of both the sheet and felt resulting from a dynamically applied load as reported as a function of time as shown in Figure 13. Davis *et al.* were the first to apply this technique and recognize its value as a tool to study the wet pressing of paper handsheets. At the time of these experiments, their interest was limited to

measurement of the overall thickness change of the felt and the sheet in response to the dynamic loading.

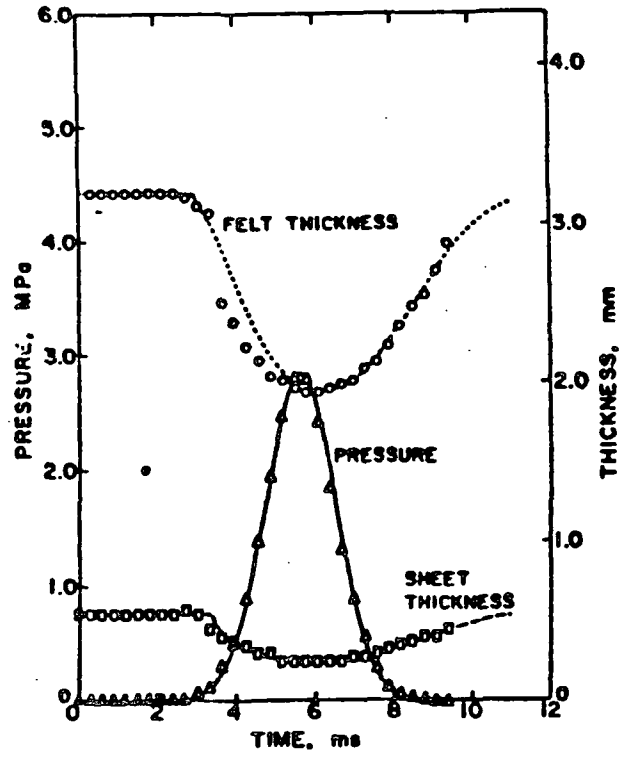

Figure 13. A comparison of calculated pressure and calculated felt and paper thickness with experimental results obtained using felt and paper simultaneously. (After Davis *et al.*, 1983)

Davis *et al.* found that for "flow-controlled" water removal the permeability of the web was more important than any other factor affecting mechanical compression. In addition, they concluded that the viscoelastic behavior of the sheet had some effect on the water removal since compression affects the permeability. They also found that the stress-strain relationship for these handsheets was highly nonlinear for the large strains

encountered, as shown in Figure 14. Davis *et al.* proposed that the area enclosed by the compression and expansion curves was related to an irreversible energy dissipation resulting from the dynamic compression process. The importance of these early experiments lies in the development of a "nonintrusive" measurement technique using open mesh targets and eddy current proximity detectors to follow the position change (at the surfaces of the sheet and the felt) of these targets. These position changes were used for calculation of the dynamic thickness change of the sheet and the felt.

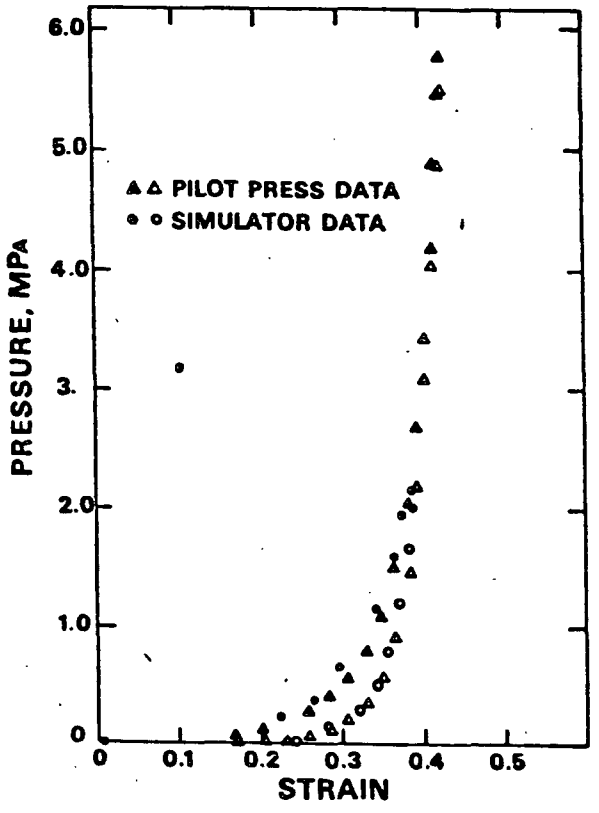

Figure 14. Comparison made by Davis *et al.* (1983) of their wet press simulator stress-strain data with pilot press data from Beck (1980).

Burton (1987), in a continuation of Davis *et al.'s* (1983) work, extended the two eddy current proximity detector system to a four detector system to measure the thickness change of multizone handsheets. This extended system enabled Burton to observe the displacement of four of the open mesh targets. These targets were embedded in the sheet to facilitate definition of three distinct zones within the sheet, which Burton referred to as Regions 1, 2, and 3. To embed the targets within the sheet, Burton constructed a special handsheet former which will be described later. Calculation of the separation distance between adjacent targets enabled Burton to measure the thickness change of each zone. The basis weights of the handsheet and each zone were carefully controlled during the handsheet forming process to facilitate accurate measurement of dynamic density development. The dynamic density was calculated by dividing the zonal basis weight by the instantaneous zonal thickness as shown in the following equation:

$$\rho_i = \frac{BW_i}{\left(d_{i+1} - d_i\right)} \qquad (2)$$

where

ρ_i = region (zonal) density, (g/cm^3)

d_i = position of target at i level, (cm)

d_{i+1} = position of target at i + 1 level, (cm)

BW_i = region (zone) basis weight, (g/cm^2)

Burton used this dynamic thickness measurement system to examine the effects of flow resistance (freeness) and moisture ratio on density development during the wet pressing of handsheets. The majority of Burton's experiments were carried out with handsheets formed from a kraft softwood pulp refined to either 735 Canadian Standard Freeness (CSF) or to 420 CSF and with an ingoing moisture ratio (MR) which varied from 4.8 to 1.4. Low flow resistance handsheets were made from the unbeaten, 735 CSF, fines-free furnish. High flow resistance sheets were made using the beaten, 420 CSF furnish.

The apparent sheet density developed in two high flow resistance handsheets is shown in Figure 15. These 53 g/m^2, 420 CSF softwood handsheets were pressed at the high and low moisture ratios of 4.8 and 1.4, respectively. Both the nip residence time and the peak applied pressure (6.9 MPa) were held constant for each of these handsheets. The desired ingoing moisture ratio for each sheet was achieved by gently pressing the high moisture ratio sheet between blotters to reduce its moisture content. The low moisture ratio sheet was pressed more heavily between blotters in a standard hydraulic press to reduce its moisture ratio.

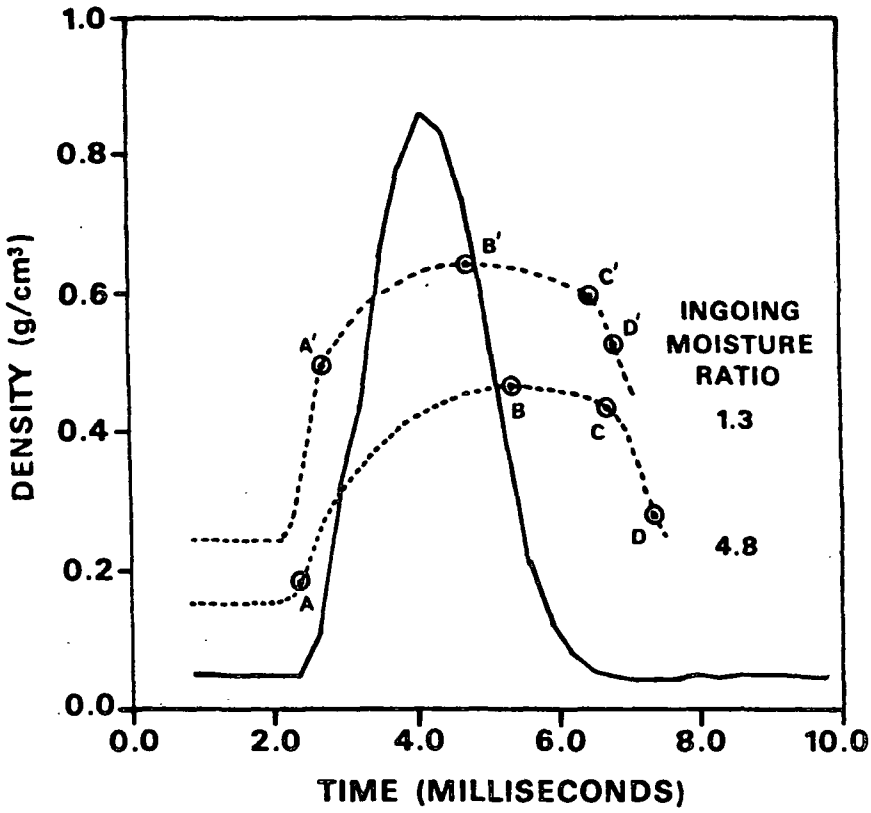

Figure 15. Sheet density-time relationships for wet pressing of sheets with different initial moisture ratios. Basis weight = 53 g/m^2; Freeness = 420 CSF; Moisture ratio = 1.4, 4.8; Peak pressure = 6.9 MPa. (After Burton, 1987)

Burton's initial wet pressing tests involved application of the technique to measure the thickness change in sheets with two equal basis weight zones. The effect of high and low freeness on density profile development in the two zones was measured. The high (735 CSF) freeness kraft softwood sheet displayed essentially the same initial densification rate for both the flow-exiting and the solid platen zones. The results do not clearly indicate the development of a flow-induced density gradient. In the case of the high freeness (735 CSF) handsheets, there was essentially no difference in the densification rate for the two zones.

The low (420 CSF) freeness softwood sheet showed a much higher densification rate in the flow-exiting zone. This was attributed to the "sieving" of fibers at the surface of the felt. As water was removed, the sheet was compressed toward the felt, and the fibers at this surface became more compacted and developed a higher fiber concentration.

In the case of the low freeness (420 CSF) furnish, there was a distinct difference in the densification rates of the two zones. In the early stages, there was little or no water flow relative to the fibers near the solid platen, yet there was a significant densification occurring in this zone. It was obvious that the fiber matrix carried a significant portion of the applied load (see Figure 16). The difference between the two density gradients was attributed to the fluid drag effect on the fibers in the flow-exiting zone and was taken as a measure of the hydraulic pressure level. It should be pointed out that the density profiles crossover early in the compression of the sheet. An explanation for this crossover was not given by Burton.

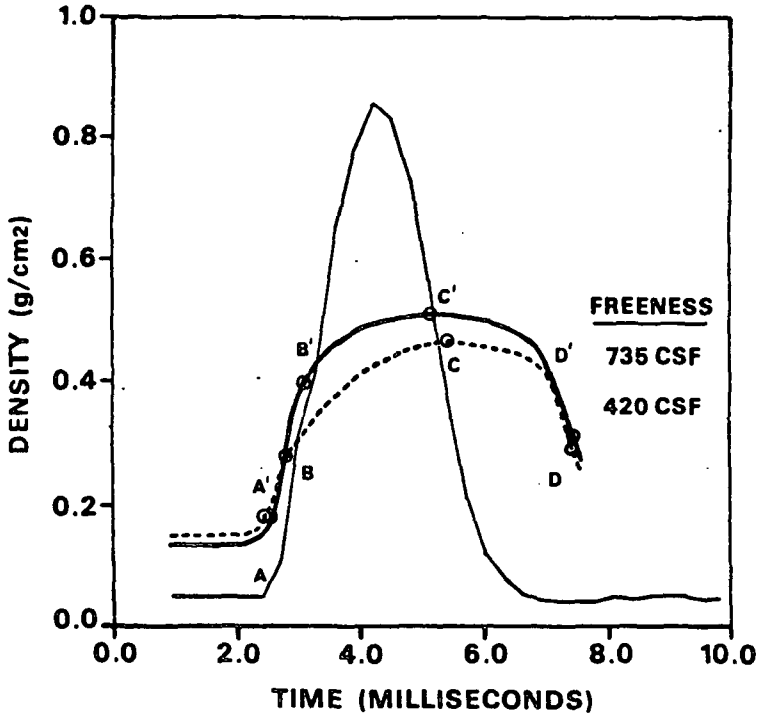

Figure 16. Density-time relationships for two wet pressing conditions of different freeness levels. Basis weight = 53 g/m^2; Moisture ratio = 4.8; Freeness = 420, 735 CSF; Peak pressure = 6.9 MPa. (After Burton, 1987)

Burton observed that the level of densification and the quantity of water removed were reduced with lower sheet freeness. He also recorded the density-time relationships for wet pressing of two different (high and low) freeness sheets with the same initial moisture ratio of 4.8 and the same nip residence time and peak applied pressure. In these tests the high freeness (low flow resistance) sheet densified to a greater magnitude before its compression was significantly resisted by the hydraulic pressure which developed.

Burton then formed three zone handsheets with a 100 g/m^2 basis weight (BW) in which the basis weight of the solid platen and flow-exiting zones was 25 g/m^2, and the middle zone was 50 g/m^2. The density-time relationship for these high and low freeness (735 and 420 CSF) sheets (shown in Figure 17) shows the effects of freeness on zonal density gradient development at a constant moisture ratio (4.0), nip residence time (4.2 msec), and peak applied pressure (7.0 MPa).

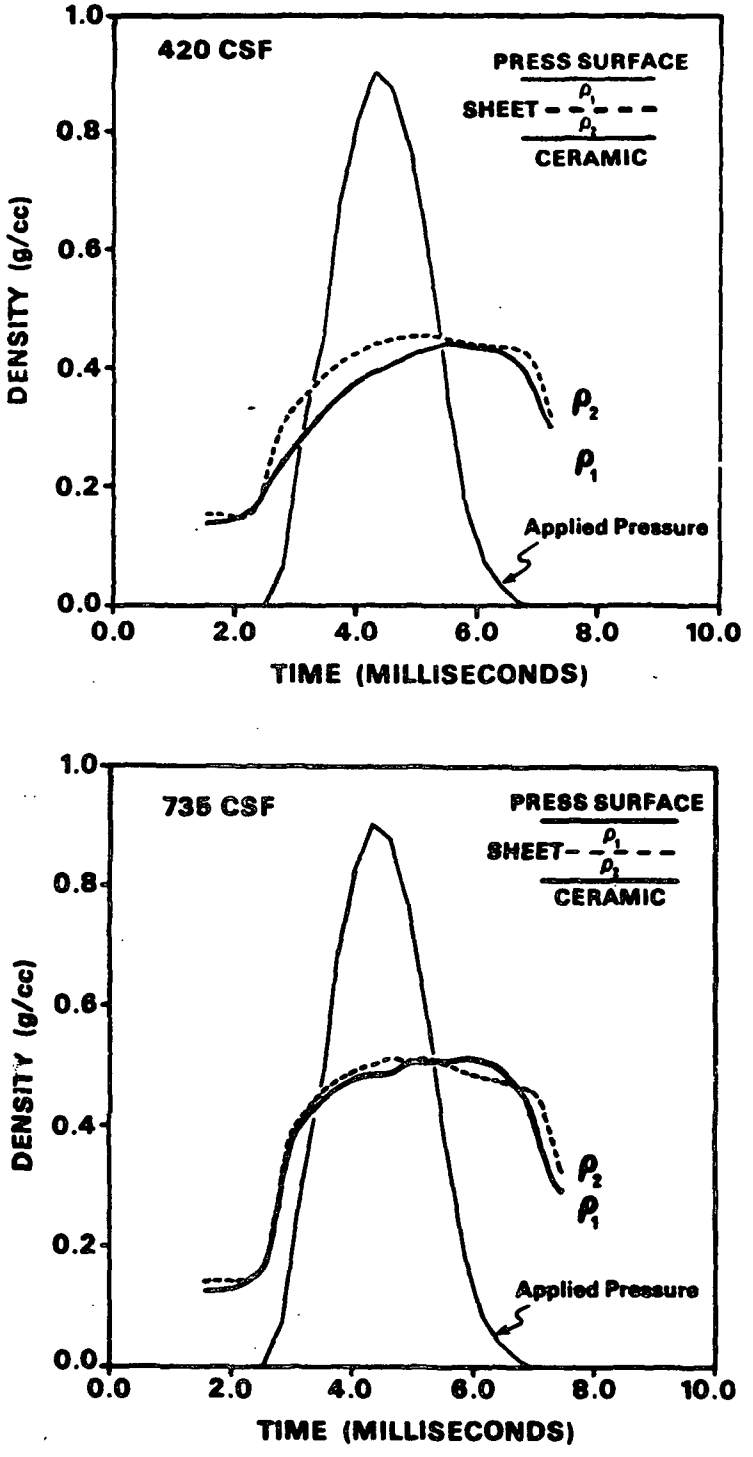

Figure 17. Internal regions density-time relationships corresponding to the sheet densities plotted in Figure 16. Regions 1 and 2 represent 50% by weight of the total sheet thickness (50 g/m^2 sheet basis weight). (After Burton, 1987)

The density-time curves for the flow-exiting zones are essentially the same for both the high and low freeness sheets. The similar initial slopes and shapes of the entire density-time curves indicate that freeness has little effect on the rate at which density development occurs early in the compression of the sheet in the flow-exiting zone.

The effect of freeness on density gradient development was more evident in the density-time curves for the remaining zones, as shown in Figure 18. For a high moisture ratio sheet (MR $\geq$ 4.0), ideally, the density gradient would be a continuous function in the z-direction. In other words, in a saturated sheet the middle zone would not be expected to densify to a lesser extent than the solid platen zone. Additionally, an individual zone would not be expected to develop its density at a higher rate initially and then develop at a lower rate than another zone. In the case of the 735 CSF sheet, the density of the solid platen zone develops more rapidly and to a greater extent than that of the middle zone. This unusual density gradient cannot be attributed to the freeness of the sheet and does not agree with the other results obtained by Burton.

It appears from Figure 19 that the target adjacent to the porous ceramic flow receiver was displaced a significant distance downward toward the proximity detector upon application of the dynamic load. The deflection of Burton's porous ceramic plate was approximately 0.025 to 0.05 mm depending on the load applied to the sheet. Burton believed that the wet sheet was the only compressible material in his press nip and had not considered that the porous ceramic plate was flexing under the applied load. The results from his multizone sheets indicate that this assumption was at least in part invalid.

The concept of embedding targets in sheets and relating their displacement during a wet pressing event to density gradient development are still valid, but proper application of these concepts requires minimizing the compressibility and flexibility of the nonpaper materials in the press nip.

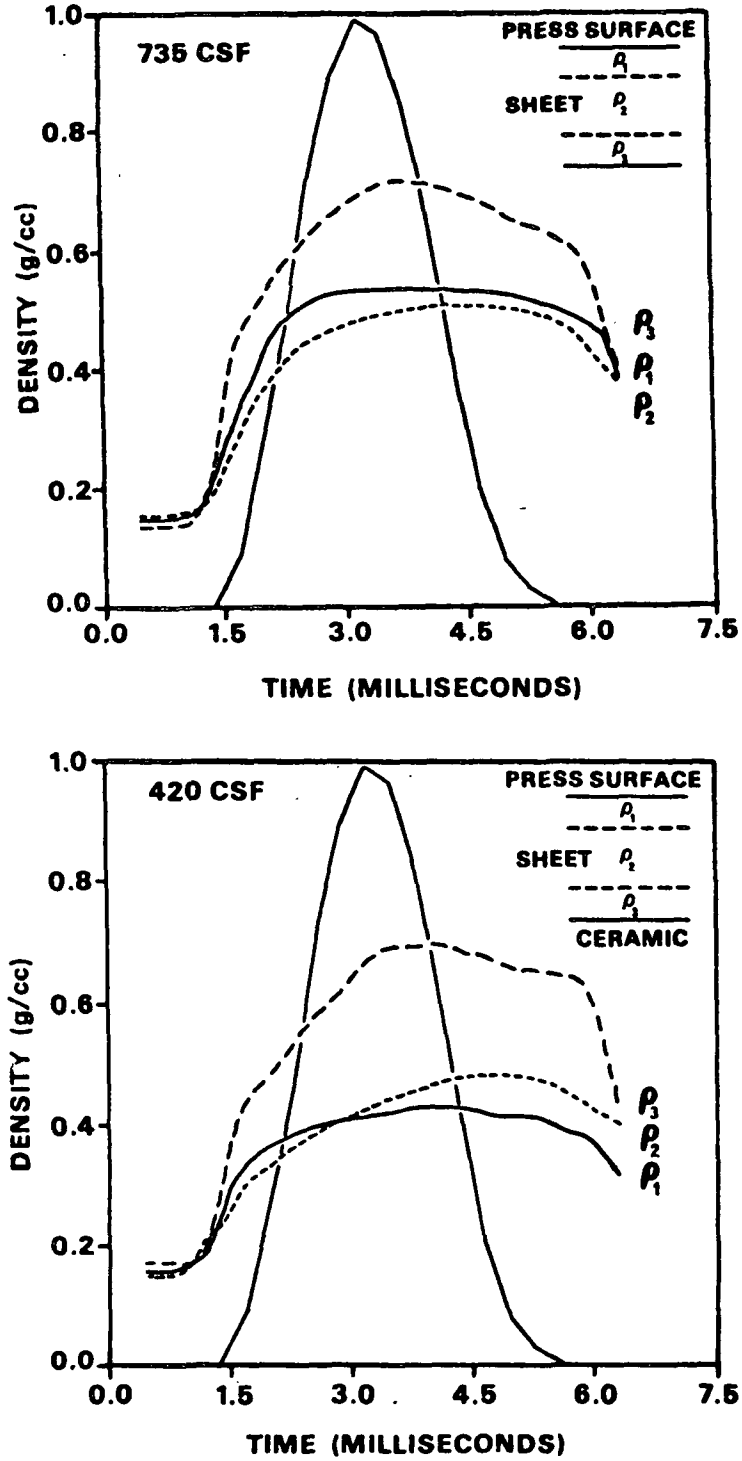

Figure 18. Internal region densities. The densities of three sheet thickness regions are depicted with a 25-50-25 split in basis weight for Regions 1-3. Basis weight = 100 g/m^2; Moisture ratio = 4.0; and Peak pressure = 7.0 MPa. (After Burton, 1987)

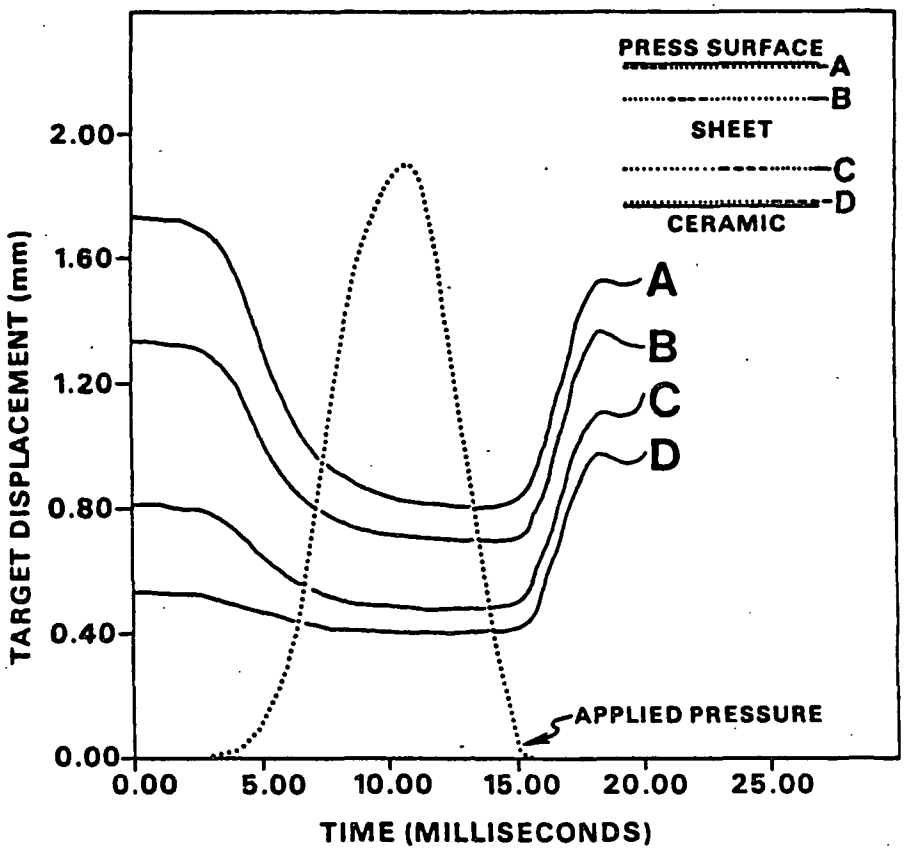

Figure 19. Typical unfiltered recordings of the target displacement histories (A-D) used in the calculation of dynamic density profiles, and the total nip pressure for wet pressing conditions at 20 °C. Peak pressure = 4.8 MPa. (After Burton, 1987)

Summary

Most of the experimental studies to date on wet pressing have dealt with measuring density development after drying the sheet. At present only one researcher (Burton, 1987) has attempted to measure density (thickness change in multizone handsheets) development inside the nip. Burton's work was focused on measurement of density development during impulse drying.

THEORETICAL BASIS FOR DENSITY GRADIENT DEVELOPMENT IN WET PRESSING

Prior to the development of suitable experimental techniques for measurement of dynamic density gradient development within the sheet by Davis *et al.*, Burton, and Szikla and Paulapuro, most previous researchers focused on development of mathematical models to understand the mechanisms of sheet densification in wet pressing. The details available on these models are limited; therefore, the results available for review are limited.

A model which provides a useful example of the basic framework used by many of the early model developers is that of Nelson (1964) and Nelson *et al.* (1964). Their work resulted in development of an approximate theory of filtration (similar to wet pressing) which could be used to describe the one-dimensional flow of fluids through deformable porous materials such as pulp or nylon fiber mats. Nelson's model characterizes a system consisting of a porous fibrous solid through which a fluid (water) is made to flow. The necessary variables are described in terms of local averages in a rectangular coordinate frame such that all quantities depend only on one spatial coordinate and on time. The independent variables are z and t (thickness and time). As shown in Figure 20, the z-direction coordinate (thickness) of Nelson's system extends from $z = 0$ upward to $z = L$. All variables associated with the fluid phase are identified by the subscripts λ and Λ, and those associated with the solid phase are identified by the subscripts ϕ and Φ. In any portion of the system, the fluid filling the available space is the fraction $\varepsilon(z,t)$.

Nelson's one-dimensional model consists of three parts. The first part describes the continuity conditions for the two phases. The second part describes a pressure relationship for the two phases, and the third part describes the resistance to fluid flow through the material due to the solid phase.

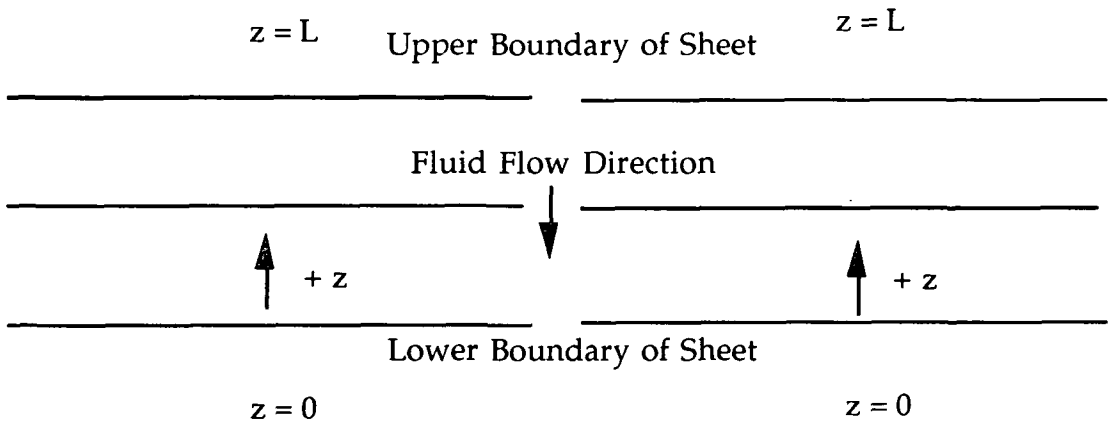

Fluid Phase	Solid Phase
fluid fraction $\varepsilon(z,t)$	solid fraction $1 - \varepsilon(z,t)$
true density ρ_{Λ}	true density ρ_{Φ}
apparent density $\rho_{\lambda}(z,t) = \rho_{\Lambda}\, \varepsilon(z,t)$	apparent density $\rho_{\phi}(z,t) = \rho_{\phi}[1 - \varepsilon(z,t)]$
pressure $p_{\lambda}(z,t)$	pressure $p_{\phi}(z,t)$
internal superficial velocity	internal superficial velocity
$U_{\lambda}(z,t) = \varepsilon(z,t)\, v_{\lambda}(z,t)$	$U_{\phi}(z,t) = [1 - \varepsilon(z,t)]v_{\phi}(z,t)$

Figure 20. Fluid and solid components of the system and their variables.

The continuity conditions for each phase are stated in terms of the averaged variables, and material compressibility is assumed (i.e., $\rho_\Lambda \neq$ constant). For the fluid phase, Nelson obtained:

$$\frac{\partial}{\partial z}\left[\rho_\Lambda U_\lambda\right] + \frac{\partial}{\partial t}\left[\rho_\Lambda \varepsilon\right] = 0 \tag{3}$$

and for the compressible solid phase ($\rho_\Phi \neq$ constant):

$$\frac{\partial}{\partial z}\left[\rho_\Phi U_\phi\right] + \frac{\partial}{\partial t}\left[\rho_\Phi (1-\varepsilon)\right] = 0 \tag{4}$$

If the fluid and the solid are actually incompressible, equations (3) and (4) can be reduced and combined to yield:

$$\frac{\partial U_\lambda}{\partial z} = -\frac{\partial U_\phi}{\partial z} \tag{5}$$

Integration of equation (5) with respect to z gives:

$$U_\lambda(z,t) = U_\lambda(0,t) - \left[U_\phi(z,t) - U_\phi(0,t)\right] \tag{6}$$

A special case was considered by Nelson in which the solid phase had an internal superficial velocity of zero at $z = 0$ (the surface at $z=0$ is not in motion), which reduces equation (6) to:

$$U_\lambda(z,t) = U_\lambda(0,t) - U_\phi(z,t) \tag{7}$$

Equations (5) and (6) are of practical importance for problems in which both phases are substantially incompressible and $U_\lambda(0,t)$ is specified. At this point in the derivation, Nelson has not assumed that the solid fraction ($1 - \varepsilon[z,t]$) is constant. The solid phase is assumed to be "compressible" or deformable.

The pressure relationship derived between the two phases assumes that the force required to produce an acceleration in the z direction, in either component, can be ignored. Therefore, Nelson obtains a simple relation connecting the pressure variables for the two phases:

$$\frac{\partial p_\phi}{\partial z} = - \frac{\partial p_\lambda}{\partial z} \tag{8}$$

Integration of equation (8) with respect to z at each surface gives:

$$p_\phi (z,t) - p_\phi (0,t) = - \left[p_\lambda (z,t) - p_\lambda (0,t) \right] \tag{9}$$

and

$$p_\phi (z,t) - p_\phi (L,t) = - \left[p_\lambda (z,t) - p_\lambda (L,t) \right] \tag{10}$$

In developing a fluid flow resistance relationship, Nelson chose the case in which the solid phase is not in motion, and the effects of acceleration can be neglected. Nelson used the following form of Darcy's law:

$$U_\lambda = - \frac{1}{\alpha} \frac{\partial p_\lambda}{\partial z} \tag{11}$$

where $\alpha = \mu r \rho_\phi$, in which μ is the fluid viscosity, and r is the local flow resistance.

In order to obtain agreement with the customary definition of r, Nelson considers a limiting case which generalizes equation (11) as:

$$U_\sigma = U_\lambda - \frac{\varepsilon}{1 - \varepsilon} U_\phi = - \frac{1}{\alpha} \frac{\partial p_\lambda}{\partial z} \tag{12}$$

The quantity on the left is called the relative superficial velocity.

The final form of the equation for U_σ becomes:

$$U_\sigma = \frac{1}{1 - \varepsilon} U_\lambda (z,t) - \frac{\varepsilon}{1 - \varepsilon} U_\lambda (0,t) \tag{13}$$

And after rearrangement equation (12) becomes:

$$U_\lambda (z,t) = \varepsilon U_\lambda (0,t) - \frac{1 - \varepsilon}{\alpha} \frac{\partial p_\lambda}{\partial z} \tag{14}$$

Substituting this result into equation (5) yields:

$$\frac{\partial \varepsilon}{\partial t} = - U_\lambda (0,t) \frac{\partial \varepsilon}{\partial z} - \frac{\partial}{\partial z} \left[\frac{1 - \varepsilon}{\alpha} \frac{\partial p_\phi}{\partial z} \right] \tag{15}$$

Nelson defined a set of boundary conditions for the model that consisted of a combination of the following quantities: the upstream fluid pressure, $p_\lambda(L,t)$; the downstream fluid pressure, $p_\lambda(0,t)$; the pressure exerted (for example, by a grid) on the lower boundary of the solid phase, $p_\phi(0,t)$; the fluid inflow rate per unit area, $-U_\lambda(L,t)$; fluid outflow rate per unit area, $-U_\lambda(0,t)$. To solve unsteady-state problems, Nelson supplied a set of initial conditions in which he specified the values as some combination of the variables listed in Figure 20 for a given value of the time. The approximate theory of filtration and retention is applied only to the retention of small particles in deformable porous solids. Unfortunately, Nelson does not present any results from solving this model in relation to the wet pressing of fiber mats.

Nilsson and Larsson (1968) also developed a mathematical model describing sheet compression and fluid flow during wet pressing. Their model was based on the following approximations: all flows are assumed perpendicular to the paper web, and the hydraulic pressure in the felt is zero; saturation of the paper web occurs simultaneously at all levels; no air is present in the sheet past the point of saturation, and Darcy's law is valid in the form of equation (16):

$$\frac{dp}{dx} = \mu FR\, v \tag{16}$$

where dp = pressure drop

dx = the distance across which the pressure drop is caused

μ = viscosity of the water

v = seeping velocity

FR = flow resistance.

Nilsson and Larsson believed that the hydraulic pressure gradient in the paper web could be of considerable magnitude and thereby affect the state of compression in different layers of the sheet. In effect, this resulted in corresponding moisture ratio and flow resistance distributions which had to be accounted for in their model. Figure 21 illustrates the distribution of hydraulic pressure, fiber structural pressure, moisture ratio, and flow resistance for a certain time t after the nip entrance. A layer with the basis weight dy at position y in the sheet is also shown. Figure 22 shows how such a layer at this height would look inside the press nip.

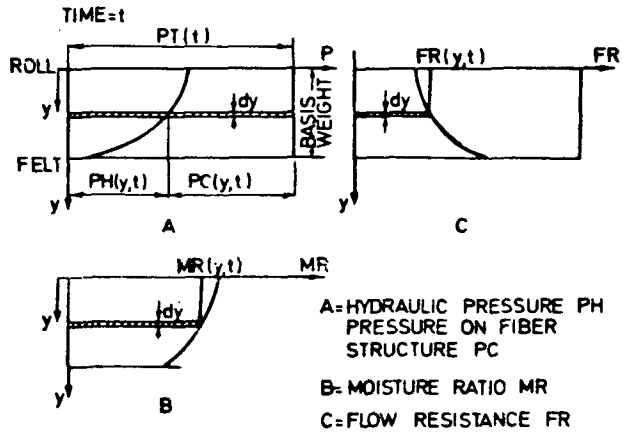

Figure 21. Distributions of hydraulic pressure, fiber structure pressure, moisture ratio, and flow resistance in the sheet at the in-going side of the nip. (After Nilsson and Larsson, 1968)

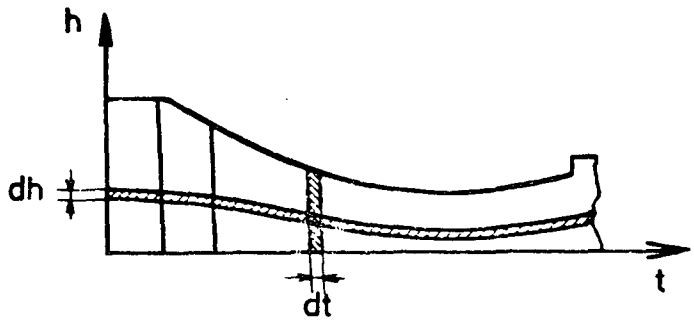

Figure 22. The change in thickness of a layer with thickness *dy* through the nip. (After Nilsson and Larsson, 1968)

Their model was constructed by splitting the whole nip into time intervals and the sheet into layers. Then an iterative trial and error method was used on the computer to solve the equations for each point in the nip. Data supplied to the computer model included the nip applied pressure curve, nip length, machine speed, sheet basis weight, web compressibility, and

the measured sheet flow resistance. Solution of the mathematical model produced values for hydraulic pressure, fiber structural pressure, thickness, and pressure drop for each layer of the sheet and for all of the 40 time intervals used. Nilsson and Larsson simulated a eucalyptus viscose pulp having a very low flow resistance and checked their results with those obtained from a practical wet press simulation (simulator). The results from the computer model (shown in Figure 23) showed that the hydraulic pressure was totally insignificant, whereas their pilot wet press measurements showed a hydraulic pressure which dominated the nip (shown in Figure 24). To address this discrepancy, Nilsson and Larsson looked for potential errors in their model. They concluded that, in order to obtain a quantitative understanding of the flow conditions in the press nip, it was not enough to statically measure the flow resistance and compressibility of handsheets and then use Darcy's law to compute the hydraulic pressure drop in the fiber bed. Initially, Nilsson and Larsson had assumed that the total pressure curve could be divided into two portions, one (static) which could be easily measured and one (dynamic) which was built up solely due to the flow of water through the fiber bed. This assumption meant that the only dynamic pressure existing inside the nip was the hydraulic pressure - which was later determined to be an incorrect assumption. Furthermore, they believed that some other sources of dynamic pressure should be considered such as inertia, flow of water from within the fibers into the transportation channels in the fiber bed, the viscoelastic behavior of the cellulose, and infiltration of fibers into the surface of the porous plate (felt) flow receiver.

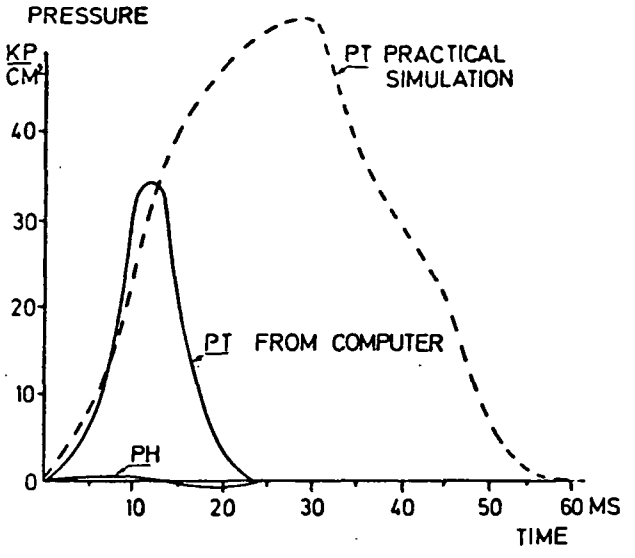

Figure 23. Pressure distribution for a eucalyptus viscose pulp as computed with Nilsson and Larsson's computer model.

Unfortunately, the only published changes in layer thickness calculated with this model are limited to those found in Figure 22. Nilsson and Larsson did not indicate whether their model actually predicted the development of a density gradient in the direction of fluid flow. However, their discussion on development of hydraulic and structural pressure gradients would indicate that a density gradient was predicted by the model.

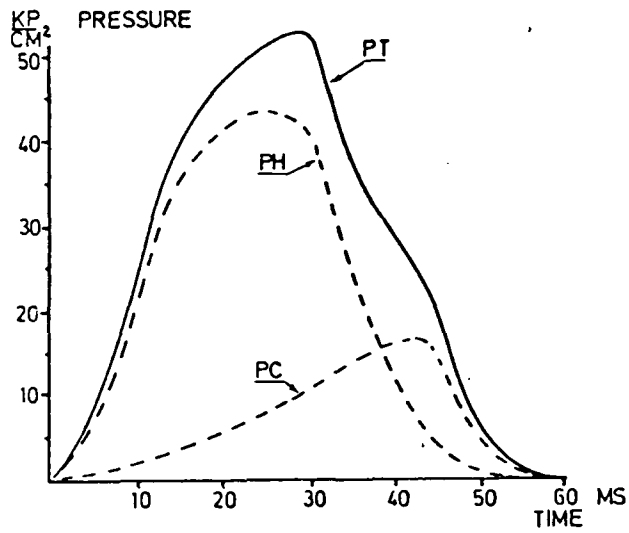

Figure 24. Pressure distribution resulting from a practical simulation test with a eucalyptus viscose pulp.

Westra (1975) analyzed Nilsson and Larsson's model and concluded that there was an error in their continuity equation. They had failed to take the divergence of the flow into account. As a consequence of this error, their calculated flows and hydraulic pressures were much lower than those measured in their pilot press simulations.

Westra derived a mathematical model of the wet pressing process similar to that of Nilsson and Larsson (1968). In analyzing the method used by Nilsson and Larsson, Westra makes the observation that the specific permeability is not constant as assumed by Nilsson and Larsson, but strongly dependent on the mat porosity. In fact, Westra used the Kozeny-Caraman equation for a large range of mat porosities to calculate the specific permeability. The Kozeny-Caraman equation states that the specific

permeability is proportional to $\varepsilon^3/(1 - \varepsilon)^2$. The porosity, ε, is defined as the fraction of the volume which is available for fluid flow.

Westra's model was capable of calculating the moisture ratios of arbitrary layers in the web as a function of position in the nip. The calculated moisture ratios for five layers and the felt-sheet interface are shown in Figure 25. The layer with the highest moisture ratio was adjacent to the hard roll ($g/G = 0.0$), and the layer with the lowest moisture ratio was the flow-exiting layer ($g/G = 1.0$).[1] The flow-exiting layer showed the most rapid change in moisture ratio as a function of press nip position. The predicted moisture ratio gradient decreased with increasing distance from the felt. The results from this model are quite interesting since this was the first wet pressing model (of saturated mats) to indicate the development of a density gradient in the direction of fluid flow.

[1] g/G is the nondimensional thickness in terms of the layer basis weight (g) in the z-direction of the web (G = sheet basis weight). $g/G = 0.0$ is adjacent to the hard roll surface, and $g/G = 1.0$ is at the flow-exiting surface of the sheet. x/B is the nondimensional machine direction position from the nip center. $x/B = 0.0$ defines the center of the nip.

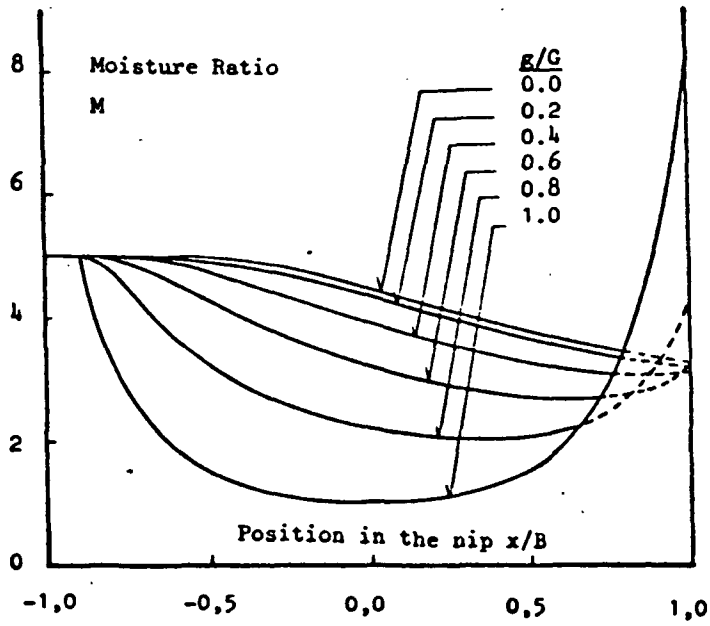

Figure 25. Moisture ratio in different layers of the web as it passes through a press nip. (After Westra, 1975)

Jewett (1980, 1984) and Jewett *et al.* (1980) at the University of Maine, have developed a more elaborate, highly empirical mathematical model of wet pressing. The full details of this model are quite lengthy; therefore, the discussion of this work will be limited to the relevant results obtained.

In Jewett's model the paper web was divided into 10 equal z-direction basis weight layers to model discrete points in the sheet. The model results show the development of a moisture gradient in the direction of fluid flow. Figure 26 illustrates what can be referred to as a consolidation wavefront which progresses from the felt toward the solid roll surface (in the opposite direction of fluid flow). Also, the points of deviation from the initially assumed uniform moisture ratio distribution are shown for various positions

in the z-direction. A delay of up to two milliseconds in initiation of the moisture ratio decrease is observed at the different locations in the z-direction. This result is similar to that obtained by Philip (1968) and described by Westra (1975). It should be noted that as the sheet passed midnip (the point of applied pressure reversal) the moisture gradient in each layer approaches the same level. The lowest moisture ratio and highest level of densification are found in the layer at the felt-sheet interface (layer MR1 shown in Figure 26). This indicates that a dense interfacial layer was formed which may have acted as a barrier to water flow. It should be noted that the moisture ratio of layer MR1 reaches a minimum at approximately 5 milliseconds into the nip (approximately midnip). After reaching a minimum, the moisture ratio begins to increase and approaches a value of 4.5 at 10 milliseconds. This indicates that water accumulates at the sheet-felt interface as the pressure is released.

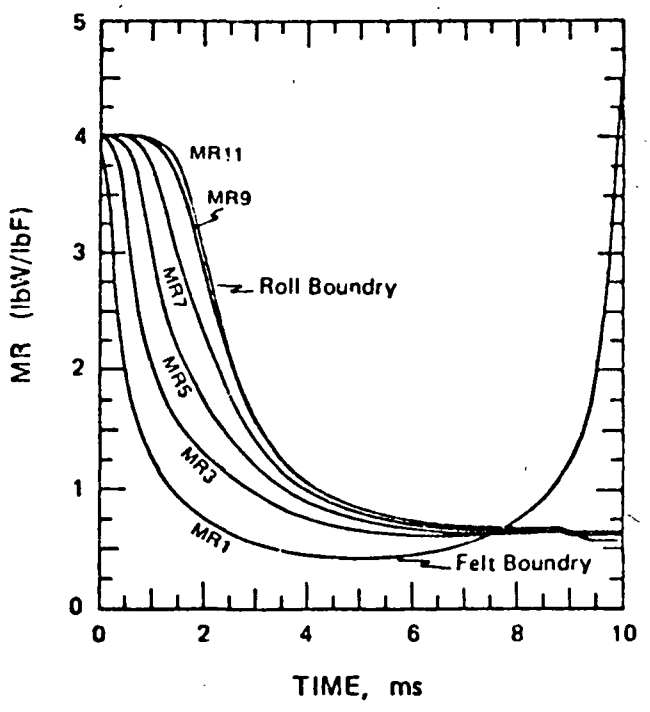

Figure 26. Z-direction moisture ratio. (After Jewett, 1980, 1984)

Figure 27 shows the change in volumetric fraction of swollen fiber (EF) in the Z-direction which, when multiplied by the density of cellulose fibers, gives the density gradient in the z-direction. Figure 27 also shows that the layer with the greatest density change is adjacent to the felt (or the flow-exiting layer), and the layer with the smallest density change is adjacent to the solid roll. This figure clearly predicts the development of a z-direction density gradient in the sheet. These model results provide added support for MacGregor's theory of sheet stratification and density gradient development in the sheet.

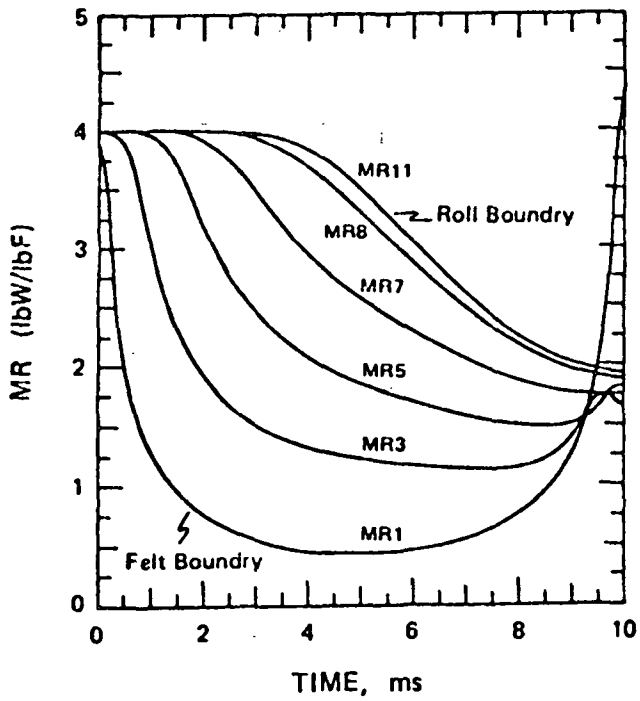

Figure 27. Compression gradient, Z-direction. (After Jewett, 1984)

Roux (1986) at L'Institut National Polytechnique de Grenoble (Grenoble, France) has also developed a wet pressing model. This model is significantly different from that of Jewett (1980, 1984) in that Roux has adopted a fundamental approach to minimize the number of empirically determined parameters. Roux's model solves elementary mechanics equations written for a small volume element consisting of three material phases (water, air, and solid fiber). In the model the paper web is divided into a rectangular domain having five equidistant layers in the z-direction of the sheet and 15 equidistant sections in the machine direction and symmetric about midnip. Roux's model also differs from Jewett's in the choice of numerical solution scheme. For the roll geometry, Roux has chosen to solve the model equations by slowly pressing the roll into the surface of the sheet. Each step increment is converged until the final sheet thickness (50% of the initial thickness) is reached.

Roux's thesis presents the results from modelling a sheet with an initial thickness of 250 μm, a dry basis weight of 70 g/m^2, and an initial moisture ratio of 2.435. The nip length is 0.030 m with a machine speed of 10 m/s which implies a press impulse duration of 3 msec. Roux's modeling approach specifies only the geometry. The total applied pressure must be indirectly known and in the absence of measurements for the elastic coefficients of the wet sheet of paper Roux adopted an order of magnitude size for the coefficients based on the elastic coefficients determined using ultrasound techniques developed for dry paper by Habeger *et al.* (1979). The calculated applied pressure profiles are in the form of parabolas centered in the middle of the nip. Since this solution is for a compression-controlled sheet, the assumption was made that the hydraulic pressure remains negligible.

Roux states that "this simulation shows the stratification phenomenon of the wet web in the press." He draws this conclusion from the two components of the displacement vector and the variations of the porosity which he attributes to the pressure gradients in the sheet. The horizontal displacement of the nodes corresponding to the middle layer of the sheet and at the horizontal positions of -0.4 and +0.4 relative to the center of the nip pass through maximum displacements of -0.87 μm (for the node at -0.4) and +0.84 μm (for the node at +0.4).[2] In other words, these two nodes move away from the nip center about 0.8 μms each. The vertical components of the mid-nip nodal displacements in the sheet follow the imposed geometry at the sheet-roll interface. Therefore, a maximal collapse of 125 μm is allowed for

[2]Note that the negative values correspond to the ingoing side of the nip, and the positive values correspond to the outgoing side of the nip.

the node at sheet-roll interface (X position inside the nip of 0.0) and the nip center as shown in Figure 28. Roux states that the thickness of the layer in contact with the roll is much larger than the thickness of the layer adjacent to the felt and that the layer thickness variation depends on the pressure gradient in the structure.

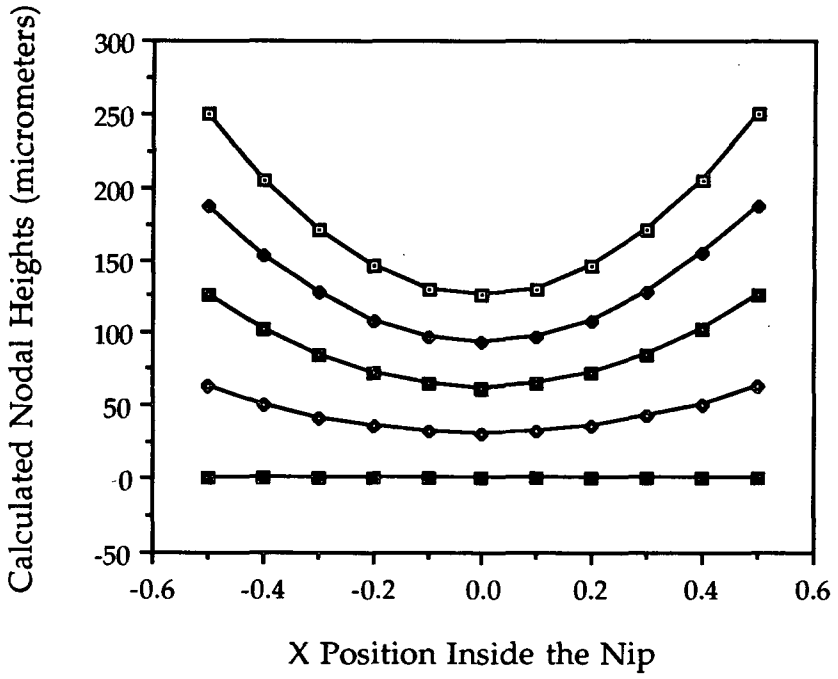

Figure 28. Distribution of calculated vertical nodal displacements. (After Roux, 1986)

Roux states that the calculated porosity (shown in Figure 29) and the saturation levels of the layers (shown in Figure 30) in the convergent geometry of the press show that at the sheet-felt interface the porosity is much lower than at the sheet-roll interface and that the saturation level is higher

toward the sheet-roll interface. Roux also observes that the most severe layer thickness compression occurs in the layer(s) adjacent to the felt. He claims that much higher gradients of porosity were calculated in the thickness direction (+y is up in all of Roux's figures) and were localized before midnip in proximity to the felt. Figure 29 shows that a small difference in the porosity occurs before midnip and increases toward the sheet-roll interface. This indicates the presence of a very small gradient in the porosity in the z-direction. Since this case was for a low initial moisture ratio sheet, there is insufficient evidence to support Roux's claim that his model predicts development of a density gradient and sheet stratification.

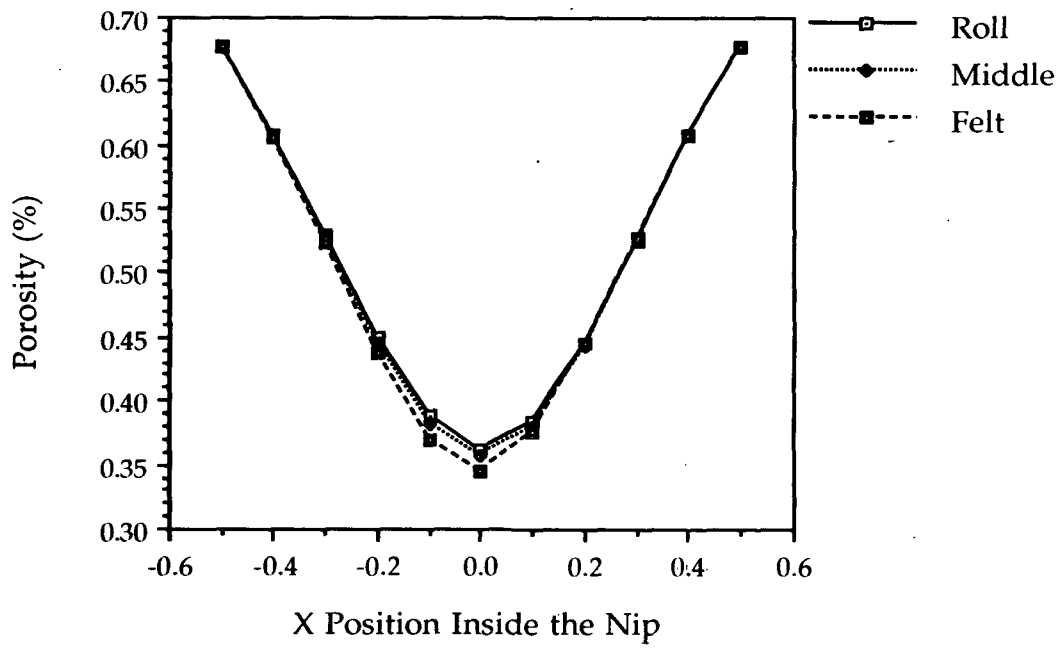

Figure 29. Distribution of porosity. (After Roux, 1986)

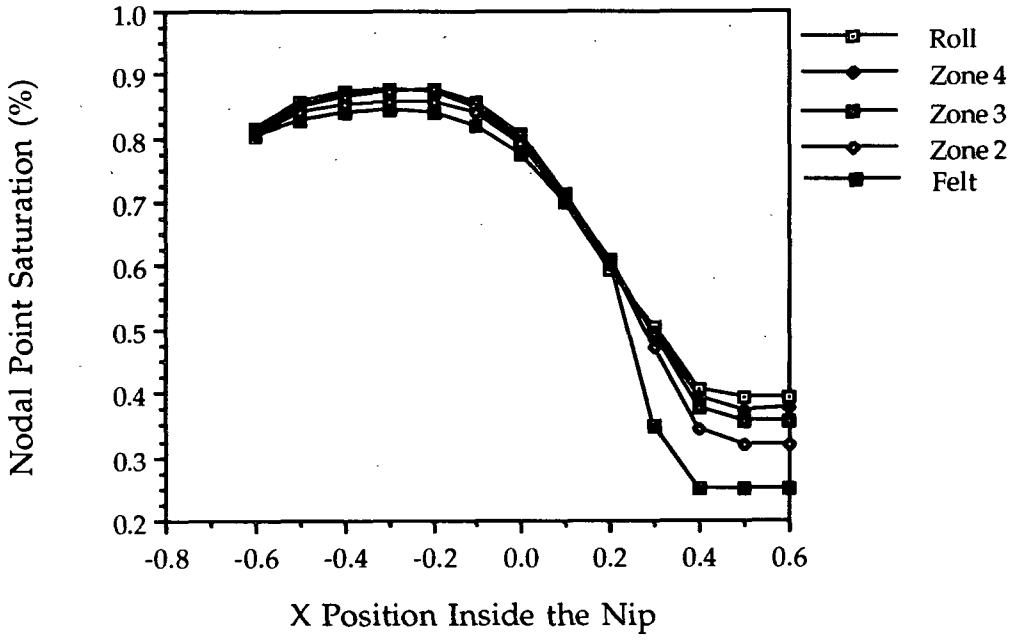

Figure 30. Distribution of external fiber saturation. (After Roux, 1986)

In addition to the early models developed for the wet pressing of fiber mats, Philip (1968) developed a model for one-dimensional consolidation of soils. Philips model is a theoretical analysis for the one-dimensional desorption (or consolidation) of a two-component paste composed of a clay-colloid and an electrolyte solution. In his analysis, Philip combined Darcy's law (for the flow of an electrolyte solution relative to the colloid particles) with the continuity requirement. The hydraulic conductivity and the moisture potential were taken to be arbitrary known functions of the volumetric solution content making these variables dependent on the level of compaction of the medium. The fundamental flow equation developed was a nonlinear partial differential equation. This equation was solved both numerically and analytically. The process of colloid displacement during consolidation can be seen in Figure 31.

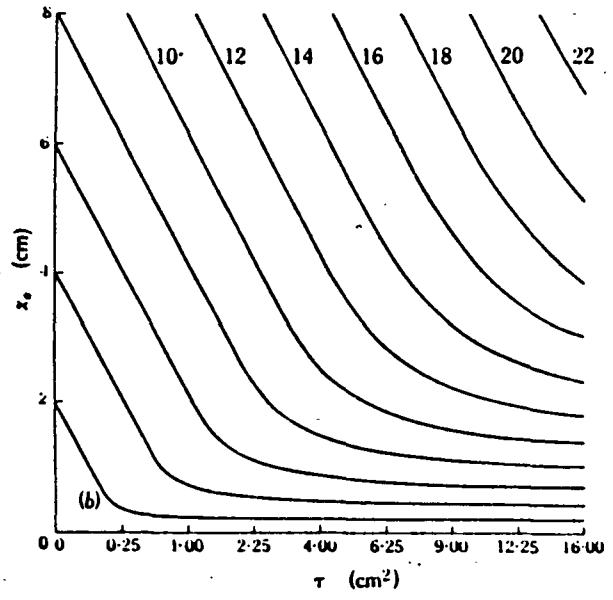

Figure 31. Numerical solution of Philip's model for one-dimensional consolidation of clay-colloid paste showing stratification. τ is time in the reduced form D*t. The scale of τ is linear in $\tau^{.5}$. (After Philip, 1968)

Figure 31 illustrates regions of parallel, linear displacement histories for the upper part of a consolidating clay-colloid paste. The bodily translation of colloid and solution is shown to occur without shrinkage in the upper part of the column (the consolidation process has not yet penetrated to these levels). The numbers in the upper part of the figure are the x_o values which are the initial elevation (in units of cm) for particles starting higher on the vertical axis. This figure clearly shows both a consolidation wavefront (stratification) and density gradient development during consolidation.

An example of the idealized compression and expansion of a porous elastic medium was modelled by Smith and Griffiths (1988). They developed a simple computer model based on the Finite Element Method (FEM) for

analysis of the behavior of porous elastic solids using Biot's theory for two-dimensional consolidation. In this program, the coupling of the fluid flow with the deformation of the solid phase requires division of the applied "total" stresses into a portion carried by the skeleton (solid phase), called the effective stress, and a portion carried by the pore water. The applicability of the model to wet pressing was investigated by this author, and the methodology and results will be presented in later sections.

SUMMARY

A considerable amount of evidence has been presented from the literature to show that both steady- and unsteady-state fluid flow through a compressible porous medium result in deformation of the medium due to drag or shear forces associated with the flow. There is also evidence that the combination of mechanical and flow-induced compression affects material properties such as permeability and compressibility. These results establish the need to develop a detailed knowledge of the strain and density distribution in compressible porous materials which undergo rapid compression such as wet paper webs. Unfortunately, given the small z-direction thickness for wet paper webs and the short duration of the wet pressing event it would be difficult to use the visual methods of these authors to observe the development of a nonuniform z-direction density profile in wet paper sheets. Since no suitable visual methods had been developed for use in the study of thin (1-2 mm thick) compressible fiber mats before this work was begun, it is obvious that an alternative method must be developed.

Considerable evidence has been presented from the literature describing the effects of freeness, basis weight, and nip residence time on the

compression and expansion behavior of saturated pulp sheets. The literature indicates that decreasing freeness tends to drive the compression behavior of the sheet toward what has been described as flow-controlled pressing. Freeness levels typical of unbeaten pulps tended to behave in a more compression-controlled manner. At low freenesses mechanical and chemical pulps tended to compress rapidly if the rise time of the applied pressure pulse was on the order of 1.5 to 5 msec. On the other hand, if the rise time was on the order of 5 to 10 msec, the compression rate was slowed considerably. Also, the compression of low freeness mechanical and chemical pulps was much less than that of higher freeness mechanical pulps which implies that the dewatering and compression behavior was more flow controlled. It has also been show that increasing sheet basis weight increases the flow resistance and the hydraulic pressure generated in the sheet. Therefore, the compression behavior as a result of increasing the basis weight was more flow-controlled.

Most of the experimental wet pressing studies to date have dealt with measuring density development after drying the sheet. At present only one researcher (Burton, 1987) has attempted to measure density (thickness change in multizone handsheets) development inside the nip. The results obtained be Burton indicate that both freeness and moisture ratio have a significant effect on density gradient development.

A number of mathematical models have been developed describing the consolidation of soils and porous fibrous materials such as pulp fiber sheets. One of the earliest of these models is probably that of Nelson. Nelson developed a simple one-dimensional model to describe the filtration of fibrous material. Unfortunately, he does not present any results from solving these equations. The next model was developed by Nilsson and Larsson in

1968. In this model the pressure in the nip was divided into two parts, one static (structural pressure) and one dynamic (hydraulic pressure). Nilsson and Larsson solved the model and compared the model hydraulic pressure predictions with measured hydraulic pressures inside the nip of a pilot press. The model predicted that the hydraulic pressure would be insignificant which was the opposite of their measurements. Upon review of their results, they concluded that a better understanding of the fundamental processes occurring inside the nip was necessary before modeling of the wet pressing of paper would be successful.

A few years later, Westra analyzed Nilsson and Larsson's model and determined that they had made an error in one of their equations. Westra corrected Nilsson and Larsson's error and developed his own model of wet pressing. The results from Westra's model showed that the most rapid change in moisture ratio in the sheet occurred in the layer adjacent to the felt, and the moisture ratio increased in the layers farther away from the felt. This was the first wet pressing model to predict the development of a density gradient in the direction of fluid flow.

In the early 1980s, Jewett and others at the University of Maine began to develop a wet pressing model. This model was based on many empirical correlations. The results from this model indicated the development of a density gradient in the direction of fluid flow similar to that predicted by Westra's model. The model also predicted that a significant quantity of water was pulled back from the felt to the interface between the sheet and the felt.

In the late 1980s, Roux and others at CTIP in Grenoble, France, developed yet another wet pressing model. This model was based on a more

fundamental approach to eliminate the need to measure the multitude of physical properties required for Jewett's model. The results presented in Roux's thesis were for the simulation of the wet pressing of a low moisture ratio (2.4) handsheet. The results indicated that a small density gradient was formed in the direction of fluid flow.

Models for the consolidation of soils were developed by Philip and Smith and Griffiths. The results from Philip's model indicated the development of a stratification or consolidation wavefront in which the layers far away from the flow-exiting surface begin to decrease in thickness at some time after the consolidation process begins. The model developed by Smith and Griffiths illustrates the coupling of fluid flow and material deformation associated with the fluid flow. The results for consolidation of a porous elastic material indicate the development of a density gradient in the direction of fluid flow.

After several researchers made unsuccessful attempts to model wet pressing, simulations based on fundamental approaches showed that MacGregor's hypothesis of the development of a density gradient did in fact have a sound theoretical basis. These results indicate that the layer at the flow-exiting surface should develop the greatest density and at the fastest rate. In addition, the point of maximum density development should occur at the point of maximum applied load in the elastic models.

PROBLEM STATEMENT

Wet pressing of saturated pulp handsheets results in flow through a saturated compressible porous medium which deforms from both mechanical compression and forces associated with fluid flow through the medium. This flow induces changes in material properties such as permeability and compressibility. The coupling of fluid flow and material deformation is believed to result in development of a density gradient in the direction of fluid flow.

The presence of this dynamic density gradient in theoretical and experimental analyses of other media suggests that it should be observable during the wet pressing of paper handsheets. Previous attempts to measure dynamic density gradient development during the wet pressing of pulp handsheets have been flawed due to inadequacies of the equipment. Therefore, development of a suitable device for measurement of dynamic density gradient development during the wet pressing is necessary.

In addition, observation and demonstration of the effects of several process variables on density gradient development would contribute to our understanding of the mechanism(s) of sheet densification inside the wet press nip. Additionally, development of better water removal methods and more desirable paper properties will result from our increased knowledge of the effects of process variables (such as nip pressure profile and pressure rise time) on the internal behavior of the sheet during wet pressing.

Therefore, the objectives of this work are 1) to develop a technique for illustration of dynamic density gradient development in handsheets pressed

in a platen press, 2) to apply the technique to measurement of the influence of process variables on density development, and 3) to develop a density profile database for future wet pressing model development.

EXPERIMENTAL PLAN

The dynamic compression and expansion behavior of wet fiber sheets is a key factor in understanding the mechanisms of wet pressing and density development. Therefore, the objectives of this work were 1) to develop a technique (including the necessary equipment) for illustration and measurement of dynamic z-directional displacement of targets embedded (density gradient development) in handsheets pressed between parallel platens, 2) to apply the technique to measurement of the influence of process variables on density development, and 3) to develop a density profile database for future wet pressing model development.

The experimental work of this thesis consisted of three parts. The first part involved the design and assembly of a data acquisition system capable of handling a wide variety of transducer signals (such as voltage, current, or thermocouple) with rapid signal processing and ultimately graphical display of the acquired data. It was essential that the data acquisition system be capable of rapidly digitizing data from several voltage signals and to acquire a sufficient number of data points to adequately resolve small or sudden changes in the short duration wet pressing events (3 to 60 milliseconds). The effectiveness of the data acquisition system was evaluated by making several measurements using a Wahren-Zotterman (1978) "rock dropper" and an MTS (Materials Testing System) servo-hydraulic press as wet press simulators.

In the second part of the experimental work, a continuous flow handsheet former was designed and constructed for the manufacture of 127-mm (5-inch) handsheets. The handsheet former was required for the production of multizone handsheets and the embedding of open mesh

copper targets, both internally and at the surfaces of these handsheets. The requirements for this new handsheet former were 1) that the handsheet former be capable of tightly controlling both the positioning of targets in the x-y plane of the handsheet for each zone and 2) to uniformly distribute fibers over the surface of each zone.

The third part of the experimental work involved the development of an instrumented wet press nip capable of accurately measuring the displacement of these embedded targets and the wet pressing of a number of these handsheets. The data from this nip had to be sufficiently accurate and reliable to measure the effects of process variables on density gradient development. In addition, the experimental nip was designed to eliminate the shortcomings encountered with Burton's wet press nip. To do this required optimization of the construction materials and the orientation of the nip such that the only significantly compressible material in the nip was the handsheet itself. Several compressible and/or flexible materials found in Burton's press nip were eliminated, and the orientation of the nip was changed. The instrumentation in the new design included five eddy current proximity detectors and a load cell (force transducer). Four of the proximity detectors tracked the positions of the four targets in the handsheets and the fifth proximity detector tracked the position of the falling press head. The load cell measured the load (force) applied to the sheet.

The influence of three process variables (furnish, freeness, and nip residence time) on the development of a dynamic z-directional density gradient was investigated in the final part of this work. Handsheets were prepared with the handsheet former from a hardwood furnish at one freeness level and a softwood furnish at two freeness levels. These handsheets were

pressed using the new press heads and a Wahren-Zotterman "rock dropper" or an MTS servo-hydraulic press as wet press simulators.

MATERIALS AND METHODS

DESIGN AND ASSEMBLY OF THE DATA ACQUISITION SYSTEM

To facilitate both acquisition and analysis of experimental data and a reduction in data analysis time, a new data acquisition system was chosen to replace the two eight-bit resolution data acquisition systems used by Burton. The short duration of the wet pressing event (3 to 60 milliseconds) and the desire to acquire as many data points as possible during the event became the most important factors in choosing the data acquisition system. A TransEra MDAS 7000 data acquisition system (TransEra Corp., Provo, Utah) was chosen because of 1) its high level of flexibility in acquiring both voltage and current signals, 2) the potential to vary the number of data channels (up to 64 channels) with multiple data acquisition cards, 3) the capability of high frequency data sampling on multiple channels (the maximum single channel sampling frequency was 540 kHz), 4) the ability to digitize the signals with 12 bits of resolution, and 5) the ability to set the number of pretrigger points to be recorded as part of the acquired signal data. The 12-bit data acquisition system resolved the signals into 4096 different levels, whereas the old eight-bit data acquisition system only resolved the signals into 256 levels. The data acquisition system was set up for each run to acquire 1000 data points, of which 450 were recorded before the system was triggered. The sampling frequency was typically 10 kHz or greater and depended on the number of channels sampled. The MDAS 7000 sampled each channel sequentially with a delay of 5.4×10^{-6} seconds between sampling of channels.

Another important requirement for improvement of the data acquisition was the elimination of the need to develop a complex control and

data analysis program. A simple control program was written in TBasic (TransEra Corp., Provo, Utah). The program capabilities included acquiring data with automatic scaling, listing the data in tabular format on the computer screen, plotting the data on the computer screen, plotting the data on a hard copy device, and saving the data to computer disk for future manipulation. (For further details of the program, see the program listing in Appendix I.) The acquired data were saved in ASCII format to facilitate transfer to other graphical or analysis software and computer systems.

The ability to immediately analyze the data after pressing each handsheet was instrumental in the detection and correction of equipment problems before the next handsheet was pressed. This reduced wastage of handsheets and target material. A full description of the proximity detectors used to instrument the wet press nip and the special requirements to interface these instruments with the data acquisition system are given in Appendix II.

Finally, the ASCII format data were transferred from an IBM compatible computer to an Apple Macintosh II computer for analysis and plotting. The Apple Macintosh was chosen based on its ability to handle large data sets and the availability of graphical analysis software. Data analysis and plotting was done with the program *Igor* ™ (Wavemetrics, Lake Oswego, Oregon). The most significant advantages of this program were 1) the ability to handle large data arrays, 2) the ability to generate graphs containing more than 5000 data points in a few seconds, and 3) the ability to manipulate the data in a spreadsheet format.

DESIGN AND CONSTRUCTION OF THE NEW HANDSHEET FORMER

Measurement of the dynamic thickness change of different layers of the handsheets with the eddy current proximity detectors required the embedding of two thin porous targets (100 lines per 25.4 mm, 25.4 μm thick electroetched copper, and an open area of 67%) within the handsheet and a target at each surface of the handsheet. In preliminary experiments with Burton's handsheet former, it was found that positioning of the targets in the handsheets was neither accurate nor repeatable. Therefore, in order to form handsheets with integrally-embedded targets and to improve the accuracy of the dynamic measurements, it was necessary to design and construct a new handsheet former. Two primary design requirements for the handsheet former were foreseen: 1) the targets had to be positioned in the sheet without disturbing the fibers around the target, and 2) the positioning of the targets had to be accurate and repeatable.

The new handsheet former design was similar to that described by Cowan (1961) and later used by Fang (1986) and Burton (1987). The improvements over the old handsheet former include attachment of the 127-mm ID (5-inch inside diameter) upper forming tube to a track-mounted slider bearing, the development of a new more accurate target insertion tool, and indexing of the rim of the upper forming tube for repeatable registration of the position of the insertion tool as shown in Figure 32. The net results of these improvements were the ability to position the targets accurately and repeatably, a reduction in time required to form a handsheet, and easier removal (couching) of the handsheets from the forming wire (face-wire).

In addition to the improved control of target positioning in the x-y plane, the new target insertion tool design prevented premature separation of the target from the insertion tool. Premature separation of the target from the insertion tool in the preliminary experiments with Burton's apparatus often resulted in random positioning of each target on the surface of a basis weight zone. Since this target would not be in the proper position above the proximity detector during wet pressing, these handsheets were abandoned, and the handsheet forming process restarted. The accuracy and repeatability of target positioning was also improved with development of an indexing system for the target insertion tool. Four notches were machined into the rim of the upper forming tube at 90° intervals. These indexed locations ensured that the targets were placed in the x-y locations which would correspond to the locations of the proximity detectors. The insertion tool was designed to gently release the targets at about 3 to 6 mm above the forming mat surface. As mentioned above, the proper positioning of the targets in the sheet required prevention of premature separation of the target from the tip of the insertion tool. Premature separation of the target from the tool often occurred upon insertion of the tool into the flowing water in the handsheet former. Prevention of target separation from the insertion tool was accomplished by drilling two holes through the plunger used to dislodge the targets. The flow of water through these holes into the tube held the target tight against the plunger. As the water level in the insertion tool tube reached the same level as in the sheet former, the target was no longer held against the plunger by the water flow. Therefore, with a slight downward movement of the plunger, the target was dislodged and sank into place on the surface of the basis weight zone.

Couching of the handsheet from the forming wire was improved by mounting the upper forming tube on a vertical track-mounted slider bearing. The forming tube could then be raised and lowered for couching of the handsheet or removal of air bubbles from beneath the forming wire. The track provided precise alignment of the upper forming tube and the base of the handsheet former which prevented leakage at the sealed interface between the two. Leakage at the seal tended to create an uneven flow of water in the tube and therefore an uneven distribution of fibers on the surface of the forming mat.

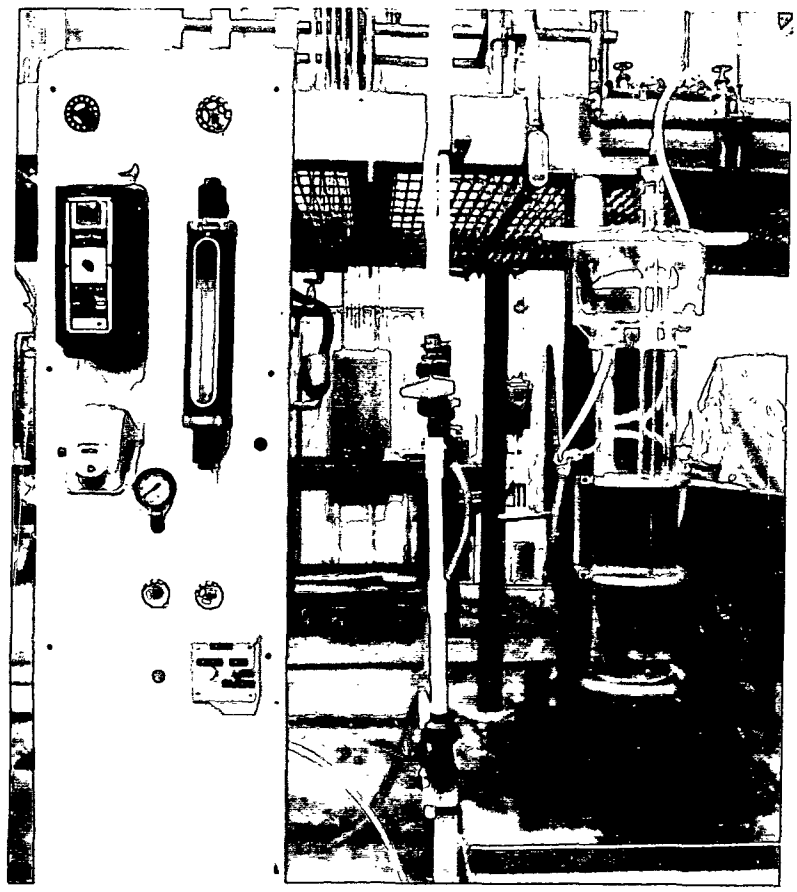

Figure 32. Forming apparatus for making handsheets used in density profile measurements.

HANDSHEET FORMING TECHNIQUE

Multizone 150 g/m^2 handsheets with targets were formed from a kraft softwood pulp (100% southern pine), a laboratory-refined sample of this same pulp, and a hardwood pulp (a mixture of ~40% maple, ~25% ash, ~20% birch, and the remainder consisting of oak, elm, and beech). Two 25 handsheet sets were formed from the refined and unrefined softwood pulp obtained from Macon Kraft Co., Macon, Georgia. A third 25 handsheet set was formed from the mill-refined kraft hardwood pulp obtained from Thilmany Pulp and Paper Co., Kaukauna, Wisconsin. The initial Canadian Standard Freeness (CSF) of the softwood pulp was 694. A 360-gram sample of this pulp was refined to 353 CSF in a laboratory Valley Beater (Valley Iron Works, Neenah, Wisconsin). The hardwood pulp was already refined to 480 CSF, and no further refining was necessary. The softwood pulp was screened to remove knots and shives, but the hardwood pulp was not screened. Neither of these pulps was fractionated to remove fines.

The first step in forming handsheets required the removal of all the air bubbles from beneath the forming wire. It was necessary to remove these air bubbles because their presence would interfere with the formation of the sheet. This was observed in preliminary handsheet formation experiments. A suction bulb was used to pull the air bubbles from the underside of the forming wire to its surface while maintaining a minimum back-flow of water through the wire. After the air bubbles were removed, the upper forming tube was gently lowered into place and slowly filled with water from the top. This procedure was adopted to prevent entrapment of air bubbles beneath the forming wire and on the walls of the forming tube. Once filled, circulation

was established in the flow loop shown in Figure 32. The flow was allowed to reach a steady-state flow rate of 6 liters/min.

In order to form handsheets with equally spaced targets and to calculate the zonal density profiles, it was necessary to make the handsheets with a known basis weight for each zone of the sheet. Therefore, the proper amount of fiber required to form each zone was measured out separately in a graduated cylinder from a well mixed fiber slurry tank having a known consistency. This pulp slurry was diluted to 0.006% consistency in the fiber supply tank (Figure 32). After mixing the stock for several minutes in this tank, handsheet forming was initiated by placing the first target on the forming wire.

The target insertion tool, with a target attached as shown in Figure 33, was inserted into the upper forming tube and indexed to the proper location. The insertion tool was then allowed to fill with water, since it was necessary to fill the tube before the target could be dislodged. It was found that the time required to fill the insertion tool tube via seepage around the plunger was too long; therefore, an alternative method was needed to decrease the time required to fill the tube. To decrease the time required to fill the tube, two holes were drilled in the plunger of the insertion tool. These holes served two purposes. First, the holes decreased the time required to fill the insertion tube to the surrounding water level. Second, the rapid flow of water upward through the holes served to keep the target attached to the surface of the plunger and push any air bubbles trapped between the target and the plunger surface through the holes in the plunger. Any remaining air bubbles were removed by rotating the plunger to allow them to be pushed through one of the holes by the rapidly flowing water. The target was dislodged from the

insertion tool when the tube was filled with water by pressing the plunger sufficiently to move the target beyond the end of the insertion tube.

After the first target settled onto the surface of the forming wire, stock flow from the fiber supply tank was initiated at a rate of approximately 0.5 liters/min. The circulation around the loop was maintained at a constant flow rate of about 6 liters/min by bleeding off the excess water introduced with the fiber slurry. After the fiber supply tank was emptied into the forming tube, the bleed valve was closed, and the flow rate in the handsheet former was restored to its previous rate.

After all the fibers were carried to the forming mat surface, the target insertion tool (with a target in place) was inserted into the sheet former at the next indexed location. The target was dislodged from the end of the insertion tool at a height of about 3 to 6 mm above the fiber mat surface to reduce disturbance of the fibers beneath the tool. In the preliminary handsheet forming experiments, it was found that the plunger traveled too close to the surface of the fiber mat. When this occurred the target was pushed down into the surface of the fiber mat disturbing the surrounding fibers. The result was placement of the target at a position which did not correspond to the surface of the basis weight zone. Placement of the target in this manner resulted in zones with unknown basis weights and violated the assumption that the initial position of the target represented the interface between two adjacent zones of equal basis weight. Placement of one of the internal targets at a position other than the interface between two basis weight zones would make it impossible to accurately calculate the density of the zones after wet pressing. To prevent disturbance of the fiber mat, a mechanical stop was attached to the plunger shaft to limit the distance the plunger could travel to release the

target. This made it impossible to press the targets down into the fiber mat and disturb the fibers.

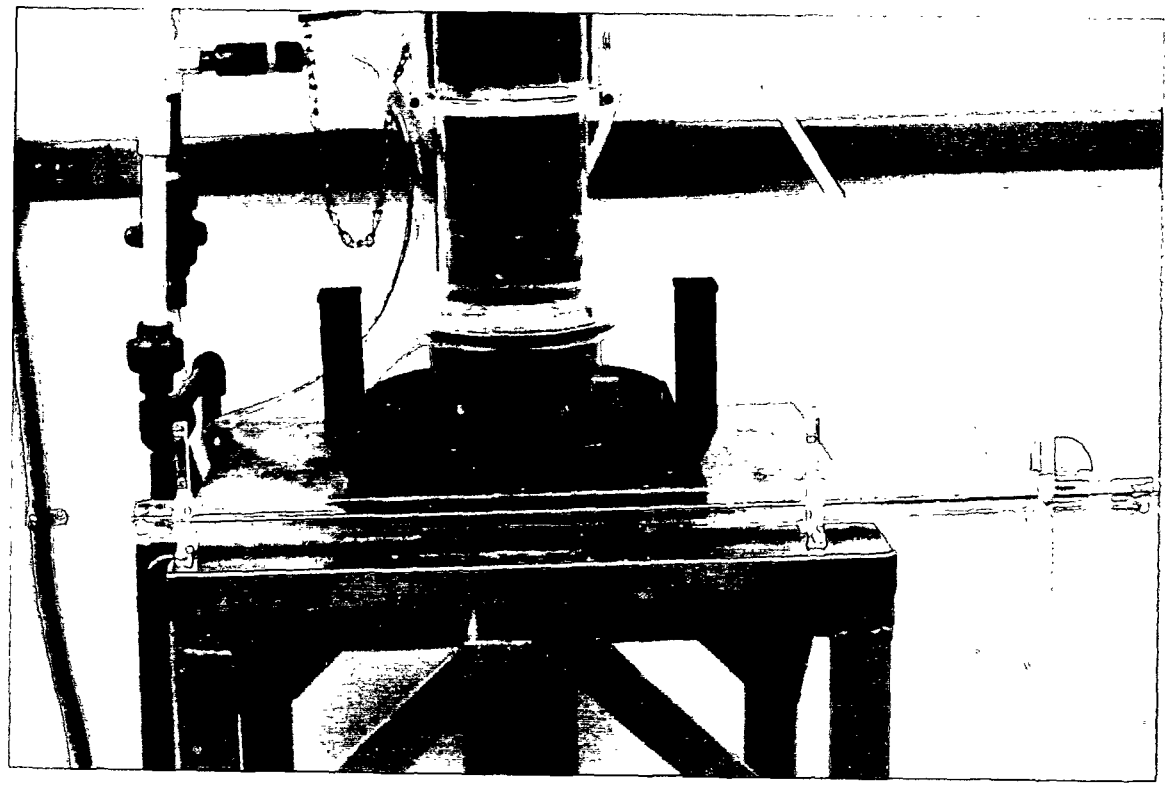

Figure 33. Target insertion tool with target attached.

After having successfully placed the target on the surface of the basis weight zone (layer), formation of the next layer was begun following the same procedure. As the fibers for the next layer were introduced into the sheet former, the target became an integral part of the sheet as shown in Figure 34. The open area of these targets was large enough to allow interaction of fibers on both sides of the target. The open area was shown by Burton to be sufficiently large in relation to the sheet pores to minimize their effect on flow resistance and interfacial effects. The sequence of indexing, target positioning, and application of the next layer of fiber was repeated until a

handsheet containing four targets was formed. The completed handsheet consisted of a target at each surface and two targets within the sheet as shown in Figure 35.

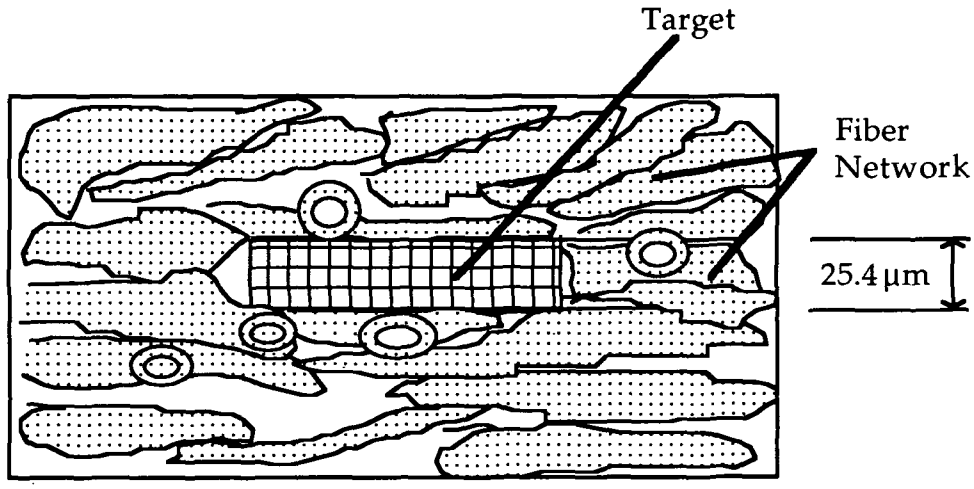

Figure 34. Conceptual interpretation of a target integrally embedded in a fiber network. Fibers and target are not drawn to scale. (After Burton, 1987)

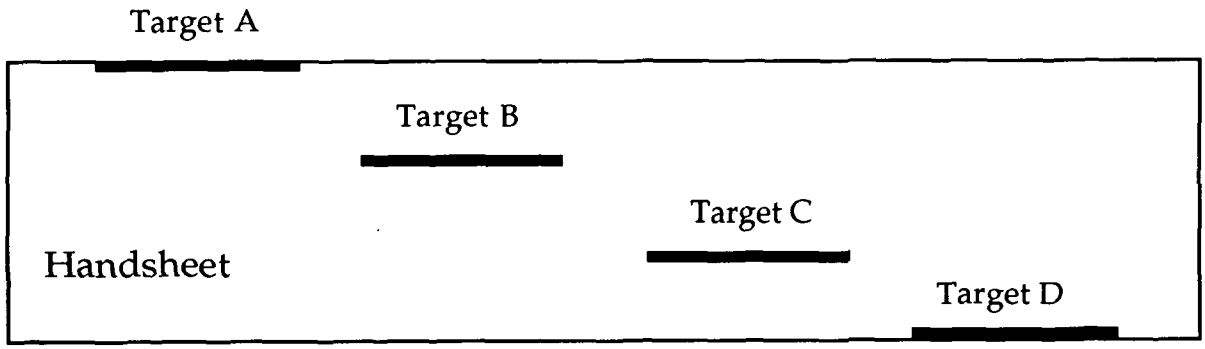

Figure 35. Side view of handsheet containing embedded targets with an equal separation distance between adjacent targets.

After placing the last target onto the surface of the sheet, the water level in the forming tube was drawn down to a level below the forming wire, and the pump was turned off. The forming tube was lifted straight up on its

track mount and pinned out of the way. A thin 150 mesh plastic face-wire was placed on the handsheet before couching from the handsheet former. Next, blotters were placed on top of the plastic face-wire to remove excess water and to couch the handsheet from the forming wire. The plastic face-wire prevented contact between fibers on the surface of the sheet with the blotter. Experience with handsheets formed before using the plastic face-wire showed that softwood fibers tended to stick to the blotters, creating an uneven z-direction fiber distribution across the surface of the sheet. The sheet was couched from the forming wire using a heavy bronze couch roll. Each couched sheet was placed in a polyethylene bag for storage until pressing.

Moisture ratio control was achieved by air drying the sheets under a slight restraint. The sheets were never pressed between blotters in a press. Previous use of a hydraulic press by Carlsson (1983), Burton (1987), and Jaavidaan (1987) to control moisture ratio may have introduced significant errors in the dynamic density determinations by changing the compression history of the sheets and the "initial" thickness of each zone. Long-term storage was avoided because Burton (1987) found that oxidation of the target material affected the displacement measurements.

ANALYSIS OF BURTON'S PRESS NIP AND DESIGN OF AN IMPROVED PRESS NIP

The original work done by Chang (1978), Davis *et al.* (1983), and Burton (1987) involved the use of a Wahren-Zotterman falling-weight press-nip simulator ("rock dropper"). The rock dropper in a comparative study by Chang *et al.* (1986) was shown to accurately duplicate the press nip impulse characteristics of the roll press geometry. Pressure profiles, pressure rise rates,

impulses, rates of caliper change, and stress strain comparisons all showed good agreement between the pilot roll press and the simulator. The rock dropper apparatus is depicted in Figure 36. The operation of this device was simple; the falling platen (carriage) was released from a specified height, fell and impacted the wet sheet, and compressed it against the stationary pedestal (lower press head). The falling platen rebounded and was caught on the rise by an air driven brake system to prevent a second impact. The pressure-time relationship was altered by adjusting the drop height and weight of the carriage.

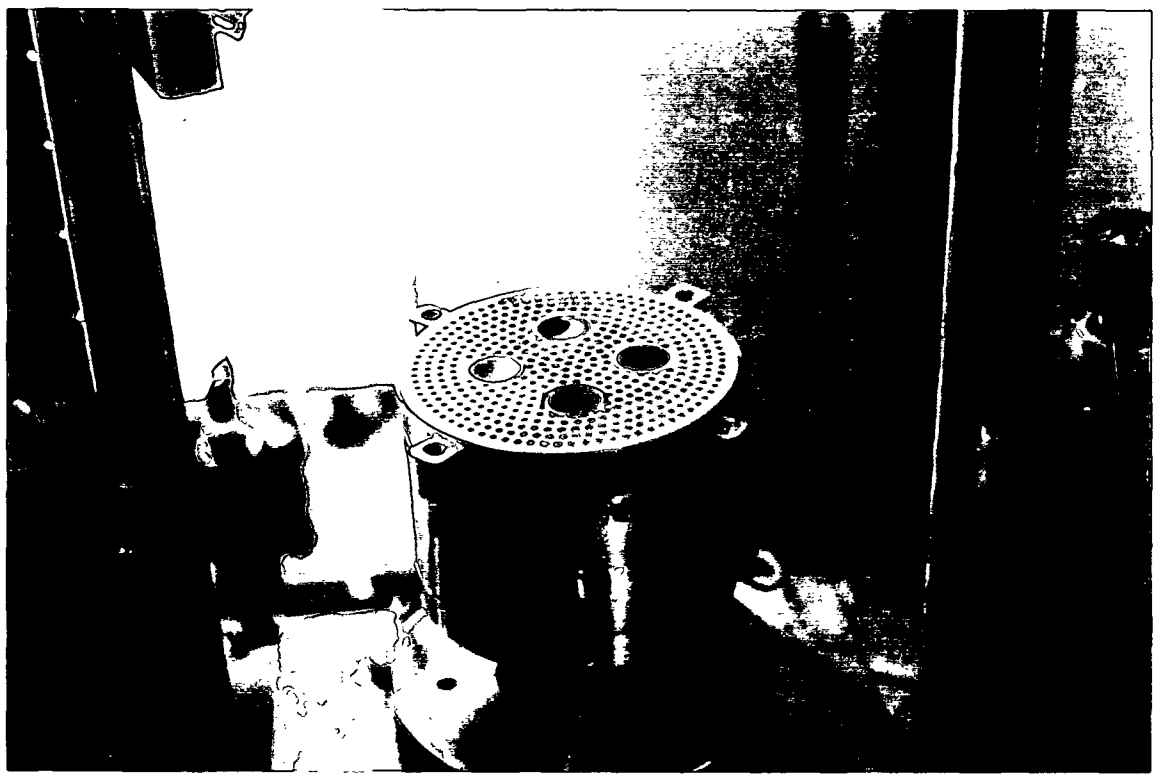

Figure 36. Picture of Burton's rock dropper and lower press head with the drilled brass plate.

The position of the lower pedestal (Figure 36) was fixed to maintain alignment between the two press heads. As the falling head compressed the sheet, water was expressed from the sheet into a ceramic flow receiver which had an average pore size of 40 μm. A vented (drilled) brass plate under the ceramic plate accepted excess water (Figure 36) and supported the porous ceramic plate during the compression and expansion of the sheet. The porous ceramic plate was used as a flow receiver to eliminate the effects of felt compressibility on dewatering, to provide a rigid support for the handsheet, and to provide a flow receiver with a constant permeability. Burton believed that by using the rigid porous ceramic plate he had limited the press nip to one compressible material (the paper sheet), and this would apply a uniform pressure distribution on the sheet. The pedestal was instrumented with a load cell which measured the impact force of the falling upper head, and four displacement transducers which provided the data necessary for determination of the sheet and zonal density profiles. The load cell sensed the total force applied to the sheet and the lower pedestal by the falling head. The factory-calibrated load cell was capable of measuring forces up to 225 kN. The press head was constructed from a high strength aluminum alloy (7575) to minimize the mass resting on the load cell.

The design of Burton's lower pedestal was based on one major assumption. He assumed that the drilled brass plate provided a rigid, non-deflecting support for the porous ceramic plate. In the initial phases of this study it became apparent (from repetition of Burton's work, using his equipment) that the brass plate was not providing uniform support for the porous plate. Evidence of the nonuniform support can be seen in a sample of Burton's data shown in Figure 37. The displacement profile of target D, on

the bottom of the sheet (i.e., in contact with the porous ceramic plate), shows a marked decrease in height (below the initial baseline) upon application of a load.

The photograph in Figure 36 and the schematic in Figure 38 show the various components of Burton's lower press head. The lower press head consists of a series of (three) machined aluminum discs and a drilled brass plate (3.175 mm thick) . The uppermost aluminum disc was machined on its upper surface to provide additional water removal space during wet pressing and for mounting the four proximity detectors. Most of the top surface of the uppermost disc was machined away, leaving a series of small columns to provide support for the drilled brass plate. Examination of these columns and their arrangement revealed that there were only three columns around each of the proximity detectors which supported the drilled brass plate. The size and irregular spacing of these support columns may have allowed an uneven deflection of the drilled brass plate upon application of a load to the handsheet. The four large holes, cut into the drilled brass plate, allowed mounting of the four proximity detectors. These four holes were large enough to prevent physical contact between the brass plate and the detectors. Apparently, these holes were drilled after the small holes as indicated by the presence of a number of partial small holes around the edge of the larger holes. Upon assembly of the three aluminum discs and the drilled brass plate it was apparent that several of the partial holes in the drilled brass plate were in alignment with one or more of the support columns on the aluminum disc which were located adjacent to the proximity detectors. It was critical to Burton's target position measurements that the support columns gave good support for the brass plate around the proximity detectors. Since there were

only three support columns around each proximity detector, any alignment of a column with a hole in the brass plate would allow a significant deflection of the brass plate at that proximity detector. Apparently, Burton did not recognize this potential for nonuniform support of the drilled brass plate when he made his dynamic thickness measurements.

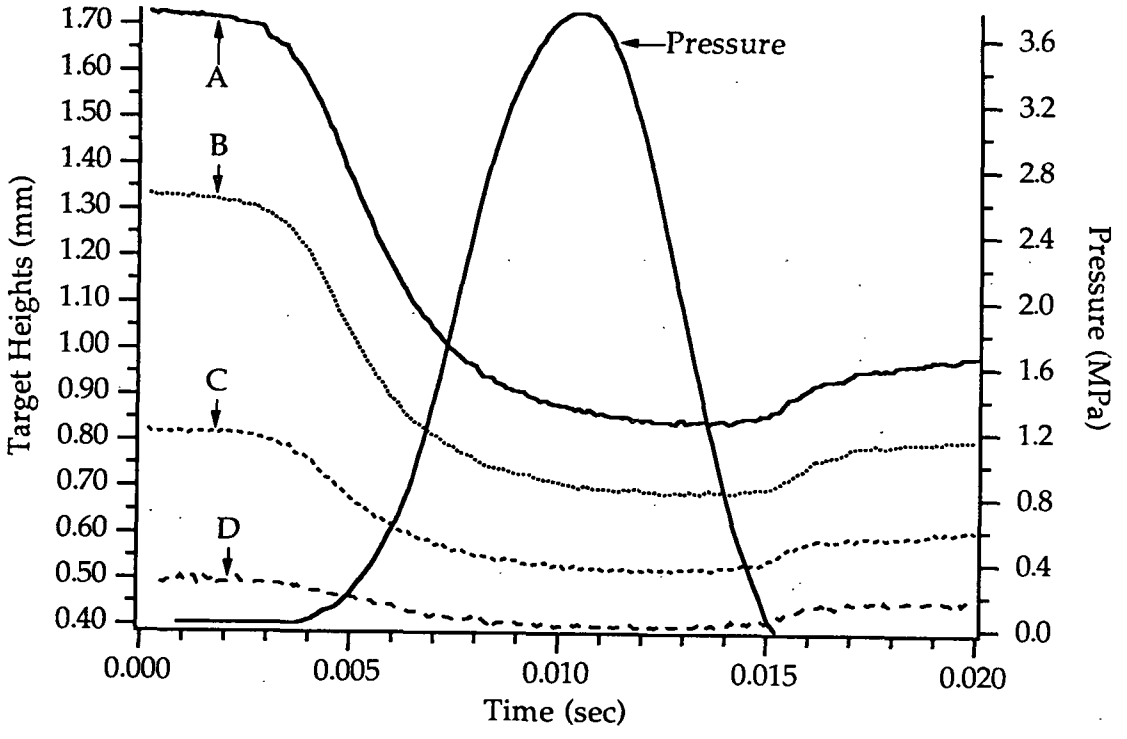

Figure 37. An example of Burton's target displacement raw data from datafile E1TNA.

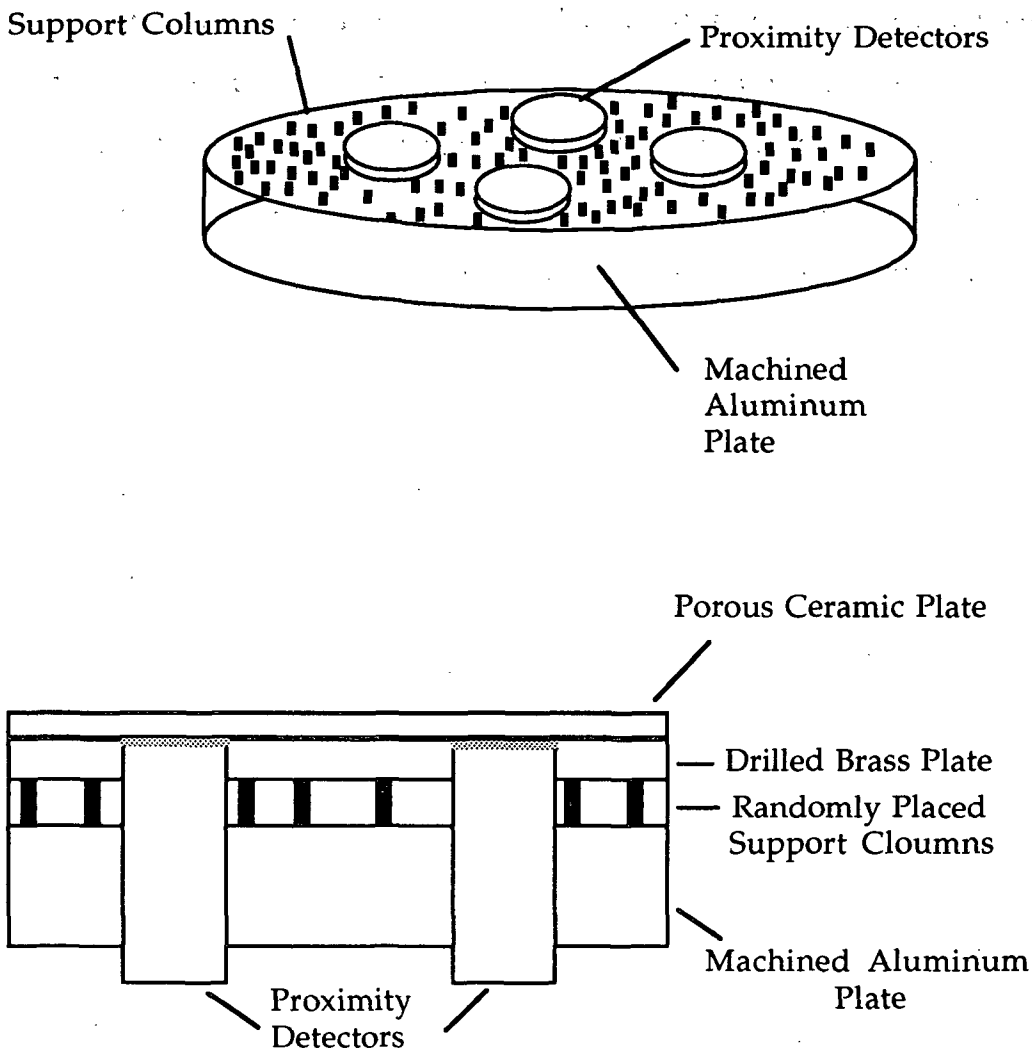

Figure 38. Schematics of the press head shown in Figure 36. The top and side views show the supporting structure, the porous ceramic plate, the proximity detectors, and the drilled brass plate of Burton's lower press head.

The target D deflection problem encountered with Burton's equipment indicated that redesign of the press nip simulator was required before more reliable data could be obtained. Therefore, after a thorough examination of all of the components of Burton's press simulator was completed, a new design was developed. The effectiveness of each component in the new design was tested before the next component was chosen. In this way the major

problems which had gone previously undetected by Burton were found and corrected.

There were three essential requirements for accurate measurement of the target motion in the handsheets during wet pressing. First, the compressibility and deflection of the porous plate had to be minimized; if the plate is compressible, this could not interfere with the measurements being made. Second, the target on the bottom of the sheet had to be in intimate contact with the supporting plate to enable accurate measurements of the compression and expansion behavior of the wet sheet. The third requirement was specific to the platen press simulator and involved the precise determination of the beginning and end of the nip: To define the precise moments at which the falling platen contacted and separated from the sheet, the positions of the falling press head and the target on the top surface of the sheet had to be known with good accuracy.

In order to meet the first requirement, it was necessary to rearrange the nip configuration used by Burton and replace the thin, flexible porous ceramic flow receiver plate with a thicker, stiffer porous ceramic plate (as described in an earlier work by Burns *et al.* (1990)). The uniform thickness of Burton's porous ceramic plates ranged from 1.67 to 2.0 mm (0.060-0.080 inch) and are shown as part of the bottom pedestal in Figure 39. These thin, flexible plates were replaced with a 9.5-mm (0.375-inch) thick plate of the same material. This ceramic plate was considerably thicker than the measuring range of the proximity detectors, so the ceramic plate was mounted on the falling platen. Mounting the thicker porous ceramic plate on the falling press head virtually eliminated the potential for flexing of the plate which had occurred with Burton's press head. The 9.5-mm porous ceramic plate was

attached to a machined solid aluminum press head which provided uniform support over the entire surface of the porous ceramic plate. With this design flexing of the porous ceramic plate did not pose a problem. In anticipation of potential compressibility problems that might occur with the thicker porous ceramic plate, the thicker plate was tested in an Instron (model 1125) tensile-compression tester for compressibility at loads up to ~13.8 MPa (2000 lb_f/in^2) and showed no appreciable compression.

Having moved the porous ceramic plate to the falling press head it was necessary to modify the lower press head to properly support the sheet during wet pressing. In order to improve the target position measurements, the structure supporting the sheet needed to possess high flexural stiffness and low compressibility while maintaining transparency to the eddy current proximity detectors. To meet these requirements, a new design was conceived as shown in Figure 40. The basic idea was to find a machinable material which possessed the desired properties. The material had to be able to be machined to achieve parallel surfaces, and four holes were needed in one surface of the material to create recesses for mounting the four proximity detectors. The total thickness of the material and the depth of the recessed holes had to be minimized to accommodate the limited range of the proximity detectors. The standoff[3] (or zero offset) of the detectors was able to be increased to compensate for the added thickness of the plate. Experiments with different materials showed that a glass-based solid ceramic material was well suited for this application. The material chosen was a solid glass-based ceramic material (914 glass ceramic) from Cotronics Corp. (Brooklyn, NY).

[3]The standoff is an offset of the zero voltage output from the eddy current proximity detectors which is used to displace or offset the transducer measuring range away from the surface of the detector.

The 914 glass ceramic was selected because of its high resistance to bending, low compressibility, and transparency to the eddy current proximity detectors. A quarter-inch thick plate of the 914 glass ceramic was selected to allow recessed mounting and minimize the zero offset required to make the proximity detectors function.

The porous ceramic plate used in these experiments had a pore size of 40 μm. The permeability of the 40 μm pore size of the porous ceramic plate was measured with a falling head permeameter (described in Appendix III). The permeability of the 40 μm pore size plate was in the range of 3.07 to 3.89×10^{-9} m^2, which was sufficiently large not to restrict the flow of water from the sheets during wet pressing.

The porous ceramic plate and the brass plate with its supporting aluminum plate (shown in Figure 39) were replaced on the lower press head with a glass-based solid ceramic plate and a half-inch thick aluminum supporting plate in which the four proximity detectors were mounted. This new aluminum plate provided a rigid flat support for the ceramic plate as shown in Figure 40. The ceramic plate and the solid aluminum plate provided a rigid lower press head which eliminated essentially all of the deflection observed with Burton's press head. By providing a more rigid lower press head, the positions of the four targets during wet pressing could be measured more accurately. The target height profile for the target adjacent to the ceramic plate showed virtually no deflection in the preliminary trials, indicating that this structure met the requirements for supporting the handsheet during wet pressing.

The second requirement of intimate contact between the target on the bottom of the sheet and the supporting ceramic plate was met by lightly pressing the sheet with a pressure of 17.9 kPa onto the surface of the solid ceramic plate. To prevent significant precompression and water removal from the sheet, the amount of force applied to get close contact between the sheet and the target on the bottom of the sheet was minimized. Close contact between the bottom target and the solid ceramic platen resulted in less potential for vertical "downward" displacement of the bottom target upon application of a load and ensured that the target on the bottom of the sheet would provide an accurate baseline for comparison with the rest of the targets.

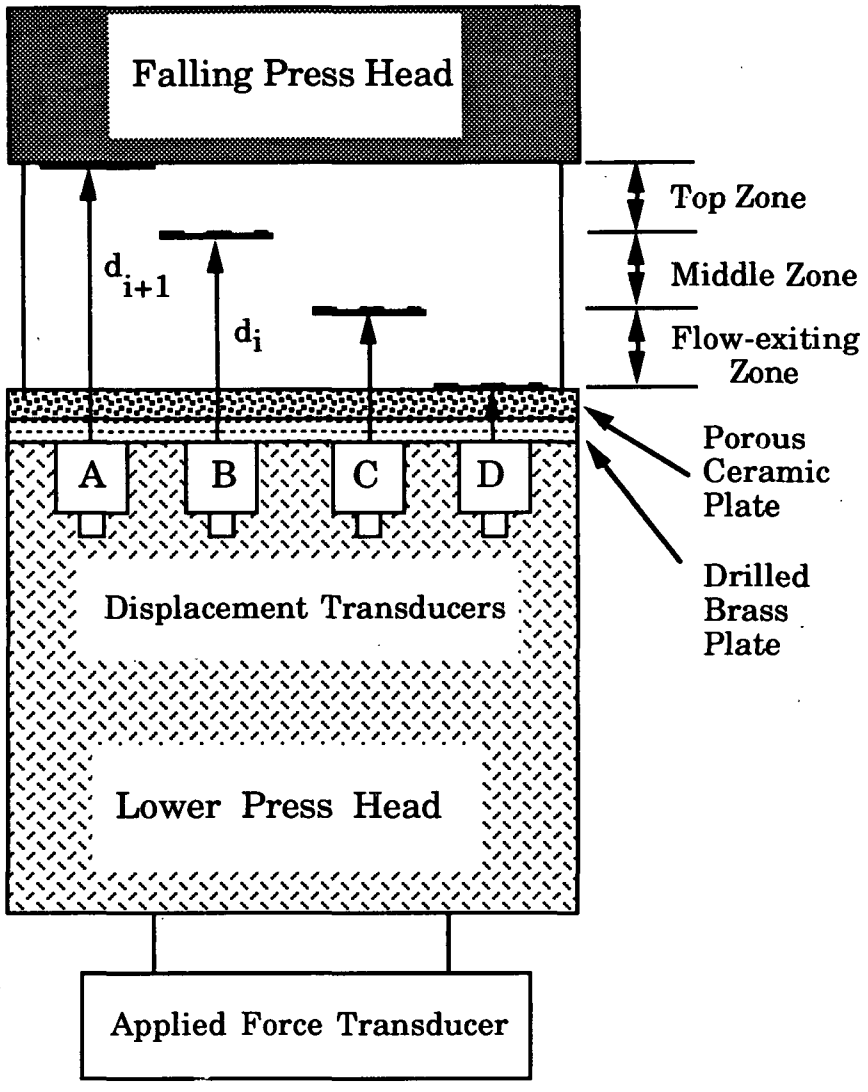

Figure 39. Schematic of Burton's press heads. (After Burton, 1987)

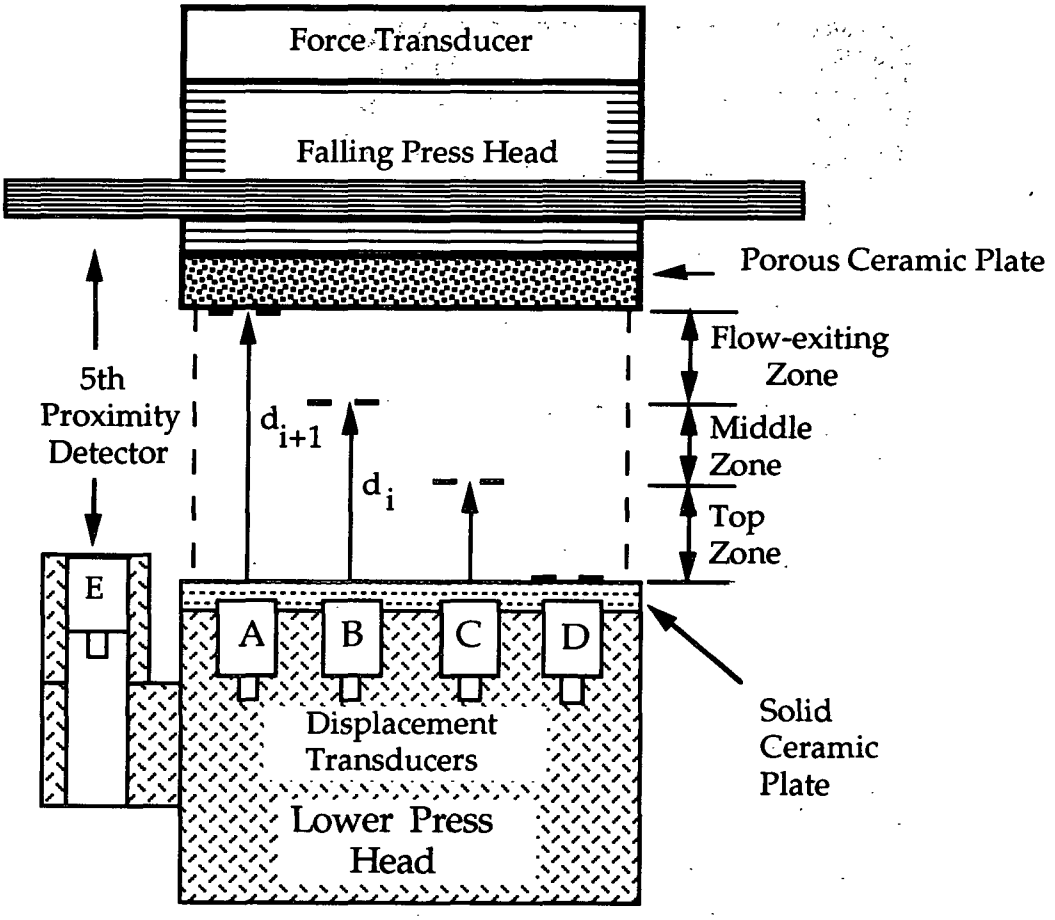

Figure 40. Schematic of new press heads with a sheet in which the solid platen zone (SPZ), the middle zone (MZ), and the flow-exiting zone (FEZ) are defined.

The third requirement for accurate wet press simulation and sheet thickness determination is specific to the platen press simulator. It is the precise determination of the beginning and end of the nip. Definition of these two points has been lacking in all of the previous press simulator designs and wet pressing work. The definition of the beginning of the nip is taken to be the point at which the falling platen contacts the target on top of the sheet, and the end of the nip is defined by the subsequent separation of these two components. In order to determine the beginning and end of the

nip, it was necessary to simultaneously record the positions of both the falling press head and the target on the surface of the sheet. This required the addition of a fifth proximity detector to follow the position of the falling press head during a pressing cycle. The fifth detector was mounted on the lower press head as shown in Figure 40.

EDDY CURRENT PROXIMITY DETECTORS

The five proximity detectors used in this study were of the eddy current type (model no. KD-2310-4S) manufactured by Kaman Instrumentation Corp. (Colorado Springs, Colorado). These transducers have a measuring range of 4.0 mm (0.160 inches) with a resolution of 0.01% of full-scale calibration. A full description of these proximity detectors and their specific requirements for proper operation are described in Appendix II.

PROXIMITY DETECTOR CALIBRATION

Accurate calibration over a measurement span of 3.0 mm (0.120 inches) was performed using a nonrotating spindle micrometer (Starrett, model no. 261, Athol, Massachusetts, with indexed increments of 0.001 inch [25.4 μm] and with a manufacturer specified precision of ±12.7 μm [±0.0005 inches]) mounted in a round plexiglass holder, shown in Figure 41. A 25.4 μm thick calibration target was glued to the target holder attached to the spindle of the micrometer and was used to calibrate the proximity detectors. This type of micrometer was chosen to prevent rotation of the calibration target in the magnetic field emitted by the proximity detector. Since the targets possessed an open mesh structure, any rotation of the target in the field would affect the voltage output from the proximity detector and decrease the accuracy and reproducibility of the target height measurements. It was also necessary

during calibration to keep the target flat on the surface of the holder so that it would be parallel to the surface of the proximity detector.

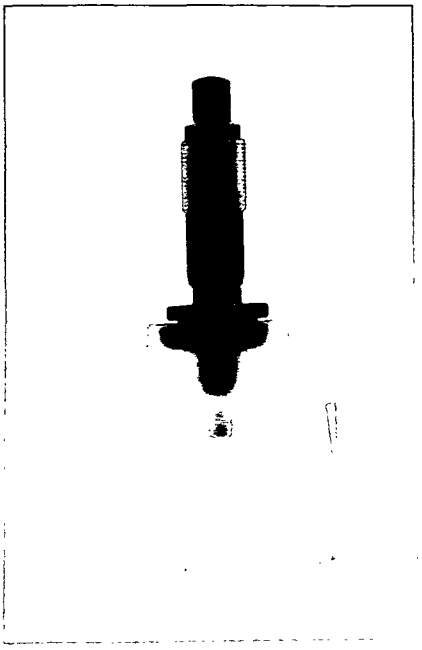

Figure 41. Picture of calibration micrometer apparatus used for calibration of the eddy current proximity detectors.

To calibrate the proximity detectors, the micrometer apparatus was centered above each proximity detector using a template. Initially, the calibration micrometer was placed in contact with the solid ceramic plate. A voltage reading was taken at this height (zero height) and at 254.0 μm (0.010 inch) increments until a total target height of 3.0 mm (0.120 inch) was reached. Linear regression of the calibration data yielded equations for calculation of the target heights. A typical calibration curve of voltage vs. displacement (target height) (shown in Figure 42) was linear with a correlation coefficient of 1.000. The proximity detectors were calibrated prior to each set of compression tests.

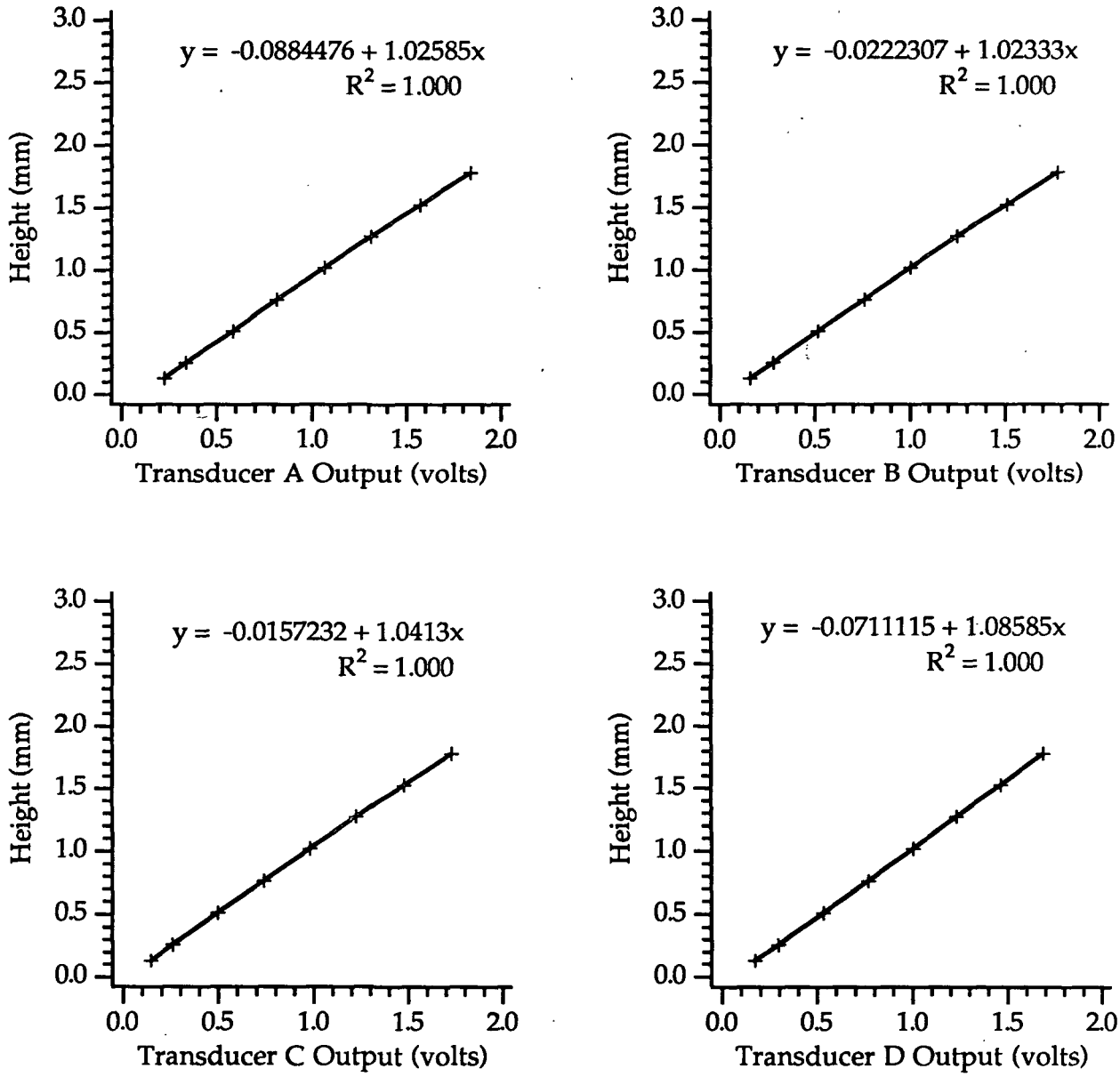

Figure 42. Typical linear calibration curves for the four proximity detectors.

APPLIED PRESSURE MEASUREMENT

The force applied to the top side of the sheet was measured by an MTS servo-hydraulic press load cell (Materials Testing Service Corp., Minneapolis, Minnesota) which was attached to the moving press head. This load cell had been recently factory-calibrated for loads ranging from 0 to ~90 kN (0 to 20,000 lb_f), which are similar to those used in wet pressing of pulp handsheets. Figure 43 shows the pressure (impact force/impact area) measured by the load cell for handsheets T4690G, T4690N, and T4690K. The overall shape of these typical pressure profile curves is similar to the pressure profile in a roll press nip (a haversine pulse). The slight asymmetry of the pulse is due to limitations in the controls of the MTS unit.

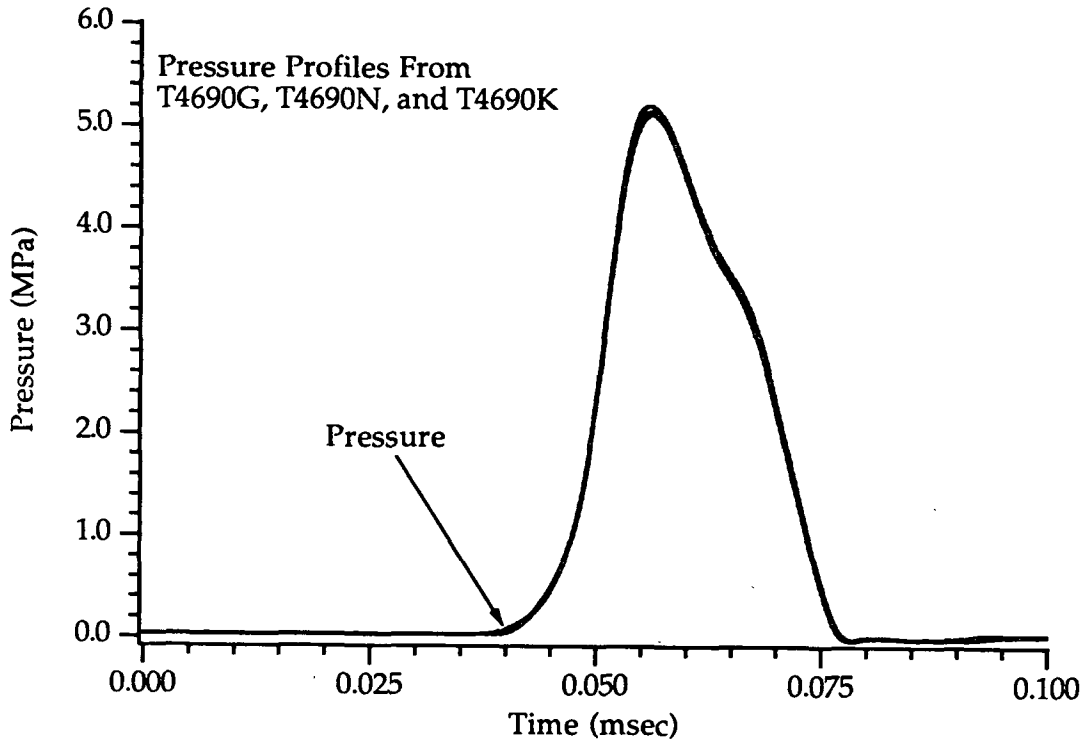

Figure 43. Applied load measured by the MTS load cell which was converted to applied pressure.

MOUNTING THE PRESS HEADS ON THE MTS

To use the MTS for these experiments, the upper press head was modified by the addition of a 215 mm (8.5 inches) extension shaft. This shaft eliminated the need to raise and lower the hydraulic unit of the MTS and saved a considerable amount of setup time. The upper press head and extension shaft were screwed directly onto the hydraulic piston of the MTS. This upper press head consisted of three circular aluminum plates and a porous ceramic plate as shown in Figure 44. The largest plate served as the target for the fifth proximity detector so that the position of the moving upper press head could be tracked. The lower press head was mounted on the fixed base of the MTS, and both the upper and lower press heads were aligned as described below. The most important requirement for simulation of wet pressing with the platen geometry was that the two press platens be parallel, since any significant deviation from parallelness between the two platens would affect the target displacements. To test the parallelness of the two platens, carbon paper-paper nip impressions were made. The uniformity of the distribution of carbon on the paper indicated the evenness of the applied pressure and, therefore, the parallel alignment of the press head surfaces. Any nonuniformity in the applied pressure was eliminated by shimming the upper press head and repeating the nip impression step. These steps were repeated until the distribution of carbon was uniform and the heads were parallel.

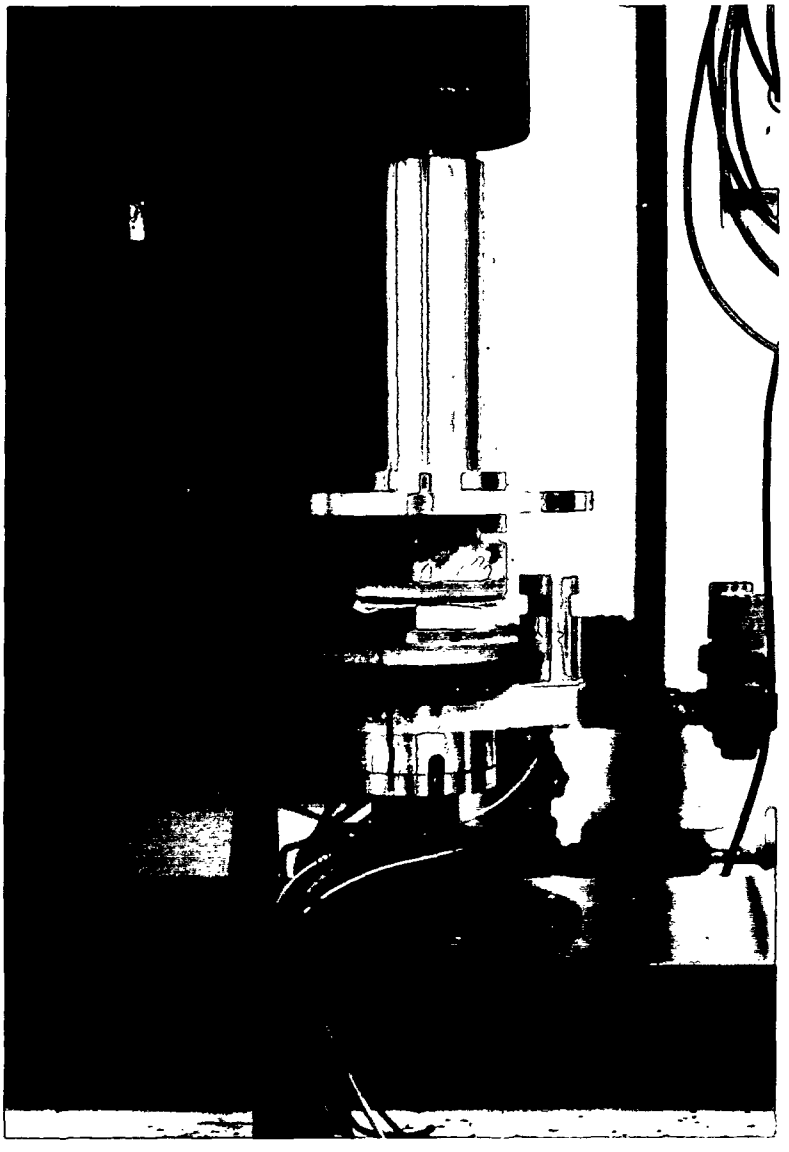

Figure 44. Upper press head with extension shaft mounted on MTS.

DYNAMIC DENSITY PROFILE DETERMINATION

In order to press the handsheets in the press simulators, the 127-mm (5-inch diameter) handsheets had to be cut with a die cutter to a diameter of 96 mm (3.75 inch) to match the size of the falling press head. The handsheets were cut prior to pressing and placed on the lower press head and aligned with the proximity detectors (using a template). As mentioned before, a small pressure of 17.9 kPa was applied to the handsheet prior to pressing to improve the contact of the bottom target with the solid ceramic platen. The feedback control system of the MTS was adjusted to yield the desired peak applied pressure and nip residence time, and the handsheets were pressed.

The trigger on the system for retraction of the hydraulic piston of the MTS was based on the length traveled by the piston. Variations in the initial thickness of the handsheets resulted in different hydraulic piston travel distances, occasionally causing an over-limit condition which prevented full retraction of the falling press head. Results obtained from these handsheets were deemed useful for observing the effects of prolonged pressing (or extended nips) on the compression and expansion behavior of the sheet. The pressure profile generated by the MTS unit was always a slightly asymmetric haversine pulse. This asymmetry is typical of the pressure profiles measured in industrial wet press nips.

During the pressing (consolidation) of the sheet, the targets moved with the surrounding fiber network in response to dewatering and densifying forces. The instantaneous (dynamic) density for each layer (zone) was calculated from the instantaneous zonal thickness and the zonal basis weights (as shown in Figure 41) using equation (2) as follows:

$$\rho_i = \frac{BW_i}{\left(d_{i+1} - d_i\right)} \qquad (2)$$

where

ρ_i = apparent zonal density, (g/cm^3)

d_i = position of target at i level, (cm)

d_{i+1} = position of target at i + 1 level, (cm)

BW_i = region (zone) basis weight, (g/cm^2)

To obtain a consistent moisture content in the porous ceramic flow receiver for each handsheet, it was necessary to adjust the moisture content of the ceramic flow receiver. After the first sheet was pressed in each handsheet series, the moisture content in the porous ceramic flow receiver was reduced by pressing blotters, in the press nip, until it was not possible to detect any further water pickup by the blotters.

SUITABILITY OF THE EQUIPMENT

In evaluating the suitability of the new handsheet former and the new press nip design for measurement of multiple target displacements, several key requirements were addressed. The major requirements for the handsheet former were 1) placement of the targets so that the center of each target was placed on the corners of a 57.15-mm (2.25-inch) square to obtain proper registry with the proximity detectors in the plane of the sheet and 2) proper

placement of the targets in the z-direction, at the interfaces between the zones. These requirements were necessary to maintain the accuracy of the target displacement measurements and to properly define the two surfaces of the sheet and the interfaces between the zones during wet pressing. The requirements for the new press nip design were 1) minimization of compressible and flexible components in the press nip, 2) the ability to accurately define the beginning and end of the nip, and 3) accurate measurement of the target displacements.

To verify the first requirement of the handsheet former, the in-plane positions of the targets were observed visually and then compared to a template of the proximity detector positions. The template was used to ensure that the targets could be centered over the detectors when placed in the press nip for wet pressing. More than 90% of the handsheets formed with the handsheet former had all four targets properly placed. Those handsheets which did not have the proper target placements were discarded.

The only method of determining whether the targets were properly placed in the z-direction in a handsheet was the physical measurement of their position when the handsheet was placed on the solid ceramic platen for wet pressing. As stated previously, all of the handsheets were pressed lightly onto the surface of the solid ceramic platen to flatten the handsheets and to achieve better contact between the target on the bottom of the sheet and the platen. An example of the initial target positions and their displacement during wet pressing is shown in Figure 45.[4] The initial positions of the targets in the handsheets presented in the next section are summarized in Table 2

[4]It should be noted that the origin of the time axis began when the data acquisition system was triggered.

(below). The target displacement signals acquired during the unrestrained portion of the process (when the press head is lifted from the sheet and the pressure has dropped to zero) may not accurately reflect the true positions of the targets in the sheet due to sticking of the sheet to the falling press head surface. When the sheets stuck to the rising press head, they often stuck to the solid platen surface, causing the sheets to be torn apart and one or more of the targets to be carried out of the calibrated measuring range of the proximity detectors.

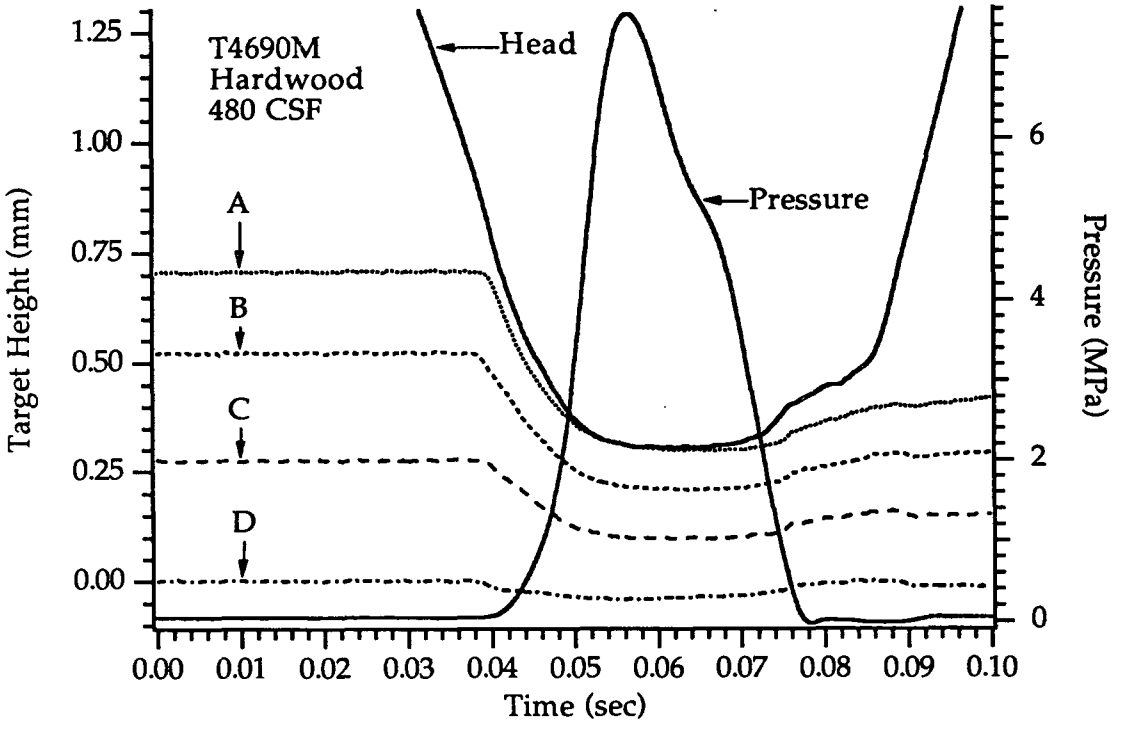

Figure 45. Typical target history data set from the redesigned press heads. Data from an MTS pressed 150 g/m^2 kraft hardwood handsheet. Moisture ratio = 3.32; Freeness = 480 CSF.

Table 2. Initial target positions and zonal thicknesses for 150 g/m^2 handsheets.[5]

Data set Name	Initial MR	Initial Target Positions(mm) A	B	C	D	Initial Zonal Thickness(mm) FEZ	MZ	SPZ
T21990A	2.63	1.22	.83	.38	0.0	.39	.45	.38
T21990E	4.31	1.02	.67	.32	0.0	.35	.35	.32
T4690G	4.74	.90	.70	.40	0.0	.20	.30	.40
T4690N	3.51	1.03	.73	.41	0.0	.30	.32	.41
T4690K	3.22	.74	.54	.30	0.0	.20	.24	.30

The initial position of target A is artificially depressed due to the load applied to the sheet; therefore, the true (or unpressed) thickness of the sheet is unknown in all of the handsheets. If it is assumed that precompression decreases the true thickness by 10%, then the initial thickness of the high freeness softwood handsheet would be 1.34 mm rather than the 1.22 mm recorded. Then, the positions of targets B and C would also be slightly higher. The position of target D is always 0.0 since it is on the surface of the solid ceramic plate. The initial thicknesses of zones FEZ, MZ, and SPZ for the high freeness softwood handsheet should be 0.45, 0.45, and 0.44 mm before the 10% precompression, respectively. It should be pointed out that some of the nonuniformity in the initial target positions and the zonal thicknesses can be attributed to the formation process itself. As each zone of the handsheet was formed, the surface of the zone was wavy in appearance. The targets, when dislodged from the insertion tool, floated down to the surface of these "waves." This resulted in an unavoidable elevation of the target during the handsheet forming process. As the next quantity of fiber was introduced into

[5]The data set names refer to the following types of handsheets: handsheets T21990A and T21990E are rock dropper pressed high (694 CSF) and low (353 CSF) freeness kraft softwood handsheets, respectively. Handsheets T4690G, T4690N, and T4690K are MTS pressed high (694 CSF) and low (353 CSF) freeness kraft softwood, and low freeness (480 CSF) kraft hardwood handsheets.

the handsheet former, this target was covered forming the next basis weight zone. Upon drainage of the handsheet former, the elevated targets and fibers settled to their proper positions.

Comparison of these ideal target positions and zonal thicknesses with the results in Table 2 indicates that the new handsheet former produced some handsheets with targets positioned at the desired positions, and the variation in zonal thickness in other handsheets was as large as ±33% of the median thickness. These results should not be interpreted as formation of handsheets with a nonuniform zonal basis weight. Instead, the results indicate that the level of consolidation was different in each zone due to the different type of furnish and its freeness. It was not possible to make handsheets with perfectly spaced targets, even though the basis weight was tightly controlled for each zone in the handsheets. This level of variation in zonal thickness during the handsheet forming process had not been previously reported. The anticipated variation in zonal thickness was ±5-10%.

The first requirement for the new press nip design was minimization of the compressibility and deflection of the materials inside the press nip. Burton had assumed that the only compressible or deflectable material inside the press nip was the handsheet itself. The inaccuracy of this assumption has been described in an earlier section in which Burton's press nip design was analyzed and a new design proposed. The improved design reduced the magnitude of the compressibility and deflection of the materials in the press nip which is evident from a comparison of the displacement histories of the target on the bottom of Burton's handsheet (Figure 37) and the target on the bottom of a handsheet pressed with the new press nip design (Figure 45). The displacements of these targets are significantly different. The new press nip

design resulted in a greater than 70% reduction in the downward displacement of the bottom target upon application of the load. The downward movement of this target is consistently on the order of 0.05 mm or less with the new press nip design, whereas Burton's target was consistently deflected downward 0.16 mm or more. These results indicate that the supporting structure (the solid ceramic plate) for the handsheet in the new press nip design was sufficiently rigid during wet pressing to reduce the previously encountered problem to an acceptable level. Subsequently, the downward displacement of target D was further reduced by machining the flat surfaces of the solid ceramic plate. This reduced the downward displacement of target D as shown in the results from the MTS pressed handsheets presented in the Results section.

The second requirement of the new press nip design was the ability to accurately define the beginning and the end of the nip. Since the data acquisition system was set up to begin recording the transducer signals just prior to the actual event, the positions of the four targets and the falling press head were recorded in the unconstrained state (as shown in Figure 45) before contact was made with the sheet. The initial positions of the four targets in the handsheet were essentially constant before compression began. The vertical position of the falling press head changed continually during the pressing event. To define the beginning and end of the nip, the positions of both the falling press head and the target on top of the sheet were recorded and compared. The displacements of these targets, E (the falling press head) and A (at the upper surface of the sheet), are shown in Figure 45. The shapes and slopes of these two target profiles (during compression and expansion of the handsheet) were very similar when the pressure in the nip was greater

than 2 MPa. When the pressure was less than 2 MPa, the profiles had similar slopes, but the position of the falling press head was slightly higher than that of target A. Apparently, the long shaft used to connect the press head to the MTS hydraulic ram provided insufficient rigidity to hold the press head in perfect alignment with the lower press head. As the pressure was increased, the head leveled itself, and as the pressure was relieved, the falling press head moved back to its original position. This also explains why the pressure in the nip does not drop to zero as the head appears to separate from the sheet. Unfortunately, these limitations could not be overcome with the time available on the MTS system. The misalignment effect is consistent in all of the results obtained. Even with this limitation, this method of defining the beginning and end of the nip provides a useful framework for future definition of the beginning and end of the nip.

An example of a typical data set containing both the raw and calculated data for an MTS pressed 150 g/m^2 high freeness, high moisture ratio handsheet (T4690A) is presented in Appendix IV. All of the target height, zonal thickness, and apparent zonal density data in this section will be presented in graphical format, and the macro used in *Igor*™ to create these graphs is presented in Appendix V. The data set contains displacement histories for the four targets embedded in the sheet and the falling press head and the pressure profile generated during the compression and expansion of the handsheet.

CALCULATION OF DENSITY GRADIENT DEVELOPMENT FOR A POROUS ELASTIC MEDIUM

The Smith and Griffiths (1988) consolidation model was used to describe a two-dimensional (x and y) sample domain which contained four nodes in the x-direction and 11 nodes in the y-direction as shown in Figure 46. A uniform load consisting of a haversine pressure pulse of 30 milliseconds duration was applied in the y-direction to the nodes at the upper surface of the sample. The vertical displacement histories of four nodes[6] (shown in Figure 46) on the left boundary of the sample were used to represent the nodes in the handsheet. The nodes are initially equally spaced, and as the solution progresses in time and as the applied load increases, the distance between the nodes decreases at different rates. The nodal separation distance decreases most rapidly toward the flow-exiting side of the medium illustrating the coupling of the fluid flow and the material deformation. These nodal displacements indicate the development of a density gradient in the direction of fluid flow. It should be noted that there is no permanent deformation in the medium, since the model was developed for a purely elastic medium in which no permanent deformation occurs.

[6]The displacements of nodes B and C were calculated as the average of the two nodes adjacent to the location of each of these two nodes.

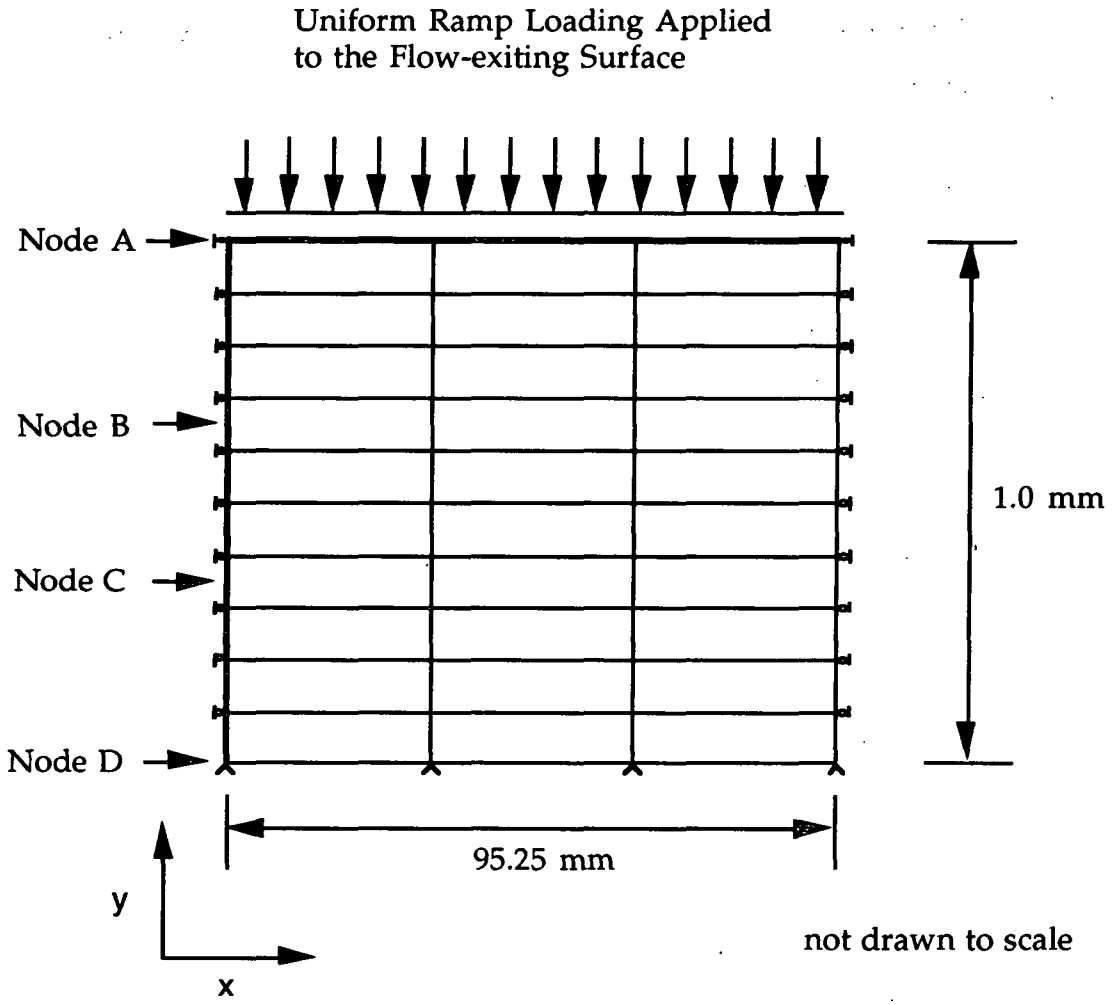

Figure 46. Mesh arrangement and data used with Smith and Griffiths' FEM model of Biot's consolidation with nodal positions corresponding to those in Figure 47.

A number of problems were encountered during development of the equipment and techniques. These problems are summarized in Appendix VI.

RESULTS

In the course of development of the experimental techniques and equipment for measurement of dynamic target displacement in handsheets, a large set of data was acquired for 150 g/m^2 handsheets. Data were collected from both high and low freeness softwood handsheets and low freeness hardwood handsheets which were pressed with either a "rock dropper" or an MTS servo-hydraulic press which were configured as wet press simulators. In addition to the experimental data, a set of data was obtained from a Finite Element Model of Biot's consolidation developed by Smith and Griffiths (1988) for an ideal porous elastic medium. The results from this model will be used to illustrate the concept of coupling of the material deformation and fluid flow processes and development of a density gradient in the direction of fluid flow.

Two sets of data, which are representative of the high and low freeness softwood handsheets and the low freeness hardwood handsheets, will be presented here along with the results obtained from Smith and Griffiths' consolidation model. The remaining data sets are listed in Appendix VII and presented in Appendix VIII. The initial conditions for these representative data sets are summarized in Table 3.

Presentation of the results will be divided into two parts. The first part will review the basic description of the handsheets used in this thesis and the medium modelled with Smith and Griffiths' consolidation program. The second part will present the recorded target displacement profiles for the high and low freeness softwood handsheets and the low freeness hardwood handsheets pressed with the "rock dropper" and the MTS servo-hydraulic

press. The key features of these profiles and the data derived from them will also be presented.

Table 3. Initial conditions of the 96-mm diameter (3.75-inch), 150 g/m^2 handsheets.[7]

Handsheet	Furnish	Freeness	Weight Ingoing (g)	Moisture Ratio	Weight Outgoing (g)	Moisture Ratio	Water Removal (g)
T21990A	SWD	694	4.100	2.63	3.786	2.43	0.314
T21990E	SWD	353	5.991	4.31	5.472	3.96	0.519
T4690G	SWD	694	6.804	4.74	3.291	3.02	3.549
T4690N	SWD	353	5.255	4.82	3.707	3.40	1.485
T4690K	HWD	480	4.886	4.48	2.995	2.75	1.891

REVIEW OF BASIC DESCRIPTION OF THE HANDSHEETS

In order to analyze the handsheet results presented in this section, it is beneficial to review the zonal definitions and their orientation as shown in Figure 47. Targets A, B, C, and D define three distinct zones within the sheet. The zone adjacent to the porous ceramic plate (flow receiver) was bracketed by targets A and B. Since water exits the sheet from this zone, it was labelled as the "Flow-Exiting Zone (FEZ)." The next zone (between targets B and C) was labelled as the "Middle Zone (MZ)." The final zone (between targets C and D) on the bottom of the sheet was labelled as the "Solid Platen Zone (SPZ)."[8] This method of labelling was adopted throughout this thesis to distinguish this nip configuration from that used by Burton (1987).

[7]The moisture ratios of these handsheets are shown in parentheses.
[8]Note. The terms zone and layer are used interchangeably.

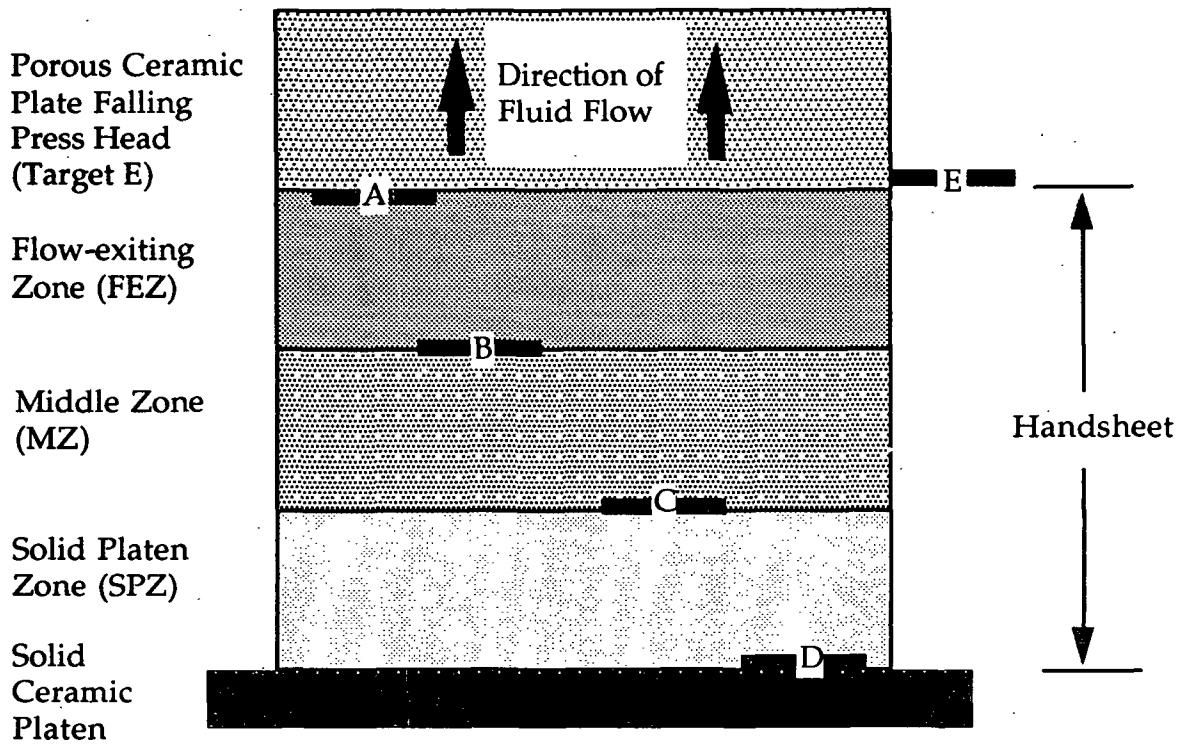

Figure 47. Handsheet orientation with definition of internal zones and the direction of fluid flow. Targets A and D are at the handsheet surface; targets B and C are located within the sheet; and target E is the lower surface of the upper press head (flow receiver).

DENSITY GRADIENT DEVELOPMENT FOR A POROUS ELASTIC MEDIUM

The Smith and Griffiths model has been used to develop a data set to illustrate the compression and expansion behavior of a saturated porous elastic medium. The nodal positions chosen for the model (shown in Figure 46) represent the formation of a handsheet with an ideal uniform placement of the targets during the handsheet forming process. The displacement histories of these nodes are used to represent the movement of targets embedded in a handsheet. As the load was increased in the simulation, nodes A, B, and C were displaced downward at different rates and to different

extents, while node D (on the bottom of the medium) remained at its fixed initial position. The difference in rates and extents of target displacements was due to the coupling between fluid flow through the medium and the medium's deformation. In this case all of the nodes reached their maximum displacement at the point of maximum applied load. As the load decreased in the totally elastic medium, it expanded back to its original thickness.

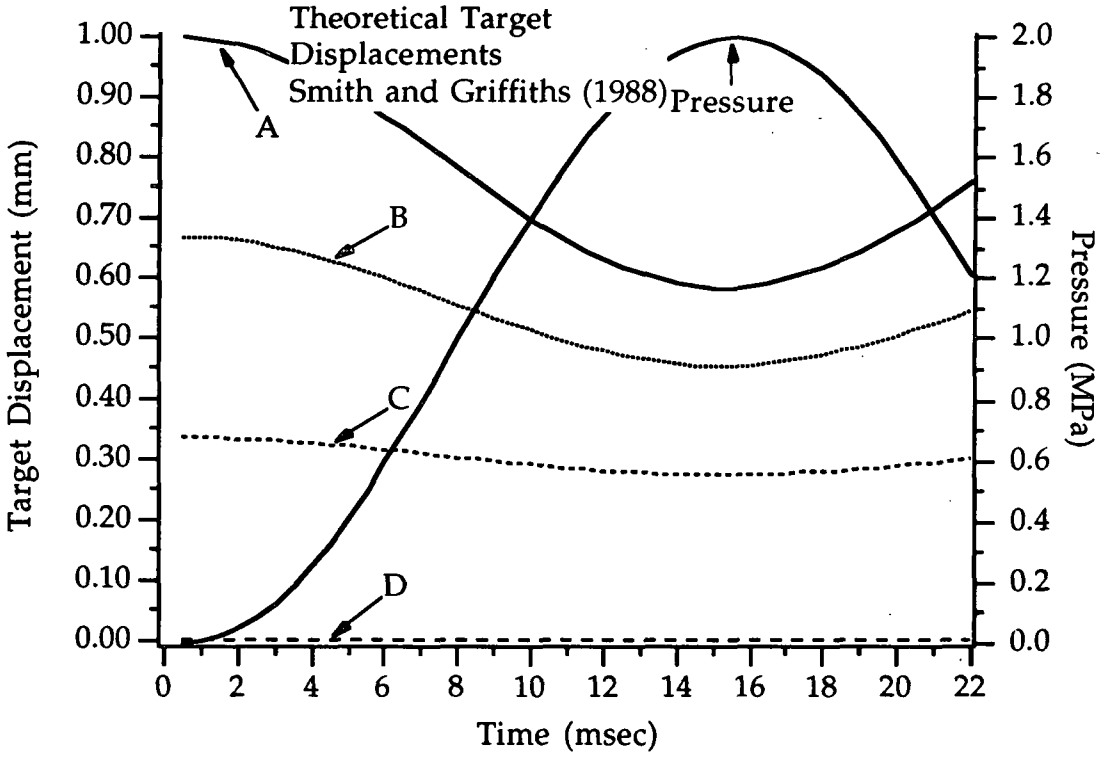

Figure 48. Nodal displacements from FEM model of Biot's consolidation developed by Smith and Griffiths (1988).

The zonal thicknesses are simply the distance between adjacent pairs of nodes or targets. The zonal thicknesses for the porous elastic medium are plotted as a function of time in Figure 49. The initial thickness of each of the zones (FEZ, MZ, and SPZ) was identical. However, as the load was applied to the sheet, each zone changed in thickness at a different rate and to a different

extent. The flow-exiting zone (FEZ) changes thickness at the greatest rate and to the greatest extent, followed by the middle zone (MZ), and then the solid platen zone (SPZ). Since this was a purely elastic medium, the point at which the minimum zonal thickness occurred was the same as the point of maximum applied load. As the load was released, the zones began to expand, eventually reaching their original thicknesses.

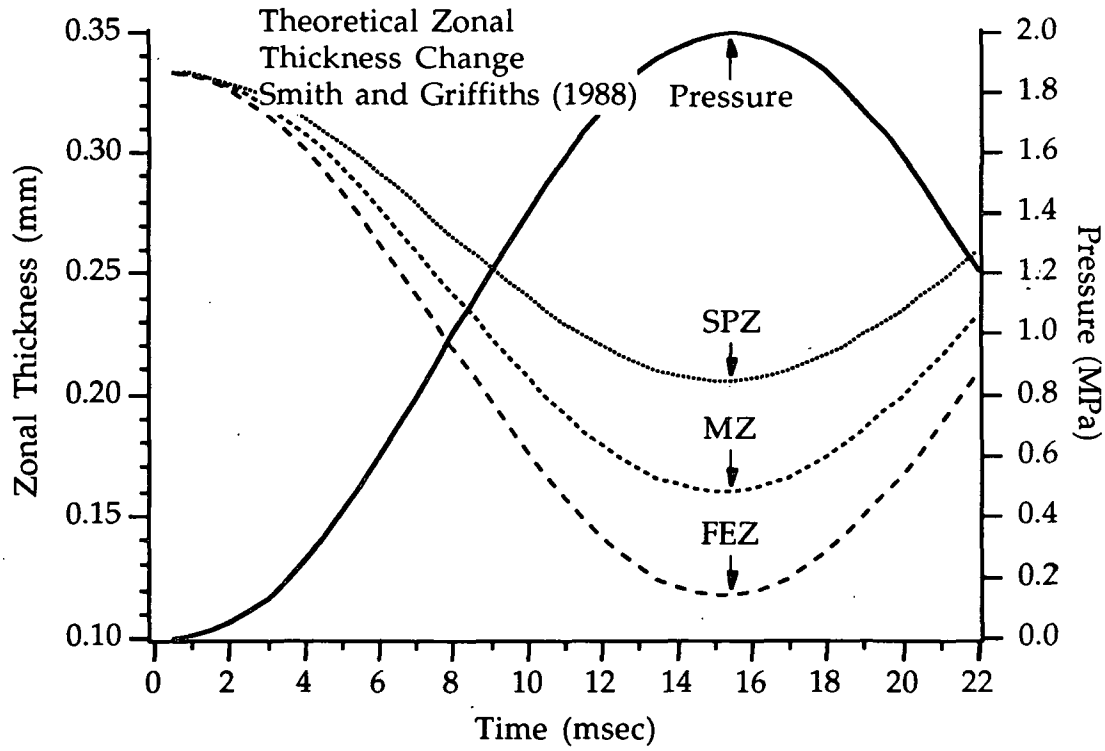

Figure 49. Hypothetical zonal thickness changes from FEM model of Biot's consolidation developed by Smith and Griffiths (1988).

The apparent zonal densities of the porous elastic medium are shown in Figure 50 and were calculated using equation (2). Since the porous elastic medium had an equal quantity of material in each of the zones, the initial apparent zonal density was the same in each zone. The flow-exiting zone

showed the most density increase and the fastest rate of density increase followed by the middle and solid platen zones.

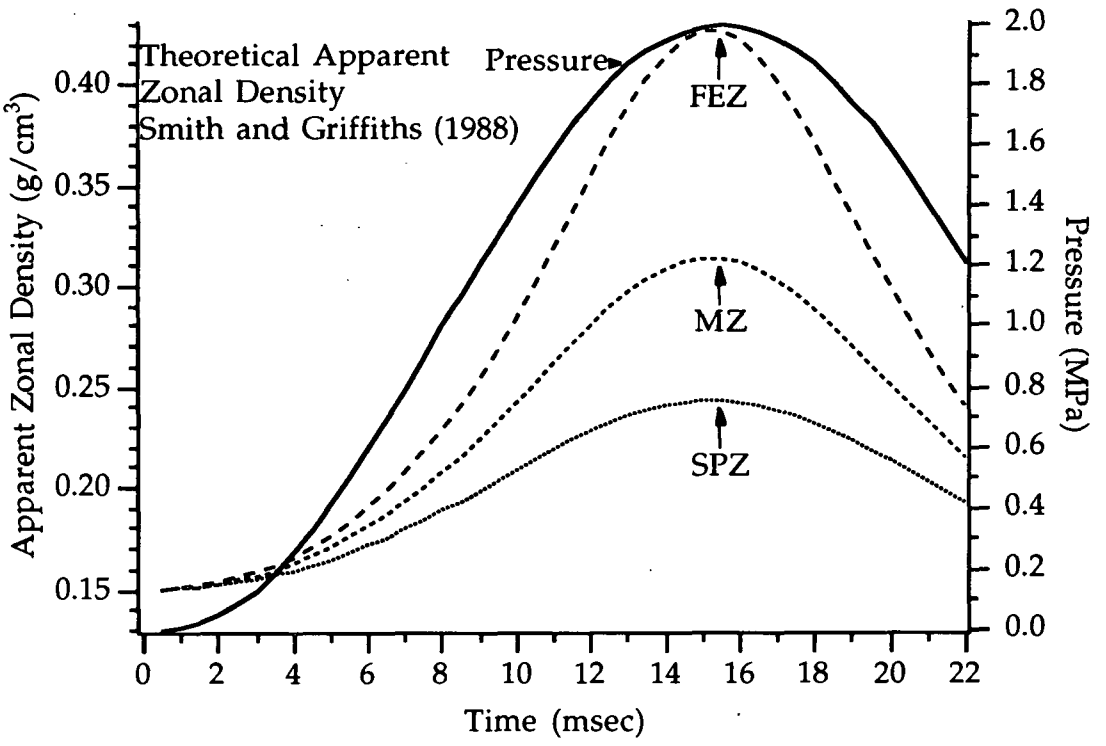

Figure 50. Hypothetical apparent zonal density change from FEM model of Biot's consolidation developed by Smith and Griffiths (1988).

"ROCK DROPPER" WET PRESS SIMULATOR

A "rock dropper" wet press simulator was used to examine the effect of short nip residences on the compression and expansion behavior of handsheets. The typical nip residence time for this press simulator was on the order of 3 to 4 milliseconds. This nip residence time was chosen to be similar to that of a typical high-speed industrial wet press. The peak pressures generated in the press nip ranged from 2 to 3 MPa which is well below those typically found in the commercial press nip (7 to 10 MPa).

The effect of short nip residence times on target displacement histories was examined with 150 g/m^2 unbleached kraft softwood handsheets at two different freeness levels (694 and 353 CSF). The target displacement histories for the high freeness softwood handsheet (694 CSF, moisture ratio = 2.63) are shown in Figure 51.

The initial target positions shown in Figure 51 indicate that the targets were distributed at roughly equal intervals in the thickness direction. More uniform distributions of targets can be seen in several of the handsheets which were very lightly pressed onto the surface of the solid ceramic plate (see Appendix VIII). In the more heavily pressed handsheets shown in this section, the zone on top of the sheet (flow-exiting zone) exhibits a consistently lower initial thickness than either of the other two zones.

High Freeness Softwood Furnish

The target displacement and nip pressure data acquired during the wet pressing of the high freeness softwood handsheet are shown in Figure 51. This handsheet was formed from a high freeness (694 CSF) kraft softwood furnish and was air dried under restraint to a prepressing moisture ratio of 2.63. The peak pressure generated during the wet pressing of this handsheet was 1.7 MPa. The displacement profiles in Figure 51 show that the displacement of the falling press head and the target on top of the sheet are similar in shape, but there are significant differences between the two profiles at the beginning and end of the nip. At the beginning of the press nip, the two profiles have similar slopes which indicate that the falling press head (target E) and target A are moving at the same rate. It is also apparent that the falling press head is in contact with the target on top of the sheet. The

difference in the positions of the falling press head and target A is probably due to a slight misalignment between the falling press head and the stationary lower pedestal. The displacement profiles of the falling press head in this and other tests indicate that the two sides of the press head dropped at slightly different rates causing one side of the press head to hit first. This initial contact on one side first resulted in a bouncing of the press head upon contact with the handsheet. The bouncing effect is evident in the rock dropper-pressed handsheets shown in Appendix VIII. These explanations for the differences between the profiles for the falling head and target A cannot completely account for the discrepancy between the two. However, they do indicate the need to pursue a better method of applying the load to the handsheets. This bouncing effect led to the use of an MTS servo-hydraulic press as a wet press simulator, as described later.

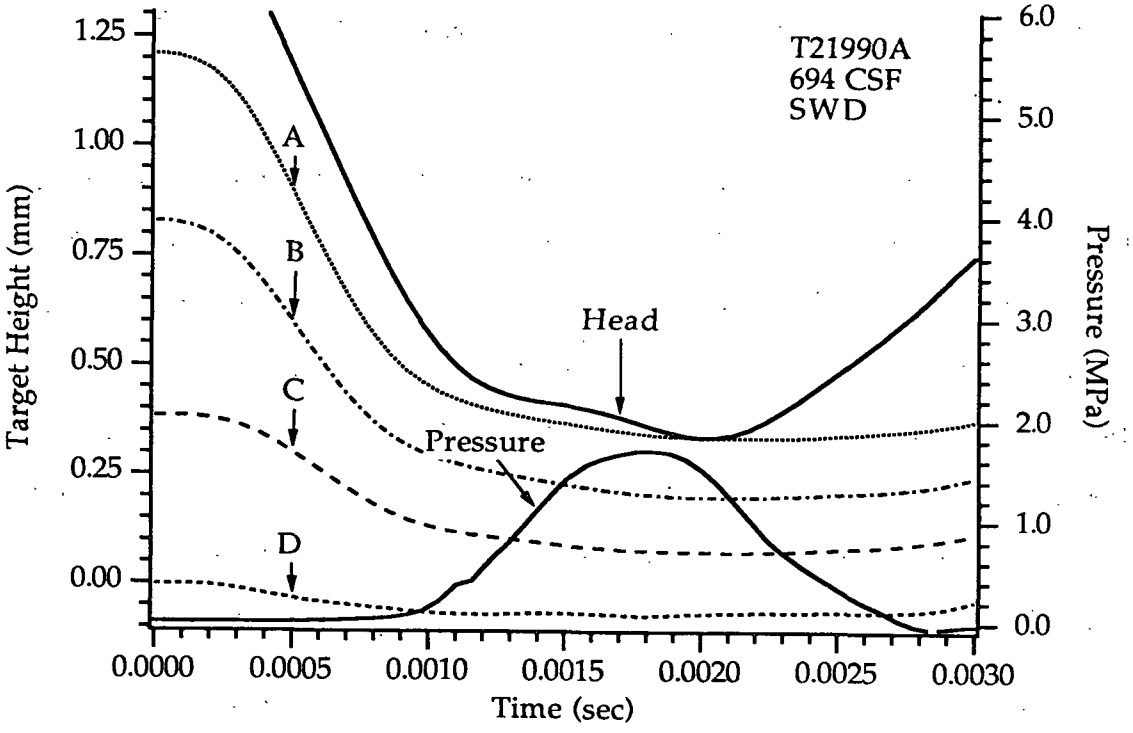

Figure 51. Target displacement histories for a "rock dropper"-pressed high freeness kraft softwood handsheet. Basis weight = 150 g/m^2; Moisture ratio = 2.63; Freeness = 694 CSF.

Under the conditions of low moisture ratio and high freeness, the displacement of target A in Figure 51 indicates that there was rapid movement of the upper surface of the handsheet during the early part of the load application. The displacement of target B was less rapid and occurred to a lesser extent than target A. Target C experienced little displacement during the early compression of the handsheet. Target D on the bottom of the sheet was displaced downward approximately 0.05 mm at the point of maximum pressure (1.7 MPa) in the nip. Each target reached its maximum displacement just after the point of maximum pressure in the nip. At this point the hydraulic pressure in the sheet reached zero. As the pressure was released,

the sheet began to expand, following the retracting press head. The sheet expanded from the minimum height (thickness) of 0.36 mm to 0.42 mm (a 16% rebound in sheet thickness) as the pressure is reduced to zero.

The zonal thickness changes (FEZ, MZ, and SPZ) during wet pressing of the handsheet are shown in Figure 52. The initial zonal thicknesses for the high freeness softwood handsheet were calculated from the target positions measured several milliseconds before the falling head makes contact with the sheets. The difference in initial thickness of each of the zones was attributable to any one (or a combination) of the following: nonuniform fiber distribution or zonal compaction during handsheet formation, improper target placement (either height placement or x-y location), or precompression of the sheet.

In the high freeness softwood handsheet, the initial thicknesses of zones FEZ, MZ, and SPZ as shown in Figure 52 are 0.342 mm, 0.43 mm, and 0.39 mm, respectively. The thickness profiles of zones SPZ and MZ appear to oscillate near the point of maximum compression of the sheet. The oscillations were due to an uneven pressure distribution resulting from the uneven initial contact between the falling head and the sheet. Zone MZ showed a higher initial thickness than either of the other two zones due to the air drying process used to reduce the initial moisture ratio of the sheet to 2.63. The moisture ratio was reduced by evaporation from both surfaces of the sheet while the sheet was held under restraint. The load used to restrain the sheet appears to have compressed the two surfaces zones slightly.

Although zones SPZ and MZ had slightly different initial thicknesses, the shapes of their profiles were similar, and most of the zonal compression occurred within the first millisecond of load application. The pressure

generated in the nip up to this point (one millisecond) was less than 0.15 MPa. Increasing the pressure to 1.8 MPa resulted in little further compression of the different zones. As the pressure was released, there was little or no zonal expansion.

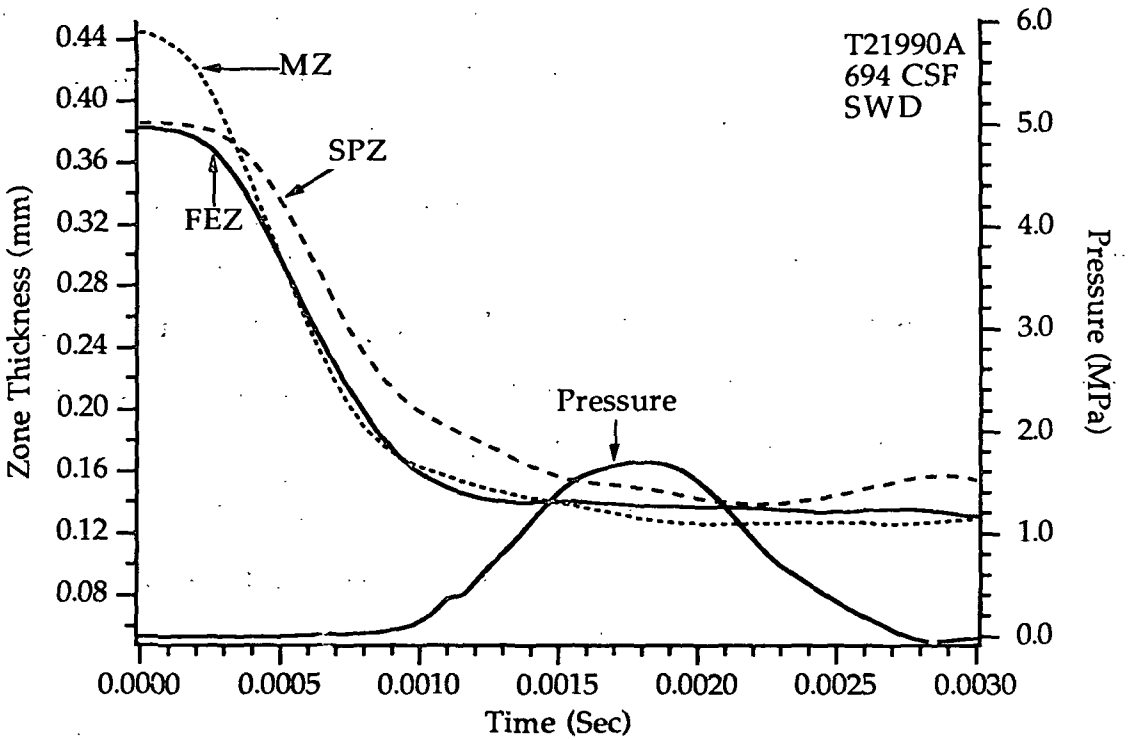

Figure 52. Zonal thickness change in a "rock dropper"-pressed high freeness softwood handsheet. Basis weight = 150 g/m^2; Moisture ratio = 2.63; Freeness = 694 CSF.

The apparent zonal densities of the high freeness softwood handsheet were calculated using equation (2) and are shown in Figure 53. The apparent zonal density is defined as the mass of dry fiber per unit volume. The

apparent zonal densities of the high freeness softwood handsheet showed little difference in the initial density of the different zones. As sheet compression began, the zones densified at slightly different rates. The flow-exiting and middle zones densified at the same rate until the pressure reached 0.1 MPa. At this point the densities of these two zones diverged slightly. The density of the flow-exiting zone appeared to oscillate as the peak pressure was reached. The densities of the middle and solid platen zones were the same until most of the pressure was released from the sheet. The small difference in densification of these two zones was due to the low initial moisture ratio of the handsheet. The air-drying process reduced the moisture level in the zones at each surface of the handsheet while leaving the middle zone virtually unchanged. At the point the nip opened, the pressure in the nip was zero, and the sheet was unrestrained. Therefore, the density profiles in this part of the graph are unreliable. Many of the handsheets stuck to the retracting upper press head and were lifted off of the solid ceramic plate. In some cases the handsheets were only partially lifted off, resulting in one or more of the targets sticking to the porous ceramic plate, while the other targets stuck to the solid ceramic plate.

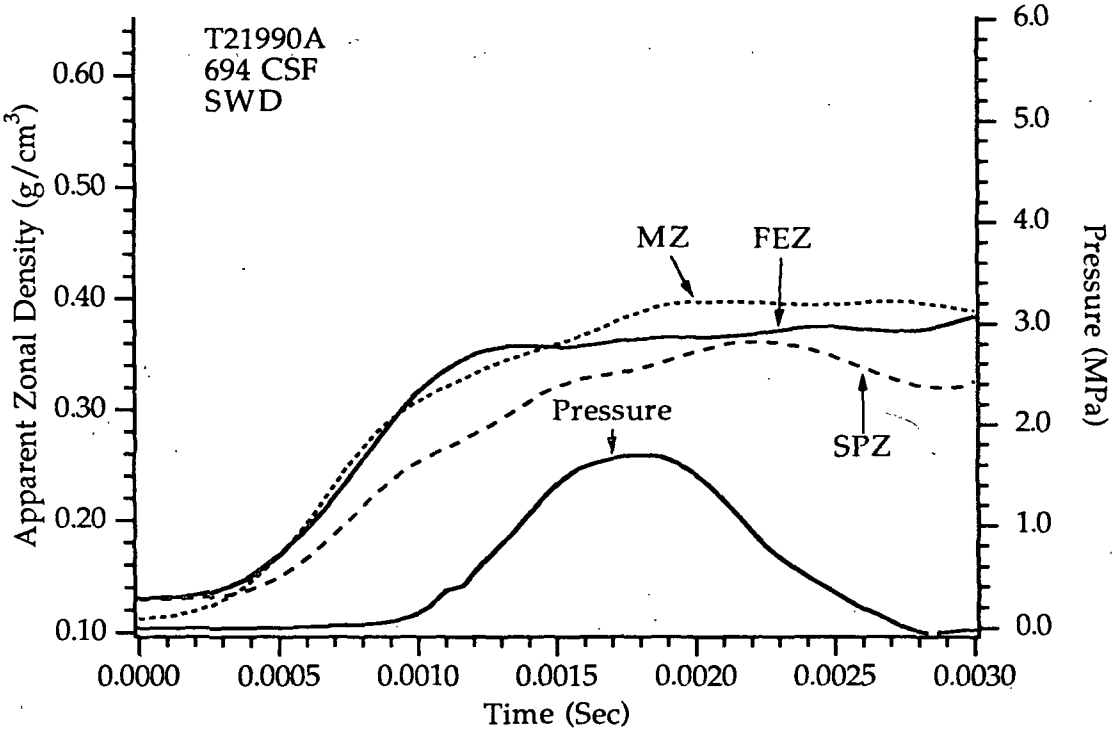

Figure 53. Zonal density histories of a "rock dropper"-pressed high freeness softwood handsheet. Basis weight = 150 g/m^2; Moisture ratio = 2.63; Freeness = 694 CSF.

Low Freeness Softwood Furnish

The displacements of the targets embedded in a low freeness softwood handsheet are shown in Figure 54. The handsheet was formed from a low freeness (353 CSF) kraft softwood furnish and had an initial moisture ratio of 4.31. The displacement profiles of the falling press head (labelled Head or target E) and the target on the top of the sheet (A) are similar in shape. The

head appears to make better contact with this handsheet and remains in contact with the sheet for a longer period of time than with the high freeness softwood handsheet. At the low pressure beginning of the press nip, the two appeared to move at different rates (the lines have different slopes), which is an indication that the falling press head hits the handsheet first on one side and then levels itself before rebounding.

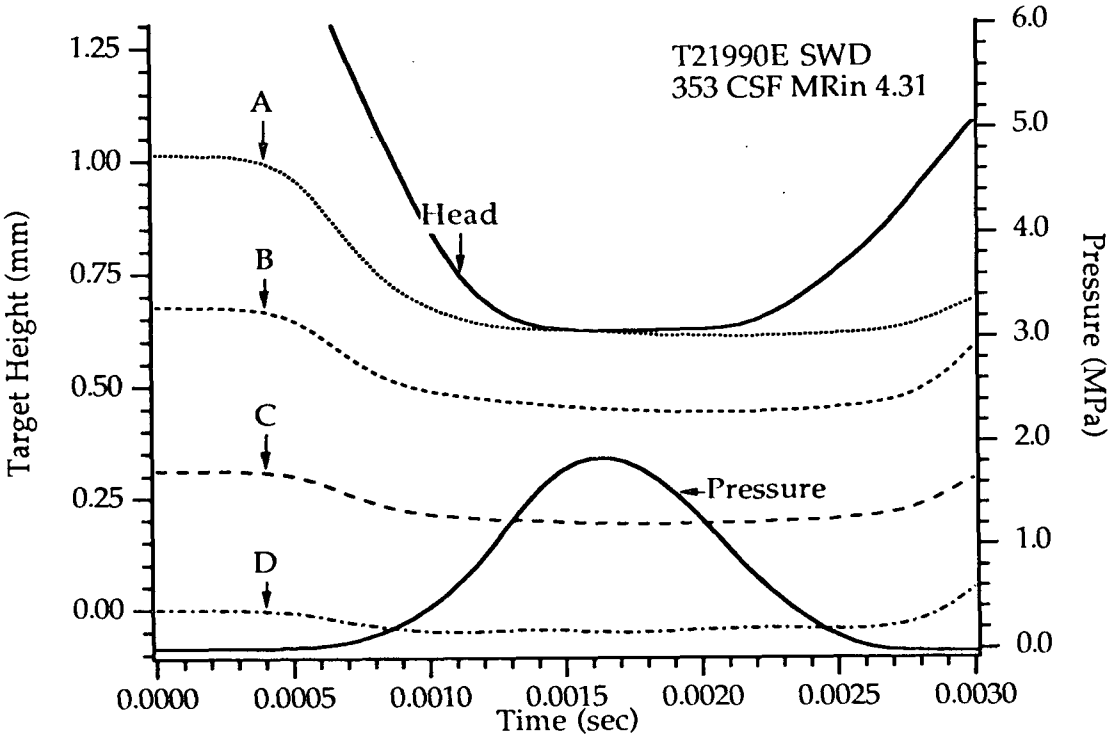

Figure 54. Target displacement histories for a "rock dropper"-pressed low freeness kraft softwood handsheet. Basis weight = 150 g/m^2; Moisture ratio = 4.31; Freeness = 353 CSF.

Early in the compression of the handsheet, targets A, B, and C move at different rates toward the bottom of the sheet. Target D shows a small

downward displacement of approximately 0.05 mm. The rate and extents of target displacements in this handsheet are significantly less than those in the high freeness softwood handsheet for the same nip residence time and peak applied pressure. There is little compression of the handsheet after the initial rapid compression of the handsheet. The sheet reaches a minimum compression height of 0.62 mm just after the point of maximum pressure. Then, the sheet expands slowly to a height of 0.68 mm as the pressure in the nip reaches zero. After the pressure is reduced to zero, the target displacement profiles become erratic. This behavior is typical of unrestrained expansion of the sheet and liftoff of the sheet from the solid ceramic plate.

Figure 55 for the low freeness softwood handsheet shows that the initial thicknesses of zones FEZ, MZ, and SPZ were 0.338 mm, 0.365 mm, and 0.389 mm, respectively. The initial thicknesses of these zones were approximately the same, indicating that precompression of the handsheet had only a small effect on the initial thickness of the flow-exiting zone. Also, the rate of zonal thickness change was different for each of the zones. During the early part of the compression cycle, the flow-exiting zone (FEZ) decreased in thickness at a much faster rate than either the middle zone (MZ) or the solid platen zone (SPZ). The solid platen zone and the middle zone decreased in thickness approximately the same amount, and the shape of the profiles were similar. From the shape of these zonal thickness curves, it is not clear that a minimum zonal thickness was reached, but rather that the zones appeared to continue to decrease in thickness during both the compression and expansion parts of the wet press cycle. This result was unrealistic and indicated that there was a problem with the target displacement measurements for this handsheet. At the end of the expansion part of the cycle, the handsheet

exhibited no expansion in the flow-exiting zone, but the middle and solid platen zones showed a slight recovery of their original thickness. It appears that the combination of high initial moisture ratio and low freeness of the furnish along with low press impulse was insufficient to significantly compress the middle and solid platen zones.

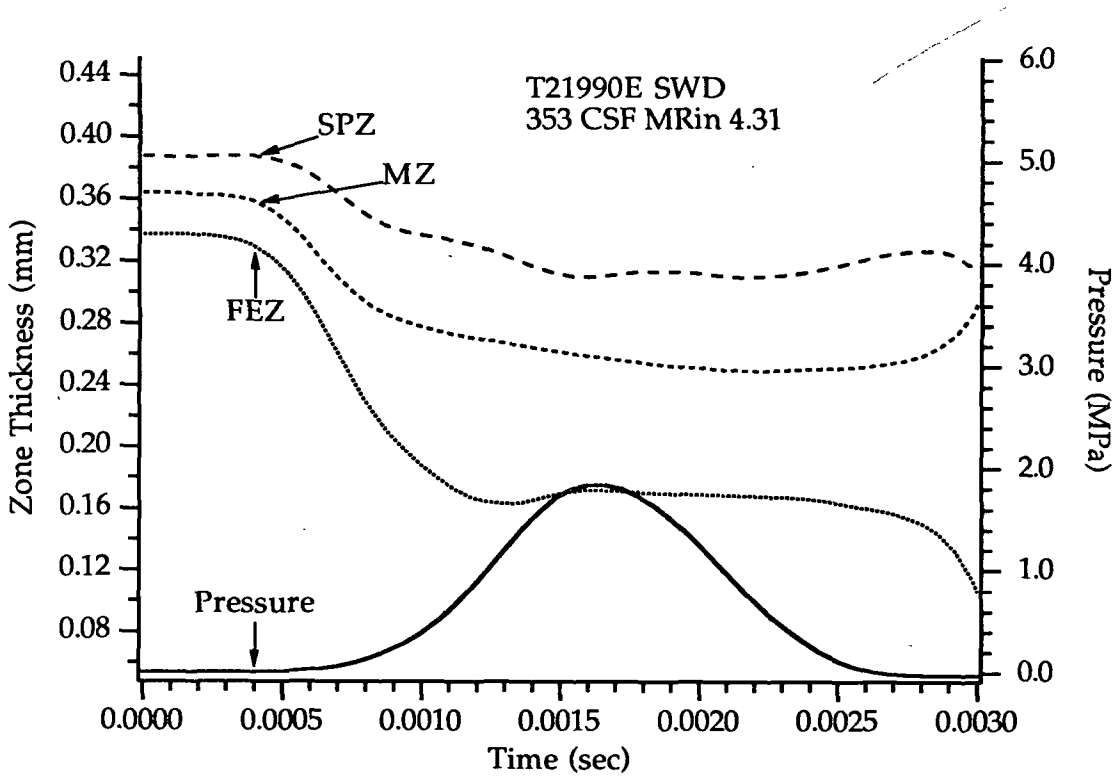

Figure 55. Zonal thickness change in a "rock dropper"-pressed low freeness softwood handsheet. Basis weight = 150 g/m^2; Moisture ratio = 4.31; Freeness = 353 CSF.

The zonal densities of a low freeness softwood handsheet are shown in Figure 56. The zonal density as used in this thesis is actually an apparent zonal density which is defined as the mass of dry fiber per unit volume. There was little difference in the initial density of the different zones in this handsheet. Each of the zones densified at a different rate, indicating the development of a density gradient in the thickness direction of the sheet. The flow-exiting zone densified to the greatest extent, followed by the middle and the solid platen zones. The deformation of the flow-exiting zone was typical of high moisture ratio, low freeness handsheets. The flow-exiting zone exhibited an unrepresentative drop in the density just prior to the peak applied pressure. The density in the flow-exiting zone increased until the nip was opened, which was also uncommon. It should be noted that this handsheet stuck to the porous ceramic plate upon retraction of the falling press head pulling the entire sheet up from the solid ceramic plate. This may explain the lack of a decrease in zonal densities upon release of the confining pressure in the nip. The middle and solid platen zones also exhibited uncharacteristic behavior in that they did not appear to reach their maximum levels at the expected points in the nip and showed little expansion as the load was reduced to zero.

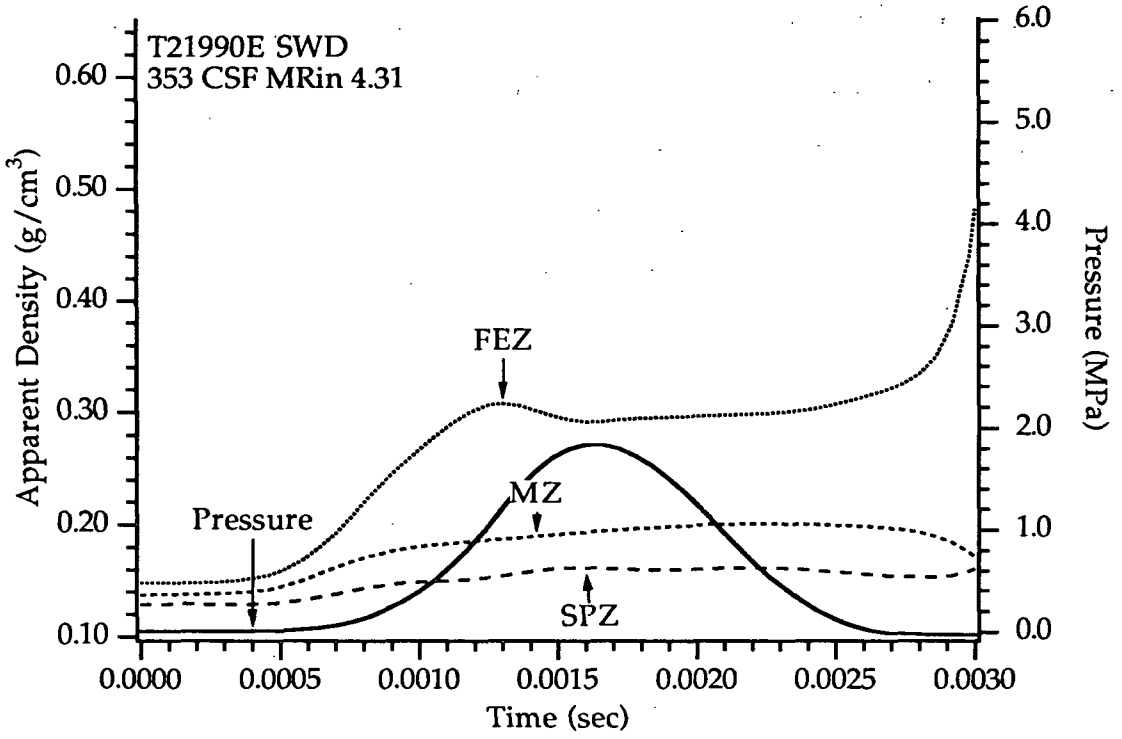

Figure 56. Zonal density histories in a "rock dropper"-pressed low freeness softwood handsheet. Basis weight = 150 g/m^2; Moisture ratio = 4.31; Freeness = 353 CSF.

"MTS SERVO-HYDRAULIC PRESS" WET PRESS SIMULATOR

The MTS wet press simulator was used to investigate the effect of much longer nip residence times (40-60 msec) on the wet pressing behavior of three types of furnishes. A representative handsheet was selected from the high freeness softwood, the low freeness softwood, and the low freeness hardwood furnishes. Data acquired during the wet pressing of these handsheets included the displacements of the targets in the handsheets, the position of the falling press head, and the pressure generated in the nip. There are three important features of the zonal density profiles: 1) the rate at

which the zones develop density, 2) the ultimate density developed in each zone, and 3) the density loss upon expansion of the sheet as the nip opens.

The capabilities of the MTS wet press simulator offered greater controllability of the nip residence times and pressure profiles which could be generated during simulated wet pressing. The MTS also provided a better means of delivering the load to the handsheet, i.e., the upper press head was connected to a single, well-lubricated shaft which guided it to the handsheet rather than the two guide shafts of the rock dropper. This reduced or eliminated the nonparallelness of the two pressing surfaces and increased confidence in the data.

HIGH FREENESS SOFTWOOD FURNISH

A high freeness softwood handsheet (shown in Figure 57) was formed from an unbleached kraft softwood (100% southern pine) furnish with a freeness of 694 CSF. The initial moisture ratio of the handsheet was 4.74. The target displacement histories for the head (target E) and target A showed that the positions of the two coincided well for most of the pressing cycle. At the beginning and end of the nip, the curves did not completely coincide due to unsteadiness in the long extension shaft used to connect the hydraulic piston of the MTS unit and the upper press head. However, the agreement between the two was much better than was observed for the rock dropper-pressed handsheets.

The initial position of target A in Figure 57 indicates that precompression of the handsheet had reduced the initial thickness of the zone defined by targets A and B. As compression of the handsheet began, targets A, B, and C moved at different rates toward target D. The slopes of the

target displacement histories indicate that each of the targets was moving at a different velocity. As the applied load increased, displacement of the targets reached a maximum just after the point of maximum pressure due to dissipation of the hydraulic pressure gradient to zero. The target positions remained essentially constant until most of the applied load was released. As the press nip opened, the target displacements indicated that there was little upward movement of the targets.

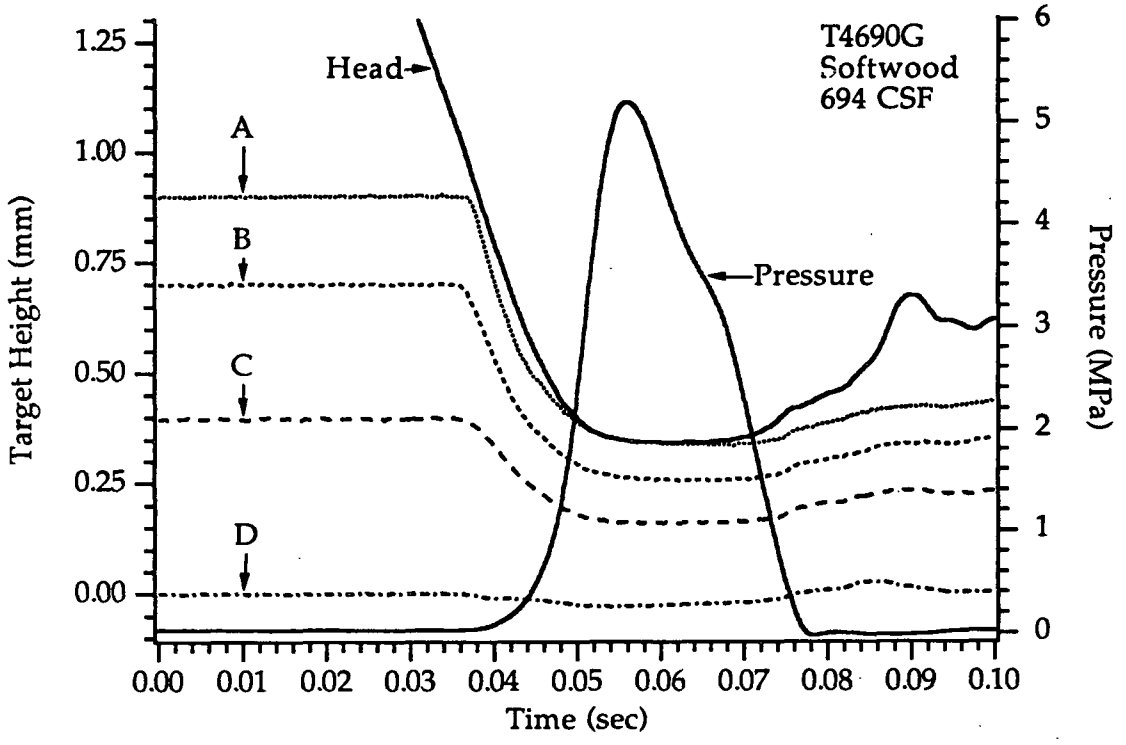

Figure 57. Target displacement histories for an MTS-pressed high freeness kraft softwood handsheet. Basis weight = 150 g/m^2; Moisture ratio = 4.74; Freeness = 694 CSF.

Target D, on the bottom of the sheet, shows a 94% reduction in vertical displacement (0.01 mm vs. Burton's 0.16 mm) when compared to the rock dropper-pressed handsheets. This reduction in displacement of target D was

due to the use of a new solid ceramic plate in the lower press head. This new solid ceramic plate was machined on both sides to increase the parallelness of these two surfaces.

The effects of longer nip residence times on the zonal thickness change for zones FEZ, MZ, and SPZ are shown in the high and low freeness softwood handsheets and the low freeness hardwood handsheet. The initial slope of the zonal thickness change curves indicates the rate of thickness change for the zone and facilitates comparison of the compression rates for the zones. The point of minimum zonal thickness and the extent of expansion are also illustrated.

The zonal thickness changes for the high freeness softwood handsheet are shown in Figure 58. The initial thicknesses of zones FEZ, MZ, and SPZ are 0.20 mm, 0.305 mm, and 0.395 mm, respectively. The large difference between the thickness of the flow-exiting zone and the other two zones was attributed to the prepressing of the handsheet described earlier. Even though the zone had a lower initial thickness, the zonal thickness decreased at about the same rate as the middle zone.

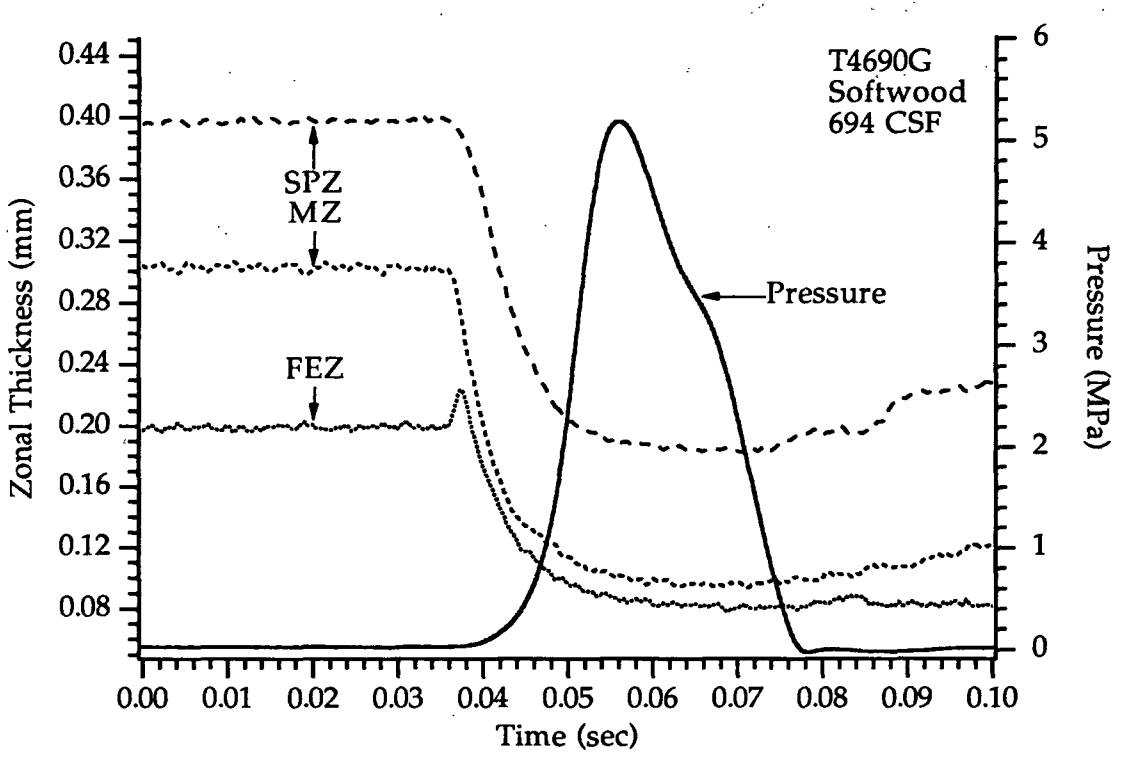

Figure 58. Zonal thickness change for an MTS-pressed high freeness softwood handsheet. Basis weight = 150 g/m^2; Moisture ratio = 4.74; Freeness = 694 CSF.

The blip in the initial part of the flow-exiting zone's thickness curve in Figure 58 was likely the result of target B being displaced (0.039 vs. 0.040 milliseconds) before target A was displaced. Movement of target B before target A caused an increase in zonal thickness to be recorded. Displacement of target B before target A could only occur if there was a small amount of fiber left on the surface of the porous ceramic platen from the previous handsheet or if the head did not drop evenly. Quite often the handsheets stuck to the porous ceramic platen and had to be scrubbed off before the next handsheet could be pressed. After this blip occurred, the compression and expansion behavior of this handsheet was similar to all the other handsheets pressed. The slope of the curves after compression began indicated that the flow-

exiting and the middle zones were compressed at approximately the same rate initially. The point of minimum thickness of each of the zones occurred just after the point of maximum pressure generation. At the end of the press nip, little zonal expansion was observed. The presence of the blip in one of the zonal thickness curves points out an important issue: errors in one zone's thickness measurements also cause errors in the thickness measurement of the other zones.

The initial densities for the three zones were similar in each handsheet and are summarized in Table 4. Before compression, the solid platen zone typically had the lowest initial density, and the flow-exiting zone had the highest initial density. The density curves will show that the zonal densities developed at different rates, with the maximum zonal density development occurring after the point of maximum applied load. The point of maximum densification occurred at different times for each zone.

Table 4. Initial Density of Zones FEZ, MZ, and SPZ, for the 150 g/m^2 MTS-pressed handsheets (SWD = softwood, HWD = hardwood, and CSF = Canadian Standard Freeness).

Handsheet	Furnish	Freeness (CSF)	Moisture Ratio	Initial Density (g/cm^3) FEZ	MZ	SPZ
T4690G	SWD	694	4.74	.255	.167	.128
T4690N	SWD	353	3.51	.168	.159	.123
T4690K	HWD	480	3.22	.26	.212	.167

The initial zonal densities of the high freeness softwood handsheet (T4690G) were 0.135, 0.165, and 0.255 g/cm^3 for the solid platen, the middle, and the flow-exiting zones, respectively. The flow-exiting zone had a higher initial density due to prepressing of the handsheet to achieve intimate contact between target D and the solid ceramic platen. The rates at which the

different zones densify early in the compression process are illustrated in the slopes of the initial portions of the density profiles. Obviously, the zone with the steepest slope densifies at the most rapid rate, as shown by the high freeness softwood handsheet. The middle zone densifies at a slower rate and the solid platen zone to an even lesser extent. The density of the middle zone is closer to that of the flow-exiting zone than the solid platen zone. The exact point at which the zones reach maximum density is unclear in Figure 59 due to the noise levels in the recorded signals. It is, however, just past midnip (point of peak pressure) for each of the zones. The solid platen zone reaches its maximum density first, followed by the middle zone and then the flow-exiting zone. In this handsheet the solid platen zone expands very little compared to the middle and the flow-exiting zones. After the pressure has been completely released, the sheet undergoes unrestrained expansion. The zonal densities measured after this point are believed to be unrealistic due to the observed tendency of the sheet to stick to the porous ceramic platen as it rebounded away from the sheet. This makes the target positions recorded during this time period suspect. Any interpretation of the density data in this period would be of little value since the target positions are unlikely to reflect the true expansion of the sheet. It is unlikely that the flow-exiting zone would increase in density with no load applied as shown in Figure 59.

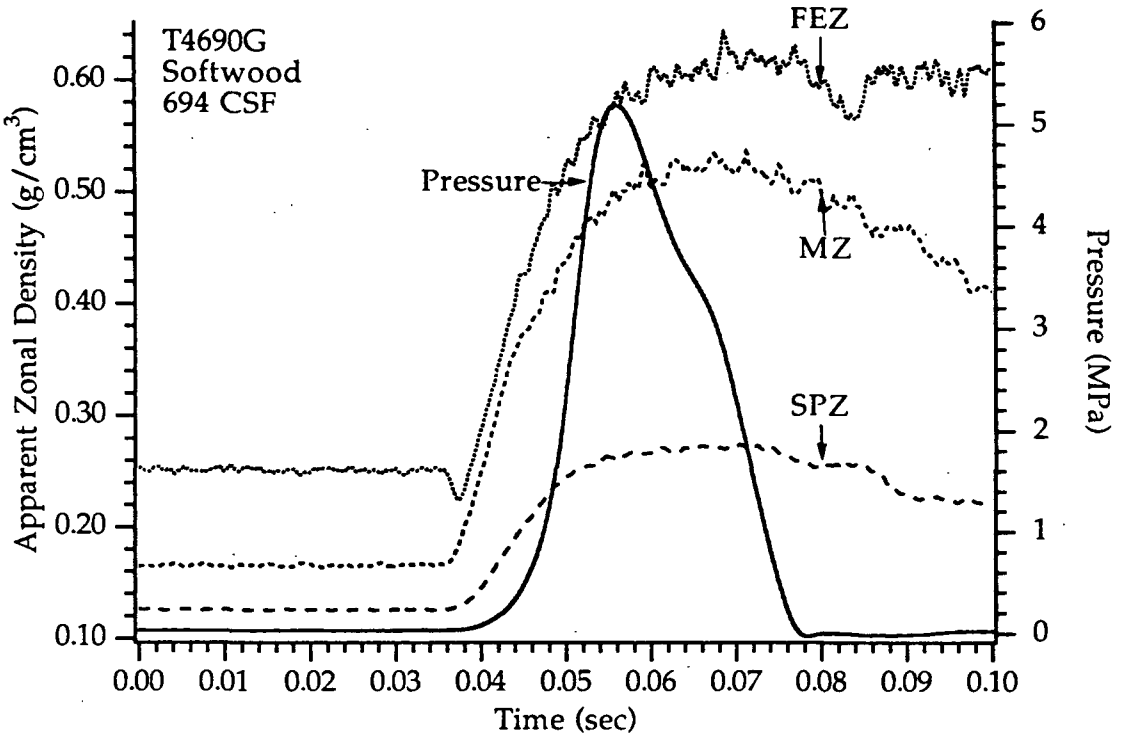

Figure 59. Zonal density change for an MTS-pressed high freeness softwood handsheet. Basis weight = 150 g/m^2; Moisture ratio = 4.74; Freeness = 694 CSF.

LOW FREENESS SOFTWOOD FURNISH

A low freeness softwood handsheet (shown in Figure 60) was formed from a refined sample of the high freeness unbleached kraft softwood furnish. The initial moisture ratio of the handsheet was 3.51 and was refined to 353 CSF. As the load was applied to the handsheet, targets A, B, and C moved at different rates. Target A was displaced at a faster rate than either B or C. The overall shape of the displacement curve for the falling press head (target E) was similar to that for target A, showing that the two are in contact

and moving together toward target D. Target D on the bottom of the sheet shows little displacement (less than 0.01 mm), even with a peak pressure of 6 MPa. As the applied load increased, the displacements of targets A, B, and C reach a maximum just past the point of maximum pressure and remain at this position until most of the applied load is released. As the press nip continues to open, there is limited additional upward movement of the targets.

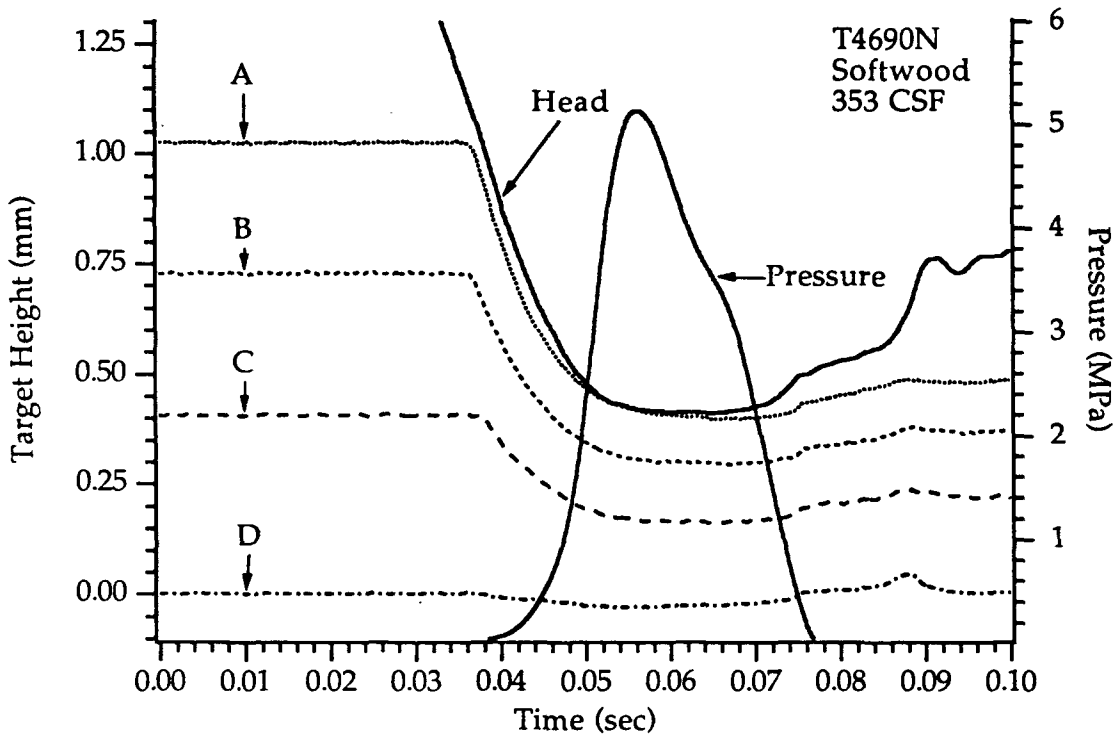

Figure 60. Target displacement histories for an MTS-pressed low freeness kraft softwood handsheet. Basis weight = 150 g/m^2; Moisture ratio = 3.51; Freeness = 353 CSF.

The zonal thickness changes for the low freeness softwood handsheet are shown in Figure 61. The initial thickness of the three zones FEZ, MZ, and SPZ are 0.30 mm, 0.32 mm, and 0.405 mm, respectively. The large difference between the thickness of the solid platen zone and the other two zones is attributed to prepressing of the handsheet necessary for intimate contact between target D and the solid ceramic platen.

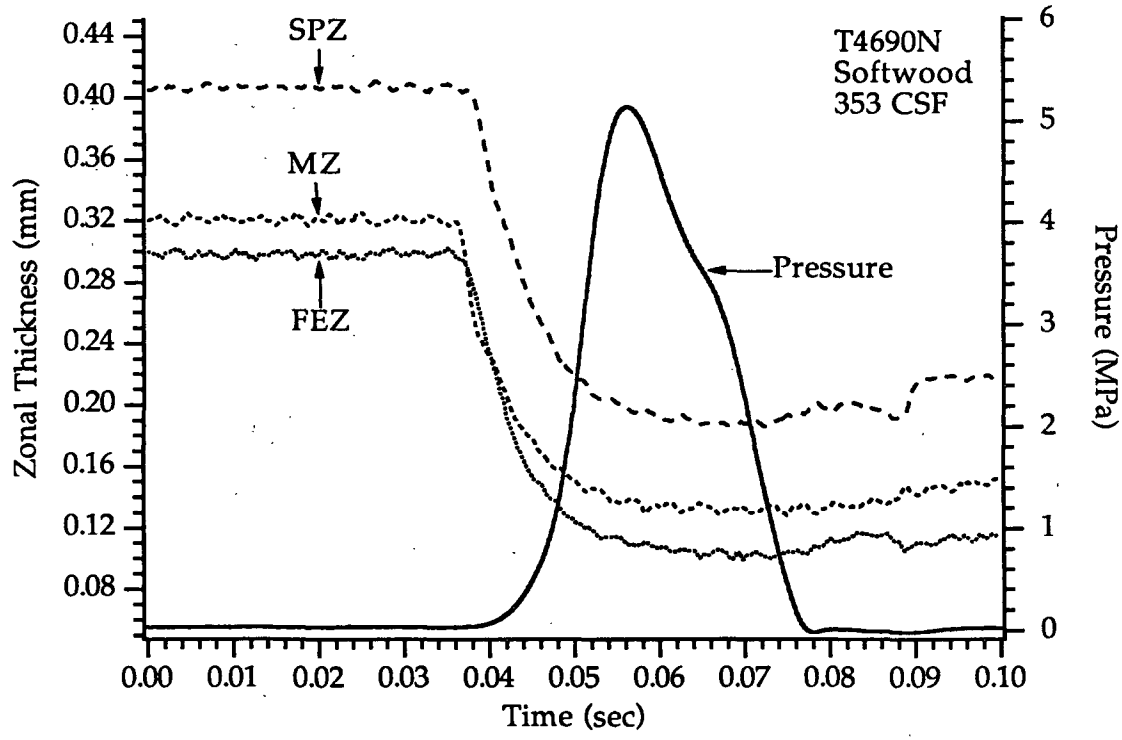

Figure 61. Zonal thickness change for an MTS-pressed low freeness softwood handsheet. Basis weight = 150 g/m^2; Moisture ratio = 3.51; Freeness = 353 CSF.

Even with its larger initial thickness, the solid platen zone decreased in thickness at about the same rate as the middle and flow-exiting zones. The slope of the curves after compression began indicates that the flow-exiting

zone and the middle zone compressed at slightly different rates initially. The flow-exiting zone compressed to a greater extent after the point of maximum pressure generation inside the nip. The point of minimum thickness of each of the zones occurred just after the point of maximum pressure generation, and after this point very little expansion was observed.

Figure 62 shows that the initial zonal densities of the low freeness softwood handsheet were 0.125, 0.158, and 0.17 g/cm^3 for the solid platen, the middle, and the flow-exiting zones, respectively. The flow-exiting zone had a slightly higher initial density due to prepressing of the handsheet. In the low freeness softwood handsheet, the flow-exiting zone densified at the most rapid rate and to the greatest extent. The middle zone densified at about the same rate as the flow-exiting zone during the first few milliseconds of the event, and then, the densification rate dropped off until the maximum density was attained. The middle zone's density lies midway between that of the flow-exiting zone and the solid platen zone. The solid platen zone density changes at a much lower rate than either of the other zones. After reaching maximum density, the zones began to expand. In this handsheet, the solid platen and middle zones expanded about the same amount, while the flow-exiting zone expanded to a greater extent and at a more rapid rate. After the pressure was released, the zonal densities became unrealistic due to uncontrolled expansion[9] or pulling apart of the sheet.

[9]Uncontrolled expansion is defined as expansion of the handsheet without restraint or applied load.

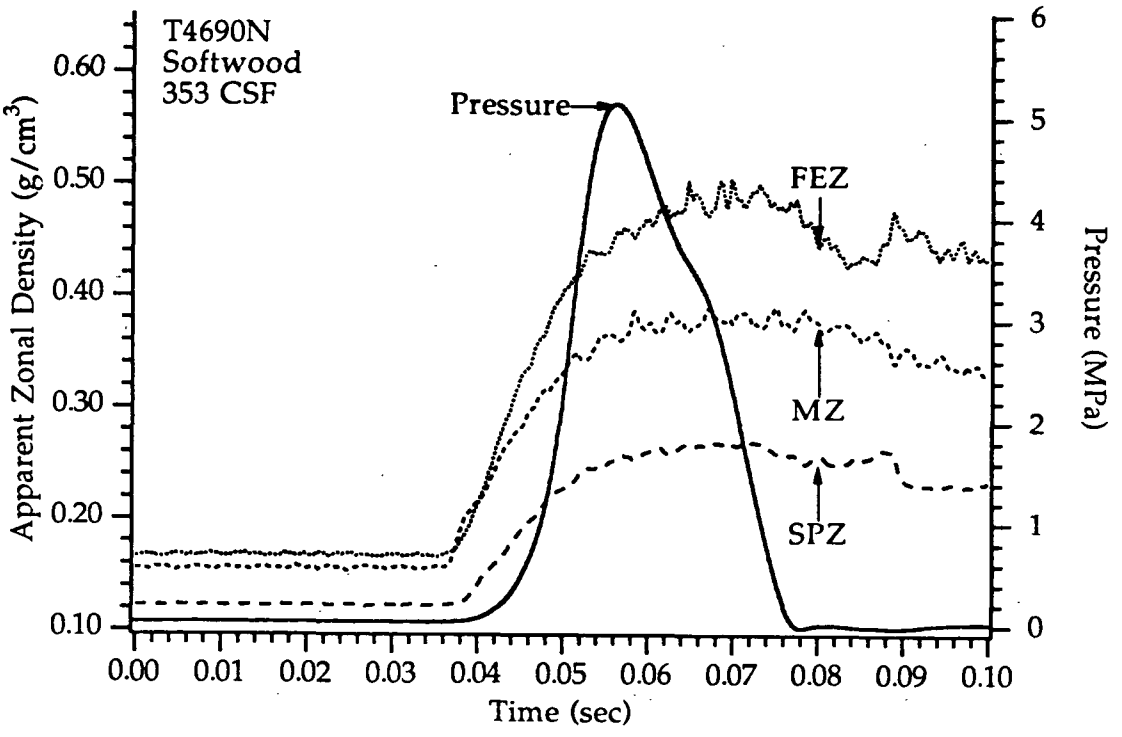

Figure 62. Zonal density change for an MTS-pressed low freeness softwood handsheet. Basis weight = 150 g/m^2; Moisture ratio = 3.51; Freeness = 353 CSF.

LOW FREENESS HARDWOOD FURNISH

The low freeness hardwood handsheet (shown in Figure 63) was formed from an unbleached kraft hardwood furnish (a mixture of ~40% maple, ~25% ash, ~20% birch, and the remainder consisting of oak, elm, and beech) refined to a freeness of 480 CSF. The initial moisture ratio of this handsheet was 3.22.

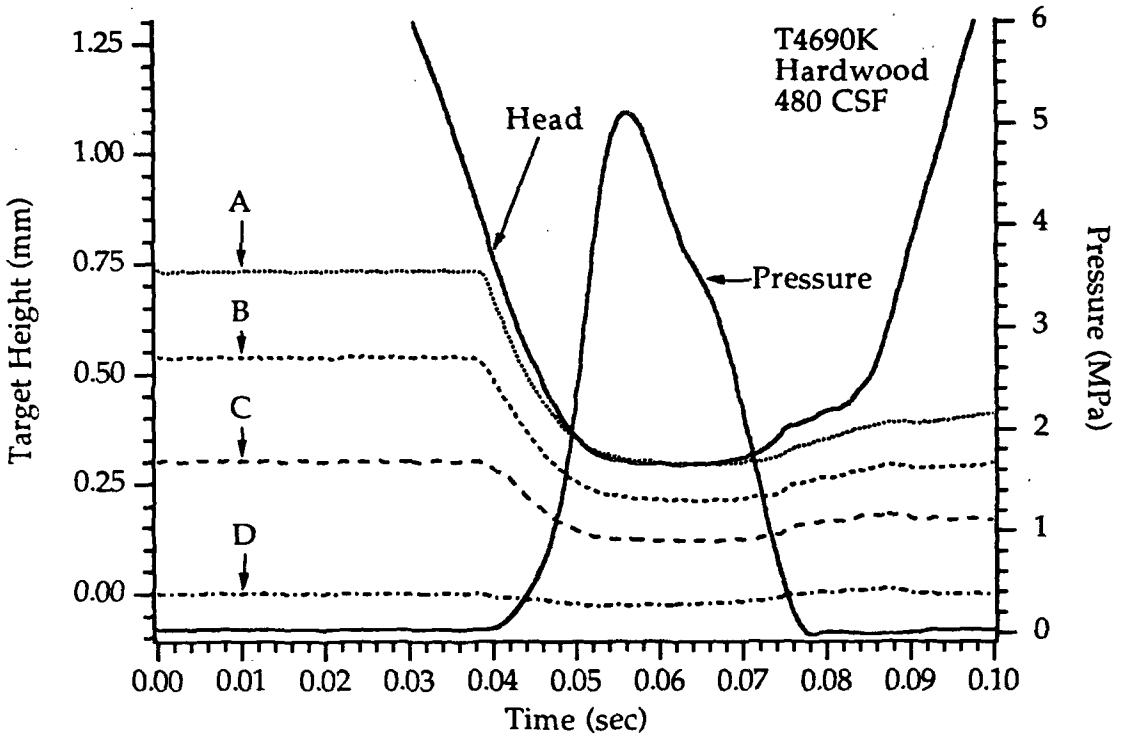

Figure 63. Target displacement histories for an MTS-pressed low freeness kraft hardwood handsheet. Basis weight = 150 g/m^2; Moisture ratio = 3.22; Freeness = 480 CSF.

The zonal thickness changes for the low freeness hardwood handsheet are shown in Figure 64. The initial thickness of each of the zones FEZ, MZ, and SPZ was 0.195 mm, 0.237 mm, and 0.30 mm. The large difference between the thickness of the solid platen zone and the other two zones was due to the prepressing of the handsheet to make intimate contact between target D and the solid ceramic plate. Even with the greater initial thickness of the solid platen zone, its thickness decreased at about the same rate as the flow-exiting and middle zones. The slope of the curves after compression begins indicates that the flow-exiting and middle zones compressed at the same rate initially, with the flow-exiting zone compressing to a greater extent after a few milliseconds. The point of minimum thickness of each of the

zones occurred just after the point of maximum pressure generation. At the end of the press nip, little zonal expansion was observed.

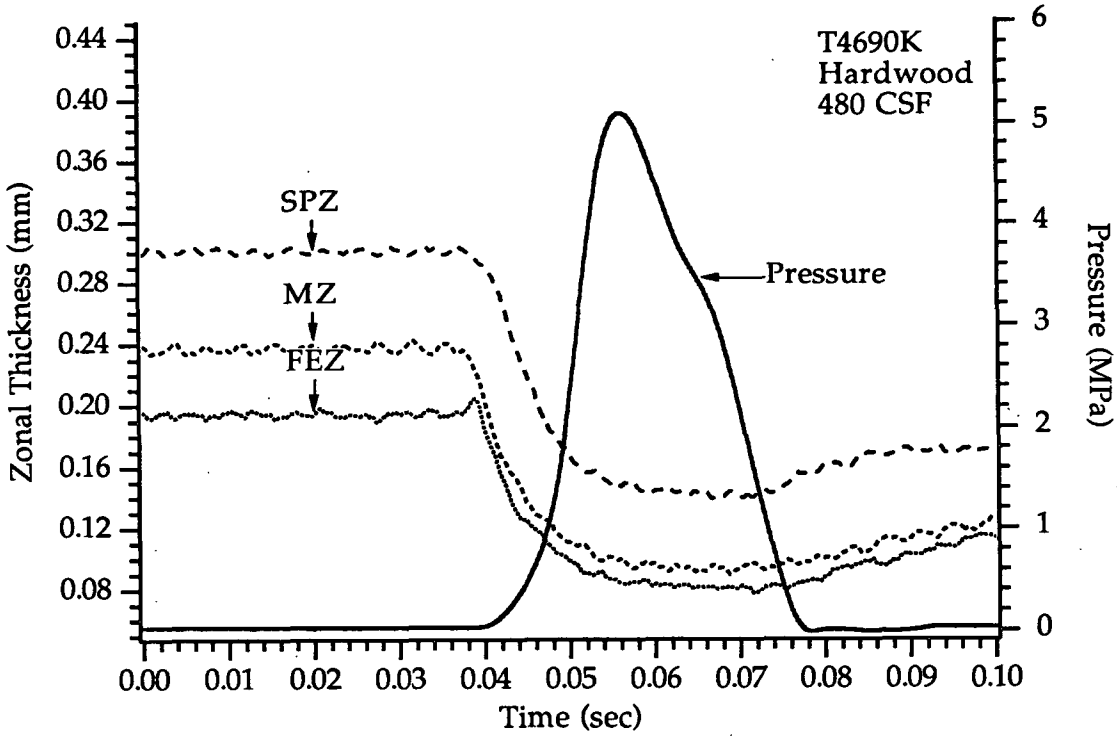

Figure 64. Zonal thickness change for an MTS-pressed low freeness hardwood handsheet. Basis weight = 150 g/m^2; Moisture ratio = 3.22; Freeness = 480 CSF.

In Figure 65 the initial zonal densities of the low freeness hardwood handsheet were 0.168, 0.211, and 0.26 g/cm^3 for the solid platen, the middle, and the flow-exiting zones, respectively. The flow-exiting zone had a slightly higher initial density, possibly due to the prepressing of the handsheet. In the low freeness hardwood handsheet, the flow-exiting zone densified at the most rapid rate and to the greatest extent. The rate of densification was approximately the same as that of the flow-exiting zone during the first 10

milliseconds of the event, and then, the densification rate dropped off. The solid platen zone densified at a much lower rate than either of the other two zones. After reaching their maximum density, the zones began to expand, and their densities decreased. In this sheet the flow-exiting and middle zones expanded to about the same amount, while the solid platen zone expanded to a lesser extent.

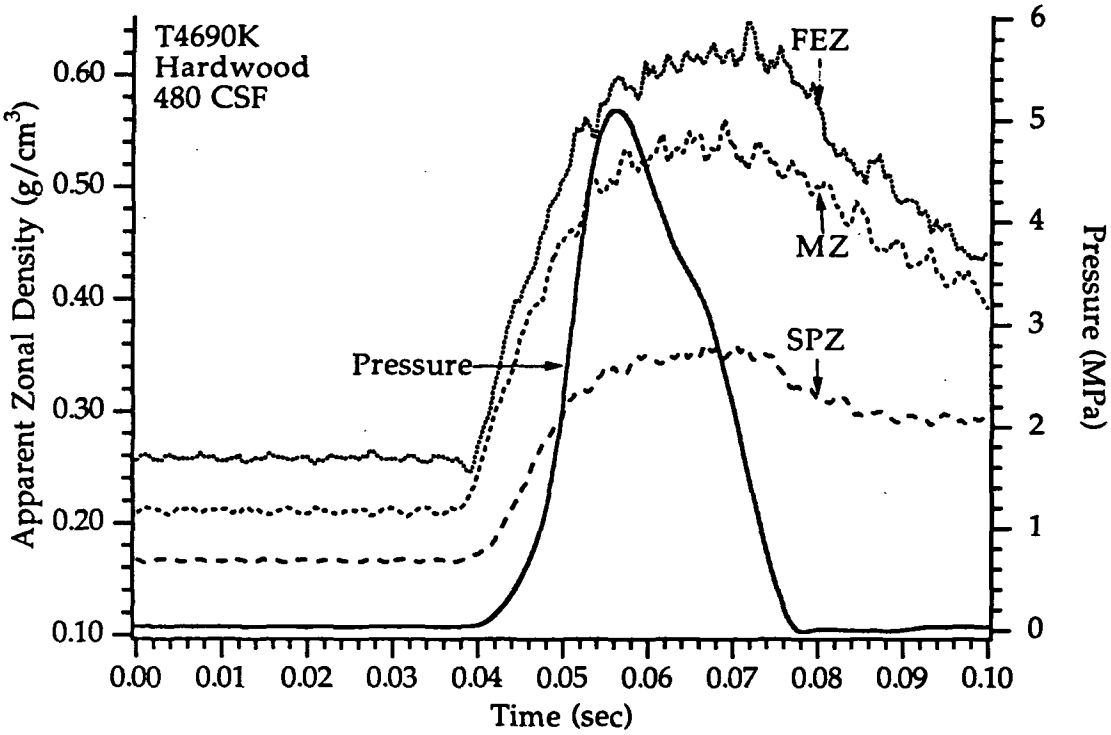

Figure 65. Zonal density change for an MTS-pressed low freeness hardwood handsheet. Basis weight = 150 g/m^2; Moisture ratio = 3.22; Freeness = 480 CSF.

SUMMARY

The results from Smith and Griffiths' Finite Element Model showed that compression (or consolidation) of a porous elastic medium results in different rates and extents of compression for the different layers, which increased in the direction of fluid flow. The maximum displacement of all points in the medium occurred when the maximum load was applied. Extrapolation of the target displacements to zonal densities indicated that the zone located nearest the flow-exiting surface developed the greatest density and at the fastest rate. At the solid platen side of the medium, there was little increase in density. These results demonstrated the development of a density gradient in the direction of fluid flow, which resulted from the coupling between fluid flow and material deformation.

The distribution of the targets in the handsheets was not as uniform as anticipated. The variation in target positions (i.e., uniformity of the zonal thicknesses) was as high as ±33%. The nonuniformity in these initial positions would seem to indicate that the zonal basis weights were not equal. In fact, this was not the case. The initial level of compression (or consolidation) of each zone was different due to different quantities of water present in the surface zones (FEZ and SPZ) and prepressing of the sheet onto the solid ceramic plate.

Wet pressing of these handsheets was carried out using two types of wet press simulators. The first wet press simulator was a "rock dropper" which was used for short nip residence times (2-3 milliseconds). An MTS servo-hydraulic press was used as the second type of wet press simulator to

produce longer nip residence times (40-60 milliseconds). The high moisture ratio (moisture ratio greater than 3.0) results from handsheets pressed with these simulators are similar to those obtained with Smith and Griffiths' consolidation model. At short nip residence times, the low moisture ratio, high freeness softwood handsheet developed approximately the same density in all three zones (no distinct density gradient was formed). At the same nip residence time, the high moisture ratio, high freeness softwood handsheet developed a significant density gradient in the direction of flow. The point at which the maximum density occurred was different in each of the zones, and the rates and extents of densification were different for each of the zones. In the longer nip residence time softwood and hardwood handsheets, the results are the same as those in the high moisture ratio, high freeness softwood handsheet, pressed in the "rock dropper." In each of these handsheets, a density gradient developed in the direction of fluid flow, and the flow-exiting zone developed the greatest density.

In all of the handsheets, there was very little expansion of the handsheet until the nip pressure was completely released. The thickness recovery, in the constrained expansion (from peak applied pressure to zero pressure) side of the nip, ranged from 5 to 10% of the minimum sheet thickness.

DISCUSSION

The compression and expansion behavior of an idealized porous elastic medium and several wet pulp fiber handsheets (pressed at two nip residence times) was presented in the last section. A comparison of the theoretical compression and expansion behavior of the porous elastic medium will be made with that of the short and long nip residence time wet pressed pulp handsheets. The effects of flow resistance (freeness) and nip residence time on sheet densification will also be discussed in this section. Furthermore, the observed effects of flow resistance and nip residence time on sheet densification will be compared to those effects reported in the literature. Finally, the contribution of this new wet pressing information to our understanding of rewet will be discussed.

COMPARISON OF THE CONSOLIDATION MODEL DATA WITH THE WET PRESS SIMULATOR DATA

The compression and expansion data from a mathematical model of consolidation of a saturated poroelastic medium were presented earlier. These data were further used for comparison with the compression and expansion behavior of pulp fiber handsheets. The data from the model, shown in Figure 48, consist of displacement profiles for two targets (nodes B and C) inside the medium and one at each surface (nodes A and D). These target displacement histories show the deformation of the medium resulting from application of a uniform haversine pressure pulse to the upper surface of the medium. Fluid was allowed to flow from this upper surface without restriction. The target positions in the medium were chosen to divide the

medium into three approximately equal height zones which would correspond to the layers in the pulp fiber handsheets.

The displacement histories of these targets show the kind of deformation that might be expected if the compression and expansion behavior of the pulp handsheets was that of an ideal porous elastic medium. In actuality, the compression and expansion behavior of pulp handsheets is more like that of a porous viscoelastic material. In Figure 48, the target displacement profiles of the porous elastic medium are smooth and well behaved, which is in sharp contrast to the target displacement curves of the high and low freeness softwood (rock dropper-pressed) handsheets, shown in Figures 66 and 67. These figures show that, in both the poroelastic material and the handsheets, the rates and extents of displacement of the targets are different. Most of the difference between the compression and expansion behavior of the poroelastic material and the handsheet was the result of changes in porosity and permeability of the pulp fiber handsheets during compression resulting from the coupling of fluid flow and material deformation. In the poroelastic material, the permeability was assumed to be constant throughout the compression and expansion process. This assumption, although invalid, was used by Smith and Griffiths to simplify the model. In the pulp fiber handsheets, the porosity and the permeability are constantly changing as a result of the coupling of fluid flow through the material and the material deformation.

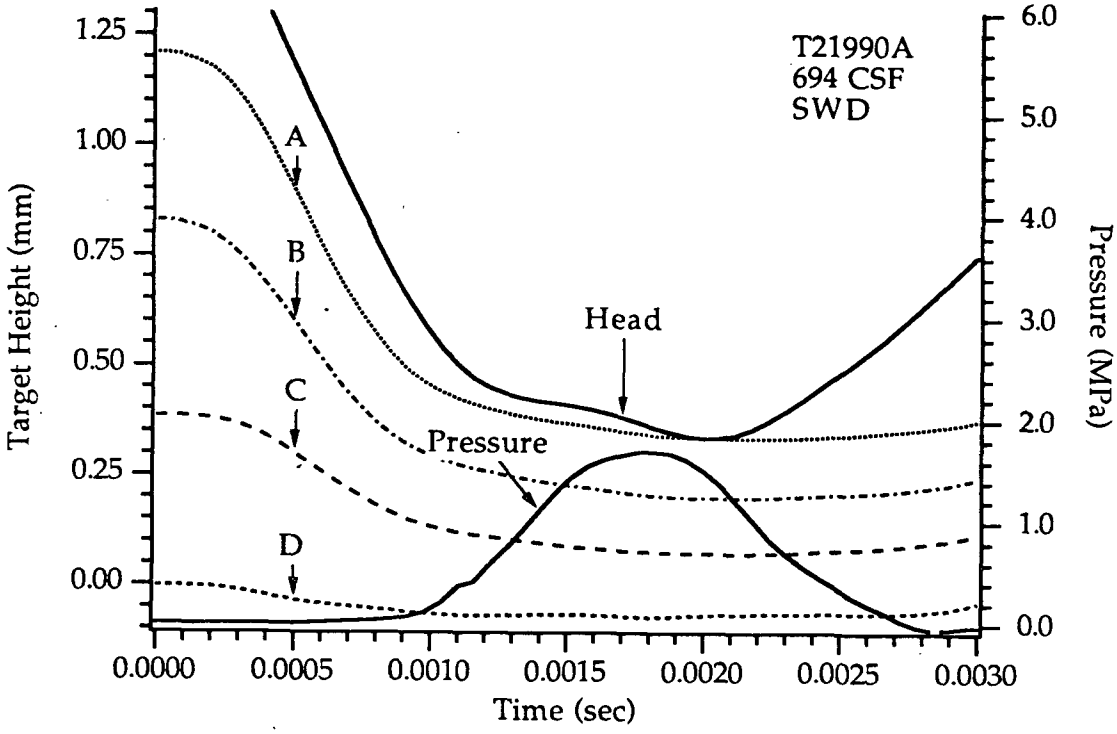

Figure 66. Target displacement in a rock dropper-pressed high freeness softwood handsheet. Basis weight = 150 g/m^2; Moisture ratio = 2.63; Freeness = 694 CSF.

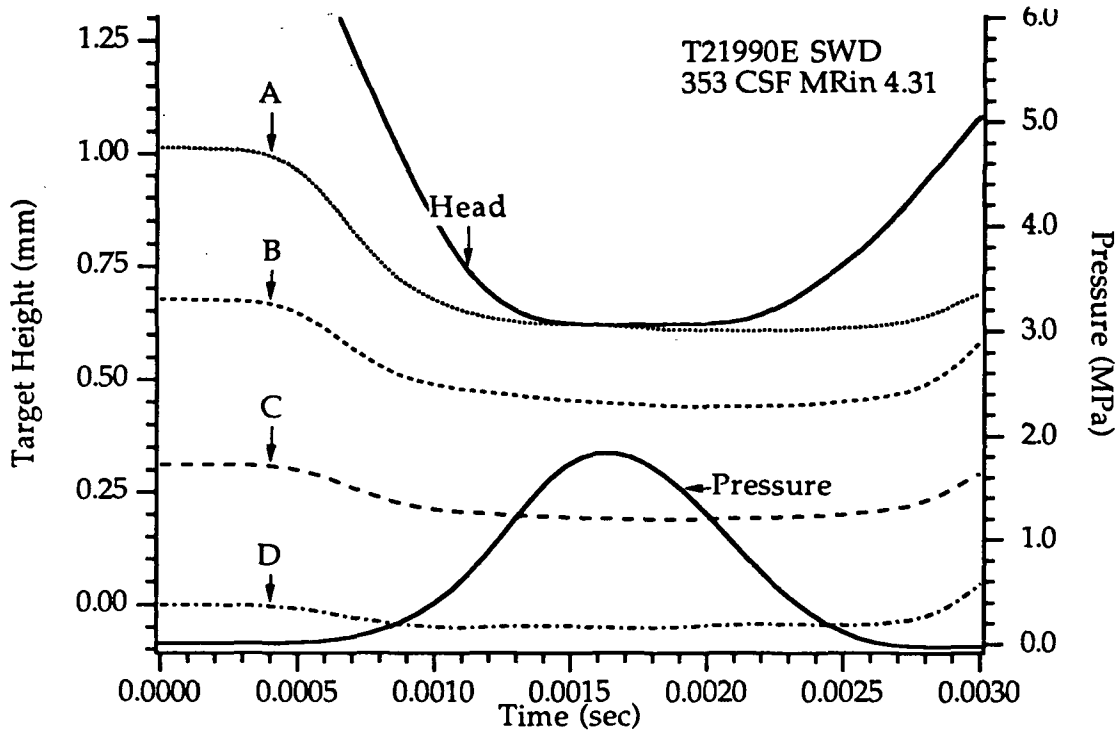

Figure 67. Target displacements in a rock dropper-pressed low freeness handsheet. Basis weight = 150 g/m^2; Moisture ratio = 4.31; Freeness = 353 CSF.

In order to compare the target displacements of the poroelastic medium and the pulp fiber handsheets, it should be recognized that the position of target D (the fixed platen) was determined by the boundary conditions in the model and, therefore, was not displaced during the loading and unloading process. However, in the handsheets it was not possible to completely fix the position of target D as shown in Figures 66 and 67. The deflection of target D was the result of movement of the target and deflection of the ceramic supporting plate. Even application of a small load (17 kPa) to the surface of the sheet to level it on the surface of the ceramic plate was not

completely successful in achieving the desired level of contact between target D and the solid ceramic plate. However, the displacement of target D and the deflection of the materials supporting the sheet during wet pressing were reduced significantly when compared to the target displacement results obtained by Burton. The new wet press nip materials and new nip configuration increased the accuracy and reproducibility of the target displacement measurements. In retrospect, application of the load (at the level used) to the handsheet to get better contact between target D and the solid ceramic plate (in the lower press head) was probably not necessary. The contact between target D and the solid ceramic plate was sufficient to accurately define the bottom surface of the handsheets.

The thickness of the zones defined by targets A-B, B-C, and C-D (zones FEZ, MZ, and SPZ, respectively) was initially equal in the poroelastic material, as shown in Figure 49. The zonal thicknesses in the high and low freeness (rock dropper-pressed) softwood handsheets (Figures 68 and 69) were not equal due to the previously described problems with handsheet formation and prepressing of the handsheets. In the model, the zonal thickness change seemed to be cumulative, in that each zone changed in thickness more than the preceding one. Yet, in the pulp handsheets, the thickness change between zones was not as uniform. In both handsheets, as the load was applied, the thickness of each zone decreased at a different rate and to a different extent indicating the buildup of a hydraulic pressure gradient and fluid flow. The high freeness softwood (low moisture ratio) handsheets showed little difference in zonal thicknesses, implying the lack of buildup of a significant hydraulic pressure gradient in the sheet. However, the low freeness (high moisture ratio) softwood handsheets showed a large change in zonal

thickness between adjacent zones. The thickness of the flow-exiting zone decreased to the greatest extent and at the fastest rate due to the cumulative effect of fluid drag as the fluid flows through the different layers of the medium. Therefore, the farther the layers were away from the flow-exiting surface, the less the effect of cumulative drag (lower hydraulic pressure) and the less the layers compressed as shown by the layer on the bottom of the medium (layer SPZ) in Figure 68. In the poroelastic material, the point at which minimum zonal thickness occurred was the same for each zone, whereas in both high and low freeness softwood handsheets, the points of minimum thickness were different for each zone due to the development of hydraulic and structural pressure gradients. In these handsheets the minimum zonal thickness occurred just after the peak pressure when the hydraulic pressure reached zero.

In the poroelastic material, the initial apparent zonal densities were equal, as shown in Figure 50. Even though the zonal basis weights were equal, the initial zonal thicknesses in the high and low freeness softwood handsheets were not equal, and therefore, the initial apparent zonal densities were not equal. As the applied load increased, the zones densify at different rates and to different extents in all cases. The density results from the ideal case and the low freeness softwood (high moisture ratio) handsheet indicated the development of a density gradient in the direction of fluid flow. The sheet stratification described by MacGregor (1983) was shown in both the consolidation model results and low freeness (high moisture ratio) handsheet. In the low moisture ratio handsheet, there was insufficient water flow to develop a significant density gradient or sheet stratification.

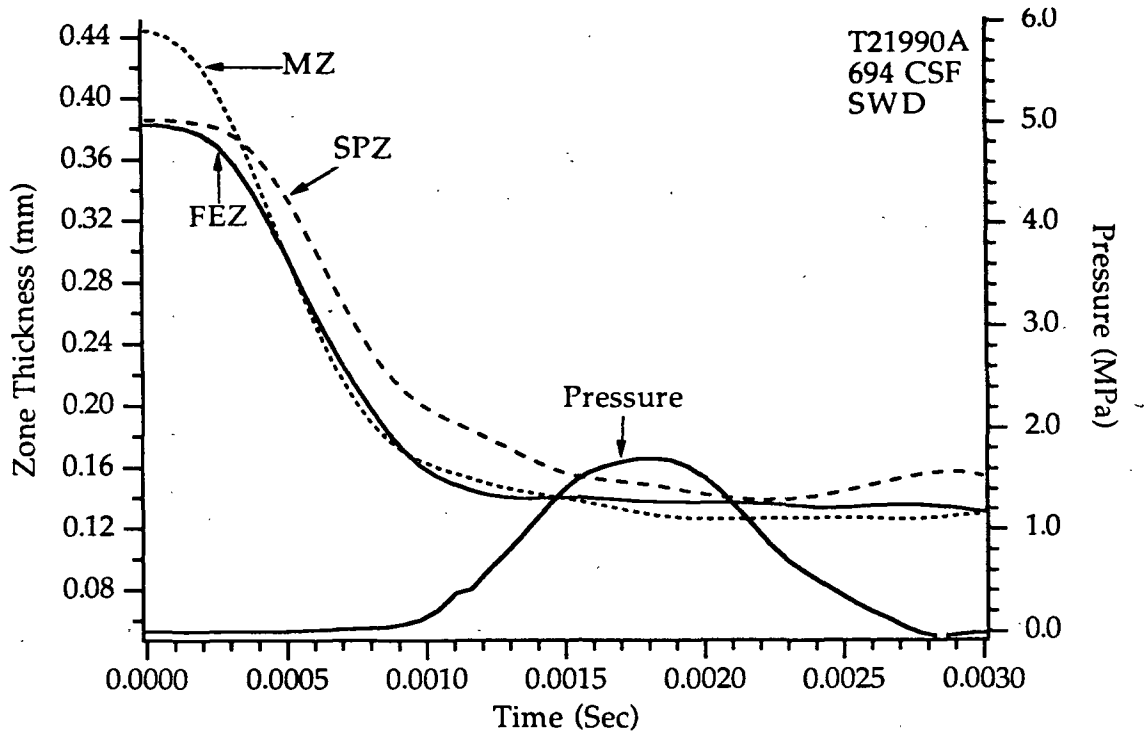

Figure 68. Zonal thickness change in a "rock dropper"-pressed high freeness handsheet. Basis weight = 150 g/m^2; Moisture ratio = 2.63; Freeness = 694 CSF.

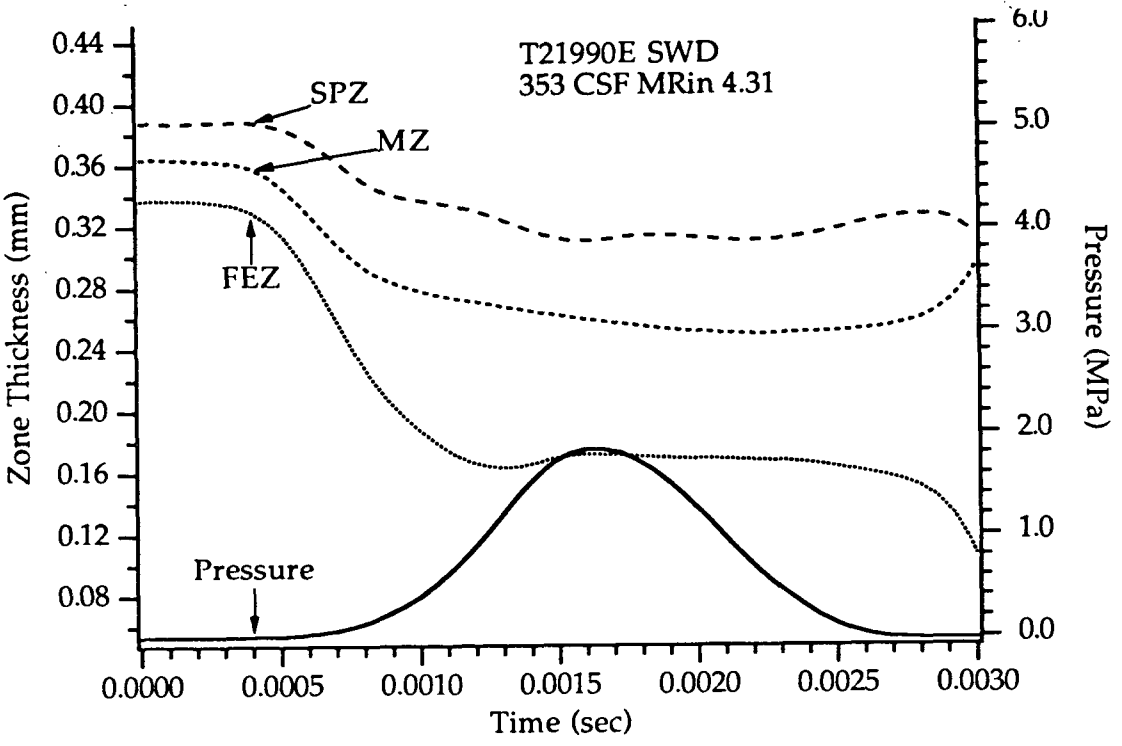

Figure 69. Zonal thickness change in a "rock dropper"-pressed low freeness handsheet. Basis weight = 150 g/m^2; Moisture ratio = 4.31; Freeness = 353 CSF.

COMPARISON OF THE COMPRESSION AND EXPANSION BEHAVIOR OF SHORT NIP RESIDENCE TIME HANDSHEETS AND A POROELASTIC MATERIAL

The nip residence time of the rock dropper was approximately 3 milliseconds, and the target displacement histories for these short nip residence time handsheets were described in the Results section. These representative handsheets were formed from an unbleached kraft softwood furnish at two freeness levels (694 and 353 CSF) and had different moisture ratios. The effects of moisture ratio and freeness on the compression and

expansion behavior of these softwood pulp handsheets are best described in terms of compression- and flow-controlled wet pressing, whereas the results from the poroelastic model would be best described as similar to flow-controlled pressing.

The target displacement histories of the rock dropper-pressed high and low freeness softwood handsheets are shown in Figures 66 and 67. The displacement histories for these handsheets show that the initial target positions and the zonal thicknesses in the low freeness softwood handsheet (.35, .35, and .32 mm) were more uniform than they were in the high freeness softwood handsheet (.39, .45, and .38 mm). The initial zonal thicknesses in the low freeness softwood handsheet were close to those of the poroelastic material (.35, .35, and .32 mm vs. .33, .33, and .33 mm for the flow-exiting, middle, and solid platen zones of the low freeness softwood handsheet and the poroelastic material, respectively). The differences in the initial zonal thicknesses of these handsheets were the result of the method used to reduce the moisture ratio and prepressing of the handsheet onto the solid ceramic plate. The process used to form the handsheets may also have contributed to the nonuniformity of the target spacing and will be discussed later.

Since the nip residence times and pressure profiles were the same for these two handsheets, the press impulse applied to both handsheets must have been the same. Even though the high freeness softwood handsheet had a lower initial moisture ratio (2.63) than the low freeness softwood handsheet (4.31), it had a higher initial thickness. The lower initial moisture content of the high freeness softwood handsheet reduced the quantity of fluid which had to be expressed from the sheet, thereby making it easier for the handsheet to compress.

Comparison of the displacement histories of these two handsheets with those of the poroelastic material shows that the targets in the high and low freeness softwood handsheets were displaced at a much more rapid rate than those in the poroelastic medium and were probably due to the viscoelastic properties of the handsheets. The target displacements in the high and low freeness softwood handsheets reached a maximum just after the point of maximum pressure generation which was different from that of the poroelastic material. In the poroelastic material, the point of maximum target displacement coincided with the point of maximum load application.

In the high and low freeness softwood handsheets, as the load approached its maximum level, the rates at which the targets were displaced decreased rapidly until maximum target displacement was reached, and then, the targets moved slowly upward as shown in Figures 66 and 67. Most of the target displacement during compression in these handsheets occurred when the load was small, and as the load reached its maximum, the target profiles became almost flat; this early, rapid target displacement is in contrast to the poroelastic material where the displacement profiles were symmetric about the midpoint.

In the poroelastic material, the initial zonal thicknesses were the same, and the zonal thickness change curves were smooth with the flow-exiting zone decreasing in thickness the most, followed by the middle zone, and then the solid platen zone. The initial zonal thicknesses in the high and low freeness softwood handsheets were approximately the same, and given the difficulties in forming the handsheets and positioning the targets in these handsheets, the uniformity of the initial zone thicknesses was quite good. It

was not possible to form a handsheet in which the thickness of all three basis weight zones was perfectly uniform. This was due in part to the formation of a wavy surface at the interface between the zones. Placement of the targets on this surface resulted in targets which were slightly elevated above the average height of the zonal interface. This accounts for most of the difference in thickness of the middle and solid platen zones. The difference in thickness between the flow-exiting zone and the other two zones is due to prepressing the handsheet onto the surface of the solid ceramic plate to achieve intimate contact between the target on the bottom of the sheet and the plate.

The thickness profiles in the high freeness softwood handsheet were approximately the same for each zone. This was due to the low initial moisture ratio of the handsheet. In the low freeness softwood handsheet, the initial thickness of the zones was less uniform than in the high freeness softwood handsheet. The zonal thickness changes in the low freeness softwood handsheet showed the development of a distinct thickness gradient in the direction of fluid flow from the sheet.

The density profiles in the poroelastic material (shown in Figure 50) showed that the zones have the same initial density, but as the load increased, the zones developed their density at different rates and to different extents. The effect of coupling between fluid flow and material deformation resulted in development of a density gradient in the direction of fluid flow similar to that shown in Figure 67 (a low freeness handsheet). The density of the flow-exiting zone developed at the fastest rate and to the greatest extent, followed by the middle and solid platen zones. It was apparent from the lack of development of a distinct density gradient in the sheet that there was insufficient water in this high freeness handsheet to develop a substantial

hydraulic pressure gradient, and therefore, the only compressive forces were those resulting from the structural pressure in the fiber network (compression-controlled wet pressing). In contrast, the low freeness softwood handsheet had a higher moisture ratio and sufficient water to develop a large hydraulic pressure gradient which affected density development during wet pressing. The flow-exiting zone developed the highest density due to the cumulative effects of fluid flow and structural pressure development. Little or no water flowed from the middle and solid platen zones, resulting in limited density development in these zones. The density profile of the flow-exiting zone in this handsheet was somewhat uncharacteristic in that it continued to increase at a slow rate throughout the press cycle, and upon release of the applied load, no density was lost. None of the other handsheets pressed in either the rock dropper or the MTS servo-hydraulic press exhibited this type of behavior.

COMPARISON OF LONG NIP RESIDENCE TIME HANDSHEETS

The target displacement histories of the long nip residence time (40 to 60 milliseconds) high and low freeness softwood handsheets and the low freeness hardwood handsheets (handsheets T4690G, T4690N, and T4690K) are shown in Figures 70, 71, and 72. Since these are representative handsheets, each has a different initial thickness, moisture ratio, and freeness. The effect these factors had on the rate of target displacement and extent of compression of the handsheets will be discussed later.

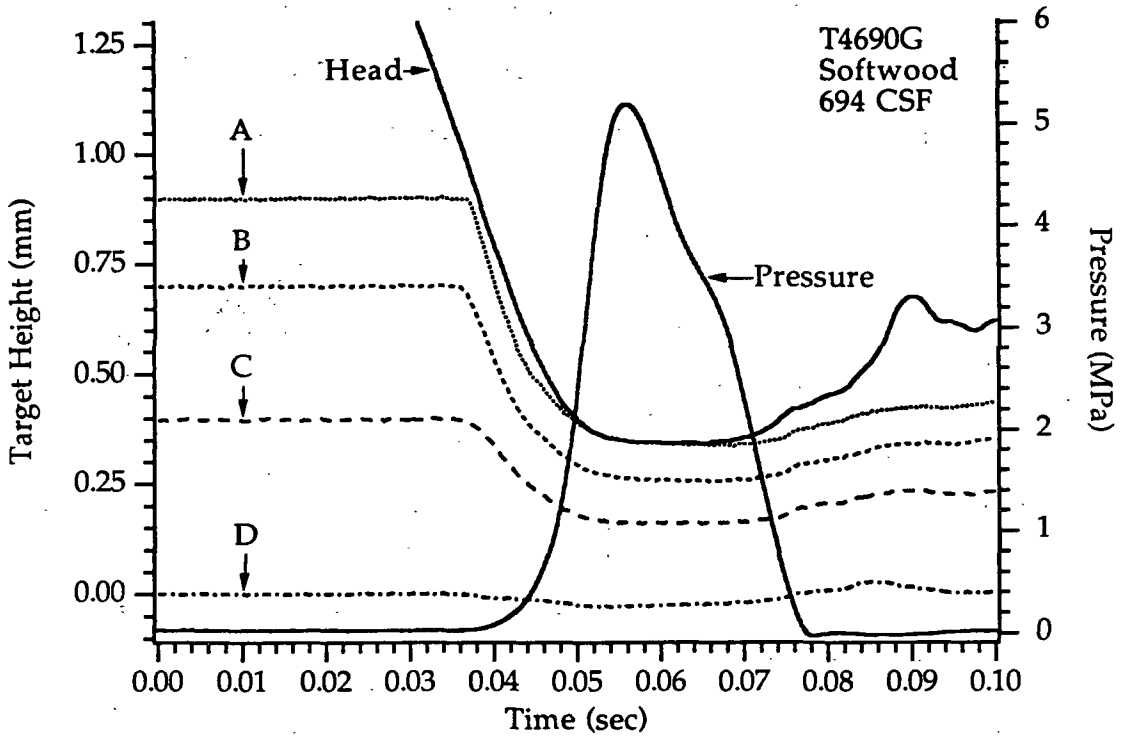

Figure 70. Target displacement histories of an MTS-pressed high freeness softwood handsheet. Basis weight = 150 g/m^2; Moisture ratio = 4.74; Freeness = 694 CSF.

Close examination of the target displacement histories for these handsheets shows that target B in the high freeness softwood and the low freeness hardwood handsheets began to move downward before target A. This was likely the result of an uneven application of pressure on the surface of the sheet. The absence of this effect on the low freeness softwood handsheet implied that movement of target B before target A was the result of debris (pulp fibers) left on the surface of the porous ceramic plate (the flow receiver) after a press run. The same porous ceramic plate was reused in each

press run, and occasionally, a sheet stuck to the porous plate and had to be physically removed by rubbing the fibers from the surface of the porous plate. Any fibers which remained on the surface of the porous plate affected the time of contact in that specific region of the porous plate with the handsheet. Apparently, the method used to remove the stuck handsheets did not remove all of the fibers from the surface of the porous ceramic plate.

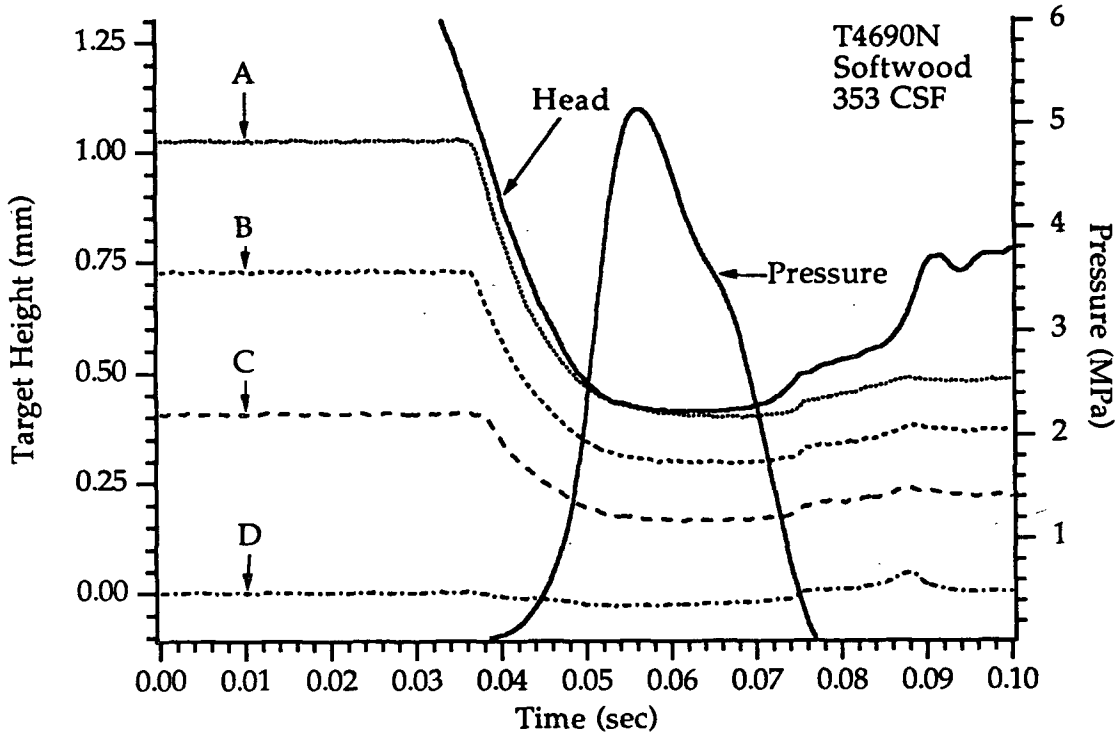

Figure 71. Target displacement histories of an MTS-pressed low freeness softwood handsheet. Basis weight = 150 g/m^2; Moisture ratio = 3.51; Freeness = 353 CSF.

In Figures 70, 71, and 72, the initial thicknesses of each of the handsheets were different as well as the zonal thicknesses. The source of the deviation from the ideal target spacing in these handsheets was the same as described for the rock dropper-pressed high and low freeness softwood

handsheets. The wet pressing behavior of these sheets was very similar in that, as the applied load increases in each of the handsheets, target A was displaced at the most rapid rate, followed by targets B and C. The displacement of target D was minimal in comparison to the displacement of the other targets. The shape of the target displacement profiles in a given handsheet was different, indicating the development of a strong z-direction hydraulic pressure gradient. The moisture ratios of the MTS-pressed handsheets (4.74, 3.51, and 3.22) were not vastly different; therefore, the overall shape of the target displacement profiles of the different handsheets was similar.

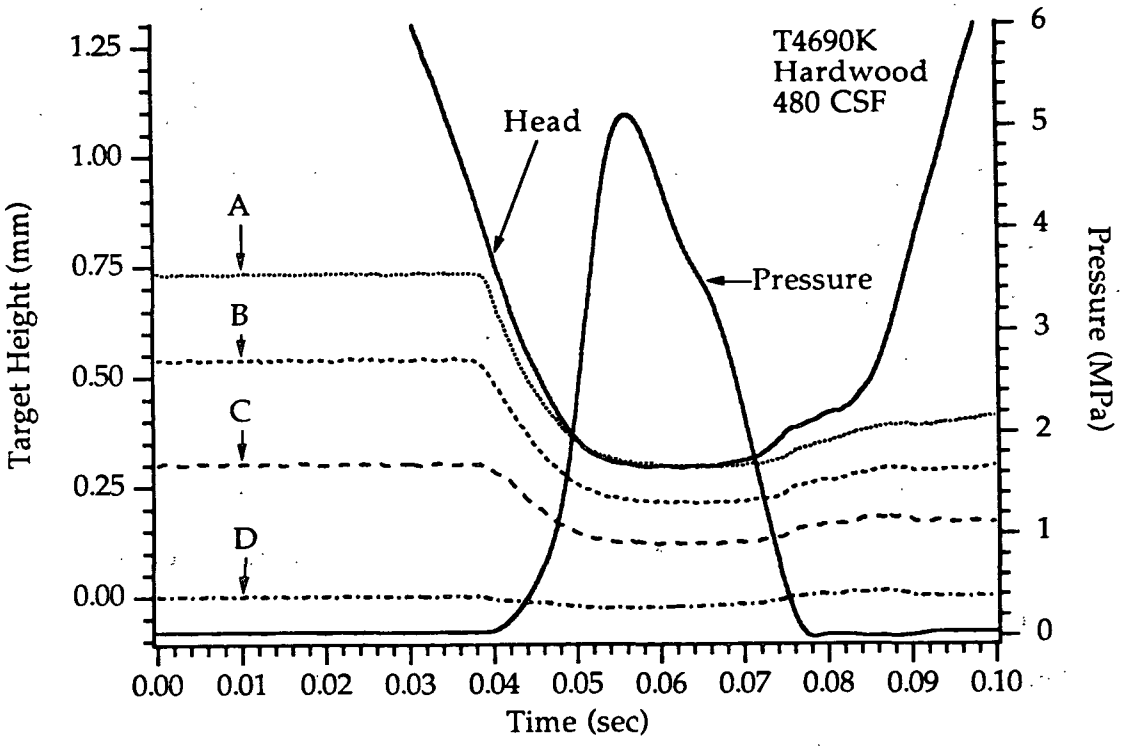

Figure 72. Target displacement histories of an MTS-pressed low freeness hardwood handsheet. Basis weight = 150 g/m^2; Moisture ratio = 3.22; Freeness = 480 CSF.

Since the initial moisture contents of the MTS-pressed high and low freeness softwood handsheets and the low freeness hardwood handsheets were similar, they all had similar initial zonal thicknesses. The flow-exiting zone had the lowest initial thickness as a result of prepressing, and upon application of the load, its thickness decreased the largest amount. The middle zone had a much greater initial thickness than the flow-exiting zone in each handsheet, yet decreased in thickness to a lesser extent than the flow-exiting zone. The solid platen zone typically had the largest initial thickness of the three zones and decreased in thickness the least amount.

The apparent zonal densities for the MTS-pressed high and low freeness softwood handsheets and the low freeness hardwood handsheets were calculated with equation (2) and are shown in Figures 73, 74, and 75. In each handsheet the zonal densities showed the development of a density gradient in the direction of fluid flow. The flow-exiting zone developed the highest density, followed by the middle and solid platen zones. The points of maximum zonal were approximately the same in each handsheet. The solid platen zone reached its maximum density first, followed by the middle and flow-exiting zones. In Figures 73 and 75 (the high freeness softwood and low freeness hardwood handsheets), the density profiles for the middle and flow-exiting zones are superimposable on each other. This implies that the differences in initial moisture ratio, freeness, and furnish type have little or no effect on density development in these two handsheets. In Figure 74 (the low freeness softwood handsheet), the effect of furnish and freeness is more evident in that the middle zone densified to a much lesser extent than in either the high freeness softwood or the low freeness hardwood handsheets. These results indicate that in the case of the high freeness softwood and the

low freeness hardwood handsheets the differences in freeness and furnish had little effect on the densification of the handsheet. In the case of the low freeness softwood handsheet, the effect of freeness is more pronounced than in the other two handsheets. The low freeness in this handsheet increases the flow resistance over the entire thickness of the sheet and results in a more uniform density development.

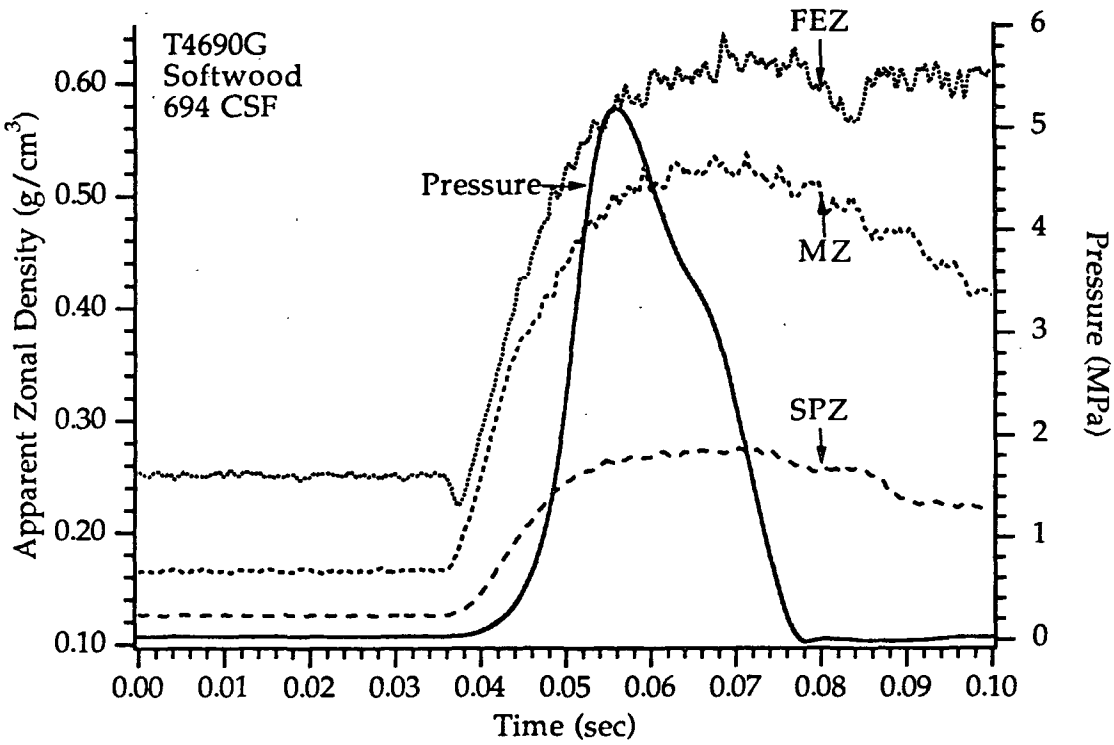

Figure 73. Apparent zonal densities of an MTS-pressed high freeness softwood handsheet. Basis weight = 150 g/m^2; Moisture ratio = 4.74; Freeness = 694 CSF.

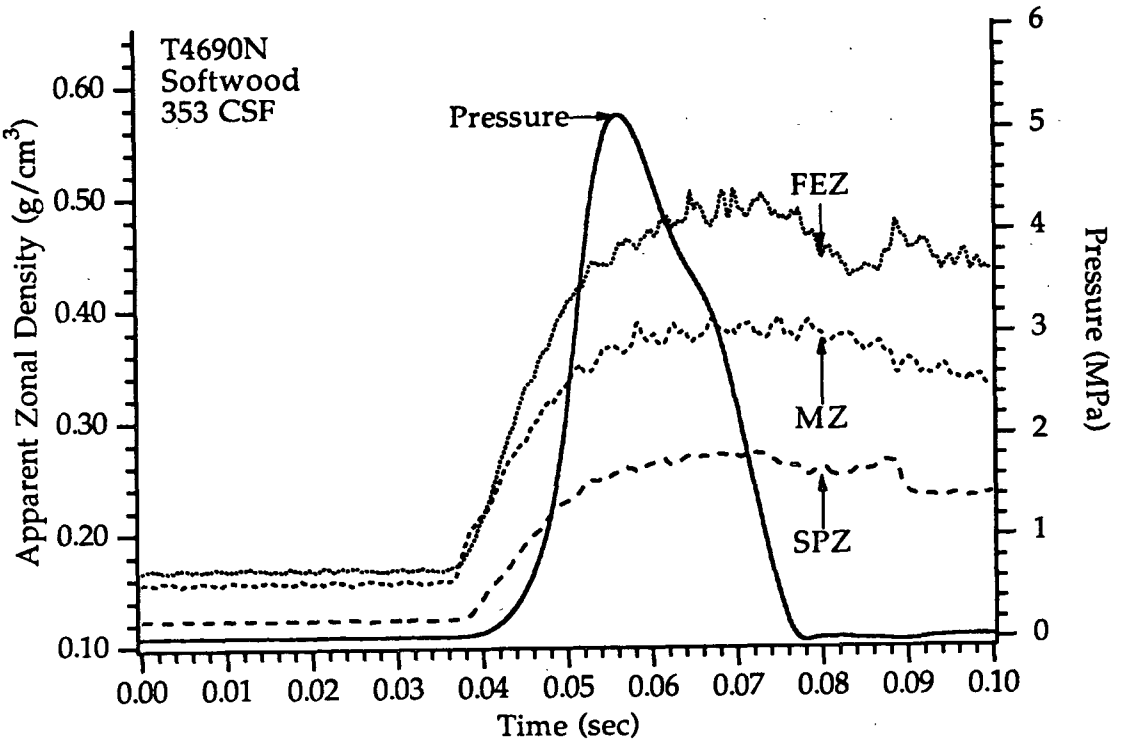

Figure 74. Apparent zonal densities of an MTS-pressed low freeness softwood handsheet. Basis weight = 150 g/m^2; Moisture ratio = 3.51; Freeness = 353 CSF.

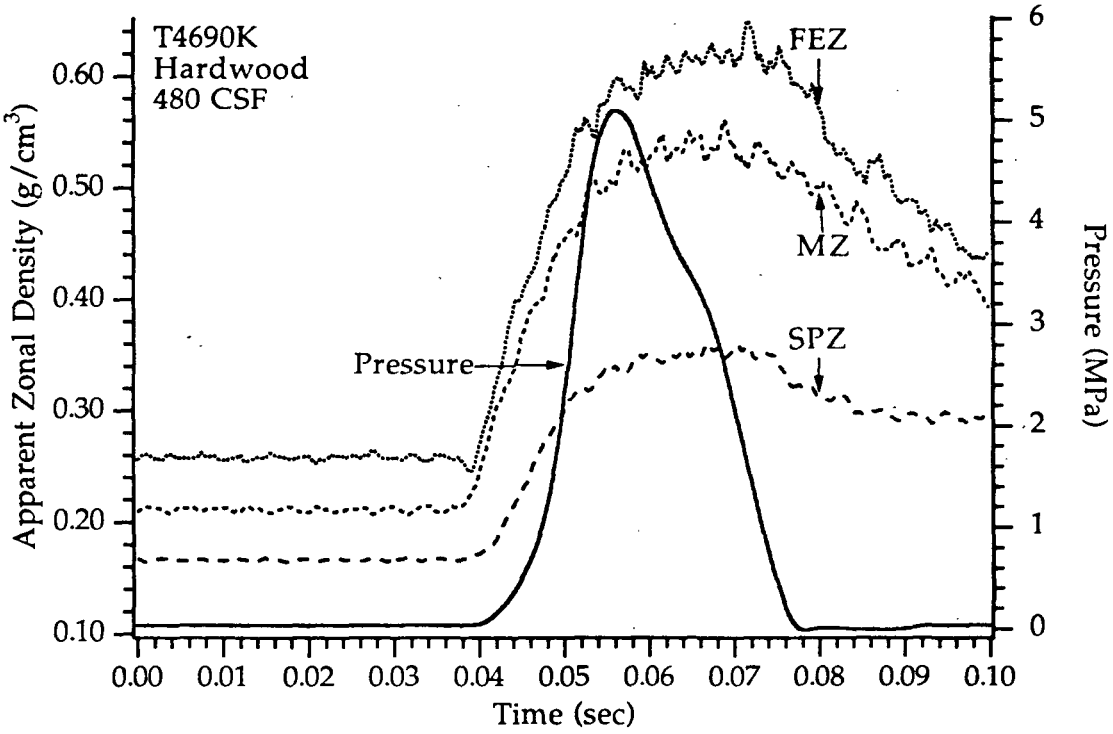

Figure 75. Apparent zonal densities of an MTS-pressed low freeness hardwood handsheet. Basis weight = 150 g/m^2; Moisture ratio = 3.22; Freeness = 480 CSF.

EFFECTS OF FLOW RESISTANCE AND NIP RESIDENCE TIME ON SHEET DENSIFICATION

As discussed in a previous section on wet pressing, handsheets which are typical of flow-controlled pressing develop lower densities during wet pressing. The typical flow-controlled handsheet possesses a high moisture ratio, a high basis weight, and a high flow resistance (low freeness). In compression-controlled pressing, density development is highly dependent on the press impulse. The typical compression-controlled sheet develops a higher density and is usually characterized as having a low initial moisture content and a low flow resistance (high freeness).

The effect of flow resistance and nip residence time on density development was examined by testing sheets with different degrees of refining and similar ingoing moisture ratios. Sheets with low flow resistance were made from an unbeaten, 694 CSF, softwood furnish, while sheets with a high flow resistance were made from both a beaten, 353 CSF, softwood furnish and a beaten, 480 CSF, hardwood furnish. Figures 76 and 77 show the total sheet density-time relationships for the three different freeness levels (and furnishes) at different nip residence times. All of the sheets were of a basis weight of 150 g/m^2.

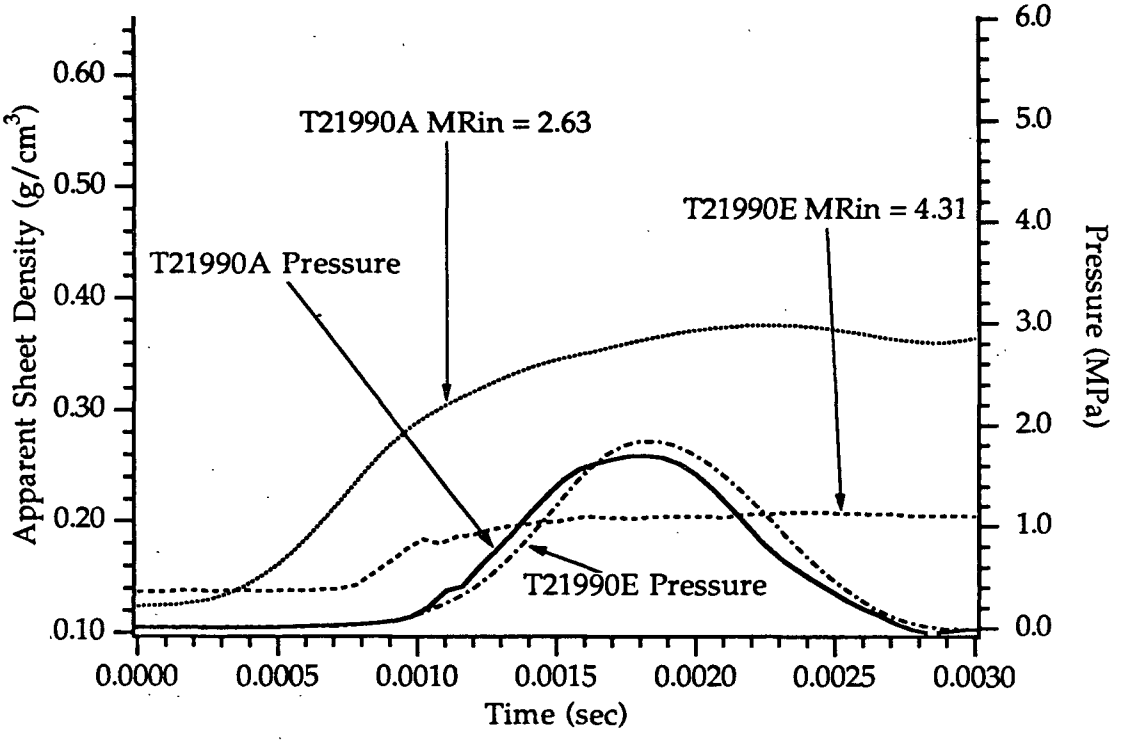

Figure 76. Sheet density-time histories for high and low freeness rock dropper-pressed handsheets. T21990A = 694 CSF softwood; T21990E = 353 CSF softwood.

The initial density of each handsheet was different because of 1) the prepressing of the sheet and 2) the type and freeness level of the furnish. It was apparent while forming the handsheets that the lower freeness pulps produced handsheets with consistently lower initial thicknesses. Refining the pulps increased the degree of fiber conformability, which resulted in the lower initial sheet thicknesses. It was also discovered that prepressing the sheet to level it on the solid ceramic plate reduced the true initial thickness of both the sheet and the flow-exiting zone. The air-drying method of reducing

the initial moisture ratio of the handsheets had little effect on the initial density of the sheet; this is in contrast to the sheets subjected to heavy pressing by Burton to reduce the initial moisture ratio of the sheets. Burton's heavily pressed sheets had a significantly higher initial density than the unpressed sheets.

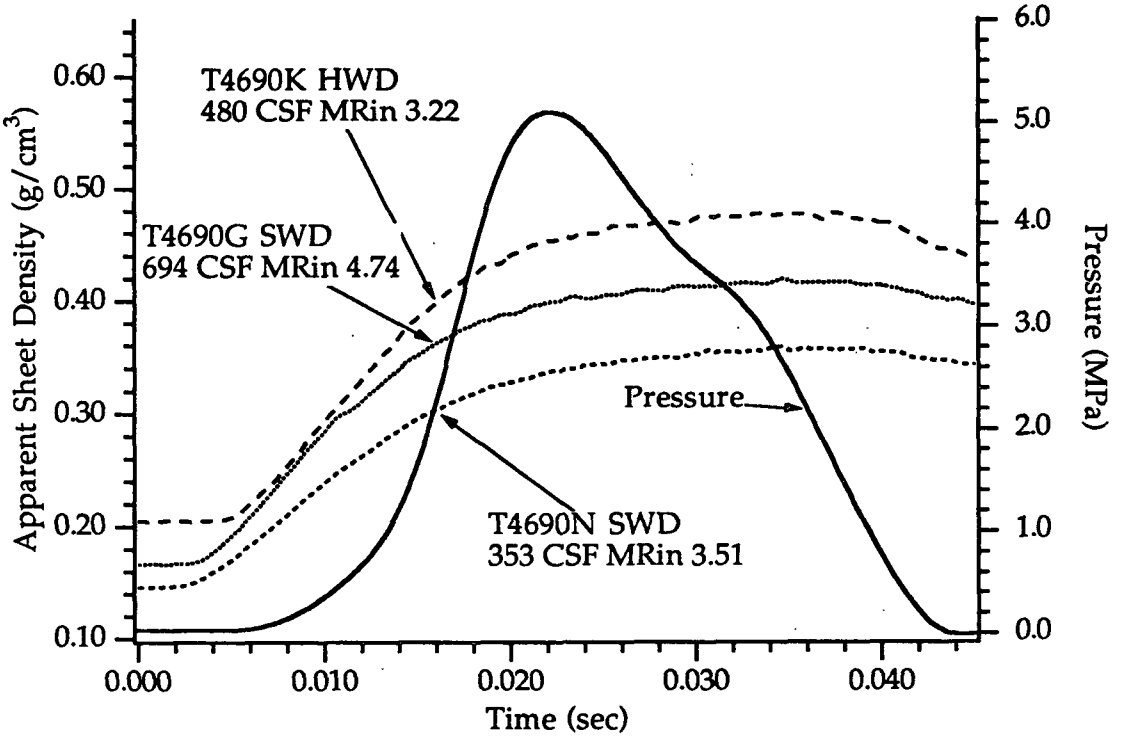

Figure 77. Sheet density-time histories for high and low freeness softwood handsheets and a low freeness hardwood handsheet.

In Figure 76, as the sheets entered the short residence time nip, some unsaturated compression occurred which compressed the fiber network and drove the air out. For these prepressed handsheets, this phase of wet pressing was very short and cannot be identified on the density profiles. For the high moisture ratio sheets, unsaturated compression represents only a small

amount of the sheet compression. As the saturation density was reached, a hydraulic pressure developed which resisted further compression. This resistance would normally be signaled by a significant change in the slope of the density-time curve in the short duration nip. In the longer duration press nip, this effect was obscured by the increased nip residence time and the reduced rate at which the compression occurred. The density-time curves in Figure 76 do show a small change in slope, but not to the extent reported by Burton. This may be due to the significantly lower press impluse applied to these handsheets. Beyond this transition point, continued dewatering and compression are controlled to a large extent by the flow resistance of the fiber network. Even though the transitions from one phase of wet pressing to the next are not as apparent as those reported by Burton, these results are still consistent with the Wahlstrom (1964) and Nilsson-Larsson (1968) wet pressing theory and with the detailed work of Carlsson (1983).

According to the Wahlstron-Nilsson-Larsson theory, the maximum density in the nip corresponds to the point at which the hydraulic pressure decays to zero. In Figure 76, it is apparent that the low moisture ratio sheet reached a higher maximum density earlier in the press nip than the high moisture sheet. The higher moisture content sheet does not appear to reach a clear maximum density. This behavior is reasonable, since the hydraulic pressure generated in the low moisture sheet should start later in the press nip and develop to a lower level when compared to the high moisture ratio sheet. After reaching the peak density, the low moisture sheet undergoes a period of constrained expansion followed by free (or unrestrained) expansion. The density data indicate that the expansion during this constrained period was not very great in the low moisture ratio sheet and was even less in the

high moisture sheet. At the point the applied pressure was released, the nip opened, and the unconstrained low moisture sheet expanded rapidly. This was not the case for the high moisture handsheet. In both of these sheets, the density profiles do not indicate the rapid sheet expansion observed by Burton. The difference in the present results and those of Burton is probably due to the use of different nip configurations and designs and the deflection of the drilled brass plate used in Burton's lower press head. As the pressure was released from the handsheet, the drilled brass plate would springback from its deflected position causing movement of the sheet away from one or more of the proximity detectors. This would result in what appeared to be rapid sheet expansion.

The differences in density-time relationships in Figure 76 demonstrate the heavy dependence of density development on sheet moisture content for the same press impulse. Most press nips have a fixed nip residence time; therefore, the more moisture present in the sheet initially, the more moisture that must be removed before a given density level can be attained. The flow resistance of the sheet inhibits the dewatering process. In order to reach the density level attained at the lower initial moisture contents and higher freeness levels, longer pressing times and/or higher press loads are required. The flow resistance in the sheet is increased by refining the furnish to a lower freeness. Subsequently, densification and dewatering are reduced as the flow resistance is increased.

Figure 77 shows the density-time relationship for three different wet pressing conditions at longer nip residence times. The initial moisture ratio, freeness, and furnish were different for each of the handsheets as summarized in Table 3. Because of its lower flow resistance, the high freeness

softwood sheet (handsheet T4690G) densifies to a greater extent than the low freeness softwood sheet (handsheet T4690N) before compression is significantly resisted by the hydraulic pressure development. The hardwood handsheet (T4690K) has the lowest moisture ratio of the three sheets, yet densifies to the greatest extent. The slope change in the low freeness softwood sheet is the most gradual of the three, suggesting a more gradual rise in the hydraulic pressure in this sheet. Of the two softwood handsheets, the high freeness sheet reaches the point of maximum density first and achieves a greater density than the low freeness sheet.

Although Figures 76 and 77 demonstrate the effects of initial moisture content, flow resistance, and nip residence time on average sheet density development, questions remain as to how this density is distributed across the sheet thickness (sheet stratification). The concept of "sheet stratification" has been described by MacGregor from both theoretical and practical aspects, and the results obtained by Burton tend to support this idea. The basic premise of sheet stratification as described by MacGregor is as follows: "... in the process of establishing flow, the sheet must deform first at the flow-exiting surface. This causes greater flow velocity and fluid shear forces here, which in turn cause even more deformation. This creates a sheet which can be more densified at the flow-exiting surface, depending on the extent of pressing." This effect was observed by Burton in the wet pressing of both high and low freeness (735 and 420 CSF) multizone (two and three zones) handsheets at short nip residence times and high moisture contents. Burton found that the initial compression of the sheet compared well with the nonuniform density development predicted by MacGregor. Burton's results showed that the hydraulic pressure gradient required for fluid flow developed

first in the flow-exiting zone (which densified first) followed by the middle and press surface zones. It was shown that the extents and rates at which the different zones densified depended heavily on the hydraulic pressure drop (flow resistance increase) across each zone as the sheet was compressing. The press surface zone encountered the greatest cumulative flow resistance and the flow-exiting zone the least; therefore, the flow-exiting zone densified to the greatest extent followed by the middle and press surface zones. Burton's results (shown in Figures 78 and 81) seem to contradict his conclusion that the density gradient is a continuous function across the sheet thickness (i.e., each zone increases in density toward the flow-exiting surface). It is obvious from Burton's figures that the density gradient was not continuously decreasing from the highest level at the flow-exiting surface to the press surface through the entire press nip. In fact, his figures (shown here as Figures 78 and 79) show that the press surface often had a higher density than the middle zone. This is in direct contrast with the density gradient proposed by MacGregor. It is believed that the inconsistency between Burton's data and MacGregor's "sheet stratification" theory is a direct result of compressibility and flexibility of the porous ceramic plate and the drilled brass plate in Burton's press nip: MacGregor's theory seems to be better supported by the work in this thesis.

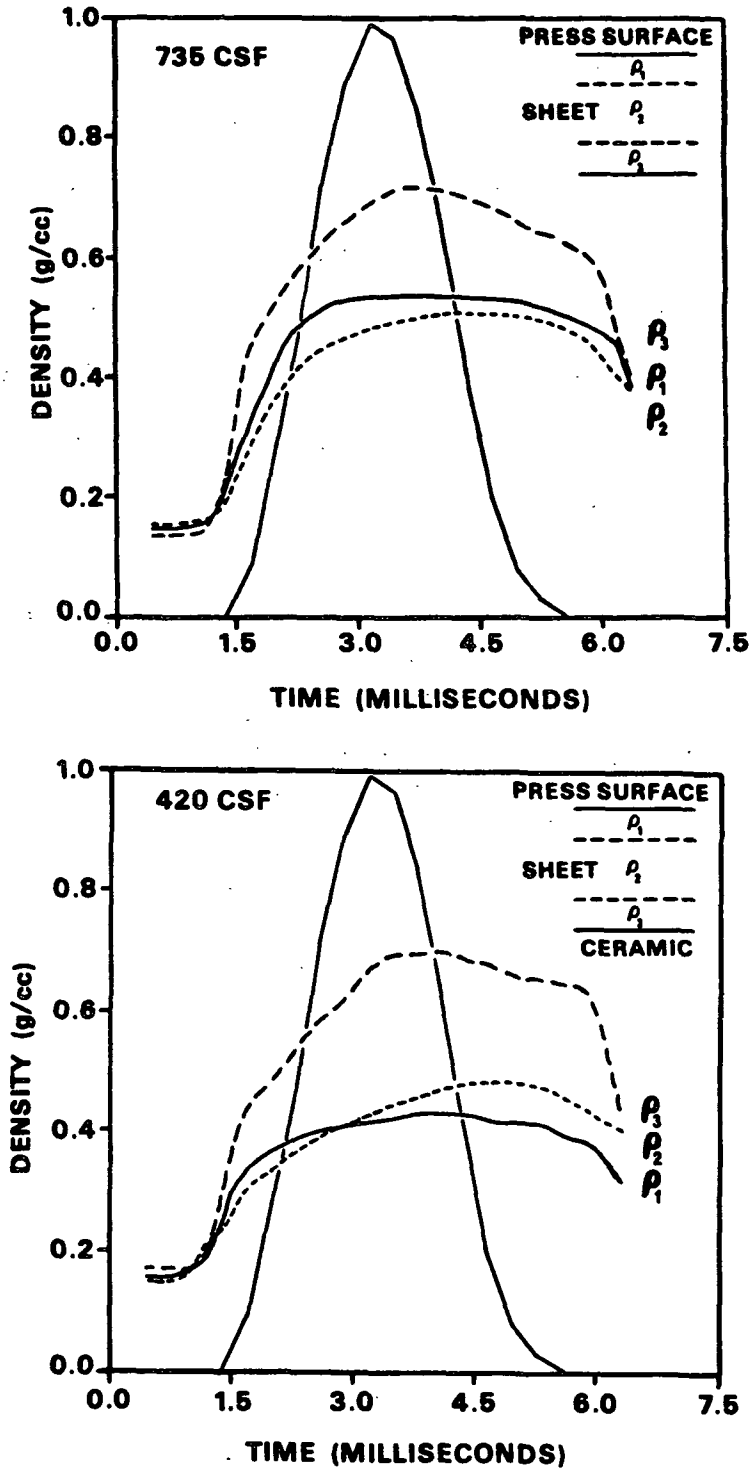

Figure 78. Densities of three sheet thickness regions having a 25-50-25 split in basis weight for regions 1-3. Basis weight = 100 g/m^2; Moisture ratio = 4.0; and Peak pressure = 7.0 MPa. (After Burton, 1987)

In contrast to the short nip residence time results obtained by Burton, a series of long nip residence time results are presented in Figures 80, 81, and 82. In these figures the density-time relationships for the high and low freeness softwood handsheets and the low freeness hardwood handsheet are plotted. The three internal zones correspond to the total sheet densities plotted in Figure 77. The solid platen zone (SPZ) represents the upper 1/3 (by weight) of the sheet adjacent to the press surface, while the middle zone (MZ) represents 1/3 (by weight) of the middle of the sheet, and the flow-exiting zone (FEZ) represents the remaining 1/3 of the sheet, next to the porous ceramic plate. In these three sheets, the flow-exiting and solid platen zones densify similarly over the entire press nip. In contrast, the middle zone in the low freeness softwood handsheet (T4690N) densifies at a lower rate initially than in either the high freeness softwood or the low freeness hardwood handsheets. Each of the zones in these handsheets indicates a growth in resistance to compression (development of hydraulic pressure) which develops immediately upon application of the compression load.

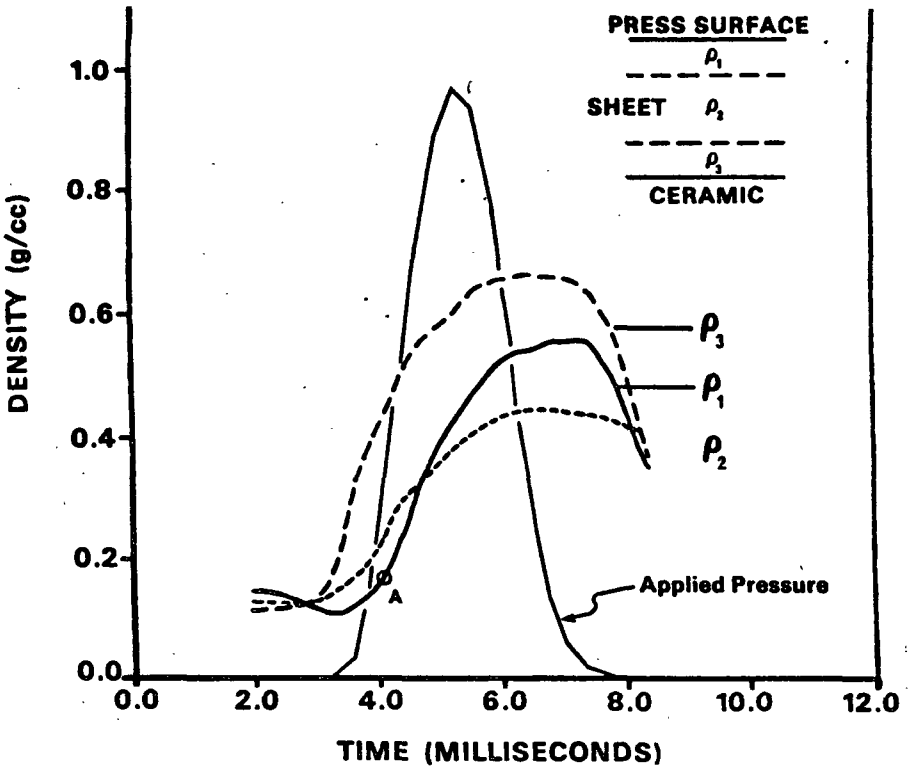

Figure 79. Density-time relationship for each of the three thickness regions. Basis weight = 170 g/m^2; Moisture ratio = 6.33; Freeness = 735 CSF; and Peak pressure = 6.5 MPa. (After Burton, 1987)

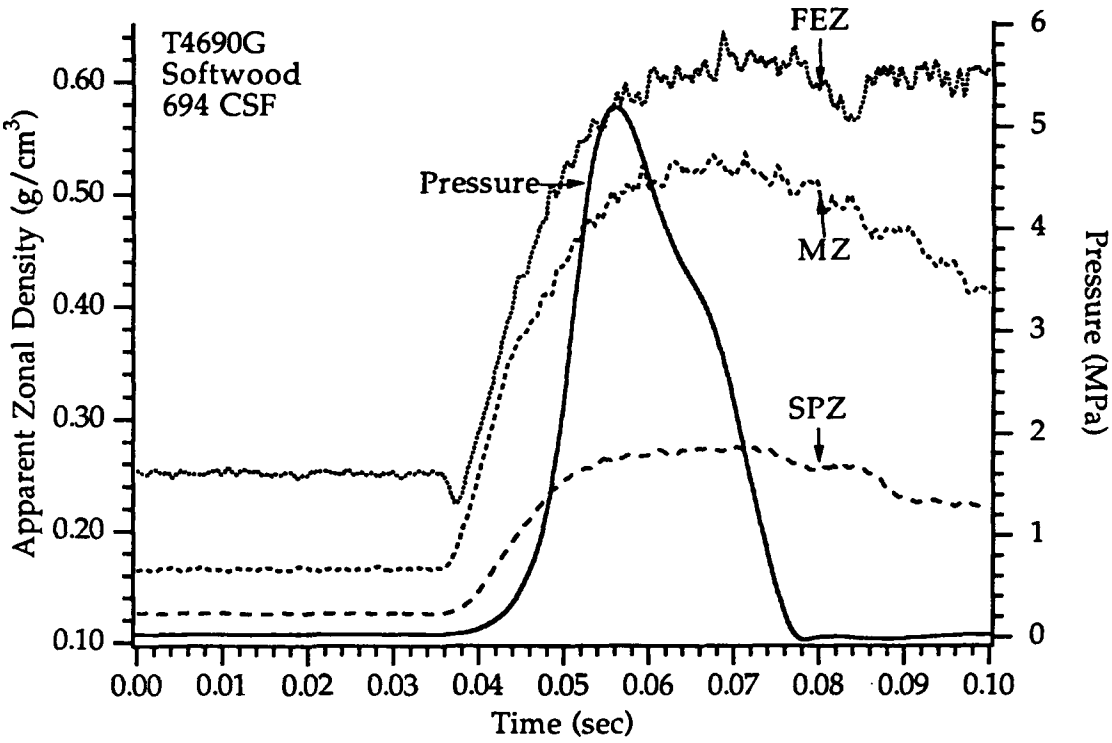

Figure 80. Density-time relationship for an MTS-pressed high freeness softwood handsheet. Basis weight = 150 g/m^2; Moisture ratio = 4.74; Freeness = 694 CSF.

The effect of long nip residence times is illustrated by the lack of a specific breakpoint in the slopes of the zonal density curves described by Burton for the short nip residence time handsheets. The zonal densities developed at different rates due to the development of a z-direction hydraulic pressure gradient which affected the compression resistance of the zones. The compression resistance was greatest at the impermeable surface and lowest at the flow-exiting surface. The effect of freeness on the rate of density development in the flow-exiting zones was not as evident as that observed by Burton (1987). Burton had observed that a large reduction in freeness (equivalent to the reduction used in these sheets) resulted in a reduction in

the rate at which densification of the sheet occurred, and therefore, a significant reduction was observed in the densification rates of the different zones in the two different freeness handsheets. In these long nip residence time wet pressing runs, the reduction of densification rate proposed by Burton was not as evident. However, it was apparent that the longer nip residence time nip reduces the freeness dependence of zonal and sheet densification as shown in Figures 80 and 81.

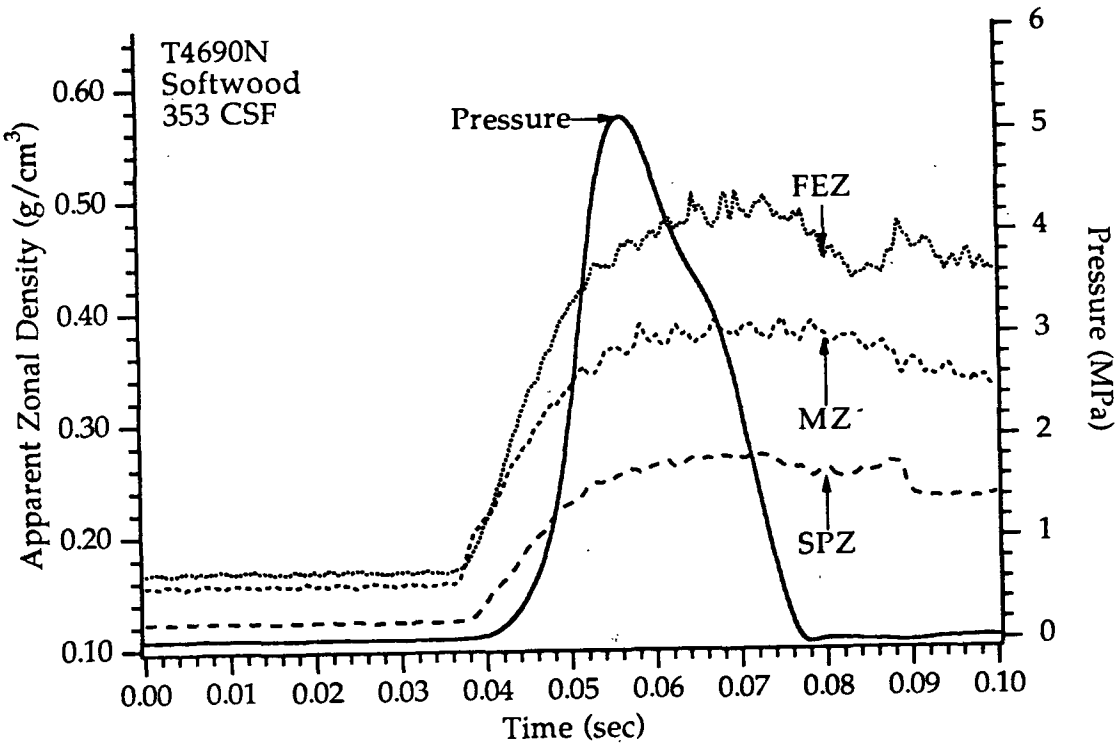

Figure 81. Density-time relationship for an MTS-pressed low freeness softwood handsheet. Basis weight = 150 g/m^2; Moisture ratio = 3.51; Freeness = 353 CSF.

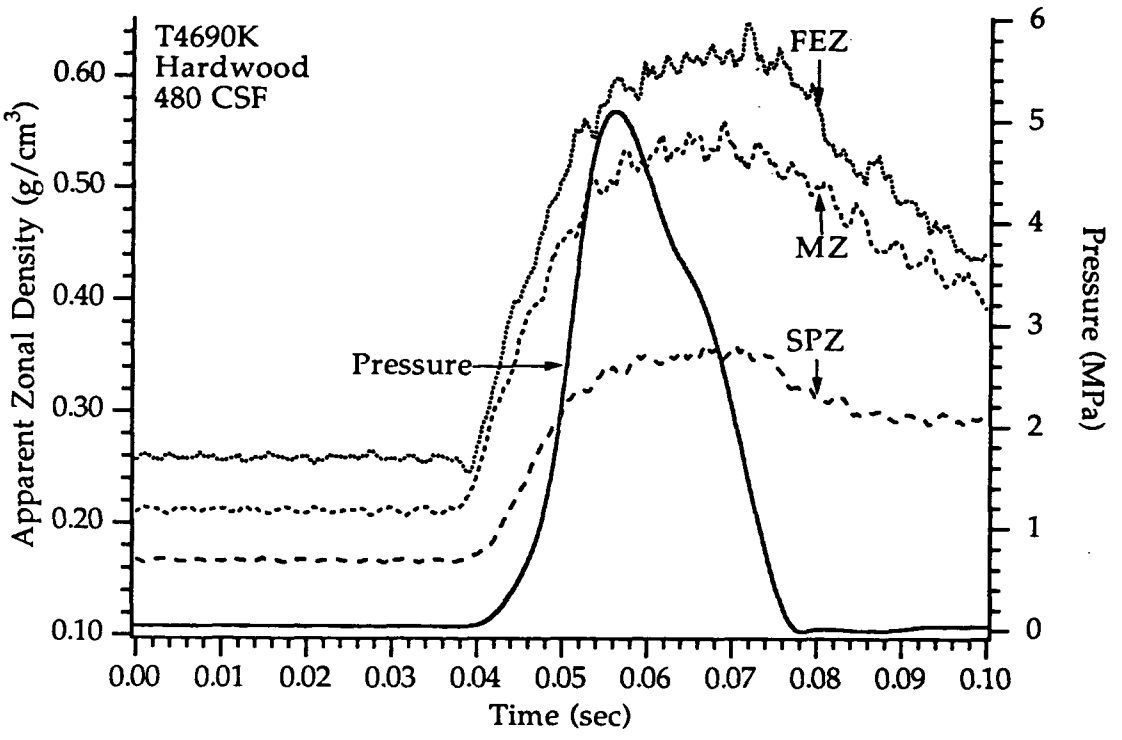

Figure 82. Density-time relationship for an MTS-pressed low freeness hardwood handsheet. Basis weight = 150 g/m^2; Moisture ratio = 3.22; Freeness = 480 CSF.

The density change observed in the zones indicates that the density increased in the direction of fluid flow. The densification wavefront is seen in the level of densification in each of the zones. The level of fiber-to-fiber transmission of the compressive force is shown in the different rates of density development in each of the zones. The level of saturation is higher in the SPZ zone and decreases in the direction of the flow-exiting surface. As water is expressed from the FEZ zone, the fibers are filtered from the consolidating fiber mat at the interface between the compressing fiber mat

and the porous ceramic plate (FEZ). This illustrates the effect of coupling the fluid flow and the mechanical compression of the sheet (development of density). The flow of fluid through the flow-exiting zone increased the density of the sheet and thereby reduced the permeability of this zone to fluid flow which increased the compressive force on the zone.

REWET IN THE EXPANSION SIDE OF THE PRESS NIP

The difference between the water removal at maximum density (minimum moisture ratio), at the exiting saturation density, and post nip gravimetric measurement indicates that only a limited amount of water is reabsorbed into the sheet as it expands inside the nip. After the nip opens, postnip rewet pulls a significant quantity of water back into the sheet. Table 5 shows the calculated water removal at midnip, exiting the nip, and after the nip opens, with the corresponding amount of reabsorbed water for each of the long nip residence time runs.

Table 5. Calculated water removal in the 150 g/m^2 handsheets at maximum density in the press nip, exiting the press nip, and post-nip, with reabsorption values for runs plotted in Figures 80, 81, and 82.[10]

Handsheet	Freeness Level (CSF)	Ingoing Moisture Ratio	Net Water Removal g/m^2 Mid-nip(MR)	Exiting-nip(MR)	Post-nip(MR)	Water Reabsorbed EN(PN)(%)
T4690G	694	4.74	466 (1.69)	448.0 (1.80)	280.1 (3.02)	3.7(39.9)
T4690N	353	3.51	221 (2.08)	205.8 (2.18)	34.1 (3.40)	6.9(84.5)
T4690K	480	3.22	180 (2.04)	156.2 (2.19)	96.0 (2.75)	13.4(46.6)

[10] The moisture ratios are in parentheses. The water reabsorbed = (midnip-exiting nip)/midnip. EN and PN are the exiting the nip and post nip water reabsorption percentages, respectively.

Ibrahim (1981) and others have described three major rewetting mechanisms which are believed to contribute to the reabsorption of water by the sheet in wet pressing. These include (1) capillary absorption in which water redistribution is due to differences in capillary structure between the flow receiver and paper, (2) film splitting in which a water film at the sheet-flow receiver interface is split as the two structures separate, and (3) mechanical absorption in which the water redistribution results from a pressure gradient. The lack of dependence of reabsorption on freeness is not consistent with the mechanism of capillary absorption. The large difference in reabsorption for the 150 g/m^2 sheets arises from the difference in initial moisture ratio. The percentage reabsorbed is approximately the same for the high freeness softwood handsheet and the low freeness hardwood handsheet. The density decrease, approximately 10%, exiting the nip, particularly in the flow-exiting zone (FEZ) provides only limited support for the theory of rewetting by mechanical reabsorption (mechanical suction or vacuum) while inside the expanding nip. There is, however, a tremendous increase in post-nip reabsorption of water, which indicates that the majority of the rewetting occurs after the nip opens in these long residence time nips.

SUMMARY

Comparison of the compression and expansion behavior of the poroelastic medium with that of the wet pressed pulp fiber handsheets indicates that in general the behavior was similar, but there are several distinct differences. In general, both exhibited different rates of compression for the different zones; a density gradient was developed in the direction of fluid flow; and the flow-exiting zone always developed the highest density.

Several differences in their compression and expansion behavior were noted. In the poroelastic medium, the point of maximum density development in each zone was the same as the point of maximum applied load, whereas in the handsheets the point of maximum density development in each zone was slightly different and occurred just past the point of maximum applied load. Also, the rates at which the zones compressed were significantly greater in the handsheets than in the poroelastic medium. This indicates that initially the handsheets were not saturated, which was a basic assumption of the poroelastic model. Also, in the handsheet most of the compression occurred within the first millisecond of load application and before the load (nip pressure) reached 0.1 MPa.

It was also apparent from examination of the zonal thickness that even with the significant refinement of the handsheet forming technique and tight control of the zonal basis weight there was little control over the thickness of the different zones. The variability in the zonal thickness was most likely the result of an uneven distribution of water in the sheet, resulting from handling of the sheet (couching, air drying, and prepressing). These conclusions are supported by the apparent lack of dependence of density development on the initial thickness or moisture content (below a certain level) of the handsheets.

Calculation of the quantity of water pulled back into the sheet, inside the nip, indicates that most of the rewet occurred after the nip opened. The quantity of water pulled back into the sheet ranged from 3.7 to 13.4% at the nip exit, whereas the postnip rewet ranged from 39.9 to 84.5% in the handsheets tested in Table 5. This conclusion is also supported by the limited

sheet expansion which was observed as the pressure in the nip was reduced to zero.

SUMMARY AND CONCLUSIONS

1. The most significant results of this investigation are the development of equipment and techniques for measurement of z-directional density gradient development. Development of this equipment and techniques offers a unique view of some of the phenomena occurring inside the wet press nip and the effects of process variables such as flow resistance (freeness), furnish, and ingoing moisture ratio on z-direction density development. As a result of this investigation, it has been possible to illustrate the coupling between fluid flow and material deformation in a highly compressible porous material and its effect on density gradient development.

2. Division of the sheet into three zones has provided the ability to examine "local" density variations in the sheet and to examine their relationship to global sheet density changes. It is the "local" density changes that have the most significant effect on the dewatering characteristics of the fiber mat, since these local density changes affect the permeability.

3. Prepressing of the handsheets to achieve better contact between the target on the bottom of the sheet and the solid ceramic plate appears to have skewed the true initial thickness of both the handsheet and the flow-exiting zone. This reduction in initial thickness of the flow-exiting zone may have affected the rate and extent of densification of this zone. The results obtained are insufficient to determine the extent to which prepressing altered the zonal compression rate and its densification.

4. In one of the short nip residence time handsheets, little difference was observed in the density of the flow-exiting zone and the middle zone. This

was attributed to the lack of development of a significant hydraulic pressure in this low moisture ratio sheet. In the high moisture ratio sheet, the hydraulic pressure gradient was probably much larger, and a large density gradient was developed across the sheet in the direction of fluid flow.

5. In the high moisture ratio longer nip residence time handsheets, a density gradient was developed which was similar to the density gradient developed in the high moisture ratio short nip residence time handsheet, which again indicates the probable development of a significant hydraulic pressure gradient.

In the high freeness softwood and the low freeness hardwood handsheets, the density profiles for the middle and flow-exiting zones were superimposable on each other. This implies that the differences in initial moisture ratio, freeness, and furnish type had little or no effect on density development above an as yet undefined minimum moisture ratio in these zones.

6. These results add support to existing wet pressing theory and to the development of sheet stratification during wet pressing.

7. Rewet in the expansion side of the nip appears to occur primarily after the nip opens. Calculation of the quantity of water pulled back into the sheet as it expands inside the nip indicates that from 3.7 to 13.4% of the water removed at the minimum sheet thickness inside the nip is pulled back into the sheet before the nip opens.

FUTURE WORK

This investigation represents a continuation of the work started by Davis *et al.* (1983) and Burton (1987) in quantitative measurement of the development of a z-direction density profile in a dynamic press nip. The results add support to existing wet pressing theory and to the development of sheet stratification during wet pressing. As a result of this work, there is an obvious need to continue refinement of the press nip and extend the technique to measurement of density gradient development in different types of press nips. It would also be useful to investigate further the effects of moisture ratio, basis weight, and pressure profile on density gradient development and develop a realistic predictive model.

The development of the density profile measurement technique is the most important instrumental contribution of this thesis. These measurements show promise for a number of other applications, such as characterization of consolidation processes, evaluation of improvements to these processes, characterization of fiber furnishes, and collection of quantitative data for process modelling. The need for fundamental information concerning permeability, porosity, and compressibility of fiber networks, especially under dynamic conditions, is a major problem in developing a mathematical model of wet pressing, and despite years of research directed at characterization of these fiber network parameters, much more work is still needed.

ACKNOWLEDGEMENTS

I would like to sincerely thank the members of my committee, Jeff Lindsay, Cyrus Aidun, and Terry Conners, for their invaluable guidance, encouragement, and contributions given throughout the course of this thesis. I am especially grateful to Dr. Terry Conners for his direction, support, and the numerous hours he devoted to advancing my work.

The financial support of this research by the Institute of Paper Science and Technology and its member companies is gratefully acknowledged. I would also like to thank Macon Kraft Co., Macon, Georgia, and Thilmany Pulp and Paper Co., Kaukauna, Wisconsin, for donating pulp for this research project.

Finally, I would like to express my appreciation to my wife, Barbara, for her continuous encouragement, love, and understanding. I would like to thank my daughter, Constance Annie, and my son, Daniel Jason, for still loving their dad after being away from home for the last two and a half years.

LITERATURE CITED

Beavers, G.S.; Hajji, A.; Sparrow, E.M. Fluid Flow Through a Class of Highly-Deformable Porous Media Part I: Experiments With Air. Trans. of ASME, J. of Fluids Engineering 103(3):432-439(September 1981).

Beavers, G.S.; Wilson, T.A.; Masha, B.A. Flow Through a Deformable Porous Material. Trans. ASME J. Applied Mechanics, 42(9):598-602(September 1975).

Beavers, G.S.; Wittenberg, K.; Sparrow, E.M. Fluid Flow Through a Class of Highly Deformable Porous Media Part II: Experiments with Water. J. of Fluids Engineering 103(3):440-444(1981).

Beck, D.A. The Dynamic Properties of Paper-machine Wet Felts in a Press Nip. 1980 Tappi Engr. Conf. pp. 181-187(1980).

Biot, M.A. General Theory of Three-Dimensional Consolidation. J. of Applied Physics 12(2):155-164(1941).

Biot, M.A. Theory of Elasticity and Consolidation for a Porous Anisotropic Solid. J. of Applied Physics 26(2):182-185(1955).

Burns, J.R.; Conners, T.E.; Lindsay, J.D. Dynamic Measurement of Density Gradient Development During Wet Pressing. Tappi 73(4):107-113(1990).

Burton, S.W.; Sprague, C.H. The Instantaneous Measurement of Density Profile Development During Web Consolidation. J. of Pulp and Paper Science 13(5):J145-J148(1987).

Burton, S.W. An Investigation of Z Direction Density Profile Development During Impulse Drying. Ph.D. Thesis. Appleton, Wisconsin. The Institute of Paper Chemistry, 1987.

Carlsson, G. Some Fundamental Aspects of the Wet Pressing of Paper. Doctor's Dissertation. Stockholm, Sweden. Dept. of Paper Tech. The Royal Institute of Technology, 1983.

Carlsson, F.; Lindstrom, T.; Norman, B. Some Basic Aspects of Wet Pressing of Paper. J. Pulp and Paper Science Canada 84(9):TR101-TR106(1983).

Caro, C.G.; Lever, M.J.; Morgan, G.E.; Parker, K.H.; Winlove, C.P. Studies of Transport in Deformable Porous Materials With Relevance to Connective Tissue Properties. J. Physiology 358:3(1984).

Ceckler, W.H.; Thompson, E.V. The University of Maine at Orono Wet Pressing Project, Final Report. University of Maine at Orono, DOE Contract No. AC02-78CS40064.M007(1982).

Ceckler, W.H.; Thompson, E.V.; Ellis, E.R.; Jewett, K.B.; Hoering, J.F.; Thorne, J.T. The University of Maine Wet Pressing Project and the Application of the Results to Optimization of Press Performance. Tappi Engr. Conf :141(1982).

Chang, N.L.; Han, S.T. Project 3258 Progress Report Two. The Institute of Paper Chemistry (July 1, 1976).

Chang, N.L. Dynamic Compression of Handsheets. 1978 Tappi Engineering Conference, Proc. Book I. San Francisco, CA. pp. 93-106(September 19-21, 1978).

Chang, N.L.; Nett, M.R.; Beck, D.A. A Comparison of a Wahren-Zotterman Press Simulator and a Pilot Press Nip. Journal of Pulp and Paper Science 12(2):J39-J43(1986).

Challen, J.M. The Solution of the Diffusion Equation With Non-Constant Diffusivity. Graduation Thesis. University of Sidney (1966).

Cowan, W.F. An Investigation of the Hot Surface Drying of Glass Fiber Beds. Ph.D. Thesis. Appleton, WI, The Institute of Paper Chemistry (June 1961).

Cribb, J.L. On the Mechanics of Sugar Cane Crushing. Australian Journal of Applied Science 15:106(1964).

Davis, E.J.; Stratton, R.A.; Chang, N.L. Water Removal Studies with the Wet Press Simulator. Journal of Pulp and Paper Science 9(3):TR68-TR73(1983).

El-Hosseiny, F. Compression Behavior of Press Felts and Wet Webs. Nordic Pulp and Paper Res. J. 5(1):28-32(March 1990)

Fang, Y.P. Unpublished Ph.D. Thesis. Appleton, WI, The Institute of Paper Chemistry (June 1986).

Gibson, R.E.; England, G.L.; Hussey, M.J.L. The Theory of One-Dimensional Consolidation of Saturated Clays 1. Finite Non-Linear Consolidation of Thin Homogeneous Layers. Geotechnique 17:261-273(1967).

Habeger, C.C.; Mann, R.W.; Baum, G.A. Ultrasonic Plate Waves in Paper. Ultrasonics 17(2):57-62(March 1979).

Heller, H.H.; Tewksbury, C.G. What Are the Limits of Paper Dryness Obtainable in a Wet Press? Tappi 55(6):893-896(1972).

Ibrahim, A.A. Survey: Understanding Rewetting Phenomenon in the Pressing Operation. Pulp and Paper Can. 82(2):T46-9(February 1981).

Jaavidaan, Y. Experimental and Theoretical Study of Two-Phase Flow Through Compressible Porous Media With Application to Sheet Rewetting in Wet Pressing of Paper. Ph.D. Thesis. University of Maine at Orono (May 1987).

Jantunen, J. Viscoelastic Properties of Wet Webs Under Dynamic Conditions. Papermaking Raw Materials. Their Interaction with the Production Process and Their Effect on Paper Properties. 8th Fundamental Research Symposium, Oxford, England, September 1985, Vol. 1, pp. 133-162(1985).

Jewett, K.B. A Two Phase Flow Model of a Transversal Flow Press Nip. M.S. Thesis, University of Maine at Orono, (December 1980).

Jewett, K.B. The Application of a Model for Two Phase Flow Through a Compressible Porous Media to the Wet Pressing of Paper. Ph.D. Thesis. University of Maine at Orono, (September 1984).

Jewett, K.B.; Ceckler, W.H.; Busker, L.; Co, A. Computer Model of a Transversal Flow Press Nip. AIChE Symposium Series New Process Alternatives in the Forest Products Industries. No. 200 vol. 76,pp. 59-70(1980).

Kerekes, R.J.; McDonald, J.D. A Decreasing Permeability Model of Wet Pressing. 76th CPPA Annual Meeting Technical Section. Montreal, Quebec (February 1-2, 1990).

Kerekes, R.J.; McDonald, J.D. A Decreasing Permeability Model of Wet Pressing: Theory. Tappi 1991 Engineering Conference, Nashville, Tennessee(1991).

Kline, S.J. The Purpose of Uncertainty Analysis. J. Fluids Eng., ASME, 107:153-160(June 1982).

Lai, W.M.; Mow, V.C. Drag-Induced Compression of Articular Cartilage During a Permeation Experiment. Biorheology 17(1/2):111-123(1980).

Lanir, Y.; Sauob, S.; Maretsky, P. Nonlinear Finite Deformation Response of Open Cell Polyurethane Sponge to Fluid Filtration. Trans. of the ASME, J. of Applied Mechanics 57(6):449-454(1990).

Lindsay, J.D. The Anisotropic Permeability of Paper: Theory, Measurements, and Analytical Tools. IPC Technical Paper Series #298, Appleton, WI (July 1988).

Lindsay, J.D. Class notes from A241 Flow Through Porous Media, Inst. of Paper Sci. and Technology(1989).

MacGregor, M.A. Pressure Profiles in a Press Nip: The Role of the Wet Felt. Tappi Engr. Conf. Hyatt Regency Hotel, Houston, Texas, pp. 41-49(Oct. 4-7, 1976).

MacGregor, M.A. Pressure Profiles in a Press Nip: The Role of the Wet Felt. Tappi 60(7):86-88(1977).

MacGregor, M.A. Tappi Engineering Conf. 1982, pp. 9-24, San Francisco Hilton, San Francisco, California (September 13-16, 1982).

MacGregor, M.A. A Description of Sheet Stratification Caused by Wet Pressing. Tappi 66(6):53-57(1983).

MacGregor, M.A. Paper Defects Caused by Fluid Shear Force During Pressing. Tappi Notes, Practical Aspects of Pressing and Drying, Geneva, Switzerland (March 16-20, 1985).

MacGregor, M.A. Practical Effects of Sheet Stratification Caused by Wet Pressing. Tappi Notes, Practical Aspects of Pressing and Drying, Geneva, Switzerland (March 16-20, 1985).

Manins, P.C.; Roberts, B.W. Compression of an Elastoporous Medium. Int. J. Non-Linear Mechanics 13:75-93(1975).

Moffat, R.J. Contributions to the Theory of Single-sample Uncertainty Analysis. J. Fluids Eng., ASME, 107:161-164(June 1985).

Nelson, R.W. Approximate Theories of Filtration and Retention. Tappi 47(12):752-764(1964).

Nelson, R.W.; Chang, N.L.; Han, S.T. Dynamic Compression of Saturated Fiber Mats. Transactions: 6th Symposium Session 4, No. 2-1(1964).

Nilsson, P.; Larsson, K.O. Paper Web Performance in a Press Nip. Pulp and Paper Mag. of Canada Technical Paper T438-T445, (12):66-73(1968).

Parker, K.H.; Mehta, R.V.; Caro, C.G. Steady Flow in Porous, Elastically Deformable Materials. Trans. of the ASME, J. of Applied Mechanics 54():794-800(1987).

Philip, J.R. Kinetics of Sorption and Volume Change in Clay-Colloid Pastes. Aust. J. Soil Res. 6:249-267(1968).

Roux, J.C. Modelisation et Optimisatioin du Fonctionnement d'une Section de Presse(s) de Machine a Papier. Ph.D. Thesis. Grenoble, France, L' Institut National Polytechnique de Grenoble (October 1986).

Smith, I.M.; Griffiths, D.V. Programming the Finite Element Method. 2nd ed. Wiley(1988).

Szikla, Z.; Paulapuro, H. Compression Behavior of Fibre Mats in Wet Pressing. Ninth Fundamental Research Symposium, Cambridge, England (September 17-22, 1989 a).

Szikla, Z.; Paulapuro, H. Changes in Z-Direction Density Distribution of Paper in Wet Pressing. J. of Pulp and Paper Sci. 15(1):J11-J17(1989 b)

Wahlstrom, P.B. A Long Term Study of Water Removal and Moisture Distribution on a Newsprint Machine Press Section. Pulp Paper Mag. Canada 61:T379,T418(1964).

Wahlstrom, P.B. Our Present Understanding of the Fundamentals of Wet Pressing. Pulp and Paper Mag. Canada 70:T349(1969).

Wahlstrom, P.B. New Developments and New Insights in Water Removal by Pressing. EUCEPA Conf. Proceedings, London pp. 92 (1979).

Wahren, D.; Zotterman, C. Paper Trade J. 162(16):37(1978).

Westra, H.A. A New Contribution to Press Nip Analysis. 1975 Int. Water Removal Symp. 109th Conf. London, Symp. Supplement to Paper Technology and Industry, pp. 66-89 (1975).

Wicks, L. The Influence of Pressing on Sheet Two-Sidedness. Tappi 65(9):73-77(1982).

APPENDIX I

Listing of Data Acquisition Program

```
100 ! This program collects, displays & stores time & thickness data
110 ! It is a limited capability program - it is not operator proof !
120 !
130 !      Written by D.R. Wheeler
140 !      2-23-87
150 !      Modified by J. R. Burns
160 !        4-6-87,4-17-87,4-20-87,4-28-87,8-12-87,9-14-87,10-7-87,10-14-87,12-3-87,6-16-88,2-5-89
170 SET DIALOG COLOR 14,1,1
180 SET CASE OFF
190 CLEAR
200 ! PRINT AT 12,10:"Pressure pulse data collection for HYDRAULIC PRESSURE"
210 ! PRINT AT 14,25:"Press <ANY KEY> to continue."
220 ! INPUT KEY WAIT Rsp$
230 ON ERROR GOTO Crisis
240 Toot$ = CHR$(7)
250 CLEAR
260 ! PRINT "Place data disk in drive A, B, or C & press <ANY KEY> when ready."
270 ! INPUT KEY WAIT Rsp$
280 CLEAR
290 ! Defining the file size ie. the number of data points per channel
300 Filsiz = 1000
310 PRINT "Setting program parameters . . ."
320 DIM Timfil[Filsiz],Dc[Filsiz],Dd[Filsiz]
330 DIM
Press[Filsiz],Hydpress[Filsiz],Totp[Filsiz],Da[Filsiz],Db[Filsiz],Lowhydpress[Filsiz],Dhead[
Filsiz]
340 Timfil = 0 ! Press = 0 ! Hydpress = 0 ! Totp = 0 ! Da = 0 ! Db = 0 ! Dc = 0 ! Dd = 0 !
Lowhydpress = 0 ! Dhead = 0 ! Filnam$ = " " ! Filnama$ = ""
350 Mflag = 0
360 Firstflag = 1
370 !
380 ! open com port 1 to receive the data
390 !
400 !
410 OPEN #1:"com1","f" ! open com port to Trans-Era
420 !
430 ! set Trans-Era parameters
440 !
450 PRINT "Defining data acquisition system . . ."
460 PRINT " Channel a1 is used for hydraulic pressure  (GAIN = 4) "
470 PRINT " Channel b1 is used for hydraulic pressure  (GAIN = 4) "
480 PRINT " Channel c1 is used for total pressure      (GAIN = 4)"
490 PRINT " Channel a3 is used for proximity detector A (GAIN = 4)"
500 PRINT " Channel b3 is used for proximity detector B (GAIN = 4)"
510 PRINT " Channel c3 is used for proximity detector C (GAIN = 4)"
520 PRINT " Channel d3 is used for proximity detector D (GAIN = 4)"
```

```
530 PRINT " Channel d1 is used for proximity detector E (GAIN = 4)"
540 !           d7
550 !
560 !
570 PRINT #1:"CAL;"
580 PRI #1:"dfn 1 1000 4 3 1000 4 4 1000 4 5 1000 4 6 1000 4 7 1000 4 8 1000 4;"
590 Defnc:
600 PRINT #1:"dfnc a1 0 1;"
610 PRINT #1:"dfnc b1 0 1;"
620 ! PRINT #1:"dfnc c1 0 1;"
630 PRINT #1:"dfnc d1 0 1;"
640 PRINT #1:"dfnc a3 0 1;"
650 PRINT #1:"dfnc b3 0 1;"
660 PRINT #1:"dfnc c3 0 1;"
670 PRINT #1:"dfnc d3 0 1;"
680 ! set the trigger channel and the trigger level also define the channel
690 ! the trigger is on the rising total force transducer channel b2
700 Trigger:
710 PRINT #1:"tri 1 b1 .05;" ! trigger off the total force
720 !
730 ! send the period to the TransEra
740 !
750 PRINT #1:"per 100e-6;"
760 !
770 ! get the error from the TransEra
780 !
790 PRINT #1:"ge;"
800 INPUT #1:Tge$
810 Wrtflag = 0
820 PRINT "Filling 'time' file . . ."
830 PRINT #1:"gper;"
840 INPUT #1:Period
850 ! fill the time array with numbers that correspond to the time
860 Timfil[1] = 0
870 FOR X = 2 TO Filsiz
880   Timfil[X] = Timfil[X-1]+Period
890 NEXT X
900 !
910 Menu:
920 !
930 CLEAR
940 Mflag = 0
950 FOR X = 1 TO 79
960   PRINT "_";
970 NEXT X
980 PRINT ! PRINT
990 PRINT " HP2.NEW the last file saves was - ";Filnama$
1000 FOR X = 1 TO 79
1010   PRINT "_";
1020 NEXT X
1030 PRINT
1040 PRINT ! PRINT ! PRINT
1050 PRINT "      1. Collect data and calculate values."
1060 PRINT "      2. View RAW data"
```

```
1070 PRINT "      3. View CALCULATED THICKNESS data"
1080 PRINT "      4. Write RAW data to disk, specify the drive 1st"
1090 PRI "      5. Write CALCULATED THICKNESSES to disk, specify the drive 1st"
1100 PRINT "      6. Make a HARDCOPY of the CALCULATED THICKNESS DATA"
1110 PRINT "      7. MAKE A PLOT OF THE CALCULATED THICKNESS DATA"
1120 PRINT "      8. Average the data before Plotting"
1130 PRINT "      9. EXIT THE PROGRAM"
1140 PRINT
1150 INPUT KEY WAIT Rsp$
1160 IF Rsp$="1" THEN GOTO Analogin
1170 IF Rsp$="2" THEN GOTO Scrnprnt
1180 IF Rsp$="3" THEN GOTO Scrnprnt1
1190 IF Rsp$="4" THEN GOTO Dskwrt1
1200 IF Rsp$="5" THEN GOTO Dskwrt
1210 IF Rsp$="6" THEN GOTO Makegraph
1220 IF Rsp$="7" THEN GOTO Makegraph
1230 IF Rsp$="8" THEN GOTO Menu
1240 IF Rsp$<>"9" THEN GOTO 1150
1250 IF Wrtflag=0 THEN GOTO 1290
1260 PRINT ! PRINT ! PRINT
1270 PRINT "  PROGRAM   HAS BEEN    TERMINATED"
1280 END
1290 PRINT ! PRINT
1300 PRINT "          ";
1310 SET DIALOG COLOR 12,1,1
1320 PRINT "      Last data file was NOT written to disk !!! ";
1330 SET DIALOG COLOR 14,1,1
1340 PRINT ! PRINT
1350 PRINT "          You have one more chance . . . "
1360 PRINT
1370 PRINT "          Press the number of your choice . . ."
1380 Wrtflag = 1
1390 GOTO 1150
1400 !
1410 Analogin:
1420 !
1430 OPEN #1:"com1","f" ! open com1 port to Trans-Era
1440 IF Firstflag=1 THEN GOTO 1470
1450 IF Wrtflag=0 THEN GOTO 1290
1460 !
1470 Firstflag = 0
1480 CLEAR
1490 PRINT "Press <ANY KEY> when ready to collect data . . ."
1500 INPUT KEY WAIT Rsp$
1510 PRINT "Waiting for trigger on channel c1 total applied force . . ."
1520 !
1530 ! set up for analog input from the channels
1540 ! define the number of data points and the number of points that are to be retained before
the
1550 ! scale the channels in the TransEra
1560 !
1570 PRINT #1:"ai 1000.450 a1 1 2 b1 3 4 d1 4 4 a3 5 4 b3 6 4 c3 7 4 d3 8 4;"
1580 PRI #1:"sca 1 1 181.0829 0;" ! scale factor for the MTS Force TD Channel A1
1590 ! PRINT #1:"sca 2 2 197.628 0;" ! scale factor for the
```

```
1600 PRINT #1:"sca 3 3 565.918 0;" ! scale factor for the PCB-896 Channel b1
1610 PRINT #1:"sca 4 4 .1488 .12874;" ! detector E 3/26/90
1620 PRINT #1:"sca 5 5 .11032 -3.2866e-3;" ! detector A
1630 PRINT #1:"sca 6 6 .10943 2.3688e-3;" ! detector B
1640 PRINT #1:"sca 7 7 .10891 1.1753e-3;" ! detector C
1650 PRINT #1:"sca 8 8 .10987 -6.0573e-3;" ! detector D
1660 PRINT #1:"ge;"
1670 INPUT #1:Rsp$
1680 PRINT "Data from channels a1,b1,c1,d1,a3,b3,c3,d3 collected & scaled."
1690 PRINT "Data transfer in progress . . ."
1700 Ti$ = TIME
1710 PRINT Ti$
1720 ! get the data from the TransEra by dumping the buffers to the computer
1730 ! input the data from the transera
1740 PRINT #1:"wr 1;"
1750 INPUT #1:Rsp$
1760 FOR X = 1 TO Filsiz
1770  INPUT #1:Lowhydpress[X]
1780 NEXT X ! channel a1 PCB
1790 PRINT " GOT CHANNEL A1"
1800 ! PRINT #1:"wr 2;"
1810 ! INPUT #1:Rsp$
1820 ! FOR X = 1 TO Filsiz
1830 ! INPUT #1:Hydpress[X]
1840 ! NEXT X ! channel b1 low hyd pressure PCB
1850 PRINT " GOT CHANNEL B1"
1860 PRINT #1:"wr 3;"
1870 INPUT #1:Rsp$
1880 FOR X = 1 TO Filsiz
1890  INPUT #1:Totp[X]
1900 NEXT X ! channel c1 total applied force
1910 PRINT " GOT CHANNEL C1"
1920 PRINT #1:"wr 4;"
1930 INPUT #1:Rsp$
1940 FOR X = 1 TO Filsiz
1950  INPUT #1:Dhead[X]
1960 NEXT X ! channel d1 proximity detector E
1970 PRINT " GOT CHANNEL D1"
1980 PRINT #1:"wr 5;"
1990 INPUT #1:Rsp$
2000 FOR X = 1 TO Filsiz
2010  INPUT #1:Da[X]
2020 NEXT X ! channel a3 proximity detector A
2030 PRINT " GOT CHANNEL A3"
2040 PRINT #1:"wr 6;"
2050 INPUT #1:Rsp$
2060 FOR X = 1 TO Filsiz
2070  INPUT #1:Db[X]
2080 NEXT X ! channel b3 proximity detector B
2090 PRINT " GOT CHANNEL B3"
2100 PRINT #1:"wr 7;"
2110 INPUT #1:Rsp$
2120 FOR X = 1 TO Filsiz
2130  INPUT #1:Dc[X]
```

```
2140 NEXT X ! channel c3 proximity detector C
2150 PRINT " GOT CHANNEL C3"
2160 PRINT #1:"wr 8;"
2170 INPUT #1:Rsp$
2180 FOR X = 1 TO Filsiz
2190  INPUT #1:Dd[X]
2200 NEXT X ! channel d3 proximity detector D
2210 PRINT " GOT CHANNEL D3"
2220 ! FOR X = 1 TO Filsiz-1
2230 ! Da[X] = Da[X+1]
2240 ! Db[X] = Db[X]-0.8*(Db[X]-Db[X+1])
2250 ! Dc[X] = Dc[X]-0.6*(Dc[X]-Dc[X+1])
2260 ! Dd[X] = Dd[X]-0.4*(Dd[X]-Dd[X+1])
2270 PRINT #1:"max 3;"
2280 INPUT #1:Peakpress
2290 PRINT #1:"min 8;"
2300 INPUT #1:Minthick
2310 PRINT #1:"max 5;"
2320 INPUT #1:Maxthick
2330 ! NEXT X
2340 ! Tb = Db-Da
2350 ! Tc = Dc-Db
2360 ! Td = Dd-Dc
2370 Ti$ = TIME
2380 PRINT Ti$
2390 PRINT "Calculations in progress "
2400 ! calculation of the distances to the targets and the pressure
2410 FOR X = 1 TO Filsiz-1
2420  Lowhydpress[X] = Lowhydpress[X]-0.2*(Lowhydpress[X]-Lowhydpress[X+1])
2430  Hydpress[X] = Hydpress[X]-0.2*(Hydpress[X]-Hydpress[X+1])
2440  Totp[X] = Totp[X]-0.2*(Totp[X]-Totp[X+1])
2450 NEXT X
2460 !
2470 ! calculation of the thickness of the layers
2480 !
2490 Wrtflag = 0
2500 GOTO Menu
2510 !
2520 Scrnprnt:
2530 !
2540 CLEAR
2550 PRINT ! PRINT
2560 PRINT "          ";
2570 SET DIALOG COLOR 10,1,1
2580 PRINT "The peak pressure was ";Peakpress;"  psi."
2590 ! PRINT "The peak hydraulic pressure was ";Peakhydpress;" psi."
2600 SET DIALOG COLOR 14,1,1
2610 PRINT
2620 PRINT "Press <ANY KEY> to look at data."
2630 PRINT ! PRINT "Press 'm' to return to menu,"
2640 PRINT
2650 PRINT "Ctrl/s will halt listing and any key will restart it."
2660 INPUT KEY WAIT Rsp$
2670 CLEAR
```

```
2680 Xs = 22 ! X = 0
2690 SLEEP 2
2700 CLEAR
2710 PRINT AT 1,1:"HydPress     Low hyd press     Totp     Time"
2720 PRINT
2730 X = X+1
2740 IF X>Filsiz THEN GOTO 2840
2750 PRI USI
"6d.5d,3x,6d.5d,3x,6d.5d,3x,0d.6d":Hydpress[X],Lowhydpress[X],Totp[X],Timfil[X]
2760 INPUT KEY M$
2770 IF M$<>"m" THEN GOTO 2800
2780 Mflag = 1
2790 GOTO 2840
2800 Xs = Xs-1
2810 IF Xs>0 THEN GOTO 2730
2820 Xs = 22
2830 GOTO 2690
2840 IF Mflag=1 THEN GOTO Menu
2850 PRINT
2860 PRINT "          Press <ANY KEY> to return to menu."
2870 INPUT KEY WAIT Rsp$
2880 Mflag = 0
2890 GOTO Menu
2900 !
2910 Scrnprnt1:
2920 !
2930 CLEAR
2940 PRINT ! PRINT
2950 PRINT "          ";
2960 SET DIALOG COLOR 10,1,1
2965 Peakpress = 0
2970 PRINT "The peak pressure was ";Peakpress;"  psi."
2975 Peakpress = 0
2980 ! PRINT "The peak hydraulic pressure was ";Peakhydpress;" psi."
2990 SET DIALOG COLOR 14,1,1
3000 PRINT
3010 PRINT "Press <ANY KEY> to look at data."
3020 PRINT ! PRINT "Press 'm' to return to menu,"
3030 PRINT
3040 PRINT "Ctrl/s will halt listing and any key will restart it."
3050 INPUT KEY WAIT Rsp$
3060 CLEAR
3070 Xs = 22 ! X = 0
3080 SLEEP 2
3090 CLEAR
3100 PRINT AT 1,1:"Time      A      B      C      D    Head"
3110 PRINT
3120 X = X+1
3130 IF X>Filsiz THEN GOTO 3230
3140 PRI USI
"0d.6d,2x,2d.5d,2x,2d.5d,2x,2d.5d,2x,2d.5d,2x,2d.5d":Timfil[X],Da[X],Db[X],Dc[X],Dd[X],Dhead[X]
3150 INPUT KEY M$
3160 IF M$<>"m" THEN GOTO 3190
3170 Mflag = 1
```

```
3180 GOTO 3230
3190 Xs = Xs-1
3200 IF Xs>0 THEN GOTO 3120
3210 Xs = 22
3220 GOTO 3080
3230 IF Mflag=1 THEN GOTO Menu
3240 PRINT
3250 PRINT "          Press <ANY KEY> to return to menu."
3260 INPUT KEY WAIT Rsp$
3270 Mflag = 0
3280 GOTO Menu
3290 !
3300 Dskwrt:
3310 GOTO Menu
3320 CLEAR
3330 PRINT ! PRINT
3340 INPUT PROMPT "Enter the CALCULATED DATA disk filename -> ":Filnam$
3350 Filnama$ = Filnam$
3360 OPEN #2:Filnama$,"w"
3370 PRINT "Writing CALCULATED DATA to disk . . ."
3380 PRINT #2:Filsiz
3390 FOR X = 1 TO Filsiz
3400  PRI #2 USI
"0d.6d,1x,6d.5d,1x,6d.5d,1x,6d.5d,1x,6d.5d,1x,6d.5d,1x,6d.5d":Timfil[X],Hydpress[X],Lowhyd
press[X],Totp[X],Tb[X],Tc[X],Td[X]
3410 NEXT X
3420 CLOSE #2
3430 Wrtflag = 1
3440 GOTO Menu
3450 !
3460 !
3470 Dskwrt1:
3480 !
3490 CLEAR
3500 PRINT " Last file written - ";Filnam$
3510 PRINT ! PRINT
3520 INPUT PROMPT "Enter the RAW DATA disk filename -> ":Filnam$
3530 Filnama$ = Filnam$
3540 OPEN #2:Filnama$,"w"
3550 PRINT "Writing RAW data to disk . . ."
3560 ! PRINT #2:Filsiz
3565 ! INPUT #2:Rsp$
3570 PRI #2:"  Time      Hyd P    L Hyd P     TotP      A         B       C       D       E"
3580 FOR X = 1 TO Filsiz
3590  PRI
#2:Timfil[X],Hydpress[X],Lowhydpress[X],Totp[X],Da[X],Db[X],Dc[X],Dd[X],Dhead[X]
3600 NEXT X
3610 CLOSE #2
3620 Wrtflag = 1
3630 GOTO Menu
3640 !
3650 Crisis:
3660 !
3670 IF Ern=6 THEN GOTO 3780
```

```
3680 SET DIALOG COLOR 0,4,4
3690 CLOSE
3700 PRINT Toot$
3710 PRI "Error # ";Ern;"  has occured at line ";Erl; ! SET DIA COL 14,1,1
3720 PRINT
3730 SET DIALOG COLOR 0,4,4
3740 PRINT "This run may still be salvagable."; ! SET DIALOG COLOR 14,1,1
3750 PRINT
3760 SET DIALOG COLOR 14,1,1
3770 PRINT
3780 PRINT "Program aborted."
3790 END
3800 !
3810 Purge:
3820 !
3830 Purgecount = 0
3840 OPEN #3:"com1","f"
3850 INPUT #3:Stuff$
3860 PRINT "Item # ";Purgecount;" = ";Stuff$
3870 Purgecount = Purgecount+1
3880 GOTO 3850
3890 Makegraph:
3900 ! This is the most current program 4/28/87 graphics routine for plotting
3910 ! pressure and calculated thickness data
3920 INPUT PROMPT "Enter the test number  ":X$
3930 IF Rsp$="6" THEN SET GRAPH DEVICE "hiplt=com2"
3940 IF Rsp$="7" THEN SET GRAPH DEVICE "gcon=ega"
3950 IF Rsp$="7" THEN SET GRAPH 4
3960 ! SET COLOR 7
3970 SET CLIP OFF
3980 Svp1 = 10 ! Svp2 = 130 ! Svp3 = 10 ! Svp4 = 90 ! Sbcol = 1
3990 !
4000 SET POINT STYLE 0
4010 CALL Make_screen(0,0,1,1)
4020 A$ = "Hyd Pressure  " & DATE & " - " & X$
4030 B$ = "       Time(msec)"
4040 L$ = "        Thickness(mils)"
4050 ! P$ = STR$(Peakpress)
4060 D$ = "     Pressure(psi) MAX = "
4070 E$ = "0     6     12     18     24     30"
4080 F$ = "0     250     500     750     1000"
4090 G$ = "20     15     10     5     0       "
4100 ! CALL Putext3(1,4,L$)
4110 CALL Putext3a(1,4,E$)
4120 CALL Putlftscal(1,4,F$)
4130 CALL Putext1(1,4,A$)
4140 CALL Putext(1,4,B$)
4150 CALL Putext2(1,4,D$)
4160 CALL Putrtscal(1,4,G$)
4170 Rxp$ = "n"
4180 SET CLIP ON
4190 IF Rxp$="y" OR Rxp$="Y" THEN SET CLIP OFF
4200 !
4210 SET POINT STYLE 0
```

```
4220 SET VIEWPORT 10,130,10,90
4230 ! set the window to match the time in milliseconds and the pressure in psi
4240 Bottom = -15.0 ! Top = 1000
4250 SET WINDOW 0,Filsiz*Period,Bottom,Top ! left, right, bottom, top
4260 SET TEXT COLOR 3
4270 SET LINE COLOR 3 ! 3 = black
4280 PLOT TEXT GDU AT 90,95:"Low Hydraulic Pressure"
4290 PLOT Timfil,Lowhydpress ! plot the hydraulic pressure second
4300 !
4310 SET LINE COLOR 4
4320 SET TEXT COLOR 4
4330 PLOT TEXT GDU AT 90,90:"Total Applied Pressure"
4340 PLOT Timfil,Totp
4350 ! make the axis tic marks for the pressure axis
4360 Thickness:
4370 Bottom = -0.1 ! Top = 0.5
4380 SET WINDOW 0,Filsiz*Period,Bottom,Top
4390 SET LINE COLOR 2 ! 2 = red
4400 SET TEXT COLOR 2
4410 PLOT TEXT GDU AT 90,85:"Da"
4420 PLOT Timfil,Da
4430 SET LINE COLOR 5
4440 SET TEXT COLOR 5
4450 PLOT TEXT GDU AT 90,80:"Db"
4460 PLOT Timfil,Db
4470 SET TEXT COLOR 6
4480 SET LINE COLOR 6
4490 PLOT TEXT GDU AT 90,75:"Dc"
4500 PLOT Timfil,Dc
4510 SET LINE COLOR 7
4520 SET TEXT COLOR 7
4530 PLOT TEXT GDU AT 90,70:"Dd"
4540 PLOT Timfil,Dd
4550 SET LINE COLOR 2
4560 SET TEXT COLOR 2
4570 PLOT TEXT GDU AT 90,65:"Dhead"
4580 PLOT Timfil,Dhead
4590 Bottom = -5.0 ! Top = 1000.0
4600 SET WINDOW 0,Filsiz*Period,Bottom,Top
4610 ! PLOT TEXT GDU AT 90,60:"Low Hyd Press"
4620 ! PLOT Timfil,Lowhydpress
4630 AXIS 0.002,100,0,-20.0,2,2
4640 ! axis x1,y1,x2,y2,x3,y3
4650 ! x1 = x-tic interval   y1 = y-tic interval
4660 ! x2 = x-intercept     y2 = y-intercept
4670 ! x3 = x-tic type      y3 = y-tic type
4680 AXIS 0.001,1,0.05,0,2,2
4690 IF Rxp$="y" OR Rxp$="Y" THEN SET CLIP OFF
4700 SET VIEWPORT 10,130,10,90
4710 ! set the window for the thickness plots in mils
4720 ! SET WINDOW 0,filsiz*period,400.0,500.0
4730 ! set the tic markslist
4740 IF Rxp$="y" OR Rxp$="Y" THEN SET CLIP OFF
4750 ! CALL Putext2(1,4,D$)
```

```
4760 Wrtflag = 3890
4770 IF Rsp$="7" THEN INPUT KEY WAIT Rsp$
4780 SET GRAPH 4
4790 SET DIALOG COLOR 14,1,1
4800 SET GRAPH DEVICE
4810 GOTO Menu
4820 ! sub Make-screen sets the two windows on the screen and the color of the border
4830 ! Zsmal, Zmedi, Zlarg, Zcol sets the # of small, medium, and large windows and Zcol is
the
 4840 SUB Make_screen(Zsmal,Zmedi,Zlarg,Zcol)
 4850  DIM Swiloc[Zsmal+Zmedi+Zlarg,2]
 4860  DECLARE LOCAL Z1,Z2,Z3,Z4
 4870  CLEAR
 4880  SET VIEWPORT Svp1,Svp2,Svp3,Svp4
 4890  SET WINDOW Svp1,Svp2,Svp3,Svp4
 4900  SET LINE COLOR Zcol
 4910   LINE Svp1,Svp3;Svp2,Svp3;Svp2,Svp4;Svp1,Svp4;Svp1,Svp3
 4920  Z2 = Zsmal+Zmedi*2+Zlarg*4
 4930  Snumwin = Zsmal+Zmedi+Zlarg
 4940  Z4 = 1 ! Z1 = Svp4
 4950  IF Zsmal=0 THEN 5020
 4960  FOR Z3 = 1 TO Zsmal
 4970   Swiloc[Z4,2] = Z1
 4980   Swiloc[Z4,1] = Z1-(Svp4-Svp3)/Z2
 4990   PLOT LINE Svp1,Swiloc[Z4,1];Svp2,Swiloc[Z4,1]
 5000   Z1 = Swiloc[Z4,1] ! Z4 = Z4+1
 5010  NEXT Z3
 5020  IF Zmedi=0 THEN 5090
 5030  FOR Z3 = 1 TO Zmedi
 5040   Swiloc[Z4,2] = Z1
 5050   Swiloc[Z4,1] = Z1-2*(Svp4-Svp3)/Z2
 5060   PLOT LINE Svp1,Swiloc[Z4,1];Svp2,Swiloc[Z4,1]
 5070   Z1 = Swiloc[Z4,1] ! Z4 = Z4+1
 5080  NEXT Z3
 5090  IF Zlarg=0 THEN 5160
 5100  FOR Z3 = 1 TO Zlarg
 5110   Swiloc[Z4,2] = Z1
 5120   Swiloc[Z4,1] = Z1-4*(Svp4-Svp3)/Z2
 5130   PLOT LINE Svp1,Swiloc[Z4,1];Svp2,Swiloc[Z4,1]
 5140   Z1 = Swiloc[Z4,1] ! Z4 = Z4+1
 5150  NEXT Z3
 5160  CALL Clr_all_wind
 5170 END SUB
 5180 ! sets the rough window
 5190 SUB Set_wind(Z1)
 5200  Swichwin = Z1
 5210  SET VIEWPORT Svp1+1,Svp2-1,Swiloc[Z1,1]+1,Swiloc[Z1,2]-1
 5220 END SUB
 5230 ! clears the window
 5240 SUB Clr_wind(Z1,Z2)
 5250  CALL Set_wind(Z1)
 5260  SET AREA STYLE 0
 5270  SET AREA COLOR Z2
 5280  SET WINDOW 0,130,0,100 ! IF Z2=0 THEN 5300
```

```
5290  PLOT AREA 0,0;130,0;130,100;0,100;0,0
5300  SET LINE STYLE 1
5310  SET LINE COLOR Sbcol
5320  ! PLOT LINE 0,50;130,50
5330  SET LINE STYLE 0
5340 END SUB
5350 ! clears the window
5360 SUB Clr_twind(Z)
5370  SET VIEWPORT 0,130,0,100
5380  SET WINDOW 0,130,0,100
5390  SET AREA STYLE 0 ! SET AREA COLOR Z
5400   PLOT AREA 1,Svp3+1;Svp1-1,Svp3+1;Svp1-1,Svp4-1;1,Svp4-1;1,Svp3+1
5410  SET LINE COLOR 15
5420   PLOT LINE 0,Svp3;Svp1,Svp3;Svp1,Svp4;1,Svp4;1,Svp3
5430 END SUB
5440 ! puts text in the window
5450 SUB Putext(Z,Z1,Z$)
5460   SET VIEWPORT 1,Svp1-1,Svp3+1,Svp4-1
5470   SET WINDOW 1,Svp1-1,Svp3+1,Svp4-1
5480  SET TEXT COLOR Z1
5490   TEXT AT Svp4-1-60*Z,1:Z$
5500 END SUB
5510 ! clears all windows and draws axis
5520 SUB Clr_all_wind ! Clears all the windows and draws the axis
5530  DECLARE LOCAL Zz1
5540  FOR Zz1 = 1 TO Snumwin
5550   CALL Clr_wind(Zz1,0)
5560  NEXT Zz1
5570 END SUB
5580 ! puts text into the window
5590 SUB Putext1(Z,Z1,Z$)
5600  SET VIEWPORT 10,20,92,100
5610  SET WINDOW 0,10,0,10
5620  SET TEXT COLOR Z1
5630  SET TEXT SIZE 3
5640  PLOT TEXT AT 1,1:Z$
5650 END SUB
5660 ! puts text into the window
5670 SUB Putext2(Z,Z1,Z$)
5680  SET CLIP ON
5690  SET VIEWPORT 0,30,0,100
5700  SET WINDOW 0,10,0,60
5710  SET TEXT COLOR Z1
5720  SET TEXT SIZE 1.0
5730  SET TEXT ANGLE 90,0
5740  PLOT TEXT AT 1,10:Z$
5750  SET TEXT ANGLE 0,0
5760  SET CLIP OFF
5770 END SUB
5780 SUB Putext3(Z,Z1,Z$)
5790  SET CLIP ON
5800  SET VIEWPORT 125,145,0,100
5810  SET WINDOW 0,10,0,60
5820  SET TEXT COLOR Z1
```

```
5830  SET TEXT SIZE 1.2
5840  SET TEXT ANGLE 270,0
5850  PLOT TEXT AT 5,50:Z$
5860  SET TEXT ANGLE 0,0
5870  SET CLIP OFF
5880 END SUB
5890 SUB Putext3a(Z,Z1,Z$)
5900  SET CLIP ON
5910  SET VIEWPORT 8,135,5,10
5920  SET WINDOW 0,78,0,5
5930  SET TEXT COLOR Z1
5940  SET TEXT SIZE 1.8
5950  SET TEXT ANGLE 0,0
5960  TEXT AT 1,1:Z$
5970  SET CLIP OFF
5980 END SUB
5990 SUB Putlftscal(Z,Z1,Z$)
6000  SET CLIP OFF
6010  SET VIEWPORT 7,12,8,90
6020  SET WINDOW 0,5,0,60
6030  SET TEXT COLOR Z1
6040  SET TEXT SIZE 1.8
6050  SET TEXT ANGLE 90,0
6060  TEXT AT 1,1:Z$
6070  SET CLIP OFF
6080  SET TEXT ANGLE 0,0
6090 END SUB
6100 SUB Putrtscal(Z,Z1,Z$)
6110  SET CLIP OFF
6120  SET VIEWPORT 132,137,9,90
6130  SET WINDOW 0,5,-60,0
6140  SET TEXT COLOR Z1
6150  SET TEXT SIZE 1.8
6160  SET TEXT ANGLE 270,0
6170  TEXT AT 1,1:Z$
6180  SET CLIP OFF
6190  SET TEXT ANGLE 0,0
6200 END SUB
6210 Makegraph1: ! THIS ROUTINE MAKES PLOTS TO THE SCREEN
6220 ! This is the most current program 9/16/87 graphics routine for plotting
6230 ! pressure and calculated thickness data
6240 SET GRAPH 4
6250 SET GRAPH DEVICE "gcon=ega"
6260 SET COLOR 7
6270 SET CLIP OFF
6280 FOR I = 1 TO Filsiz-4
6290  Press[I] = (Press[I]+Press[I+1]+Press[I+2]+Press[I+3]+Press[I+4])/5.0
6300  Hydpress[I] =
(Hydpress[I]+Hydpress[I+1]+Hydpress[I+2]+Hydpress[I+3]+Hydpress[I+4])/5.0
6310  Totp[I] = (Totp[I]+Totp[I+1]+Totp[I+2]+Totp[I+3]+Totp[I+4])/5.0
6320 NEXT I
6330 Svp1 = 10 ! Svp2 = 130 ! Svp3 = 10 ! Svp4 = 90 ! Sbcol = 1
6340 !
6350 SET POINT STYLE 0
```

```
6360 CALL Make_screen(0,0,1,1)
6370 A$ = "HPM white press, green hpress, purple totp"
6380 B$ = "      Time(msec)"
6390 L$ = "        Thickness(mils)"
6400 P$ = STR$(Peakpress)
6410 D$ = "     Pressure(psi) MAX = " & P$
6420 E$ = "0    10    20    30    40    50"
6430 F$ = "0    250   500   750   1000"
6440 G$ = "20   15    10    5     0     "
6450 CALL Putlftscal(1,4,F$)
6460 CALL Putext3a(1,4,E$)
6470 CALL Putext1(1,4,A$)
6480 CALL Putext(1,4,B$)
6490 CALL Putrtscal(1,4,G$)
6500 CALL Putext3(1,4,L$)
6510 CALL Putext2(1,4,D$)
6520 SET CLIP OFF
6530 SET POINT STYLE 0
6540 SET VIEWPORT 10,130,10,90
6550 ! set the window to match the time in milliseconds and the pressure in psi
6560 SET WINDOW 0,0.05,0.0,1000.0
6570 FOR I = 1 TO Filsiz
6580   PLOT POINT Timfil[I],Press[I]
6590 NEXT I
6600 ! make the axis tic marks for the pressure axis
6610 SET CLIP ON
6620 AXIS 0.005,50,0,0,2,2
6630 SET CLIP OFF
6640 SET VIEWPORT 10,130,10,90
6650 ! set the window for the thickness plots in mils
6660 ! SET WINDOW 0,0.05,0,5.0
6670 SET POINT COLOR 2
6680 FOR J = 1 TO Filsiz
6690   PLOT POINT Timfil[J],Hydpress[J]
6700 NEXT J
6710 ! SET WINDOW 0,0.05,0,20 ! AXIS 0,1,0.05,0,2,2
6720 SET POINT COLOR 0
6730 SET POINT COLOR 5
6740 FOR I = 1 TO Filsiz
6750   PLOT POINT Timfil[I],Totp[I]
6760 NEXT I
6770 ! set the tic marks
6780 SET CLIP ON
6790 ! AXIS 0.01,2.0,0.05,0,-1,-1
6800 SET CLIP OFF
6810 Wrtflag = 0
6820 INPUT KEY WAIT Rsp$
6830 SET GRAPH 0
6840 SET DIALOG COLOR 14,1,1
6850 SET GRAPH DEVICE
6860 GOTO Menu
6870 Ti:
6880 Timfil[1] = 0
6890 FOR I = 2 TO Filsiz
```

```
6900   Timfil[I] = Timfil[I-1]+5.E-05
6910 NEXT I
6920 Aver:
6930 Lhp = Lowhydpress
6940 FOR I = 3 TO Filsiz-3
6950   Totp[I] = (Totp[I-2]+Totp[I-1]+Totp[I]+Totp[I+1]+Totp[I+2])/5.0
6970 NEXT I
6980 Lowhydpress = Lhp
7000 GOTO Menu
```

APPENDIX II

Factors Important to Density Profile Determination

A number of factors are critical to accurate layer thickness and density determinations. These include proper choice of the target material, target thickness, target shape, target surface characteristics, target alignment relative to the sensor, proper transducer calibration, and parallelism between the pressing surfaces. To achieve a high degree of accuracy, the effect ofeach of these factors on the target displacement measurement was addressed.

The basic principles of the inductive displacement measuring technique are well known.[11] An alternating current (AC) flowing through a coil causes the field of one winding to add to the field of the next winding. The fields pulsate, in turn generating a pulsating electromagnetic field surrounding the coil. Placing the coil a nominal distance from a metal target induces a current flow on the surface and within the target (because of the circular pattern, the induced current is called an "eddy current"). The induced current produces a secondary magnetic field that opposes and reduces the intensity of the original field. The depth of eddy current penetration can be controlled to "look" only at the surface, or into the metal to locate cracks, seams, or inclusions by selecting the proper operating frequency. Such discontinuities upset the eddy current flow and are picked up by the detection system.

---

[11] Application note number 108 382, General Application Considerations, Inductive Measuring Systems, 1982 KAMAN Instrumentation Corp.

The sensing coil is normally a section or leg of a balanced bridge network. As the target moves toward the coil, more eddy currents are generated in the material, and losses within the bridge network increase. As the target moves away, the losses decrease. Such unbalanced conditions are sensed and converted into a signal directly proportional to the distance between coil and target as shown in the block diagram in Figure 83.

Target Material

It was desired to minimize flow resistance of the target material while maximizing the openness and interaction between fibers on opposite sides of the target. In choosing the target material, it was necessary to consider not only the electrical parameters of resistivity and magnetic permeability but the openness of the target material on the performance of the inductive system. Metals such as copper, aluminum, and brass have a low resistivity and, therefore, have a high output sensitivity in terms of impedance change per unit displacement. These materials have a permeability of one and are classified "nonmagnetic" which made them a good choice for targets. The material chosen was an electro etched copper mesh material.

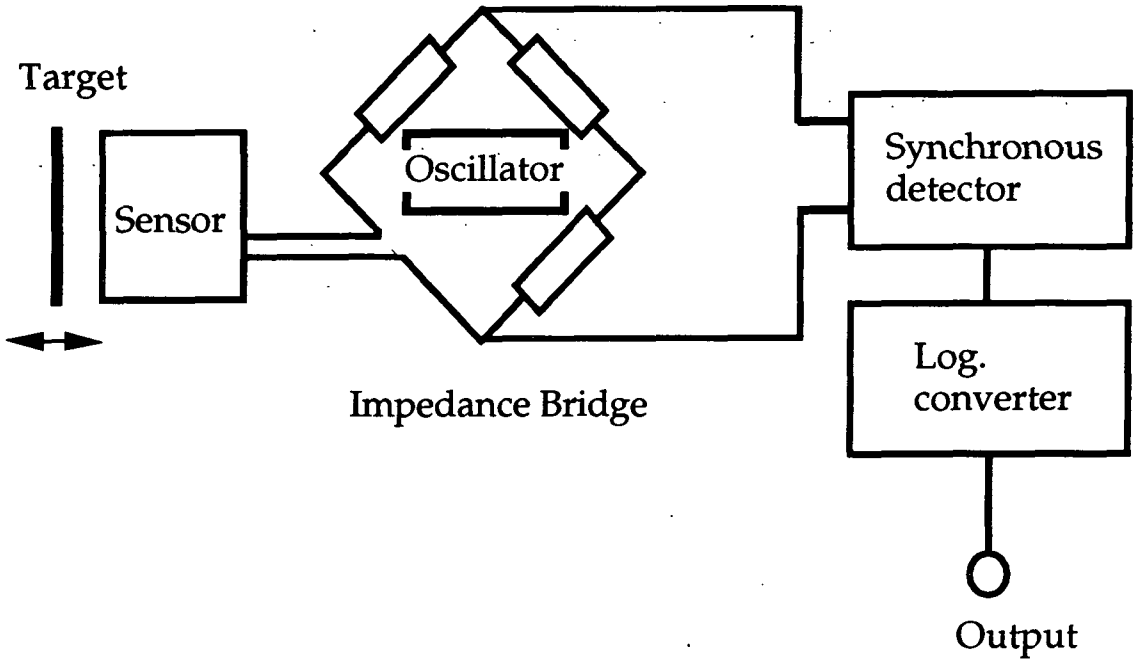

Figure 83. Block Diagram for KD-2310 series. (KAMAN Instrumentation Corp. Application Note 108 382)

Target Thickness and Diameter

Eddy current density is at a maximum on the surface of a target. There is a penetration below the surface; the extent is a function of the resistivity, the permeability of the material, and system oscillator frequency. At one "skin depth (δ)," the current density is only 36% of the surface density, and at two, it is only 13% (See Figure 84 for skin depth). Skin depth is defined by the following equation:

$$\delta = 50.3 \left(\frac{\rho}{f\mu_r} \right)^{\frac{1}{2}} , \text{mm}$$

where ρ = target material resistivity (Microhm-cm); μ = magnetic permeability; and f = oscillator frequency (KAMAN Instrumentation Corp. Application Note 108 382).

For good conductors (i.e., aluminum), operation is virtually independent of the target thickness down to one-fourth of a skin depth. Displacements of conductive surfaces as thin as 0.5 mil (0.0005 inch or 0.013 mm) have been measured successfully. This indicates that target thickness generally is not a limiting factor. To avoid variations caused by temperature changes of the target, the recommended minimum thickness should be three skin depths. Since the temperature was held constant at room temperature for all tests, changes in target properties with temperature were not a problem.

The one-inch diameter copper mesh targets were die-punched from a six inch by six inch stock material which was 0.001 inch thick (BuckBee-Mears, Minneapolis, Minnesota). The mesh was etched to 100 lines per inch. This thickness and type of material was chosen because it had been shown by Burton (1987) not to interfere with the movement of fibers or water flow during the compression process.

A flat circular target equal to the diameter of the transducer is essentially as good as an infinite plane. However, sensitivity falls off rapidly for small diameter targets and is reduced 50% when the target diameter is 50% of the sensor diameter. To maximize the sensitivity, all targets were made with diameters equal to 1.3 times the diameter of the sensor.

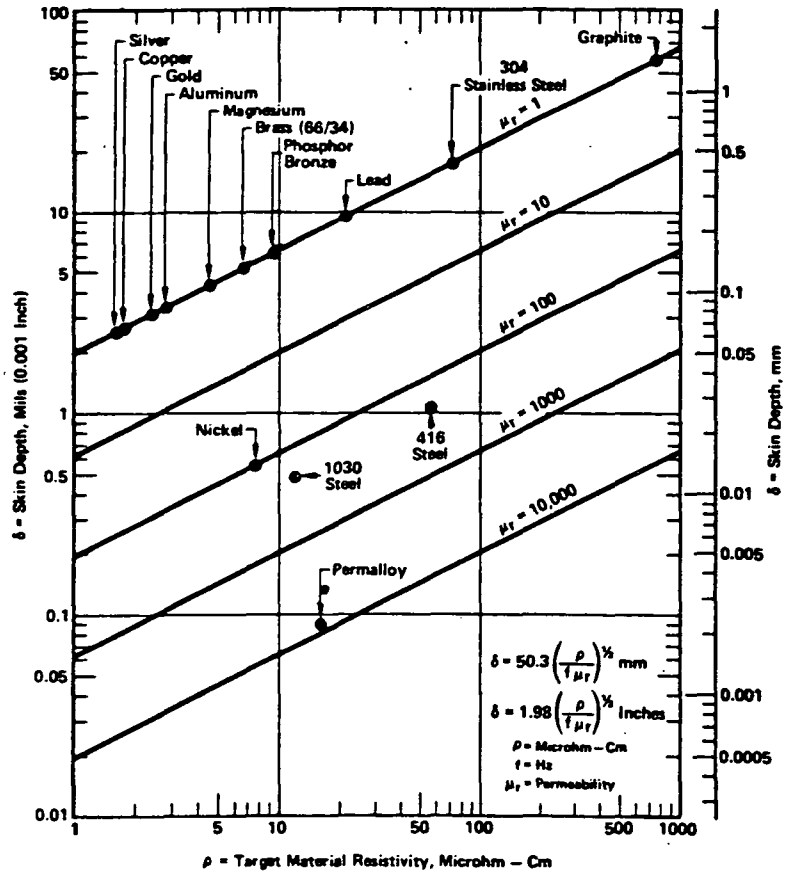

Figure 84. Skin Depth at 1 MHz. (KAMAN Instrumentation Corp. Application Note 108 382)

Target Surface

Generally, there is no difference in target effectiveness between smooth and rough surfaces since the total area beneath the sensor is averaged. Impurities such as oil, grease, and dirt have negligible effects. Cracks in the target itself, if deep enough, may appear as a discontinuity. Cracks of less than two skin depth have minimum effect. The 65% open area of the copper mesh targets did not significantly affect the thickness measurements since each detector was sensing the same type of target. A comparison of static thicknesses of several layers of mylar sheets with targets placed between the layers agreed well with the micrometer measured thickness of the mylar

sheets. The difference in thickness was less than 1% which indicated that the mesh structure of the targets would not introduce a significant error in the thickness measurements.

Target Alignment

Normally, the target and transducer surfaces should be parallel. However, if the unexpected target excursion is less than full range, some nonparallelism can exist without appreciable error in the target position determination. The transducer senses the average distance to the target, such that the nonparallelism effect is small up to 15 degrees.

APPENDIX III

Measurement of the Permeability of the Porous Ceramic Plate

The permeability of the beaded porous ceramic plate was measured using a "falling head permeameter" which was described by Lindsay (1989). In unsteady "permeametry" the pressure difference across a porous medium is allowed to decrease gradually as a result of flow. The "falling head permeameter" concept is shown in Figure 85, and the data characterizing the permeability of the beaded porous ceramic plate are summarized in Table 6 below.

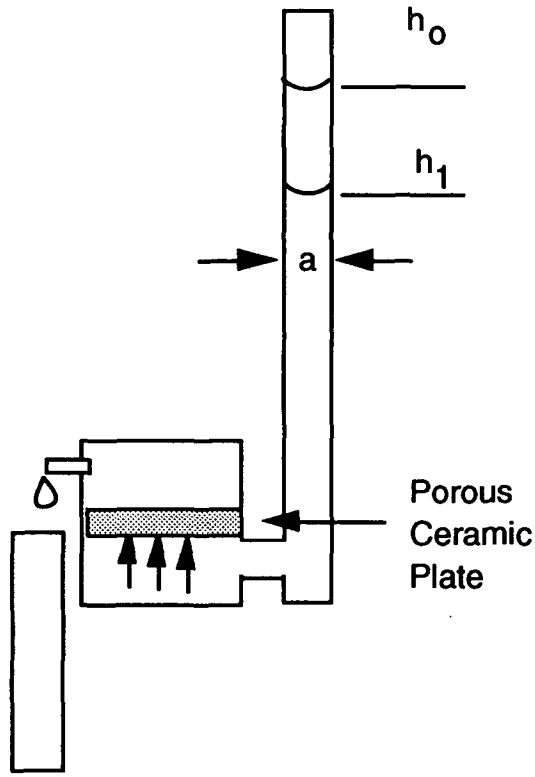

Figure 85. Falling head permeameter.

The permeability of the porous medium is related to the drop in water column height versus time via the following equation:

$$k = \left(\frac{aL\mu}{At\rho g}\right) \ln\left(\frac{h_0}{h_1}\right)$$

where a is the diameter of the tall tube; L is the thickness of the porous sample; A is porous medium cross-sectional area; and t is the time it takes for the column to fall from h_0 to h_1.

a = 95.25 mm (3.75 inches)

L = 9.52 mm (.375 inches)

A = 95.25 mm x 9.52 mm (3.75 inches x .375 inches) = 906.78 mm^2

t = measured variable, sec

h_0 = measured variable, mm

h_1 = measured variable, mm

μ = $1x10^{-3}$ viscosity of water, Pa.s

ρ = 1000 density of water, kg/m^3

g = 9.81 gravitational constant, m/s^2

Table 6. Falling head permeameter data for porous plate permeability measurement.

Elapsed Time (sec)	t	h_0(mm)	h_1(mm)	Permeability (m^2)
15.	15.	146.05	139.70	3.76e-9
32.	17.	139.70	133.35	3.47e-9
48.	16.	133.35	127.00	3.87e-9
66.	18.	127.00	120.65	3.61e-9
84.	18.	120.65	114.30	3.81e-9
104.	20.	114.30	107.95	3.63e-9
129.	25.	107.95	101.60	3.06e-9

APPENDIX IV

Numerical Data From Handsheet T4690A.

Point	MTSP.y	A.y	B.y	C.y	D.y	EE.y	ThickA.y	ThickB.y	ThickC.y	SheetThick.y	DenA.y	DenB.y	DenC.y	SheetDen.y
0	3.68046	0.105349	0.074105	0.0346085	-0.00540714	0.219786	0.0312167	0.0395202	0.0399905	0.110727	0.160171	0.126518	0.12503	0.135468
1	3.94571	0.105346	0.0741089	0.0346004	-0.0054057	0.219775	0.031205	0.0395268	0.0399799	0.110712	0.160231	0.126497	0.125063	0.135487
2	3.59204	0.10532	0.0741182	0.0345815	-0.00539679	0.219756	0.0311173	0.0395447	0.0399473	0.110665	0.160396	0.126439	0.125165	0.135544
3	3.68046	0.105248	0.0741195	0.0345475	-0.00537702	0.219741	0.0311313	0.0395693	0.0398908	0.110591	0.160611	0.126361	0.125343	0.135635
4	3.94571	0.105137	0.0740885	0.03449	-0.0053537	0.219712	0.0310992	0.0395968	0.0398106	0.110507	0.160777	0.126273	0.125597	0.135739
5	3.68046	0.105033	0.0740157	0.0343965	-0.00533392	0.219626	0.0310973	0.0396237	0.0397135	0.110435	0.160787	0.126187	0.125904	0.135827
6	3.94571	0.104998	0.0739264	0.0342725	-0.00531611	0.219453	0.031136	0.0396443	0.0396174	0.110398	0.160588	0.126122	0.126209	0.135872
7	3.59204	0.105051	0.0738551	0.0341589	-0.00530223	0.219202	0.0312058	0.0396469	0.0395495	0.110402	0.16023	0.126114	0.126425	0.135867
8	3.59204	0.105138	0.0738073	0.0341129	-0.00530472	0.218927	0.0312796	0.039618	0.0395358	0.110433	0.159851	0.126206	0.126469	0.135829
9	3.59204	0.105184	0.0737724	0.034168	-0.00532934	0.218669	0.0313262	0.039555	0.0395855	0.110467	0.159613	0.126408	0.126311	0.135788
10	3.59204	0.105168	0.0737608	0.0343095	-0.00536077	0.218427	0.0313258	0.0394753	0.0396809	0.110482	0.159615	0.126663	0.126008	0.135769
11	3.59204	0.105119	0.0737971	0.0344766	-0.00537544	0.218175	0.0312796	0.039411	0.0397846	0.110475	0.159851	0.126869	0.125679	0.135777
12	3.68046	0.10508	0.0738847	0.0345948	-0.00536226	0.21792	0.0312077	0.0393896	0.0398588	0.110456	0.16022	0.126938	0.125444	0.135801
13	4.03413	0.105083	0.0739985	0.0346291	-0.00532582	0.217712	0.0311376	0.039416	0.0398853	0.110439	0.16058	0.126853	0.12536	0.135822
14	4.03413	0.105138	0.074102	0.034607	-0.00527785	0.21761	0.0310899	0.03947	0.0398714	0.110431	0.160825	0.126679	0.125404	0.135831
15	4.03413	0.105208	0.0741624	0.0345814	-0.00523216	0.217587	0.0310699	0.0395226	0.0398409	0.110433	0.160928	0.126511	0.1255	0.135828
16	4.03413	0.105239	0.0741686	0.0345763	-0.00520239	0.217536	0.0310694	0.0395563	0.0398177	0.110443	0.16093	0.126402	0.125573	0.135816
17	4.03413	0.105232	0.0741463	0.0345812	-0.00519899	0.217384	0.0310754	0.0395741	0.0398149	0.110464	0.160899	0.126345	0.125581	0.13579
18	4.03413	0.105235	0.0741442	0.0345889	-0.00522413	0.21717	0.0310779	0.0395916	0.0398318	0.110501	0.160886	0.12629	0.125528	0.135745
19	4.03413	0.10528	0.074194	0.0346047	-0.0052649	0.216977	0.0310728	0.0396224	0.0398564	0.110552	0.160912	0.126192	0.125451	0.135683
20	4.03413	0.105344	0.0742787	0.0346209	-0.00529676	0.216827	0.0310609	0.0396684	0.0398715	0.110601	0.160974	0.126045	0.125403	0.135623
21	4.03413	0.105388	0.0743469	0.034611	-0.00530384	0.21668	0.0310464	0.0397204	0.0398642	0.110631	0.16105	0.125881	0.125426	0.135586
22	3.85177	0.105384	0.074357	0.0345599	-0.0052941	0.216532	0.0310361	0.0397647	0.0398338	0.110635	0.161103	0.12574	0.125522	0.135582
23	3.30467	0.105316	0.0743054	0.0344798	-0.00529246	0.216429	0.0310403	0.0397915	0.0397927	0.110625	0.161081	0.125655	0.125652	0.135594
24	4.12255	0.105223	0.0742159	0.0343951	-0.00532214	0.216366	0.0310705	0.0397995	0.0397575	0.110627	0.160926	0.12563	0.125763	0.13559
25	4.38781	0.105196	0.0741217	0.0343275	-0.00538296	0.216238	0.0311307	0.0397968	0.0397367	0.110664	0.160616	0.125638	0.125829	0.135545
26	4.03413	0.105283	0.0740622	0.0342959	-0.00543997	0.215958	0.0312085	0.039797	0.0397251	0.110731	0.160216	0.125638	0.125865	0.135484
27	4.03413	0.105428	0.0740691	0.0343	-0.00545009	0.21557	0.0312783	0.0398114	0.0397091	0.110799	0.159858	0.125592	0.125916	0.135381
28	4.03413	0.105522	0.0741303	0.0343048	-0.00540904	0.215204	0.0313192	0.0398393	0.0396794	0.110838	0.159648	0.125505	0.12601	0.135333
29	4.03413	0.105519	0.0741844	0.0342751	-0.00535481	0.214945	0.0313315	0.0398645	0.0396418	0.110838	0.159584	0.125425	0.12613	0.135333
30	4.03413	0.105463	0.0741775	0.0342295	-0.00532341	0.21479	0.031335	0.0398631	0.0396152	0.110813	0.159566	0.12543	0.126214	0.135363
31	4.03413	0.105426	0.0741167	0.0342242	-0.00532122	0.214678	0.0313494	0.0398181	0.0396192	0.110787	0.159493	0.125572	0.126202	0.135395
32	4.03413	0.105429	0.0740482	0.0342841	-0.00533579	0.214527	0.0313803	0.0397299	0.0396589	0.110769	0.159336	0.125852	0.126076	0.135417
33	4.03413	0.105429	0.0739946	0.0343801	-0.00535089	0.214302	0.0314219	0.0396144	0.0397211	0.110757	0.159126	0.12622	0.125879	0.135431
34	4.03413	0.105396	0.0739392	0.0344686	-0.00535526	0.214045	0.0314688	0.0394941	0.0397822	0.110745	0.158889	0.126604	0.125685	0.135446
35	4.03413	0.105361	0.073866	0.0345226	-0.00535269	0.213829	0.0315188	0.0393895	0.0398205	0.110729	0.158637	0.126939	0.125564	0.135466
36	4.03413	0.105363	0.0737819	0.0345246	-0.00535525	0.213678	0.0315654	0.0393147	0.0398247	0.110705	0.158402	0.12718	0.12555	0.135495
37	4.03413	0.105365	0.0736999	0.0344699	-0.00535971	0.213565	0.0315929	0.039274	0.0397985	0.110665	0.158264	0.127311	0.125633	0.135544
38	4.03413	0.105302	0.0736357	0.0343925	-0.00534746	0.213435	0.0315863	0.039263	0.0397586	0.110608	0.158298	0.127347	0.12576	0.135614
39	4.03413	0.105188	0.0736188	0.0343536	-0.00531505	0.213224	0.0315465	0.0392714	0.039728	0.110546	0.158498	0.127319	0.125856	0.13569
40	4.03413	0.105119	0.0736691	0.0343814	-0.00528636	0.212915	0.0314925	0.039289	0.0397234	0.110505	0.15877	0.127262	0.125871	0.135741
41	4.03413	0.105152	0.0737581	0.0344439	-0.00528458	0.212587	0.0314455	0.039308	0.0397457	0.110499	0.159006	0.127201	0.1258	0.135748
42	4.03413	0.105238	0.0738285	0.034493	-0.00530535	0.212343	0.0314101	0.0393249	0.0397824	0.110517	0.159185	0.127146	0.125684	0.135725
43	4.03413	0.105284	0.0738563	0.0345169	-0.00532613	0.212184	0.0313714	0.0393415	0.0398166	0.110529	0.159382	0.127092	0.125576	0.13571
44	4.03413	0.105247	0.0738694	0.0345321	-0.0053312	0.212013	0.03131	0.0393649	0.0398363	0.110511	0.159697	0.127017	0.125514	0.135733
45	4.03413	0.105154	0.0739046	0.0345412	-0.00532114	0.211772	0.0312205	0.0394033	0.0398382	0.110462	0.160156	0.126893	0.125508	0.135793
46	4.03413	0.105058	0.0739677	0.0345297	-0.00530693	0.211522	0.0311182	0.0394593	0.0398256	0.110403	0.160682	0.126714	0.125548	0.135866
47	4.03413	0.104998	0.0740351	0.034499	-0.00529961	0.211366	0.0310285	0.0395263	0.0398064	0.110361	0.161145	0.126499	0.125608	0.135917
48	4.03413	0.104992	0.0740845	0.0344701	-0.00530184	0.211327	0.0309707	0.0395938	0.0397901	0.110355	0.161444	0.126283	0.125659	0.135925
49	4.03413	0.105036	0.0741188	0.0344533	-0.00531081	0.211331	0.0309488	0.0396538	0.0397837	0.110386	0.161557	0.126092	0.12568	0.135886
50	3.94571	0.105103	0.0741557	0.0344435	-0.00532777	0.211299	0.0309541	0.039703	0.0397894	0.110447	0.16153	0.125935	0.125662	0.135812
51	3.68046	0.10517	0.0741992	0.0344408	-0.00535815	0.211198	0.0309747	0.0397406	0.0398028	0.110518	0.161422	0.125816	0.125619	0.135724
52	4.03413	0.105229	0.0742342	0.0344471	-0.00539233	0.211027	0.0310035	0.0397653	0.0398137	0.110582	0.161273	0.125738	0.125585	0.135645
53	4.03413	0.105274	0.0742448	0.034451	-0.005403	0.210801	0.0310379	0.0397761	0.0398116	0.110626	0.161094	0.125704	0.125592	0.135592
54	4.03413	0.105301	0.074229	0.0344418	-0.00537193	0.210548	0.0310771	0.0397737	0.0397944	0.110645	0.160891	0.125711	0.125646	0.135568
55	4.03413	0.105321	0.0742019	0.0344313	-0.00531552	0.210296	0.031118	0.0397603	0.0397715	0.11065	0.16068	0.125754	0.125718	0.135563
56	4.03413	0.105354	0.0741835	0.034439	-0.00527261	0.210053	0.0311542	0.0397395	0.0397579	0.110652	0.160493	0.125819	0.125761	0.135561
57	4.03413	0.105388	0.0741786	0.0344653	-0.00526821	0.209805	0.0311775	0.0397156	0.0397619	0.110655	0.160372	0.125895	0.125749	0.135556
58	4.03413	0.105396	0.0741783	0.0344937	-0.00529291	0.209534	0.0311811	0.0396932	0.0397787	0.110653	0.160354	0.125966	0.125696	0.135559
59	4.03413	0.105364	0.0741749	0.0345106	-0.00531578	0.20925	0.031163	0.0396778	0.0397946	0.110635	0.160447	0.126015	0.125645	0.135581
60	4.12255	0.1053	0.0741638	0.0345118	-0.00531548	0.208986	0.0311276	0.0396762	0.0397978	0.110602	0.16063	0.12602	0.125635	0.135622
61	4.38781	0.105235	0.074153	0.0345006	-0.00529796	0.208755	0.0310833	0.039696	0.0397847	0.110564	0.160859	0.125958	0.125677	0.135668
62	4.03413	0.105203	0.0741725	0.0344795	-0.00528415	0.208551	0.0310417	0.0397399	0.0397586	0.11054	0.161074	0.125819	0.125759	0.135697
63	4.03413	0.105215	0.0742393	0.0344428	-0.00528638	0.208385	0.0310177	0.0397979	0.0397248	0.11054	0.161199	0.125636	0.125866	0.135697
64	4.03413	0.105255	0.0743067	0.0343881	-0.00530157	0.208266	0.0310279	0.0398451	0.0396869	0.11056	0.161147	0.125487	0.125987	0.135673
65	4.03413	0.10529	0.0742884	0.0343264	-0.00532082	0.208123	0.0310823	0.0398543	0.0396473	0.110584	0.160867	0.125458	0.126112	0.135644

Point	MTSP.y	A.y	B.y	C.y	D.y	EE.y	ThickA.y	ThickB.y	ThickC.y	SheetThick.y	DenA.y	DenB.y	DenC.y	SheetDen.y
66	4.03413	0.105299	0.0741508	0.0342712	-0.00533462	0.207862	0.0311729	0.0398148	0.0396086	0.110596	0.160401	0.125583	0.126236	0.135628
67	4.03413	0.105288	0.0739616	0.0342333	-0.00533046	0.207486	0.0312715	0.0397424	0.0395745	0.110588	0.159895	0.125812	0.126344	0.135638
68	4.03413	0.10528	0.0738336	0.0342286	-0.00529891	0.207098	0.0313422	0.0396679	0.0395503	0.11056	0.159532	0.126048	0.126422	0.135673
69	4.03413	0.105275	0.0738235	0.0342643	-0.00524897	0.206775	0.0313624	0.0396159	0.0395402	0.110519	0.159428	0.126212	0.126454	0.135724
70	3.94571	0.105256	0.0738911	0.034317	-0.00520977	0.206504	0.0313357	0.0395921	0.0395441	0.110472	0.159564	0.126288	0.126441	0.135781
71	3.68046	0.105208	0.0739504	0.0343534	-0.00520616	0.206243	0 0312873	0 0395876	0.0395549	0.11043	0.159811	0.126302	0.126407	0 135833
72	4.03413	0.105143	0.0739541	0.0343624	-0.00523052	0.205975	0.0312475	0.0395931	0.0395595	0.1104	0.160014	0 126285	0.126392	0.13587
73	4.03413	0.105108	0.0739257	0.034348	-0 0052469	0 205716	0.0312355	0.0396073	0.0395453	0.110388	0.160075	0.126239	0 126438	0 135884
74	4.03413	0.105142	0.073914	0.0343107	-0.00522922	0.205477	0.0312519	0.0396331	0.0395088	0.110394	0.159991	0.126158	0.126555	0.135877
75	4.03413	0.105226	0.0739292	0.0342579	-0.0051886	0.20526	0.0312815	0.0396683	0.0394599	0.11041	0.15984	0.126045	0.126711	0.135858
76	4.03413	0.105296	0.0739449	0.034214	-0.00515578	0.205075	0.0313031	0.039705	0.0394172	0.110425	0.159729	0.125929	0.126849	0.135838
77	4.03413	0.105308	0.0739512	0.0342012	-0.0051464	0.20493	0.0313014	0.0397353	0.0393971	0.110434	0.159738	0.125833	0.126913	0.135828
78	4.03413	0.105267	0.0739713	0.0342166	-0.0051571	0.204792	0.0312755	0.0397562	0.0394059	0.110438	0.159871	0.125767	0.126885	0.135823
79	4.03413	0.105224	0.0740129	0.0342353	-0.0051875	0.204606	0.0312365	0.0397664	0.03944	0.110443	0.16007	0.125734	0.126775	0.135817
80	4.03413	0.105212	0.0740395	0.0342381	-0.00524268	0.204362	0.0311956	0.0397613	0.0394914	0.110448	0.16028	0.125751	0.12661	0.13581
81	4.03413	0.105197	0.0740169	0.0342375	-0.0053097	0 204118	0.031153	0.039737	0.0395517	0.110442	0.160499	0.125828	0.126417	0.135818
82	4.03413	0.105118	0.0739663	0.0342653	-0.00535601	0.203907	0.0311009	0.0396983	0.0396126	0.110412	0.160769	0.12595	0.126223	0.135855
83	4.03413	0.104987	0.0739421	0.0343256	-0.00536539	0.203692	0.0310385	0.039661	0.0396651	0.110365	0 161092	0.126069	0.126056	0.135913
84	4.12255	0.104892	0.0739684	0.0343811	-0.00535542	0.203461	0.0309786	0.0396426	0.0397008	0.110322	0 161403	0.126127	0.125942	0.135966
85	4.38781	0.104898	0.0740203	0.0343995	-0.00534653	0.20328	0.0309368	0.0396511	0 0397153	0.110303	0.161621	0.1261	0.125896	0 135989
86	4.03413	0.104976	0.0740666	0.0343913	-0.00533584	0.203177	0.0309153	0.0396822	0.0397104	0.110308	0.161732	0.126002	0.125912	0 135983
87	4.03413	0.105048	0.0741077	0.0343831	-0.00531271	0.203059	0.0309023	0.0397245	0.0396935	0.11032	0.161801	0.125867	0.125965	0 135968
88	4.12255	0.105068	0.0741592	0.0343822	-0.0052795	0.202816	0.0308871	0.0397658	0.0396755	0.110328	0 16188	0.125737	0.126022	0.135958
89	4.38781	0.105053	0.0742153	0.0343865	-0.00525006	0.202488	0.0308753	0.0397946	0.0396678	0.110338	0.161942	0.125646	0 126047	0.135946
90	4.03413	0.105054	0.0742463	0.0343987	-0.00524352	0.202216	0.0308847	0.0398018	0.0396775	0.110364	0.161894	0.125623	0 126016	0.135914
91	4.03413	0.105095	0.0742278	0.0344116	-0.00527613	0.202062	0.0309278	0.0397846	0.0397048	0.110417	0.161669	0.125677	0.12593	0.135849
92	4.03413	0.105158	0.074164	0.0344097	-0.00534113	0.201946	0.0309976	0.0397488	0.0397416	0.110488	0.161306	0.12579	0.125813	0 135762
93	4.03413	0.105215	0.0740913	0.0343987	-0.00540062	0.201751	0.031069	0.0397061	0.0397766	0.110552	0.160935	0.125926	0.125702	0 135683
94	4 03413	0.105247	0.0740544	0.0344076	-0.00541465	0.201449	0.0311147	0.0396692	0.0398014	0.110585	0.160697	0.126043	0.125624	0 135642
95	4.03413	0.105245	0.074068	0.0344478	-0.0053787	0.201111	0.0311202	0.039648	0.0398132	0.110581	0.160668	0.12611	0.125586	0.135647
96	4.03413	0.105218	0.0741084	0.0344948	-0.00532604	0.200836	0.0310891	0.0396485	0.0398141	0.110552	0.16083	0 126108	0 125584	0.135683
97	4.03413	0.105192	0.0741548	0.0345188	-0.00529375	0.200645	0.0310362	0.039672	0 0398064	0.110515	0.161104	0 126034	0.125608	0.135729
98	4.03413	0.105181	0.0742131	0.0345138	-0.00528898	0.200457	0.0309794	0.0397121	0 039791	0.110482	0.161399	0 125907	0.125657	0.135768
99	4.03413	0.105176	0.074278	0.0344924	-0.00529077	0.20019	0.0309352	0.0397541	0 0397671	0.110456	0.161629	0.125774	0.125732	0 1358
100	4.03413	0.10516	0.074302	0.0344645	-0.00528156	0.199862	0.030916	0.0397819	0.0397356	0.110434	0.161729	0.125685	0.125832	0 135826
101	4.03413	0.105132	0.0742467	0.0344292	-0.005266	0.19955	0.0309252	0.0397894	0.0397023	0.110417	0.161681	0.125662	0.125937	0.135849
102	4.03413	0.105108	0.0741486	0.0343852	-0.00525992	0.199295	0.0309539	0.0397854	0.039678	0.110417	0.161531	0.125674	0.126015	0.13584
103	4.03413	0.105112	0.0740938	0.0343502	-0.00527459	0.199063	0.0309849	0.0397872	0.0396728	0.110445	0.16137	0.125669	0.126031	0.135814
104	4.03413	0.10516	0.0741259	0.0343503	-0.00531048	0.198798	0.0310028	0.0398076	0.0396887	0.110499	0.161276	0.125605	0 125981	0.135748
105	4.03413	0.105236	0.074212	0.0343797	-0 00535396	0.198483	0.031	0.0398474	0.039716	0.110563	0.16129	0.125479	0 125894	0.135669
106	4.03413	0.105301	0.0742987	0.0343988	-0.00538239	0.198146	0.0309772	0.0398964	0.0397392	0.110613	0.16141	0.125325	0.125821	0.135608
107	4.03413	0.105316	0.0743624	0.0343885	-0.00538278	0.197832	0.0309412	0 0399375	0.0397492	0.110628	0.161598	0.125196	0.125789	0.13559
108	4.03413	0.105273	0.0743918	0.034373	-0.00536497	0.197563	0.0309053	0.0399538	0 0397491	0.110608	0.161785	0 125145	0.125789	0.135614
109	4.03413	0.1052	0.0743699	0.034377	-0.00534977	0.197321	0.0308871	0.0399359	0.0397481	0.110571	0.16188	0.125201	0.125792	0.135659
110	4.03413	0.105142	0.0743028	0.034398	-0.00534624	0.197073	0.0309021	0.0398883	0.0397517	0.110542	0.161803	0.125351	0.125781	0.135695
111	4.03413	0.105137	0.0742304	0.0344234	-0.00534649	0.196813	0.0309566	0.0398264	0.0397561	0.110539	0.161519	0.125546	0.125767	0.135699
112	4.03413	0.105197	0.0741819	0.0344429	-0.00533961	0.196578	0.0310449	0.0397673	0.0397517	0.110564	0.161062	0.125732	0 125781	0.135668
113	3.85177	0.105299	0.0741473	0.0344449	-0.00531993	0.196385	0.031151	0.0397202	0.0397312	0.110602	0.160514	0.125881	0.125846	0.135621
114	3.30467	0.105398	0.0741042	0.034424	-0.00528566	0.196205	0.0312533	0.0396849	0.0396958	0.110634	0.159987	0.125993	0.125958	0.135582
115	4.03413	0.105444	0.0740457	0.0343882	-0.00524655	0.195995	0.0313313	0.039657	0.039657	0.110645	0.159587	0.126081	0.126082	0 135568
116	4.03413	0.105411	0.0739805	0.03435	-0.00523087	0.195742	0.0313749	0.0396322	0.0396314	0.110638	0.159364	0.12616	0.126163	0 135577
117	4 03413	0 105326	0.0739254	0.0343203	-0.00526258	0 195478	0.0313894	0.0396076	0.039631	0.110628	0.15929	0.126238	0.126164	0 13559
118	4.03413	0.105262	0.0738957	0.0343077	-0.00532812	0 195251	0.0313895	0.0395794	0.0396568	0.110626	0.159289	0.126328	0.126082	0.135592
119	3.94571	0.105266	0.0738896	0.0343195	-0.00538234	0.195084	0.0313862	0.0395413	0.0397	0.110628	0 159306	0.12645	0 125945	0.13559
120	3.68046	0.105296	0.0738866	0.0343639	-0.00539276	0.194861	0.0313796	0.0394884	0.0397479	0.110616	0.159339	0.12662	0 125793	0.135604
121	3.94571	0.105269	0.0738686	0.0344377	-0.00536866	0.194615	0.031364	0.0394238	0.0397892	0.110577	0.159419	0.126828	0.125663	0.135652
122	3.59204	0.105168	0.0738322	0.0345072	-0.0053419	0.194366	0.0313395	0.0393619	0.0398153	0.110517	0.159543	0.127027	0.12558	0.135726
123	3.59204	0.105062	0.0737836	0.0345264	-0.00533137	0.19414	0.0313137	0.0393223	0.0398222	0.110458	0.159675	0.127155	0.125558	0 135798
124	3.68046	0.105022	0.0737411	0.0344864	-0.00533591	0.193887	0.0312903	0.0393204	0.0398138	0.110425	0.159794	0.127161	0.125585	0.135839
125	4.03413	0.10505	0.073741	0.0344284	-0.00534838	0.193565	0.0312616	0.0393585	0.0398011	0.110421	0.159942	0.127038	0.125625	0 135844
126	3.94571	0.10509	0.073815	0.0344018	-0.00536221	0.193215	0.0312161	0.0394247	0.0397958	0.110437	0.160175	0.126825	0.125642	0.135825
127	3.59204	0.105106	0.0739472	0.03442	-0.00537099	0.192912	0.0311558	0.0394968	0.0398021	0.110455	0.160486	0.126594	0 125622	0.135802
128	3.68046	0.105102	0.0740709	0.0344579	-0.00536981	0.19267	0.0311013	0.0395508	0.0398146	0.110467	0.160767	0.12642	0.125582	0.135787
129	3.94571	0.105111	0.0741236	0.0344878	-0.00535645	0.192437	0.031078	0.0395711	0.0398238	0.110473	0.160887	0.126355	0.125553	0.13578
130	3.59204	0.105145	0.0740963	0.0345049	-0.00533366	0.192145	0.031095	0.0395574	0.0398226	0.110475	0.160799	0.126399	0.125557	0.135777
131	3.59204	0.105178	0.0740238	0.0345128	-0.00531061	0.191787	0.0311388	0.0395256	0.0398088	0.110473	0.160573	0.126501	0.125601	0.13578

Point	MTSP.y	A.y	B.y	C.y	D.y	EE.y	ThickA.y	ThickB.y	ThickC.y	SheetThick.y	DenA.y	DenB.y	DenC.y	SheetDen.y
132	3.59204	0.10518	0.0739499	0.0345023	-0.00529607	0.191428	0.0311851	0.0394982	0.0397832	0.110466	0.160334	0.126588	0.125682	0.135788
133	3.59204	0.105159	0.0739092	0.0344656	-0.00529044	0.191133	0.0312166	0.0394915	0.0397491	0.110457	0.160172	0.12661	0.125789	0.135799
134	3.59204	0.105146	0.0739108	0.0344158	-0.00528887	0.190903	0.0312307	0.0395058	0.0397117	0.110448	0.160099	0.126564	0.125908	0.13581
135	3.59204	0.105156	0.0739295	0.0343755	-0.00528742	0.190706	0.0312332	0.0395285	0.0396769	0.110439	0.160086	0.126491	0.126018	0.135822
136	3.59204	0.105172	0.0739331	0.0343555	-0.00528185	0.190511	0.0312272	0.0395449	0.0396489	0.110421	0.160117	0.126439	0.126107	0.135844
137	3.59204	0.105162	0.0739151	0.0343529	-0.00526793	0.190292	0.0312078	0.0395497	0.0396291	0.110387	0.160217	0.126423	0.12617	0.135886
138	3.59204	0.105106	0.0738946	0.0343614	-0.00524772	0.190023	0.0311683	0.0395495	0.0396172	0.110335	0.160421	0.126424	0.126208	0.13595
139	3.68046	0.105024	0.073897	0.0343743	-0.00522907	0.189685	0.0311083	0.0395553	0.0396136	0.110277	0.160731	0.126405	0.126219	0.136021
140	3.94571	0.104965	0.0739392	0.0343871	-0.00521643	0.189279	0.031038	0.0395727	0.039621	0.110232	0.161095	0.12635	0.126196	0.136077
141	3.59204	0.104953	0.0740141	0.0344042	-0.0052094	0.18885	0.0309736	0.0395971	0.0396435	0.110214	0.16143	0.126272	0.126124	0.136099
142	3.59204	0.104974	0.07409	0.0344395	-0.00521246	0.188467	0.0309295	0.0396194	0.0396833	0.110232	0.161659	0.126201	0.125998	0.136076
143	3.59204	0.105012	0.0741398	0.0344959	-0.00523403	0.188164	0.0309124	0.039637	0.0397353	0.110285	0.161748	0.126145	0.125833	0.136012
144	3.68046	0.10507	0.0741683	0.034549	-0.00527063	0.187904	0.03092	0.0396584	0.039786	0.110364	0.161708	0.126077	0.125673	0.135914
145	3.94571	0.10515	0.0742068	0.0345647	-0.00530585	0.18763	0.0309453	0.0396954	0.03982	0.110461	0.161576	0.12596	0.125565	0.135795
146	3.59204	0.105244	0.0742732	0.0345365	-0.00532888	0.187327	0.030982	0.0397493	0.0398279	0.110559	0.161385	0.125789	0.12554	0.135674
147	3.59204	0.105346	0.0743389	0.0344902	-0.00533925	0.187018	0.0310262	0.0398064	0.0398102	0.110643	0.161155	0.125609	0.125596	0.135572
148	3.59204	0.105433	0.0743542	0.0344498	-0.00533446	0.186727	0.0310726	0.039848	0.0397747	0.110695	0.160914	0.125477	0.125708	0.135507
149	3.68046	0.105461	0.0743108	0.0344173	-0.00531238	0.186467	0.0311134	0.0398649	0.0397319	0.11071	0.160703	0.125424	0.125844	0.135489
150	3.94571	0.105415	0.0742479	0.034387	-0.00528597	0.186249	0.031144	0.0398614	0.0396922	0.110698	0.160545	0.125435	0.12597	0.135504
151	3.59204	0.10535	0.0742018	0.0343591	-0.00527659	0.186057	0.0311701	0.0398469	0.0396644	0.110681	0.160411	0.12548	0.126058	0.135524
152	3.68046	0.105337	0.0741755	0.0343384	-0.00528872	0.185829	0.0312035	0.0398268	0.0396539	0.110684	0.160239	0.125544	0.126091	0.135521
153	4.03413	0.105385	0.0741558	0.0343358	-0.00530531	0.185502	0.0312519	0.0398009	0.039661	0.110714	0.159992	0.125626	0.126069	0.135485
154	3.94571	0.105456	0.0741381	0.0343627	-0.00531011	0.185094	0.0313107	0.0397693	0.0396812	0.110761	0.159691	0.125725	0.126004	0.135426
155	3.59204	0.105529	0.0741324	0.0344109	-0.00530359	0.184691	0.031366	0.0397354	0.0397071	0.110808	0.15941	0.125833	0.125922	0.135369
156	3.68046	0.105589	0.0741405	0.0344491	-0.00529724	0.184359	0.0314022	0.0397028	0.039732	0.110837	0.159225	0.125936	0.125843	0.135334
157	4.03413	0.105595	0.0741364	0.0344546	-0.00530197	0.184086	0.0314111	0.0396708	0.0397536	0.110836	0.15918	0.126038	0.125775	0.135336
158	4.03413	0.105515	0.0740977	0.0344414	-0.00532083	0.183799	0.0313954	0.039635	0.0397739	0.110804	0.159259	0.126152	0.125711	0.135374
159	4.03413	0.105392	0.0740413	0.0344413	-0.00534637	0.183462	0.0313674	0.0395929	0.0397949	0.110755	0.159401	0.126286	0.125645	0.135434
160	4.03413	0.105309	0.0739999	0.034463	-0.00536522	0.183127	0.0313413	0.039547	0.0398139	0.110702	0.159534	0.126432	0.125584	0.135499
161	4.03413	0.105292	0.0739776	0.034485	-0.00536816	0.182883	0.0313236	0.0395013	0.039825	0.11065	0.159624	0.126579	0.125549	0.135563
162	4.03413	0.105281	0.0739524	0.0344904	-0.0053532	0.182738	0.031312	0.039458	0.0398243	0.110594	0.159683	0.126717	0.125551	0.135631
163	4.03413	0.105219	0.0739112	0.034491	-0.00532115	0.182584	0.0313028	0.0394191	0.0398147	0.110537	0.15973	0.126842	0.125582	0.135702
164	4.03413	0.105143	0.0738715	0.0345087	-0.00527877	0.182306	0.0312977	0.0393907	0.0398035	0.110492	0.159756	0.126934	0.125617	0.135757
165	4.03413	0.105141	0.073867	0.0345402	-0.00524489	0.181913	0.0313014	0.0393824	0.0397967	0.110481	0.159738	0.12696	0.125638	0.135771
166	4.03413	0.105225	0.0739112	0.0345549	-0.00524013	0.181524	0.0313151	0.0393987	0.0397953	0.110509	0.159667	0.126908	0.125643	0.135735
167	3.94571	0.105317	0.0739731	0.0345322	-0.00526862	0.18123	0.0313352	0.0394312	0.0397962	0.110563	0.159565	0.126804	0.12564	0.13567
168	3.68046	0.105353	0.0739992	0.0344874	-0.00531343	0.181009	0.0313568	0.0394617	0.0397956	0.110614	0.159455	0.126705	0.125642	0.135607
169	4.03413	0.105341	0.0739676	0.0344527	-0.00534592	0.180767	0.031376	0.0394768	0.039792	0.110645	0.159358	0.126657	0.125653	0.135569
170	4.03413	0.105323	0.0739152	0.0344433	-0.0053442	0.180427	0.0313868	0.039478	0.0397865	0.110651	0.159303	0.126653	0.125671	0.135561
171	4.03413	0.105326	0.0738999	0.034457	-0.00531282	0.179995	0.0313788	0.0394805	0.0397821	0.110641	0.159344	0.126645	0.125685	0.135573
172	4.03413	0.105344	0.0739451	0.0344889	-0.00528	0.179536	0.0313422	0.0395018	0.0397803	0.110624	0.159531	0.126577	0.125691	0.135594
173	4.03413	0.105344	0.0740307	0.0345236	-0.00526816	0.179122	0.0312758	0.0395518	0.0397772	0.110605	0.159871	0.126418	0.1257	0.135618
174	4.03413	0.105309	0.0741247	0.0345263	-0.00527491	0.178786	0.0311919	0.0396271	0.0397663	0.110585	0.160301	0.126178	0.125735	0.135642
175	4.03413	0.105268	0.0742052	0.0344759	-0.0052858	0.178534	0.0311112	0.0397109	0.0397453	0.110567	0.160717	0.125912	0.125801	0.135664
176	4.03413	0.105258	0.0742594	0.0344058	-0.00528986	0.178353	0.0310518	0.0397781	0.0397222	0.110552	0.161023	0.125698	0.125874	0.135683
177	4.03413	0.105271	0.0742787	0.0343827	-0.00527963	0.178184	0.0310204	0.0398085	0.0397099	0.110539	0.161185	0.125602	0.125913	0.135699
178	4.03413	0.105267	0.074264	0.0344317	-0.00525794	0.177937	0.0310125	0.0398017	0.0397148	0.110529	0.161226	0.125623	0.125898	0.135711
179	4.03413	0.105245	0.0742333	0.0344982	-0.00524816	0.177575	0.0310193	0.0397782	0.0397298	0.110527	0.16119	0.125697	0.12585	0.135713
180	4.03413	0.105237	0.0742092	0.0345067	-0.00527266	0.177154	0.0310328	0.0397644	0.03974	0.110537	0.16112	0.125741	0.125818	0.135701
181	4.03413	0.10525	0.0741952	0.0344468	-0.00531777	0.17676	0.031047	0.0397737	0.0397345	0.110555	0.161046	0.125711	0.125835	0.135679
182	4.03413	0.105258	0.0741843	0.0343757	-0.00534384	0.176433	0.031057	0.0398028	0.0397129	0.110573	0.160994	0.12562	0.125904	0.135657
183	3.85177	0.105257	0.0741856	0.0343416	-0.00533317	0.176146	0.0310613	0.0398409	0.0396832	0.110585	0.160972	0.125499	0.125998	0.135642
184	3.30467	0.105266	0.074212	0.034336	-0.0053071	0.175847	0.0310636	0.0398798	0.0396543	0.110598	0.16096	0.125377	0.12609	0.135627
185	4.03413	0.105299	0.0742524	0.0343286	-0.00529238	0.175499	0.0310701	0.0399143	0.0396314	0.110616	0.160926	0.125269	0.126163	0.135605
186	4.03413	0.105353	0.0742835	0.0343174	-0.00528963	0.175108	0.031083	0.0399397	0.0396157	0.110638	0.16086	0.125189	0.126213	0.135577
187	4.03413	0.105415	0.0742979	0.0343213	-0.00528059	0.174736	0.0310964	0.0399527	0.0396053	0.110654	0.160791	0.125148	0.126246	0.135557
188	4.03413	0.10545	0.0743064	0.0343469	-0.00525338	0.174437	0.0311015	0.0399545	0.0395967	0.110653	0.160764	0.125142	0.126273	0.135559
189	4.03413	0.105428	0.0743206	0.0343802	-0.00521517	0.17419	0.0310982	0.0399517	0.0395859	0.110636	0.160781	0.125151	0.126308	0.13558
190	4.03413	0.105379	0.0743328	0.0343956	-0.0051862	0.173915	0.0311017	0.0399502	0.0395706	0.110622	0.160764	0.125156	0.126356	0.135596
191	4.03413	0.105369	0.0743212	0.0343698	-0.00518397	0.173559	0.0311324	0.039949	0.0395536	0.110635	0.160606	0.12516	0.126411	0.135581
192	4.03413	0.105428	0.0742771	0.0343049	-0.00521164	0.173142	0.0311989	0.039938	0.0395444	0.110681	0.160266	0.125194	0.12644	0.135524
193	4.03413	0.105512	0.0742071	0.0342398	-0.00526014	0.172722	0.0312865	0.0399021	0.0395568	0.110745	0.159818	0.125308	0.126401	0.135446
194	4.03413	0.105555	0.0741184	0.0342251	-0.00531579	0.172335	0.0313643	0.0398323	0.0396006	0.110797	0.15942	0.125528	0.126262	0.135383
195	4.03413	0.105527	0.0740316	0.034284	-0.00536383	0.171978	0.0314027	0.0397341	0.0396731	0.11081	0.159224	0.125839	0.126032	0.135367
196	4.03413	0.105445	0.0739826	0.034392	-0.00539233	0.171624	0.0313886	0.0396275	0.0397564	0.110772	0.159296	0.126177	0.125767	0.135413
197	4.03413	0.105332	0.0739754	0.0344938	-0.00539705	0.171248	0.0313293	0.0395366	0.0398261	0.110692	0.159598	0.126467	0.125547	0.135511

Point	MTSP.y	A.y	B.y	C.y	D.y	EE.y	ThickA.y	ThickB.y	ThickC.y	SheetThick.y	DenA.y	DenB.y	DenC.y	SheetDen.y
198	4.03413	0.105203	0.0739696	0.0345445	-0.00538094	0.170845	0.0312449	0.0394794	0.0398652	0.110589	0.16003	0.126649	0.125423	0.135637
199	4.03413	0.105087	0.0739507	0.0345447	-0.00535108	0.170444	0.0311562	0.039464	0.0398727	0.110493	0.160485	0.126698	0.125399	0.135756
200	4.03413	0.105029	0.0739677	0.034532	-0.00531742	0.170089	0.0310778	0.039489	0.0398613	0.110428	0.160889	0.126618	0.125435	0.135835
201	4.03413	0.105049	0.0740604	0.0345368	-0.0052911	0.169802	0.0310196	0.0395432	0.0398459	0.110409	0.16119	0.126445	0.125484	0.135859
202	3.94571	0.105118	0.0741861	0.0345509	-0.00528087	0.169538	0.0309922	0.0396066	0.0398331	0.110432	0.161332	0.126243	0.125524	0.13583
203	3.68046	0.105191	0.0742607	0.0345467	-0.00528826	0.169231	0.0310041	0.039657	0.0398216	0.110483	0.16127	0.126082	0.12556	0.135768
204	4.12255	0.105252	0.074244	0.0345147	-0.00530382	0.168852	0.0310544	0.0396807	0.0398081	0.110543	0.16101	0.126006	0.125603	0.135694
205	4.38781	0.105307	0.0741671	0.034474	-0.00531159	0.168434	0.0311267	0.0396785	0.0397952	0.1106	0.160637	0.126013	0.125643	0.135623
206	4.03413	0.105358	0.0741027	0.0344539	-0.00530418	0.168028	0.0311951	0.039661	0.0397915	0.110648	0.160284	0.126068	0.125655	0.135568
207	4.03413	0.105401	0.0741035	0.0344708	-0.0052944	0.167668	0.0312392	0.0396381	0.0398053	0.110683	0.160056	0.126141	0.125612	0.135523
208	4.03413	0.105418	0.0741443	0.0345141	-0.00530391	0.167359	0.0312552	0.0396124	0.0398372	0.110705	0.159974	0.126223	0.125511	0.135496
209	4.03413	0.1054	0.0741565	0.034557	-0.005336	0.167078	0.0312529	0.0395837	0.0398768	0.110713	0.159985	0.126315	0.125387	0.135485
210	4.03413	0.105358	0.0741222	0.0345836	-0.00536698	0.166798	0.0312444	0.0395566	0.0399075	0.110708	0.160029	0.126401	0.12529	0.135491
211	4.03413	0.105329	0.0740881	0.0345932	-0.00537032	0.166507	0.0312346	0.0395423	0.0399153	0.110692	0.160079	0.126447	0.125266	0.135511
212	4.03413	0.105326	0.0740874	0.0345821	-0.00534621	0.166199	0.0312205	0.0395506	0.0398966	0.110668	0.160151	0.126421	0.125324	0.135541
213	4.03413	0.105323	0.0741065	0.0345421	-0.00531967	0.165857	0.0311983	0.0395815	0.0398594	0.110639	0.160266	0.126322	0.125441	0.135576
214	4.03413	0.105297	0.0741242	0.0344861	-0.00530894	0.165449	0.031168	0.039624	0.0398183	0.11061	0.160421	0.126187	0.125571	0.135611
215	4.12255	0.105266	0.074141	0.0344498	-0.00530625	0.164958	0.0311343	0.0396647	0.0397868	0.110586	0.160595	0.126057	0.12567	0.135641
216	4.38781	0.105257	0.0741659	0.0344545	-0.00529498	0.164424	0.0311026	0.0396965	0.0397719	0.110571	0.160759	0.125956	0.125717	0.135659
217	4.03413	0.105271	0.0741996	0.0344841	-0.00527567	0.163936	0.0310747	0.039722	0.0397739	0.110571	0.160903	0.125875	0.125711	0.13566
218	4.03413	0.105294	0.0742393	0.03451	-0.00526689	0.163558	0.0310484	0.0397495	0.0397885	0.110586	0.161039	0.125788	0.125664	0.135641
219	4.03413	0.105319	0.0742876	0.0345227	-0.00528401	0.163273	0.0310189	0.0397871	0.039809	0.110615	0.161193	0.125669	0.1256	0.135606
220	4.03413	0.105341	0.0743443	0.0345235	-0.00532299	0.163009	0.0309825	0.0398379	0.0398257	0.110646	0.161382	0.125509	0.125547	0.135567
221	4.03413	0.105342	0.0743952	0.0345031	-0.00536604	0.162694	0.0309398	0.0398989	0.0398286	0.110667	0.161605	0.125318	0.125538	0.135542
222	4.03413	0.105307	0.0744202	0.034449	-0.0053975	0.162298	0.0308963	0.0399618	0.0398125	0.110671	0.161833	0.12512	0.125589	0.135537
223	4.03413	0.105249	0.0744154	0.0343697	-0.00541224	0.161848	0.0308623	0.0400144	0.0397833	0.11066	0.162011	0.124956	0.125681	0.13555
224	4.03413	0.1052	0.0743965	0.0343003	-0.00541605	0.161386	0.0308497	0.0400424	0.0397554	0.110647	0.162077	0.124868	0.125769	0.135566
225	4.03413	0.105196	0.0743801	0.0342813	-0.005418	0.160932	0.0308675	0.0400345	0.0397415	0.110643	0.161984	0.124893	0.125813	0.135571
226	4.03413	0.105237	0.0743616	0.0343221	-0.00541505	0.16051	0.0309182	0.0399884	0.0397428	0.110649	0.161719	0.125037	0.125809	0.135563
227	4.03413	0.105289	0.074314	0.0343866	-0.00539158	0.160167	0.0309945	0.0399153	0.0397496	0.110659	0.161322	0.125267	0.125787	0.135551
228	4.03413	0.105322	0.0742258	0.0344273	-0.00534643	0.159928	0.0310806	0.039838	0.0397514	0.11067	0.160875	0.12551	0.125782	0.135538
229	4.03413	0.105346	0.07414	0.0344318	-0.00530797	0.159724	0.0311583	0.0397809	0.0397456	0.110685	0.160473	0.125689	0.1258	0.13552
230	4.03413	0.105381	0.0741215	0.0344202	-0.00530362	0.159457	0.0312165	0.0397554	0.0397361	0.110708	0.160173	0.125769	0.12583	0.135492
231	4.03413	0.105426	0.07417	0.0344088	-0.00532318	0.159106	0.0312572	0.0397526	0.0397254	0.110735	0.159964	0.125778	0.125864	0.135458
232	4.03413	0.105467	0.0742051	0.0343984	-0.00533135	0.158739	0.0312895	0.0397505	0.0397122	0.110752	0.159799	0.125785	0.125906	0.135438
233	4.12255	0.105487	0.0741635	0.0343887	-0.00531129	0.158408	0.0313156	0.039732	0.039696	0.110744	0.159665	0.125844	0.125957	0.135448
234	4.38781	0.10547	0.0740754	0.0343848	-0.00527819	0.158086	0.0313234	0.0396974	0.0396815	0.110702	0.159626	0.125953	0.126003	0.135499
235	4.03413	0.105403	0.0740183	0.0343937	-0.00525362	0.157719	0.0312971	0.0396597	0.0396765	0.110633	0.159761	0.126073	0.126019	0.135583
236	4.03413	0.105293	0.0740272	0.0344195	-0.00524437	0.157287	0.0312365	0.03963	0.0396867	0.110553	0.160072	0.126167	0.125987	0.135681
237	4.03413	0.105183	0.0740697	0.0344524	-0.00524813	0.15682	0.0311638	0.0396072	0.0397129	0.110484	0.160445	0.12624	0.125904	0.135767
238	4.03413	0.105114	0.0740886	0.034475	-0.00526518	0.156372	0.0311106	0.0395806	0.039753	0.110444	0.160719	0.126325	0.125777	0.135815
239	4.03413	0.105095	0.0740612	0.0344907	-0.00529594	0.15597	0.0310968	0.0395416	0.0398035	0.110442	0.160789	0.12645	0.125618	0.135818
240	4.03413	0.105118	0.0740194	0.0345273	-0.0053305	0.155575	0.0311225	0.0394917	0.039858	0.110472	0.160657	0.12661	0.125446	0.135781
241	4.03413	0.105175	0.0740043	0.034591	-0.00534966	0.155116	0.0311738	0.0394412	0.0399055	0.11052	0.160393	0.126772	0.125296	0.135722
242	4.03413	0.10525	0.0740135	0.0346436	-0.00534275	0.154587	0.0312351	0.0394008	0.0399335	0.110569	0.160078	0.126901	0.125208	0.135661
243	4.03413	0.10532	0.0740138	0.03465	-0.00531989	0.154064	0.0312941	0.0393741	0.0399354	0.110604	0.159776	0.126987	0.125202	0.13562
244	4.03413	0.10536	0.0739881	0.0346254	-0.00529782	0.153633	0.0313402	0.0393582	0.0399141	0.110612	0.159541	0.127038	0.125269	0.135609
245	4.03413	0.105357	0.0739477	0.0346045	-0.00527793	0.153325	0.0313641	0.039351	0.0398778	0.110593	0.159418	0.127062	0.125383	0.135633
246	4.03413	0.105318	0.0739156	0.0345925	-0.00524893	0.153094	0.0313607	0.0393564	0.0398348	0.110552	0.159436	0.127044	0.125519	0.135683
247	4.03413	0.105269	0.0739154	0.0345773	-0.00520787	0.152834	0.0313322	0.0393815	0.039792	0.110506	0.159581	0.126964	0.125654	0.13574
248	4.03413	0.105248	0.0739613	0.0345617	-0.00516924	0.152458	0.0312878	0.0394289	0.0397567	0.110473	0.159808	0.126811	0.125765	0.135779
249	4.03413	0.10527	0.0740421	0.0345526	-0.00515331	0.151979	0.031239	0.0394914	0.039735	0.110465	0.160057	0.126611	0.125834	0.135789
250	4.03413	0.105307	0.0741254	0.0345425	-0.00516937	0.151483	0.031196	0.0395535	0.0397279	0.110477	0.160278	0.126412	0.125856	0.135774
251	4.03413	0.105315	0.0741741	0.0345242	-0.00520891	0.151001	0.0311662	0.0395989	0.0397295	0.110495	0.160431	0.126267	0.125851	0.135753
252	4.03413	0.105281	0.0741609	0.0344998	-0.00525186	0.150502	0.0311528	0.0396193	0.03973	0.110502	0.160499	0.126201	0.12585	0.135744
253	4.03413	0.105232	0.0740907	0.034467	-0.00527873	0.149982	0.0311521	0.0396187	0.0397225	0.110493	0.160503	0.126203	0.125873	0.135755
254	4.03413	0.105199	0.0740163	0.0344274	-0.00527973	0.149496	0.0311518	0.0396084	0.039709	0.110469	0.160505	0.126236	0.125916	0.135784
255	4.03413	0.105188	0.0739981	0.0344077	-0.00525834	0.149087	0.0311373	0.0395981	0.0396985	0.110434	0.16058	0.126269	0.125949	0.135828
256	4.03413	0.105171	0.0740394	0.0344377	-0.00522903	0.148728	0.0311027	0.0395907	0.0396993	0.110393	0.160759	0.126292	0.125947	0.135879
257	4.03413	0.10513	0.0740917	0.0345051	-0.00520648	0.148354	0.0310562	0.0395868	0.0397094	0.110352	0.161	0.126305	0.125915	0.135928
258	4.03413	0.105092	0.0741214	0.0345604	-0.00519459	0.147926	0.0310142	0.0395903	0.0397169	0.110321	0.161217	0.126294	0.125891	0.135966
259	4.03413	0.105093	0.0741351	0.0345631	-0.00518936	0.147451	0.0309895	0.0396049	0.0397092	0.110304	0.161345	0.126247	0.125916	0.135988
260	4.03413	0.105117	0.0741426	0.0345109	-0.00518798	0.146953	0.0309858	0.0396263	0.0396853	0.110297	0.161365	0.126179	0.125992	0.135996
261	4.03413	0.105116	0.0741327	0.0344401	-0.00518693	0.146442	0.0310022	0.0396399	0.0396577	0.1103	0.161279	0.126136	0.126079	0.135993
262	4.03413	0.105094	0.0740969	0.034406	-0.00518176	0.145945	0.0310387	0.039632	0.0396443	0.110315	0.161091	0.126161	0.126122	0.135974
263	4.03413	0.105112	0.0740504	0.0344372	-0.00517914	0.145519	0.0310922	0.0396036	0.0396534	0.110349	0.160814	0.126252	0.126093	0.135932

Point	MTSP.y	A.y	B.y	C.y	D.y	EE.y	ThickA.y	ThickB.y	ThickC.y	SheetThick.y	DenA.y	DenB.y	DenC.y	SheetDen.y
264	4.03413	0.105197	0.0740204	0.0344987	-0.00519279	0.145176	0.0311493	0.039572	0.0396772	0.110399	0.160519	0.126352	0.126017	0.135871
265	4.03413	0.105293	0.0740237	0.0345264	-0.00521863	0.144843	0.0311879	0.0395567	0.0396986	0.110443	0.16032	0.126401	0.125949	0.135817
266	4.03413	0.105316	0.0740516	0.0345026	-0.00523332	0.144446	0.0311914	0.0395637	0.039705	0.11046	0.160302	0.126379	0.125929	0.135796
267	4.03413	0.10525	0.0740761	0.0344684	-0.00522443	0.143981	0.0311643	0.0395832	0.0396967	0.110444	0.160441	0.126318	0.125955	0.135815
268	4.03413	0.10516	0.0740822	0.0344604	-0.00520617	0.143507	0.0311325	0.0396014	0.0396825	0.110416	0.160605	0.126258	0.126	0.135849
269	4.03413	0.105122	0.0740801	0.0344667	-0.00520012	0.143079	0.031127	0.0396116	0.03967	0.110409	0.160633	0.126226	0.12604	0.135859
270	4.03413	0.105161	0.0740696	0.0344531	-0.00521256	0.142698	0.0311645	0.039614	0.0396628	0.110441	0.160441	0.126218	0.126063	0.135819
271	3.94571	0.10525	0.074029	0.0344078	-0.00523902	0.142324	0.0312354	0.0396112	0.0396654	0.110512	0.160078	0.126227	0.126055	0.135732
272	3.68046	0.105343	0.0739674	0.0343579	-0.00527884	0.141919	0.0313075	0.0396059	0.0396851	0.110599	0.159709	0.126244	0.125992	0.135626
273	3.94571	0.105404	0.0739439	0.0343541	-0.0053278	0.141485	0.0313432	0.0396032	0.0397263	0.110673	0.159527	0.126252	0.125862	0.135535
274	3.68046	0.105419	0.0740038	0.0344231	-0.00536528	0.141056	0.031321	0.0396108	0.03978	0.110712	0.15964	0.126228	0.125692	0.135487
275	3.94571	0.105397	0.0741249	0.034524	-0.00536944	0.140631	0.0312467	0.0396333	0.0398237	0.110704	0.160022	0.126157	0.125554	0.135497
276	3.68046	0.105361	0.074239	0.0345766	-0.00534169	0.140176	0.0311458	0.0396653	0.0398345	0.110646	0.16054	0.126055	0.12552	0.135568
277	4.03413	0.105297	0.0742852	0.0345449	-0.00530358	0.139682	0.0310478	0.0396892	0.0398051	0.110542	0.161046	0.125979	0.125613	0.135695
278	3.85177	0.105168	0.0742377	0.0344688	-0.00527199	0.139199	0.0309755	0.0396837	0.0397483	0.110408	0.16142	0.125997	0.125793	0.135861
279	3.21625	0.104979	0.0741087	0.034409	-0.0052455	0.138783	0.030944	0.0396399	0.0396862	0.11027	0.161584	0.126137	0.125989	0.13603
280	3.68046	0.104823	0.0739455	0.0343866	-0.0052171	0.138449	0.0309594	0.0395714	0.0396382	0.110169	0.161503	0.126355	0.126141	0.136155
281	4.03413	0.104799	0.0738191	0.0343849	-0.0051944	0.138151	0.0310129	0.0395081	0.0396144	0.110135	0.161226	0.126557	0.126217	0.136196
282	3.94571	0.104908	0.0737814	0.0343853	-0.00519675	0.137808	0.0310764	0.0394786	0.0396168	0.110172	0.160896	0.126652	0.126209	0.136151
283	3.59204	0.10505	0.0738296	0.0343877	-0.0052302	0.13735	0.0311132	0.0394942	0.0396413	0.110249	0.160705	0.126602	0.126131	0.136056
284	3.68046	0.105131	0.0739333	0.0344063	-0.00527271	0.136784	0.031099	0.0395468	0.0396783	0.110324	0.160779	0.126434	0.126014	0.135963
285	4.03413	0.105142	0.0740749	0.0344512	-0.00528999	0.136201	0.0310392	0.0396168	0.0397141	0.11037	0.16109	0.12621	0.1259	0.135906
286	4.03413	0.105129	0.0742256	0.0345073	-0.00526784	0.135695	0.0309669	0.0396822	0.0397364	0.110385	0.161466	0.126002	0.125829	0.135887
287	4.03413	0.105132	0.0743213	0.0345399	-0.00522611	0.13529	0.0309219	0.0397253	0.03974	0.110387	0.1617	0.125865	0.125818	0.135885
288	4.03413	0.105168	0.0743192	0.0345344	-0.0051949	0.13492	0.0309255	0.0397378	0.0397297	0.110393	0.161681	0.125825	0.125851	0.135878
289	4.03413	0.105226	0.0742565	0.0345167	-0.00518153	0.134482	0.0309695	0.0397228	0.0397162	0.110409	0.161451	0.125872	0.125893	0.135859
290	4.03413	0.105271	0.0742037	0.0345165	-0.00517298	0.133925	0.0310277	0.0396914	0.0397101	0.110429	0.161148	0.125972	0.125913	0.135834
291	4.03413	0.105288	0.0741798	0.0345322	-0.00516595	0.133312	0.0310755	0.0396555	0.0397168	0.110448	0.1609	0.126086	0.125891	0.135811
292	4.03413	0.105289	0.0741619	0.0345479	-0.00517307	0.132763	0.0310991	0.0396231	0.0397368	0.110459	0.160777	0.126189	0.125828	0.135797
293	4.03413	0.10529	0.0741493	0.0345637	-0.00519643	0.132326	0.0310936	0.0395975	0.0397663	0.110457	0.160805	0.126271	0.125735	0.135799
294	3.94571	0.105268	0.0741597	0.0345889	-0.00521813	0.131949	0.0310613	0.0395786	0.0397984	0.110438	0.160973	0.126331	0.125633	0.135822
295	3.68046	0.105191	0.0741825	0.0346175	-0.0052276	0.131547	0.0310158	0.0395651	0.0398248	0.110406	0.16121	0.126374	0.12555	0.135863
296	4.03413	0.105083	0.0741815	0.0346274	-0.00523681	0.131081	0.0309827	0.0395566	0.0398381	0.110377	0.161382	0.126401	0.125508	0.135897
297	4.03413	0.105031	0.0741427	0.0346049	-0.00525587	0.130564	0.0309849	0.0395558	0.0398343	0.110375	0.161371	0.126404	0.12552	0.1359
298	4.03413	0.105094	0.0740961	0.0345603	-0.00527247	0.130045	0.0310234	0.0395674	0.0398146	0.110405	0.16117	0.126367	0.125582	0.135863
299	4.03413	0.105224	0.0740865	0.0345152	-0.00526897	0.129554	0.0310756	0.0395918	0.0397862	0.110454	0.1609	0.126289	0.125672	0.135804
300	4.03413	0.105308	0.0741241	0.0344865	-0.00524829	0.129069	0.0311153	0.0396214	0.0397605	0.110497	0.160694	0.126195	0.125753	0.13575
301	4.03413	0.1053	0.0741666	0.0344794	-0.00523323	0.128545	0.0311356	0.0396442	0.0397481	0.110528	0.160588	0.126122	0.125792	0.135712
302	4.03413	0.105263	0.074165	0.0344868	-0.00524262	0.127989	0.0311495	0.0396545	0.039753	0.110557	0.160517	0.126089	0.125777	0.135677
303	4.03413	0.10528	0.074131	0.0344983	-0.00527204	0.127468	0.0311694	0.0396591	0.0397696	0.110598	0.160414	0.126074	0.125724	0.135626
304	4.03413	0.105364	0.0741351	0.0345116	-0.00529845	0.127023	0.0311928	0.0396704	0.0397856	0.110649	0.160294	0.126039	0.125674	0.135564
305	4.03413	0.105457	0.0742092	0.0345243	-0.0053022	0.126617	0.0312073	0.0396914	0.0397879	0.110687	0.160219	0.125972	0.125667	0.135518
306	4.03413	0.105496	0.0742797	0.0345199	-0.00528365	0.12618	0.0312029	0.0397109	0.0397707	0.110685	0.160242	0.12591	0.125721	0.13552
307	4.03413	0.105445	0.0742484	0.0344811	-0.00526104	0.125682	0.0311752	0.039715	0.0397393	0.110629	0.160385	0.125897	0.12582	0.135588
308	4.03413	0.105303	0.0741251	0.0344192	-0.00525506	0.125145	0.0311205	0.0397018	0.0397079	0.11053	0.160669	0.125939	0.12592	0.13571
309	4.03413	0.105112	0.0740184	0.0343725	-0.00527292	0.12461	0.0310388	0.039685	0.0396906	0.110414	0.161093	0.125992	0.125974	0.135852
310	3.94571	0.104935	0.0740057	0.0343676	-0.00530391	0.124121	0.0309458	0.0396808	0.0396912	0.110318	0.161578	0.126006	0.125973	0.135971
311	3.68046	0.104835	0.074067	0.0343901	-0.00532997	0.123692	0.0308762	0.039694	0.0397004	0.110271	0.161941	0.125964	0.125943	0.136029
312	4.03413	0.104855	0.0741388	0.0344055	-0.00533664	0.123279	0.030869	0.0397146	0.0397035	0.110287	0.16198	0.125898	0.125934	0.136009
313	4.03413	0.104998	0.0741757	0.0344037	-0.00531362	0.122804	0.0309421	0.0397261	0.0396919	0.11036	0.161601	0.125862	0.12597	0.135919
314	4.03413	0.105218	0.0741642	0.0344055	-0.00526001	0.122246	0.0310767	0.0397175	0.0396689	0.110463	0.160904	0.125889	0.126044	0.135792
315	3.94571	0.105429	0.0741188	0.0344233	-0.00519683	0.121672	0.0312239	0.0396902	0.0396469	0.110561	0.160144	0.125976	0.126113	0.135672
316	3.68046	0.105548	0.0740751	0.0344432	-0.00515902	0.121155	0.0313312	0.0396545	0.0396399	0.110626	0.159591	0.126089	0.126136	0.135593
317	3.94571	0.10554	0.0740618	0.0344533	-0.00516487	0.120697	0.0313724	0.0396177	0.0396563	0.110646	0.159378	0.126207	0.126084	0.135567
318	3.68046	0.105442	0.0740729	0.0344673	-0.00520189	0.12025	0.0313596	0.0395764	0.0396959	0.110632	0.159442	0.126339	0.125958	0.135585
319	3.94571	0.105334	0.0740727	0.0345038	-0.0052451	0.119787	0.0313304	0.0395208	0.0397505	0.110602	0.159591	0.126517	0.125785	0.135622
320	3.68046	0.105273	0.0740252	0.0345523	-0.00527865	0.119304	0.0313181	0.039447	0.0398077	0.110573	0.159653	0.126754	0.125605	0.135657
321	4.03413	0.105252	0.0739303	0.034585	-0.00529759	0.118794	0.0313308	0.0393645	0.0398573	0.110553	0.159588	0.12702	0.125448	0.135682
322	4.03413	0.105237	0.0738397	0.0346008	-0.00530121	0.118246	0.0313545	0.0392921	0.0398969	0.110543	0.159467	0.127253	0.125323	0.135693
323	4.03413	0.105224	0.0738188	0.0346281	-0.00529282	0.117685	0.0313739	0.0392456	0.0399299	0.110549	0.159369	0.127403	0.12522	0.135686
324	4.03413	0.105245	0.0738804	0.0346805	-0.00527955	0.11716	0.0313894	0.0392277	0.0399597	0.110577	0.15929	0.127461	0.125126	0.135652
325	4.03413	0.105328	0.0739706	0.0347366	-0.0052668	0.11669	0.0314132	0.0392287	0.0399841	0.110626	0.15917	0.127458	0.12505	0.135592
326	3.94571	0.105452	0.074022	0.0347686	-0.00525614	0.116252	0.0314509	0.0392345	0.0399969	0.110682	0.158979	0.127439	0.12501	0.135523
327	3.68046	0.105553	0.074018	0.0347708	-0.00524758	0.115815	0.0314909	0.0392368	0.0399923	0.11072	0.158777	0.127431	0.125024	0.135477
328	4.03413	0.105567	0.073983	0.0347535	-0.00523925	0.115351	0.0315121	0.0392379	0.0399873	0.110717	0.15867	0.127428	0.125103	0.13548
329	4.03413	0.105485	0.0739367	0.0347197	-0.00522908	0.114838	0.0315002	0.0392497	0.0399211	0.110671	0.15873	0.12739	0.125248	0.135537

Point	MTSP.y	A.y	B.y	C.y	D.y	EE.y	ThickA.y	ThickB.y	ThickC.y	SheetThick.y	DenA.y	DenB.y	DenC.y	SheetDen.y
330	4.03413	0.105356	0.073885	0.0346586	-0.00522232	0.114278	0.0314555	0.0392897	0.0398541	0.110599	0.158957	0.127261	0.125459	0.135625
331	3.94571	0.105246	0.0738459	0.0345579	-0.00523192	0.113713	0.0313858	0.0393727	0.0397685	0.110527	0.159311	0.126995	0 125729	0.135714
332	3 68046	0.105179	0.0738528	0.0344166	-0.00526284	0.113173	0.0312975	0.0395015	0.0396709	0.11047	0.159761	0.126583	0.126039	0.135784
333	4.03413	0.105136	0.0739184	0.0342563	-0.00529878	0.112649	0.0311954	0.0396581	0.0395744	0.110428	0.160285	0.126083	0 126346	0.135835
334	4.03413	0.105089	0.0740141	0.0341238	-0.00531515	0.112109	0.0310889	0 039808	0.0394985	0.110395	0.160834	0.125607	0.126588	0.135875
335	4.03413	0.105041	0.0740972	0.0340684	-0.00530554	0.111536	0.0309949	0.0399156	0.0394639	0.110374	0 16132	0.125267	0.126699	0.135901
336	4.03413	0.105025	0.074159	0.0341123	-0.00528562	0.110942	0.0309323	0.0399622	0.0394823	0.110377	0.161645	0.125119	0.12664	0.135898
337	3 94571	0.105075	0.0742273	0.034237	-0.00527104	0.110364	0.0309145	0.0399506	0.039549	0.110414	0.161738	0.125155	0.126427	0.135852
338	3.68046	0.105192	0.0743106	0.0343911	-0.00526366	0.109829	0.0309458	0.0398943	0.0396434	0.110484	0.161575	0.125333	0.126126	0.135767
339	3.94571	0.105336	0.0743627	0.0345186	-0.00526113	0.10933	0.031021	0.0398034	0 0397394	0.110564	0.161185	0.12562	0.125822	0.135668
340	3.68046	0.105441	0.0743276	0.0345942	-0.00526573	0.108838	0.0311273	0.0396803	0.0398164	0.110624	0.160637	0.126011	0.125577	0.135595
341	4.03413	0.105456	0.0741942	0.0346257	-0.00527765	0.108339	0.0312486	0.039526	0 0398652	0.11064	0.160014	0.126505	0.125423	0.135575
342	4.03413	0.105371	0.073987	0.0346266	-0.00528955	0.107851	0.0313726	0.0393494	0.0398869	0.110609	0 159381	0.127074	0.125355	0.135613
343	4.03413	0.105232	0.0737424	0.0346043	-0.00529575	0.107391	0.0314948	0.0391684	0.03989	0.110553	0.158762	0.12766	0.125345	0.135681
344	4.03413	0.105123	0.073515	0.03457	-0.0053026	0.106946	0.0316151	0.0390018	0.0398867	0.110504	0.158158	0.128205	0.125355	0.135742
345	4.03413	0.105102	0.07336	0.0345401	-0.00532204	0.106481	0.0317311	0.0388559	0.0398892	0.110476	0.157579	0.128685	0.125347	0.135776
346	3.94571	0.105143	0.0732732	0.0345258	-0.00535618	0.105968	0.0318333	0.0387172	0.0399061	0.110457	0.157072	0.129146	0.125294	0.1358
347	3.68046	0.105138	0.0731709	0.0345233	-0.00539852	0.105407	0.031906	0.0385577	0.0399421	0.110406	0.156713	0.129683	0.125182	0.135863
348	3.94571	0.10498	0.0729645	0.034517	-0.00545176	0.104804	0.0319323	0.0383518	0 0400015	0.110286	0.156583	0.130385	0.124997	0.136011
349	3.68046	0.104644	0 0726506	0.0345003	-0 00553503	0.104174	0.0319011	0.0380898	0.0400909	0.110082	0.156737	0.131289	0.124719	0.136264
350	4.03413	0.104178	0.0722985	0.0344864	-0.00566827	0.103552	0.0318132	0.0377772	0.0402164	0.109807	0.157174	0.132382	0.124332	0.136606
351	4.03413	0.103648	0.0719497	0.0344867	-0.00585198	0.102974	0.0316823	0.037425	0.0403774	0.109485	0.157826	0.133634	0.123838	0.137009
352	4.03413	0.103092	0.0715754	0.0344931	-0.00606464	0.102435	0.0315278	0.0370415	0.0405643	0.109134	0.158601	0.135023	0.123268	0.13745
353	4.03413	0.102515	0.0711483	0.0344926	-0.00628079	0.101895	0.0313634	0.0366326	0.0407622	0.108758	0.159433	0.136536	0.12267	0.137925
354	4.03413	0.101911	0.0706952	0.0344838	-0.00648974	0.101321	0.0311932	0.0362036	0 0409573	0.108354	0 160304	0.138159	0 122085	0.13844
355	4.03413	0.101274	0.0702454	0.034469	-0.00669436	0.100717	0.031017	0.0357563	0.0411405	0.107914	0.161215	0.139893	0.12154	0.139006
356	4.12255	0.1006	0.0697736	0.034441	-0.00689445	0.100108	0.0308367	0.0352877	0.0413076	0.107432	0.162158	0.141759	0.121048	0.139631
357	4.29939	0.0998821	0.0692376	0.0343965	-0.0070802	0.099508	0.0306566	0.034794	0 0414584	0.106909	0.163111	0.14378	0.120606	0.140315
358	3.76888	0.0991327	0.0686502	0.0343563	-0.00724386	0.0989178	0.0304779	0.0342785	0.0415953	0.106352	0.164067	0.14595	0.120209	0.141052
359	4.47623	0.0983866	0.0680757	0.0343445	-0.00738716	0.0983485	0.0302983	0.0337529	0.0417194	0.105771	0.16504	0.148226	0.119851	0.141827
360	4.47623	0.0976738	0.0675533	0.0343499	-0.00751184	0.0978247	0.0301142	0.0332299	0.0418283	0.105172	0 166051	0.150559	0.119538	0.14263
361	4.47623	0.0969812	0.0670522	0.0343392	-0.00761483	0.0973545	0.0299232	0.0327151	0.0419185	0.104557	0.167112	0.152928	0.11928	0.143476
362	4.47623	0.0962651	0.0665243	0.0343075	-0.00769763	0.0969106	0.0297236	0.0322078	0.041989	0.10392	0.168237	0.155337	0.11908	0.144355
363	4.47623	0.095508	0.065974	0.0342812	-0.00776935	0.0964436	0.0295148	0.03171	0.0420409	0.103266	0.169429	0.157774	0 118932	0.145271
364	4.38781	0.0947425	0.0654433	0.0342657	-0.00783856	0.0959123	0.0292999	0.0312314	0 0420723	0 102604	0.170672	0.160184	0.118843	0.1462
365	4.12255	0.0940072	0.0649428	0.0342241	-0.00791031	0.0953111	0.0290854	0.0307857	0 0420752	0.101946	0.17193	0.162491	0.118835	0.147
366	4.38781	0.0933042	0.0644443	0.0341196	-0.00798645	0.0946727	0 0288771	0.0303807	0 0420395	0.101297	0.173169	0.164644	0.118937	0.148
367	4.12255	0.0926128	0.0639352	0.033957	-0.00805912	0.0940301	0.0286751	0.0300141	0.0419597	0.100649	0.174389	0.166645	0.119164	0.1
368	4.47623	0.0919192	0 0634333	0.0337713	-0.00810958	0.0933921	0.0284743	0.0296756	0.0418381	0.099988	0.175619	0.16854	0.119512	0.
369	4.47623	0.0912209	0.0629425	0.0335898	-0.00812282	0.0927655	0.0282682	0.029355	0.041683	0.0993062	0.176902	0.170378	0.119958	0.151067
370	4.47623	0.0905141	0.0624441	0.0334131	-0.00810535	0.0921697	0.0280509	0.0290489	0.0415053	0.0986051	0.178276	0.172169	0.120473	0.152142
371	4.65307	0.0897905	0.0619396	0.0332236	-0.00808865	0.0916021	0.0278188	0.0287616	0.0413157	0.0978961	0.179768	0.173883	0.121026	0.153244
372	5.27201	0.0890512	0.0614593	0.0330076	-0 00810787	0.0910242	0.0275732	0.0284989	0.0411205	0.0971926	0.181374	0.175479	0.121601	0.154353
373	4.91833	0.0883141	0.0610104	0.0327673	-0 00816757	0.0904168	0.0273231	0.0282599	0.0409181	0.0965011	0.183033	0.176959	0.122203	0.155458
374	5.00675	0.0875916	0.0605527	0.0325093	-0.00823614	0.0898223	0.0270824	0.0280371	0.0406995	0.095819	0.184656	0.178362	0.122862	0.156565
375	5.36042	0.086871	0.0600447	0.0322246	-0.00828323	0.0892976	0.0268607	0.0278242	0.0404559	0.0951409	0.186175	0.179725	0.123604	0.157681
376	5.36042	0.0861431	0.0594955	0.0319017	-0 00830962	0.0888355	0 0266572	0.0276219	0.0401874	0.0944665	0.187592	0.181039	0.124432	0.158807
377	5.36042	0.0854308	0.0589569	0.0315584	-0.00833173	0.0883648	0.0264626	0.0274356	0.039905	0.0938033	0.188971	0.182264	0.125314	0.159929
378	5.45437	0.0847645	0.0584791	0.0312368	-0.0083563	0.0878252	0.0262677	0.0272673	0.0396228	0.0931578	0.190375	0.183386	0.126206	0.161036
379	5.83015	0.0841416	0.0580703	0.0309566	-0.00838093	0.087219	0.0260706	0.0271092	0.039347	0.0925268	0.191815	0.184455	0.12709	0.162134
380	5.91857	0.0835264	0.0576778	0.0306913	-0.00840438	0.0865869	0.0258787	0.0269453	0.0390725	0.0918964	0.193235	0.185581	0.127983	0.163247
381	6.18383	0.0828727	0.0572136	0.0303966	-0.00842795	0.085961	0.0257021	0.0267602	0 0387888	0.0912512	0.194557	0.186871	0.128921	0.164403
382	5.73621	0.082158	0.056637	0.0300565	-0.00845336	0.0853511	0.0255456	0.0265494	0 0384905	0.0905855	0.195745	0.188362	0.129923	0.165613
383	5.54279	0.0814138	0.0560088	0.0296983	-0.00847851	0.0847609	0.0254051	0.0263214	0.038181	0.0899075	0.196825	0.189997	0.130977	0.166862
384	6.36067	0.0807051	0.0554284	0.0293637	-0.00849239	0.084196	0.0252725	0.0260905	0.0378684	0.0892314	0.197857	0.191678	0.132059	0.168126
385	6.71435	0.0800641	0.0549241	0.0290687	-0.00848283	0.0836531	0.02514	0.0258665	0.0375595	0.0885661	0.1989	0.193335	0 133144	0.169389
386	6.71435	0.0794609	0.0544472	0.0287958	-0.00845506	0.0831147	0 0250005	0.0256515	0.037257	0.0879089	0.200013	0.194954	0.134225	0.170655
387	6.71435	0.07884	0.0539552	0.0285185	-0.00843385	0.0825619	0.0248447	0.0254446	0.0369603	0.0872496	0.201274	0.196537	0.135302	0.171945
388	6.80277	0.0781662	0 0534492	0.0282225	-0.00844053	0.0819814	0 0246626	0.025248	0 036668	0.0865786	0 20277	0.198064	0.13638	0.17328
389	7.24486	0.0774386	0.0529444	0.0279089	-0.00847275	0.0813625	0.0244489	0.0250674	0.0363771	0.0858934	0.204554	0.199486	0.137471	0.174663
390	7.59854	0.0766868	0.0524573	0.0275864	-0.0085085	0.0807069	0.0242088	0.0249063	0.0360852	0.0852003	0.206592	0.200771	0 138584	0.176085
391	7.69249	0.0759562	0 0520124	0.0272668	-0.00852645	0.0800414	0.0239588	0.0247598	0 0357927	0.0845113	0.208749	0.201957	0.139716	0.17752
392	8.15669	0.0752744	0.0516087	0.0269592	-0.00852535	0.0794056	0.0237215	0.0246106	0.0355057	0.0838378	0.210828	0.203187	0.140845	0.178945
393	8.51037	0.0746276	0.0511872	0.0266656	-0.00852839	0.0788237	0.0235167	0.0244347	0.0352323	0.0831838	0.212649	0.204663	0.141935	0.180351
394	8.51037	0.0739796	0.0506809	0.0263841	-0.00856236	0.0782886	0.023351	0.0242159	0.0349763	0.0825432	0.214146	0.206531	0.142972	0.18175
395	8.59879	0.073305	0.0500924	0.0261106	-0.00862672	0.0777683	0.0232138	0.0239578	0.0347312	0.0819028	0 215406	0.20877	0.143981	0.183172

Point	MTSP.y	A.y	B.y	C.y	D.y	EE.y	ThickA.y	ThickB.y	ThickC.y	SheetThick.y	DenA.y	DenB.y	DenC.y	SheetDen.y
396	9 04088	0 072597	0 0494803	0 0258313	-0 00869162	0 0772286	0.0230836	0 0236838	0 0344825	0.0812499	0 216623	0 211186	0.145021	0.184646
397	9 48298	0 0718678	0 0488879	0.0255287	-0 00873004	0.0766552	0 022938	0.0234245	0.0342177	0.0805802	0 218007	0.213512	0.146147	0 186183
398	9 83666	0.0711512	0 0483375	0 0252058	-0 00874057	0 076056	0.0227608	0.0232015	0.0339351	0 0798974	0 21972	0.215545	0 147367	0.187775
399	9 9306	0 0704703	0 0478601	0 0248905	-0 00873666	0.0754414	0.0225446	0 02302	0.0336438	0.0792084	0.221846	0.217231	0.148644	0.18941
400	10 3948	0 0698036	0 0474673	0 0246082	-0 00872512	0 0748108	0.022294	0 0228687	0 0333556	0 0785183	0 224357	0.21866	0 149927	0.191075
401	10 7485	0.0691243	0 047119	0 0243652	-0 00869897	0.0741679	0 022028	0 0227283	0 0330769	0 0778333	0.227068	0.220011	0.151188	0.192756
402	10 9253	0 068462	0 0467655	0 0241534	-0 00865092	0 0735345	0 0217747	0 0225818	0.0328074	0 0771639	0 229695	0.221443	0 15243	0.194427
403	11 6327	0 0678667	0 0463867	0 0239495	-0 00859429	0 072933	0.0215553	0 0224225	0.0325435	0 0765213	0 232014	0.223021	0.153666	0.196057
404	11 7211	0 0673184	0 0459691	0 0237178	-0 00856191	0.0723686	0.0213701	0 0222558	0.0322835	0.0759093	0 234011	0.224693	0.154903	0 197635
405	12 1687	0.0667387	0 0455045	0 0234378	-0.00857763	0.0718357	0 0212007	0.0220943	0 0320287	0.0753237	0.23588	0.226331	0.156134	0.199169
406	12.6329	0 0661015	0 0450319	0 0231291	-0 00863462	0.0713215	0 0210255	0.0219516	0 0317812	0 0747583	0.237853	0.227795	0.157349	0.200674
407	13 075	0 0654721	0 0446227	0.0228322	-0 00870257	0 0708001	0.0208358	0.0218337	0.0315402	0.0742096	0.240026	0.229018	0.158551	0.202157
408	13 5171	0 0649135	0 0442956	0 0225651	-0 00875047	0 0702434	0.020638	0.0217338	0 0313007	0 0736726	0 242327	0.230068	0.159764	0.20363
409	13 9592	0 0644037	0.0439867	0 0223106	-0.00876435	0 0696422	0.0204433	0.0216337	0 0310591	0.0731361	0.244632	0.231137	0.161008	0.205125
410	14 4068	0.0638796	0 0436292	0.0220558	-0 00874948	0 0690146	0.0202555	0.0215139	0.0308175	0.0725869	0 246898	0.232433	0.16227	0.20668
411	14 9595	0 0633215	0 043231	0 0218251	-0.00872017	0.0683951	0 0200683	0.0213664	0.0305837	0 0720183	0.249206	0.234048	0.163509	0.208314
412	15 7552	0 0627487	0 042844	0 0216483	-0.00868938	0.0678136	0 0198712	0.0212001	0.0303626	0.0714339	0.251688	0.235887	0.164697	0.21002
413	16 1973	0 0621687	0 0424884	0 0214984	-0 00866673	0 0672772	0 0196592	0.0210352	0.0301497	0 0708442	0.254414	0.237731	0.16586	0.211769
414	16 7334	0.0615764	0 0421415	0.0213053	-0 00866096	0 0667699	0.0194356	0.0208906	0.0299347	0 0702609	0.257349	0.239367	0.167053	0.213526
415	17 5513	0.0609845	0 0417887	0 0210463	-0.00867461	0 0662642	0.0192097	0.0207725	0 0297114	0 0696936	0.260374	0 240719	0.168311	0.215262
416	18.0818	0 06042	0 0414486	0 0207746	-0 00869518	0.0657356	0.0189923	0 0206734	0.0294814	0 0691471	0.263346	0 241869	0.169625	0.216961
417	18 8775	0 0598984	0 0411387	0.02054	-0.0087041	0.0651884	0.0187924	0 020578	0.0292504	0.0686208	0 266133	0 242993	0.170964	0.218623
418	19.4136	0.0594063	0.0408327	0 0203281	-0.00869788	0 0646619	0.0186163	0.020472	0.0290226	0 0681108	0.268635	0.244256	0.172306	0.220259
419	20 2315	0.0589089	0 0404769	0.0200981	-0.00869317	0.0641841	0.0184645	0.0203491	0.028802	0.0676156	0 27083	0 245738	0.173624	0.221871
420	20.8559	0 0583859	0.0400602	0 0198429	-0 00871336	0 0637303	0.0183301	0.0202134	0.0285957	0.0671393	0.272809	0.24739	0.174872	0.223443
421	22 0275	0 0578628	0 0396424	0.0195937	-0 00876997	0 0632628	0.0182002	0.0200773	0 0284107	0.0666883	0.274758	0.249065	0.176006	0.224951
422	22 558	0 0573872	0 0392963	0.0193828	-0 00884506	0 0627902	0.0180609	0.0199537	0.0282468	0.0662615	0.276888	0.250601	0.177024	0.226398
423	23.4477	0 056971	0 0390358	0 0192112	-0.0088995	0 0623413	0.0179029	0.0198478	0.0280939	0.0658447	0.279348	0 251932	0.177987	0.227832
424	24 4424	0.0565632	0 0388104	0.0190505	-0.00891584	0.0619007	0 0177249	0.0197541	0.027938	0.065417	0.282169	0.253126	0.178983	0.229324
425	25.5919	0 0560952	0.0385572	0.0188727	-0.0089171	0.0614183	0.0175347	0.0196613	0.0277697	0 0649657	0.285237	0.254321	0.18007	0.230921
426	26 2163	0 0555607	0.0382498	0 018671	-0 00892786	0 0608777	0 0173477	0.0195621	0 0275885	0.0644983	0.288303	0.255614	0.181256	0.232595
427	27 4763	0.0550285	0 0379062	0.018454	-0.0089455	0.0603123	0.017181	0.0194574	0 0274004	0.0640387	0.29108	0 256992	0.182501	0.234262
428	28.4545	0.0545626	0 0375627	0.0182301	-0.00896681	0.0597563	0.0170444	0 0193535	0.0272143	0 0636122	0.29339	0.25837	0.183748	0.235828
429	29.7144	0.0541625	0 0372449	0.018004	-0.0090073	0.0592185	0.0169367	0.0192544	0.0270386	0.0632297	0 295241	0.259698	0.184939	0.23725
430	30 5157	0 0537956	0 036954	0.0177827	-0 00907235	0.0587125	0.0168484	0.0191553	0.026878	0.0628818	0.296782	0.261043	0.18604	0.23856
431	31.3391	0 0534384	0 0366697	0.0175812	-0 00913805	0 0582636	0.016768	0.0190448	0.0267322	0.0625451	0 298204	0.262566	0.187053	0.239845
432	33.3065	0.0530688	0 036368	0 0174115	-0.00918104	0 0578651	0.0166847	0.0189131	0 0265966	0.0621945	0.299696	0.264407	0.188005	0.2412
433	34.373	0 0526605	0 0360402	0.0172639	-0.00920549	0.0574667	0.0165892	0.0187598	0.0264654	0.0618143	0.301433	0.266579	0.188938	0.242688
434	35 9867	0 0522101	0.0357014	0.0171172	-0.00922377	0.0570335	0.0164741	0.0185939	0.0263343	0.0614023	0.303553	0.268961	0.189878	0.24432
435	37.0533	0 0517455	0 0353804	0 0169701	-0.00923119	0 0565852	0 0163369	0.0184278	0.0262034	0.0609681	0.30612	0.271383	0.190827	0.246063
436	38.8493	0.0512938	0.0350959	0.0168413	-0.00921984	0.0561526	0.0161811	0.0182704	0.0260759	0.0605274	0.309083	0.273714	0.191759	0.247854
437	40.5513	0.0508578	0 0348435	0 0167355	-0 0092013	0 055738	0.0160158	0.018126	0.0259567	0.0600985	0.312277	0.275886	0.192638	0.249621
438	41 9716	0.0504385	0.0346115	0 0166366	-0.00919688	0.0553374	0.015854	0.0179959	0.0258474	0.0596973	0.315456	0.277873	0.193451	0.251294
439	43.6792	0.0500587	0 0343934	0 0165307	-0.00921454	0.0549565	0.0157075	0 0178792	0.0257452	0.0593319	0.318382	0.279682	0.194218	0.252837
440	45.1215	0.0497329	0.0341807	0.0164135	-0.00924303	0.0545817	0.0155813	0.0177721	0.0256445	0.058998	0.320942	0.281364	0.194981	0.254265
441	46 912	0 0494329	0.0339623	0.0162871	-0.00926366	0.0541714	0 0154722	0.0176687	0.0255411	0.0586821	0.323195	0.28301	0.195771	0 255632
442	48.5091	0.0491165	0.0337375	0.0161612	-0.00926945	0.0537006	0.0153732	0.0175627	0.0254351	0.0583711	0.325272	0.284721	0.196587	0.256995
443	49.6862	0.0487744	0.0335062	0.0160431	-0.00927564	0.0531994	0.0152806	0 0174505	0.025329	0.0580601	0.327241	0 286556	0.197411	0.258372
444	51 8359	0.0484261	0 0332548	0.0159197	-0.00930443	0.052731	0.0151949	0 017333	0.0252235	0.0577514	0.329083	0.288502	0.198236	0.259752
445	53.7148	0.0480869	0.0329771	0.0157732	-0.009357	0.0523386	0 0151153	0.0172149	0.0251157	0.0574458	0.330813	0.29048	0.199089	0.261134
446	55.9308	0.0477563	0.0326984	0.0156124	-0.00940658	0.0520161	0.0150362	0.0171026	0.0250001	0.057139	0.332555	0.292383	0.200011	0 262537
447	58.1689	0.0474252	0.0324499	0.0154656	-0 00942404	0.051724	0.0149513	0.0170017	0.0248736	0.0568265	0.33445	0.294112	0.201031	0.263982
448	60.407	0.0470892	0.0322308	0.0153383	-0.00940911	0.0514233	0.0148604	0.0169172	0.0247365	0.0565141	0.336498	0.295573	0.202147	0.26544
449	62 7391	0.0467643	0 0320199	0.0152041	-0 00939046	0.051099	0.014771	0.0168537	0 0245937	0.0562184	0.33853	0.29668	0.203322	0.266834
450	65.353	0.0464827	0.0318173	0.0150416	-0.00939528	0.0507567	0.0146917	0.0168118	0.0244532	0.0559568	0.340349	0.297413	0.204488	0.268077
451	67 5911	0 0462625	0.0316474	0.0148664	-0.00942575	0.0504014	0.0146251	0.0167839	0.024324	0.055733	0.341893	0.297907	0.205572	0.26915
452	69.8292	0.0460856	0.0315164	0.0147195	-0 00946168	0.0500303	0 0145671	0.0167531	0.0242109	0.0555311	0.343251	0.29846	0.206528	0.270128
453	72.1557	0 0459057	0.0313889	0.0146248	-0.00947951	0 0496524	0.0145111	0.0167027	0.0241105	0.0553244	0.344577	0.299367	0 207387	0.271139
454	74.7475	0.0456797	0.0312191	0.0145641	-0.0094729	0.0492966	0.0144516	0.0166298	0.0240104	0.0550918	0.345999	0.300685	0.208254	0.272287
455	77.0741	0.045399	0.0309999	0.0144893	-0 0094552	0.048982	0.0143857	0.016549	0.0238958	0.0548305	0.347587	0.302154	0.209257	0.273587
456	79.7543	0.0450935	0.0307714	0.0143563	-0.00944079	0 0486884	0.0143144	0.0164806	0.0237603	0.0545553	0.349322	0.3034	0.210456	0 274968
457	82.4345	0.0448072	0.0305761	0.0141681	-0.00943305	0.0483758	0.014243	0.0164332	0.0236112	0.0542874	0.351072	0.304269	0.211786	0.276323
458	85.1202	0.0445647	0.0304145	0 0139836	-0.00943287	0.048031	0.0141796	0.0163969	0.0234648	0.0540412	0.352636	0.304941	0.213105	0.277579
459	87.8226	0.0443518	0.0302494	0.013851	-0.00944795	0.0476844	0.0141293	0.0163555	0.0233321	0.0538169	0.353883	0.305716	0.214313	0.278734
460	90.5028	0.0441337	0.0300476	0.0137411	-0.00948509	0.0473765	0.0140877	0.0163026	0.0232101	0.0536004	0.354928	0.306711	0.215438	0.27986
461	93.2714	0.0438906	0.0298117	0 0135935	-0.00953255	0.0471054	0.014038	0.0162463	0.0230863	0.0533705	0.356202	0.307773	0.216596	0.281069

Point	MTSP.y	A.y	B.y	C.y	D.y	EE.y	ThickA.y	ThickB.y	ThickC.y	SheetThick.y	DenA.y	DenB.y	DenC.y	SheetDen.y
462	96.3053	0.0436196	0.0295774	0.013409	-0.00956005	0 0468234	0 0139562	0 0161994	0 0229535	0.0531091	0.358334	0 308659	0.217851	0 282458
463	99 1679	0 0433126	0.0293882	0.0132421	-0 00955011	0 0464911	0.0138249	0 0161681	0.0228181	0 0528111	0 361806	0 309254	0 219143	0 284057
464	102.578	0 0429609	0.0292661	0.0131216	-0.00952503	0 0461245	0.0136488	0 0161461	0.0226952	0.0524901	0.366532	0 309675	0.220326	0 285796
465	105.44	0.0425851	0 0291846	0 0130276	-0.00952647	0.045777	0.0134599	0 0161171	0.0225961	0 0521731	0 371667	0 310237	0 221286	0.28753
466	109 027	0.0422356	0.0290712	0.0129342	-0 00956821	0.0454856	0 0133031	0.0160632	0.0225214	0.0518877	0 375976	0.311292	0.222016	0.289105
467	112.597	0 0419584	0.0288685	0.0128385	-0.00962462	0 0452384	0 0132075	0 0159775	0.0224623	0 0516472	0 378625	0 312977	0 222599	0 290445
468	116.189	0.0417552	0.0286033	0.0127496	-0.00966761	0 0449924	0.0131672	0.0158728	0 0224068	0.0514468	0 379749	0 315044	0 22315	0 291573
469	119 775	0 041577	0.0283655	0 0126642	-0 00969909	0 0447171	0.0131499	0 0157753	0 0223448	0 05127	0 38024	0.31698	0 223771	0 292577
470	123.433	0 0413729	0 028202	0 0125585	-0.00973816	0 0444146	0.0131257	0.0157054	0.0222698	0 0511009	0 380945	0.318376	0 224527	0 293545
471	127 468	0 0411424	0 0280683	0 012413	-0.00978876	0 0441008	0.0130863	0.0156633	0 022182	0 0509316	0.382092	0.319223	0 225419	0 294521
472	131 496	0 0409176	0.0279033	0 0122402	-0.00983754	0.0437867	0.0130405	0 0156309	0.0220897	0 050761	0 383434	0.319886	0.22636	0.295511
473	135.508	0 0407072	0.0277084	0.0120776	-0.00988231	0 0434843	0.0129962	0.015585	0 0220074	0.0505885	0.38474	0.320838	0.227204	0.296519
474	139 631	0.0404902	0.0275187	0.0119576	-0 00993862	0.0432062	0.0129529	0 0155095	0.0219469	0 0504093	0.386025	0.322418	0 227827	0 297575
475	144.107	0.0402494	0.0273374	0.0118888	-0.0100051	0 0429435	0.0129077	0.0153998	0 0219076	0 0502151	0 387379	0.324738	0 228233	0 298727
476	148 672	0.0399905	0.0271412	0.0118573	-0.0100474	0 0426651	0.0128613	0.0152638	0.0218759	0.050001	0.388777	0.327649	0 228564	0.30001
477	153 596	0.0397373	0.0269305	0.0118373	-0 0100392	0 0423538	0 012817	0.0151197	0 0218339	0 0497705	0.390117	0.330772	0.229006	0.3014
478	158 536	0.0395096	0 0267328	0 011802	-0.0100006	0.042035	0.0127766	0 0149897	0 0217698	0 0495361	0.391349	0.333618	0 229685	0.302826
479	163 543	0.0393016	0.0265603	0 0117288	-0.0099763	0 0417543	0.0127395	0.0148904	0 0216809	0 0493108	0.392489	0.335818	0 23063	0.304208
480	168 903	0.0390913	0 0263926	0 0116028	-0 00999046	0 0415229	0 0127053	0 0148245	0.0215709	0 0491007	0.393543	0 337292	0.231812	0.305507
481	174 269	0.038869	0.0262059	0 0114275	-0 0100328	0 0412993	0 0126751	0.0147818	0.0214464	0.0489033	0.394478	0.338261	0 233161	0.30674
482	179 74	0 0386403	0 0259972	0.0112304	-0 0100777	0 0410363	0.0126488	0.0147461	0.021317	0 048712	0.395298	0.339079	0.234576	0.307944
483	185 637	0.0384114	0 0257794	0 0110502	-0 0101105	0 040729	0 0126221	0.0147056	0 0211949	0 0485227	0.396136	0.340016	0.235923	0.309146
484	191.82	0.03819	0 0255764	0.0109166	-0.0101346	0 0404035	0.0125868	0.0146589	0.0210893	0.0483349	0 397255	0 341101	0.2371	0.310346
485	197 827	0.0379894	0 0254187	0.0108326	-0.0101543	0 0400777	0.0125343	0.014614	0.0210004	0.0481487	0.398935	0 342145	0.2381	0.311546
486	204 542	0 0378124	0 0253201	0.0107734	-0.0101621	0 0397468	0.0124609	0.0145806	0.0209197	0.0479612	0 401304	0 342925	0.239018	0.312765
487	211 162	0.0376381	0 0252571	0 0107087	-0.0101515	0.0394036	0.0123714	0.0145615	0.0208358	0.0477686	0 404221	0.343373	0.239983	0.314027
488	217 595	0 0374404	0 0251833	0 0106226	-0.0101336	0 0390582	0 0122784	0 0145505	0.0207429	0 0475718	0 407278	0 343631	0.24106	0 315326
489	224 773	0.03722	0.0250659	0.0105104	-0.0101296	0.0387324	0.012197	0.0145378	0.0206442	0.047379	0 409977	0.343933	0.242213	0.316608
490	231 93	0.0370089	0 0249118	0 0103783	-0.0101482	0.0384435	0 0121359	0.0145155	0.0205489	0 0472002	0.412022	0.344465	0.243335	0.317805
491	239 263	0.0368378	0.024753	0.0102535	-0.0101801	0.0381977	0.0120907	0.0144813	0.0204658	0 0470377	0.413557	0.34528	0.244319	0.318902
492	247.221	0.0366931	0.0246087	0 0101644	-0 010213	0 0379822	0.012045	0.01444	0 0203969	0 046882	0.415134	0.34627	0.245141	0 319962
493	254 93	0.0365193	0 0244772	0.0101031	-0.0102433	0.0377661	0.0119819	0.0144022	0 0203354	0 0467196	0.417346	0.347175	0.245882	0.321075
494	262 976	0 0362878	0.0243632	0.0100314	-0 0102709	0 03753	0.0118978	0.0143798	0.0202686	0.0465462	0.420319	0.347713	0.246696	0.322273
495	271 133	0 0360448	0.0242777	0.00992835	-0 0102907	0 0372939	0.011809	0.0143777	0.0201854	0.0463721	0.423475	0.347763	0.247718	0.323482
496	279 637	0 0358603	0.0242056	0.00980663	-0.0102971	0 0370907	0.0117424	0.0143901	0.0200816	0.0462141	0.425847	0.347464	0.249005	0.324585
497	288.308	0 035746	0.0241043	0.00967753	-0.0102978	0 0369124	0.0117167	0.0144052	0.01996	0 0460819	0.426762	0 347099	0.250528	0.325513
498	297.636	0 0356549	0.0239465	0.00952373	-0.0103116	0 0367107	0 0117279	0 0144133	0.0198288	0 04597	0.42635	0.346902	0.252187	0.326304
499	306 583	0 0355432	0.0237526	0.00933213	-0.0103465	0 0364598	0 0117524	0.0144085	0 0197017	0.0458627	0 425459	0.347019	0 25381	0.327068
500	315 607	0 0353988	0 0235708	0.00914653	-0.0103852	0.0361911	0 0117623	0.0143849	0 0195967	0 0457439	0 425099	0.347596	0 255162	0.327919
501	325.113	0 0352305	0.023438	0.00904842	-0.0104027	0.0359541	0.0117425	0.0143365	0.0195286	0 0456076	0 425825	0.348781	0 256043	0.328901
502	334 949	0.0350635	0 0233598	0.00906878	-0.0103884	0.0357698	0 011696	0.0142642	0.0195	0.0454602	0 427524	0.350561	0.256413	0.329968
503	344.791	0.0349296	0 0233143	0.00915126	-0.0103521	0.0356248	0.0116372	0.0141803	0 0194978	0.0453154	0 429687	0.352636	0.25644	0.331022
504	354.739	0 034836	0.0232706	0.00921485	-0 0103164	0.0354882	0.0115777	0.0141049	0.0195014	0.045184	0.431894	0.35451	0.256393	0 331982
505	365.023	0 0347523	0.023217	0.00921866	-0.0103051	0.0353314	0 0115192	0.0140546	0.0194937	0.0450675	0.434088	0.355767	0.256495	0.332839
506	375.324	0.0346387	0.0231599	0.00915965	-0.0103307	0.0351472	0 0114582	0.0140322	0.0194679	0.0449583	0 436403	0.356328	0.256836	0.333648
507	385.696	0.0344761	0.0230876	0.00904859	-0 0103901	0.0349508	0.0113952	0.0140251	0.0194255	0 0448458	0 438817	0.356506	0.257398	0.334485
508	396.356	0.0342733	0.0229688	0.00890811	-0 010469	0.0347631	0.0113375	0.0140133	0.0193718	0.0447226	0 441041	0.356808	0.258114	0 335408
509	406.746	0.0340621	0.0227995	0.0087738	-0.0105398	0.034599	0.011293	0.0139817	0.0193129	0.0445876	0 442768	0.357623	0.2589	0 336425
510	417 561	0.0338776	0.0226222	0.0086784	-0.0105691	0 0344584	0 0112623	0.0139276	0.019256	0.0444458	0.443967	0.359021	0.259665	0.337498
511	428 663	0.0337331	0.0224833	0.00863081	-0.0105514	0 0343221	0.011239	0.0138589	0.0192091	0 044307	0.444884	0.360804	0.260297	0.338555
512	439 411	0 0336174	0.0223918	0.00861423	-0.0105263	0.0341667	0.011216	0.0137852	0.0191794	0.0441806	0.445799	0.362734	0.260698	0.339522
513	450.248	0.0335108	0.0223216	0 00860595	-0.010537	0.0339868	0.0111909	0.0137108	0.0191689	0 0440707	0 446797	0.364702	0 26084	0.340367
514	461.345	0.0333941	0.0222379	0 00859198	-0.010583	0.0337933	0.0111664	0.0136361	0.0191707	0.0439733	0.447777	0 366701	0.260815	0 34112
515	471.983	0.033256	0.0221208	0 00856288	-0 0106363	0.0336008	0.0111454	0 0135631	0.0191722	0.0438807	0.448619	0.368673	0.260794	0.341839
516	482 554	0.033106	0.0219795	0.00851084	-0.0106812	0.0334267	0 0111273	0.0134986	0 0191628	0 0437888	0.449347	0.370427	0.260924	0.342557
517	494 099	0.0329699	0.021847	0.00843746	-0.0107164	0.033289	0.0111082	0.0134507	0.0191401	0 043699	0 450121	0.371739	0.261233	0 343261
518	505.112	0.0328597	0.0217578	0.00835947	-0.01074	0.0331884	0.0110856	0.0134199	0.0191114	0.0436169	0 451043	0.372586	0.261626	0 343906
519	515.502	0.0327701	0.0217201	0.00830335	-0.0107542	0.0331028	0.011064	0 0133954	0.0190871	0.0435465	0.451924	0.373269	0 261959	0.344462
520	526.228	0.032704	0.0216997	0.00828614	-0.0107671	0.0330082	0.011054	0.0133602	0.0190727	0.0434869	0 452334	0.374261	0 262155	0.344933
521	536.888	0.0326621	0 0216395	0.00829332	-0.0107821	0.0328973	0 0110628	0.0133038	0.0190639	0.0434305	0 451976	0 375861	0.262277	0 345381
522	547.277	0.0326062	0.0215105	0.00828347	-0.0108002	0.0327746	0.0110853	0.0132315	0.0190491	0.0433659	0 451057	0.377921	0.262482	0.345896
523	557.827	0.032486	0.0213364	0.00822244	-0.0108296	0.0326423	0.0111067	0.0131619	0 0190181	0.0432868	0.450185	0.379911	0.262912	0.34653
524	567.774	0.0323093	0.0211648	0.00810919	-0 010878	0.0324959	0.0111141	0.0131146	0 0189689	0 0431975	0 449885	0 38127	0.263596	0.347246
525	577.97	0.0321425	0.0210322	0.00797302	-0.0109334	0.0323382	0.0111048	0.0130972	0.0189089	0.0431108	0.450261	0.381767	0.264434	0.347944
526	587.829	0.0320406	0.0209573	0.00785908	-0.0109674	0.0321939	0 0110844	0.0131026	0.0188505	0.0430375	0.451091	0.381607	0.265251	0.348536
527	597.577	0.0320057	0.0209423	0.00780592	-0.0109636	0.0320923	0.0110589	0.0131146	0.0188051	0.0429785	0.452133	0.381258	0.265889	0.349013

Point	MTSP.y	A.y	B.y	C.y	D.y	EE.y	ThickA.y	ThickB.y	ThickC.y	SheetThick.y	DenA.y	DenB.y	DenC.y	SheetDen.y
528	606.883	0 031999	0.0209634	0 00781351	-0 0109384	0 0320309	0.0110314	0.0131175	0.0187768	0 0429256	0 453261	0.381173	0 266288	0 349443
529	615 836	0 0319718	0.0209721	0 00784021	-0 0109221	0 0319714	0 0110036	0 0131037	0.0187604	0 0428677	0.454405	0 381577	0.266519	0.349916
530	624.788	0.0318995	0.0209307	0 00784605	-0.0109224	0 0318804	0.0109768	0.0130763	0 0187446	0 0427977	0 455513	0.382379	0 266745	0.350489
531	633 652	0 0318001	0.0208491	0.00782521	-0 0109209	0 0317634	0 0109501	0 0130474	0.0187184	0 0427159	0.456623	0 383225	0.267119	0.351161
532	642.068	0 0317119	0.0207745	0 00778942	-0.0109065	0 0316484	0.0109189	0.0130315	0.018677	0.0426274	0 457936	0 383692	0 267714	0 351891
533	650.115	0 0316471	0 0207415	0 00774212	-0 0108892	0 031547	0 0108768	0.0130359	0 0186222	0 0425349	0 459719	0.383562	0 268504	0 352656
534	658	0 0315794	0 0207388	0.00768029	-0.0108803	0.0314495	0.0108206	0.0130551	0 0185603	0 042436	0.462123	0 382997	0 2694	0 353479
535	665.245	0 0314787	0 0207237	0.00761074	-0 0108763	0.031353	0 0107517	0 0130747	0.0184994	0 0423258	0.465102	0 382421	0 270285	0.3544
536	672.755	0 0313468	0 0206711	0.00755483	-0 0108675	0.0312693	0 010673	0.0130832	0.0184475	0.0422037	0.468542	0 382173	0 271044	0 355427
537	679.735	0 0312117	0.0206071	0 00753192	-0 0108519	0.0312025	0 0105858	0 0130815	0.0184088	0 042076	0 472423	0.382222	0.271612	0.356506
538	686 096	0.031095	0.0205828	0.00753854	-0.0108355	0.031141	0 0104908	0.013081	0.0183814	0.0419531	0 476717	0.382237	0 272016	0 357549
539	692.633	0.0309951	0.0206121	0 00754853	-0.0108247	0.0310783	0.010395	0 0130921	0.0183571	0.0418442	0.481102	0.381914	0.272376	0.358478
540	698 458	0 0309039	0.0206484	0 00753239	-0.0108211	0.0310286	0.0103134	0.0131159	0 0183261	0 0417554	0.484876	0.381222	0 272839	0.359238
541	704.177	0 0308287	0.0206354	0.00747752	-0.0108243	0.0310097	0 0102603	0.0131458	0.0182833	0.0416894	0.487349	0.380355	0 273479	0 359805
542	709 56	0 030787	0 0205765	0 00739863	-0.0108317	0.0310149	0.010238	0 0131747	0.0182318	0.0416444	0.48839	0 379519	0.274253	0 360193
543	714.655	0.0307802	0 0205288	0.00732798	-0.0108352	0 0310165	0 010235	0 0131975	0.0181805	0 041613	0.488526	0.378863	0 275025	0.360465
544	718.866	0.0307794	0.0205224	0.00728794	-0.0108251	0.0310004	0 0102369	0 013208	0.0181409	0.0415859	0.488431	0.378561	0.275623	0 3607
545	723.696	0 0307539	0 0205239	0.00727648	-0.0108067	0.0309757	0 0102381	0.0131976	0.0181228	0 0415586	0.488372	0 378865	0 275898	0.360937
546	727.995	0 0307058	0.0204894	0 00728228	-0.0108036	0.0309433	0.0102426	0.0131594	0.018132	0.0415341	0 488158	0.379977	0 275759	0.361149
547	731 582	0 0306585	0.0204192	0 00730151	-0 0108344	0.0308846	0 0102558	0.0130951	0.0181666	0.0415175	0.487536	0 381857	0.275236	0.361294
548	735.058	0.0306198	0.0203418	0.00733213	-0.0108908	0.0307951	0.0102771	0.0130161	0.0182151	0.0415083	0.486527	0 384181	0.274503	0.361374
549	738.186	0.0305799	0.0202706	0 00736034	-0 0109425	0.0306974	0.0103004	0.0129388	0.0182605	0.0414996	0 485425	0.386468	0 27382	0 361449
550	741 242	0.0305345	0.0202017	0 00736451	-0 0109662	0.030614	0.0103175	0.0128771	0.01829	0.0414846	0.484616	0 388306	0.273375	0 36158
551	743.922	0 030491	0 0201417	0.00733667	-0.0109704	0.0305501	0 0103213	0.0128356	0 0183044	0 0414613	0.484441	0.38955	0 27316	0 361784
552	746.425	0 0304498	0 0201089	0.00729939	-0.0109835	0 030501	0 0103082	0.0128079	0.0183151	0.0414311	0.485061	0 39039	0 273	0.362047
553	748 221	0 0303947	0 0201032	0.00729003	-0.0110153	0.0304604	0 0102825	0 0127803	0.0183332	0.0413961	0 486278	0 391235	0 27273	0 362354
554	750.017	0 0303142	0.0200903	0.00731591	-0.0110488	0.0304291	0.0102562	0.0127428	0.0183598	0.0413588	0.487523	0.392393	0 272336	0.36268
555	751.719	0 0302273	0.0200327	0.00733973	-0 0110735	0.030422	0.0102408	0.0126978	0.0183862	0.0413248	0 48825	0.393785	0 271945	0 362978
556	752.963	0 0301745	0.0199419	0.00733017	-0 0110953	0.0304511	0.0102352	0.012661	0.0184027	0.041299	0.488519	0.394928	0 271699	0.363206
557	753.958	0.0301742	0.0198876	0.00730673	-0.0111103	0.030499	0.0102224	0.0126506	0.0184055	0 0412785	0.489151	0 395251	0.271659	0.363386
558	755 107	0.0301958	0 0199321	0.00730634	-0.0111005	0.0305266	0.0101836	0.0126734	0.0183952	0.0412522	0.49105	0.394545	0 271811	0.363619
559	755.555	0.0301869	0.0200511	0 00732561	-0.0110642	0.0305093	0.010119	0.012717	0.0183742	0.0412102	0.494209	0 393194	0.272122	0.363989
560	755 93	0 0301264	0.020144	0.00732718	-0.0110263	0.0304524	0.0100544	0.0127553	0 0183457	0 0411554	0 497373	0 392012	0 272545	0.364474
561	755.93	0 0300439	0.0201333	0.00729231	-0.0110131	0.030379	0 010026	0.0127624	0 0183151	0.0411036	0.498771	0.391794	0 273	0.364933
562	755.93	0.0299899	0.0200277	0 00724231	-0.0110266	0.030315	0.0100556	0.0127276	0 0182887	0 0410719	0 497339	0 392878	0 273393	0 365214
563	755.837	0 0299931	0 0198876	0 00721265	-0.0110441	0.0302762	0 0101358	0.0126608	0.0182697	0 0410663	0.493446	0 394964	0.273677	0.365263
564	755.284	0.0300434	0.0197673	0 00721959	-0.0110407	0.0302594	0.0102349	0.0125879	0.0182551	0.0410778	0.488665	0.397247	0.273897	0 365161
565	754.488	0.0301056	0.019701	0.00724531	-0.0110137	0.030248	0 0103135	0.012538	0.0182373	0.0410887	0.484889	0.398813	0.274165	0 365064
566	753.952	0.030144	0.0197046	0 00725226	-0.0109813	0.0302255	0 0103451	0.0125275	0.0182098	0.0410824	0 483369	0.399137	0.274581	0 365121
567	752.957	0.0301373	0.019763	0.00722465	-0.010956	0 0301809	0.0103279	0.0125502	0.0181722	0.0410503	0.484166	0.398416	0.275149	0 365407
568	751.626	0.0300874	0.0198257	0.00718874	-0.0109289	0.0301142	0.0102828	0.0125814	0 0181317	0.0409959	0 486289	0.397425	0.275763	0.365892
569	750.277	0.03002	0.0198373	0 0071771	-0.0108921	0.0300395	0.010237	0.0125977	0.018098	0 0409326	0.488454	0.396907	0.276276	0.366458
570	748 857	0.0299665	0 0197879	0 00718772	-0 0108651	0.0299793	0.0102051	0 0125953	0.0180757	0.0408761	0.489966	0.396979	0 276616	0.366964
571	747.061	0 0299366	0.0197284	0.00719284	-0.0108751	0.0299586	0.0101826	0.0125911	0.0180595	0 0408332	0.491043	0 397114	0.276864	0.367349
572	745 265	0.0299127	0.019716	0 00717076	-0 0109086	0.0299875	0.0101564	0.0126048	0 0180368	0.0407981	0 492316	0.396685	0 277214	0.367665
573	743.469	0.0298758	0.0197489	0 0071209	-0.010917	0.0300351	0.0101209	0.0126415	0.0179979	0.0407603	0.49405	0 395541	0.277816	0 368006
574	741.584	0 0298332	0.0197807	0 00706352	-0.01088	0 030039	0.0100836	0.0126881	0 0179451	0.0407168	0.495874	0 394088	0.278635	0 3684
575	739.346	0.0298099	0.0197881	0.00702405	-0.0108307	0.0299691	0.0100575	0.012725	0.0178919	0.0406744	0.497154	0.392938	0.279462	0.368784
576	736.931	0.0298118	0.0197842	0.00700808	-0.0108065	0.0298677	0.0100502	0.0127371	0.0178527	0 04064	0.497509	0.392563	0.280073	0 369095
577	734.074	0.0298137	0.0197685	0.00700224	-0.0108104	0.0298034	0.0100607	0.0127177	0.0178327	0.040611	0.496991	0.39317	0.280385	0.369358
578	732.101	0 0297876	0 0197119	0 0070012	-0.0108241	0.0298057	0.0100808	0.0126697	0 0178264	0 0405769	0.496001	0.394669	0 280484	0 36967
579	729.421	0.0297317	0.0196099	0.00701211	-0.0108267	0.0298579	0 0100978	0.012608	0.0178226	0.0405284	0.495169	0.396605	0.280543	0 370113
580	726.741	0.0296698	0.0195193	0.00703236	-0.0108028	0.0299273	0.0100978	0.0125559	0.017812	0 0404656	0.495173	0 398243	0.280711	0.370688
581	723 967	0.0296249	0.0195063	0.00704651	-0.0107575	0.0299839	0 0100737	0 0125326	0.0177908	0 0403972	0.49637	0 398971	0 281045	0.371316
582	720.822	0.0295985	0.0195676	0.00704611	-0.0107142	0.0300129	0.010032	0 0125405	0.0177615	0.040334	0.498441	0.398719	0.28151	0.371897
583	717.789	0 029575	0.0196301	0.00703526	-0.0106885	0.0300225	0.00999131	0.0125646	0.0177293	0.0402852	0.500463	0.39795	0 282022	0 372346
584	714.926	0.0295433	0.0196289	0.00701426	-0.0106809	0.030025	0.00997123	0.0125886	0.0176991	0.0402589	0.501461	0.39719	0 282502	0.372589
585	711.428	0.0295125	0.0195692	0.0069713	-0.0106938	0.0300128	0.00998041	0.0126075	0.0176758	0.0402637	0.501001	0.396594	0.282874	0.372545
586	708.3	0.0295081	0.0195048	0.00690322	-0.0107332	0.0299705	0.0100129	0.0126284	0.0176645	0.0403058	0.499383	0.395938	0.283054	0.372158
587	705.067	0.0295466	0.0194764	0.00683741	-0.0107975	0.0299076	0.0100528	0.0126612	0.017668	0.0403819	0.497399	0.39492	0.282999	0.371459
588	701.497	0.0296168	0.0194937	0.00680628	-0.0108736	0.0298575	0.0100827	0.01271	0.0176812	0.0404739	0.495915	0.393412	0.282788	0.370615
589	697 911	0.0296909	0.0195558	0.00680153	-0.0109344	0.0298467	0 0100917	0.0127697	0.0176913	0.0405526	0 495468	0 39158	0.282627	0.369894
590	694.341	0.0297434	0.0196464	0.00678945	-0 0109433	0 029873	0 0100803	0.012823	0.0176877	0 040591	0 496027	0.389949	0.282684	0.369542
591	690.754	0.0297556	0.0197149	0.00677006	-0.0108917	0.029913	0 0100595	0.0128438	0.017675	0.0405782	0.497054	0.389323	0 282889	0.369659
592	687.184	0.029719	0.0197074	0.00678145	-0.0108216	0.0299373	0.0100421	0.0128094	0.0176724	0.0405239	0.497911	0.390397	0.282932	0.370155
593	683.592	0.0296471	0.0196243	0.00684778	-0.0107817	0.0299184	0.0100332	0.0127182	0 0176993	0.0404507	0.498351	0 39324	0 282506	0.370826

Point	MTSP.y	A.y	B.y	C.y	D.y	EE.y	ThickA.y	ThickB.y	ThickC.y	SheetThick.y	DenA.y	DenB.y	DenC.y	SheetDen.y
594	679.917	0.0295722	0.0195249	0.0069552	-0 0107768	0 0298482	0.0100265	0.012595	0 0177585	0.04038	0 498683	0.3971	0.281569	0 371473
595	675.994	0.0295167	0.0194697	0 00707073	-0.0107853	0.0297566	0 0100108	0 0124787	0.0178327	0 0403222	0.499476	0.400769	0 280398	0 372005
596	672.313	0 0294779	0.0194725	0.00715899	-0.0107972	0 0296988	0.00997976	0.0124004	0.0178946	0.0402747	0 501038	0 403253	0 279424	0 372443
597	668.373	0 0294458	0.0195104	0 00719516	-0.0108025	0.0297096	0 00993926	0.0123683	0.0179219	0.0402295	0.503085	0.404273	0 278994	0 372862
598	664.715	0.0294207	0.0195552	0 00718582	-0 0107748	0.0297762	0.00990629	0.0123669	0 0179084	0 0401816	0.504756	0 404313	0.279204	0 373307
599	660 681	0.0294107	0.0195819	0.00716466	-0 0107044	0 0298584	0.00990169	0 0123685	0 0178657	0 0401359	0 505001	0 40426	0 279874	0 373732
600	656 741	0 0294259	0 0195638	0.00715427	-0.0106266	0 0299215	0.00993872	0.0123499	0.0178155	0.0401041	0 503159	0 404878	0 280661	0 374027
601	653.082	0 0294672	0 0194871	0 00715025	-0.0105858	0 0299542	0.010013	0 0123046	0.0177775	0 0400951	0.499468	0.406381	0 281257	0 374111
602	649.136	0 0295157	0 0193771	0.00714882	-0.0105854	0.0299719	0 0101011	0 012246	0.0177598	0.0401068	0.495109	0 408329	0 281536	0 374002
603	645.456	0.0295479	0.0192936	0.00715881	-0.0105967	0 0299959	0.0101714	0.0121991	0.0177576	0.0401281	0 491642	0.409891	0.28157	0 373803
604	641.427	0.0295593	0 0192819	0.00717452	-0.0106015	0.0300243	0 0102011	0 012186	0.0177604	0.0401475	0.490179	0.410325	0 281526	0.373622
605	637.504	0.02956	0.0193339	0 00716985	-0.0106061	0.0300392	0.0101855	0.012213	0.0177593	0.0401578	0.490933	0 409424	0 281543	0 373526
606	633.912	0.0295556	0.0194065	0.00713545	-0.0106196	0.0300401	0 0101345	0 012267	0 0177523	0.0401538	0 493422	0.407629	0 281654	0 373564
607	630.237	0.0295385	0 0194656	0.00709788	-0.0106349	0.030045	0.0100619	0 012324	0.0177432	0.0401291	0.497005	0.405736	0 281798	0 373794
608	626.313	0.0294944	0 0195041	0.0070918	-0.0106336	0.0300633	0 0099786	0 0123633	0.0177371	0.040079	0.501168	0.404433	0 281896	0 374264
609	622 633	0.0294205	0.0195328	0.00712707	-0.0106038	0 0300897	0.00989501	0.0123768	0 0177362	0.040008	0.505396	0.403985	0 28191	0 374929
610	618.604	0 0293411	0.0195612	0.00718363	-0 0105557	0 0301162	0.0098255	0.012368	0 0177392	0.0399327	0 508944	0.404274	0 281861	0 375635
611	614.769	0 0292968	0.0195836	0.0072324	-0.0105137	0 0301305	0.00978605	0.0123446	0.0177432	0.0398739	0 510967	0 405042	0 281798	0 376188
612	611 442	0 0293105	0.0195866	0.00726321	-0 0104883	0 0301162	0.00978464	0.012314	0 0177446	0.0398433	0 511034	0 40605	0 281775	0 376476
613	607 502	0.0293677	0.0195666	0.00728819	-0 0104643	0.030064	0.00981263	0 0122843	0.0177401	0.0398371	0.50958	0.407031	0 281847	0.376534
614	603 932	0.0294319	0.0195411	0.00731472	-0.0104276	0.0299838	0.0098465	0.0122678	0 0177269	0.0398412	0.507824	0.40758	0 282059	0.376495
615	600 434	0.0294702	0 0195392	0 00732742	-0.0103909	0.0299018	0 0098606	0.0122787	0.0177031	0 0398424	0.507094	0.407229	0 282438	0 376484
616	597 218	0 0294666	0.0195738	0 00730423	-0.0103771	0.0298435	0 00984245	0.0123242	0.0176694	0.0398361	0 508038	0 405742	0 282979	0.376543
617	593.631	0.02943	0.0196297	0 00724359	-0.0103885	0.0298162	0.00979934	0.0123973	0 017629	0.0398256	0.510283	0.403365	0.283628	0 376642
618	590.061	0.0293927	0.0196813	0 00716985	-0.0104083	0.0298141	0.00975139	0 0124773	0 0175878	0.0398164	0 512783	0 400773	0.284293	0 376729
619	586.563	0.0293856	0.0197124	0.0071135	-0.0104203	0.0298316	0 00971693	0.0125403	0.0175522	0.0398094	0 514584	0.398741	0.284868	0 376795
620	583.347	0.029406	0 01972	0.00709156	-0.0104167	0.0298609	0.00970174	0.0125694	0.0175268	0 0397979	0 515377	0 397806	0 285278	0 376904
621	579.849	0 0294194	0.0197107	0.00710494	-0 0103957	0 0298842	0 0096998	0 0125597	0 0175127	0.0397722	0 515476	0 398114	0 285507	0.377149
622	576.633	0.0293957	0.019686	0.00714142	-0.0103621	0 0298844	0.00970246	0.0125179	0 0175078	0.0397282	0.515334	0 399451	0 285587	0 377568
623	573.046	0 0293361	0 0196378	0.00717933	-0.0103271	0.0298629	0 00970586	0.0124583	0.0175094	0.0396736	0.515153	0.401366	0.285561	0 378087
624	569.565	0.0292712	0 0195711	0.00720088	-0.0103067	0.0298412	0 00971013	0 0123983	0.0175158	0.0396243	0.514927	0 403303	0.285457	0 378558
625	566.509	0.029235	0 0195152	0 00720361	-0.0103146	0.0298414	0 00971386	0 0123527	0.0175252	0 0395917	0 51473	0 404783	0 285305	0 378868
626	563.74	0.0292277	0 0194916	0.007194	-0.0103496	0.0298648	0 00971196	0 0123287	0 0175332	0 0395738	0 514833	0.405564	0 285174	0.379039
627	560 524	0 029212	0 0194881	0 00717621	-0.0103864	0.0298941	0 00969979	0 0123245	0 0175333	0 0395576	0 515483	0 405696	0 285172	0.379194
628	557 114	0 0291656	0.0194842	0.00715297	-0.0103924	0 029914	0.00967915	0.0123328	0 0175222	0 0395342	0 516584	0.405424	0 285353	0 379419
629	554 434	0.0291177	0.019483	0.00713337	-0.0103619	0.029925	0.00965929	0.0123447	0.0175049	0.0395089	0.517645	0 405032	0 285636	0 379662
630	551.66	0.0291136	0.0194979	0.00713169	-0 0103236	0.0299392	0.00965162	0.0123531	0.0174935	0 0394983	0.518056	0.404757	0.285821	0 379764
631	548.604	0.029161	0 0195257	0.00715461	-0 010306	0.0299658	0.00966292	0.0123538	0.0174988	0 0395156	0.517455	0 404733	0.285735	0.379598
632	545.923	0.0292281	0.0195493	0.00719306	-0.0103141	0 0299959	0.00969243	0 0123478	0.0175214	0 0395616	0 515889	0 404932	0.285368	0 379158
633	543.243	0 0292836	0 0195545	0.00722683	-0.0103416	0.0300028	0 00973344	0 0123424	0.0175498	0 0396257	0 513721	0 40511	0 284906	0 378545
634	540.563	0.0293219	0 019537	0.00723	-0.0103835	0.0299668	0.00977611	0 0123495	0.0175674	0 039693	0 511476	0 404881	0 284621	0 377903
635	537.971	0.0293495	0.0195094	0 00717962	-0.0104307	0.029899	0 00980975	0 0123773	0 0175626	0 0397497	0 509713	0 40398	0 284698	0.377363
636	535.639	0.0293596	0.0194945	0 0070804	-0.0104698	0.0298323	0.00982625	0 0124208	0.0175379	0 039785	0 508849	0.40257	0.2851	0 377027
637	533.025	0.0293375	0.0194945	0.00697754	-0 010496	0.02979	0.00982357	0.0124601	0 0175086	0 0397922	0.508987	0.4013	0.285578	0.376959
638	530.699	0.0292846	0.0194796	0.00692339	-0.0105169	0.0297701	0.00980552	0 0124712	0 0174928	0 0397695	0 509927	0.40094	0 285835	0.377175
639	528.107	0.0292131	0.0194289	0 00693215	-0.0105375	0.0297628	0.00977677	0 012443	0.0174989	0.0397186	0 511433	0.401861	0 285735	0 37766
640	525.869	0.0291245	0.0193625	0.00697734	-0.0105501	0.0297735	0 00973938	0.0123833	0 017521	0.0396437	0 513405	0.403809	0.285374	0 378375
641	523.631	0.0290174	0 0193117	0.00702436	-0.0105458	0.0298137	0.00969573	0.0123111	0.017546	0.0395529	0.515722	0.406174	0 284967	0 379245
642	521.393	0 0289117	0 0192813	0.00705754	-0.0105248	0 0298708	0 00965354	0 0122426	0 017564	0 0394602	0.517972	0 408438	0 284673	0.380135
643	519.248	0 0288409	0.0192599	0.00708247	-0.0104921	0 0299094	0.00962502	0 0121833	0.017575	0.0393833	0 519496	0 41042	0.284495	0 380875
644	517.386	0 0288185	0 01924	0.00710792	-0 0104593	0 0299116	0 00961972	0 0121313	0.0175863	0 0393373	0 519779	0.412173	0 284313	0 381319
645	515 148	0 0288292	0.019214	0 00713246	-0.0104484	0.0298955	0.00963797	0.0120853	0 0176053	0.0393286	0 518799	0 413739	0 284008	0.381403
646	512.998	0 028854	0.0191806	0 00715336	-0.0104709	0 0298803	0.00967053	0.012049	0 0176325	0 039352	0.517056	0 414981	0 28357	0 381176
647	511.202	0.0288909	0.0191633	0 00717556	-0.0105061	0.0298562	0 00970425	0.0120302	0 0176591	0.0393936	0 515254	0 415625	0 283142	0 380774
648	509.406	0.0289445	0 0191912	0.00719893	-0.0105193	0.0298033	0.00972936	0.0120346	0 0176715	0.0394354	0 513916	0 415476	0.282944	0 38037
649	507.61	0.0290037	0 0192535	0.00720737	-0.0104979	0.0297335	0 00974333	0.0120588	0 0176598	0.039462	0 513175	0 414644	0 283132	0 380113
650	505 82	0.0290452	0.0193	0.00718712	-0 0104558	0 0296903	0.00974827	0.0120907	0.0176257	0.0394647	0 512913	0.413549	0 283682	0.380087
651	504.134	0.029058	0.0193013	0.00715246	-0.0104102	0 0297043	0.00974487	0.0121164	0.0175818	0.039443	0.513095	0.412671	0 28439	0 380296
652	502.692	0.0290472	0.0192839	0.0071376	-0 0103694	0 02976	0 0097301	0.0121288	0.0175435	0 0394023	0 51388	0.412245	0 28501	0 38069
653	500.99	0.0290156	0.0192877	0.00715892	-0 0103369	0.0298157	0.00970235	0.0121307	0.017519	0 039352	0.515359	0 412177	0 285407	0.381176
654	499.569	0.0289675	0.0193125	0.00719419	-0 0103161	0.0298448	0.0096677	0.0121305	0 0175052	0 0393034	0.517208	0.412186	0 285629	0.381648
655	497.862	0.0289215	0.0193238	0.0072031	-0 0103107	0.0298529	0.00963839	0.0121358	0.0174925	0 0392666	0.518774	0.412007	0.285838	0.382004
656	496 514	0.0288947	0.0193008	0.00716514	-0 0103246	0.0298565	0.00962345	0.0121505	0.017472	0 039246	0 519571	0.411508	0 286174	0.382205
657	495 182	0.0288844	0.0192603	0.00709599	-0 0103541	0 0298552	0 00962123	0.0121748	0.0174408	0 0392368	0 519687	0.410692	0 286687	0.382294
658	493 828	0.0288745	0.019231	0.00702671	-0.0103808	0 0298332	0.0096217	0.0122057	0.0174007	0 0392281	0 519661	0 409652	0.287349	0.382379
659	492.479	0.028851	0.0192167	0 00697299	-0.0103858	0.0297887	0.00961515	0.0122407	0.0173552	0.0392111	0 520017	0 408481	0 288103	0 382545

Point	MTSP.y	A.y	B.y	C.y	D.y	EE.y	ThickA.y	ThickB.y	ThickC.y	SheetThick.y	DenA.y	DenB.y	DenC.y	SheetDen.y
660	491 148	0 0288112	0.0192032	0 0069307	-0 0103732	0 0297474	0 00959858	0.0122795	0 0173083	0.0391864	0.520918	0.407196	0.288884	0.382787
661	489 888	0 0287684	0.0191932	0 00688905	-0 0103661	0 0297318	0 00957613	0 012323	0.0172645	0 0391636	0 522141	0 40576	0 289616	0 383009
662	488 909	0 0287433	0 0192034	0 00683902	-0 010376	0 0297279	0.00955588	0 0123687	0.0172299	0 0391545	0 523245	0 404263	0.290196	0 383098
663	487 649	0 0287472	0 0192296	0 00678543	-0 0103921	0.0297001	0 0095455	0 0124053	0.0172139	0 0391646	0 523812	0.403068	0.290467	0.382999
664	486 76	0 0287729	0 0192456	0 00675696	-0 0104068	0 0296349	0 00954763	0 012417	0 0172269	0 0391916	0.523694	0 402687	0 29025	0.382736
665	485 765	0 0287998	0.0192366	0 00678552	-0 0104304	0 0295602	0.0095571	0 0123959	0.0172739	0 0392269	0 523176	0.403379	0 289467	0 382392
666	484 616	0 0288088	0 0192163	0 00686822	-0 0104704	0 029522	0.00956288	0 0123521	0 0173456	0 0392606	0 522861	0 404814	0 288274	0 382063
667	484 08	0 0287967	0 0192088	0 00695953	-0 0105117	0 0295434	0 00955474	0 012311	0 0174195	0 0392852	0 523312	0 406162	0 287049	0 381824
668	483 173	0 0287769	0 0192279	0 00700742	-0 0105339	0 0296033	0 00952982	0 0122971	0 0174713	0 0392982	0 524689	0 406616	0 286191	0 381697
669	482 289	0 0287665	0 0192743	0 0069968	-0 010536	0 0296563	0 00949474	0 0123173	0.0174898	0.0393018	0 526631	0.405952	0.285884	0 381662
670	481 399	0 0287681	0.0193314	0 00695373	-0 0105332	0.0296758	0 00946292	0.0123555	0.01748	0 0392984	0.528398	0.404698	0.286043	0.381695
671	480 581	0 0287666	0.0193637	0 0069107	-0 0105371	0 029668	0.00944909	0 0123824	0.0174558	0 0392873	0.529168	0 403816	0 28644	0.381803
672	479 957	0 028749	0 0193365	0 00688175	-0 0105423	0 02965	0 00946285	0.0123735	0.0174285	0.0392648	0.528411	0.404117	0 286889	0.382022
673	478 785	0.0287163	0 0192419	0 00686856	-0 0105342	0 029628	0.00950293	0.0123233	0.0174032	0.0392294	0.526202	0.405779	0.287305	0.382367
674	478 343	0 028675	0 0191047	0 00686867	-0 0105091	0 0296014	0 00955573	0 01225	0.0173813	0 039187	0.523297	0.408214	0.287667	0.382781
675	477 813	0.0286341	0 0189815	0 00687312	-0 0104809	0 0295749	0 00960181	0.0121847	0 0173645	0 039151	0.520769	0 410388	0 287945	0 383133
676	477 012	0 0286158	0 0189417	0 00687407	-0 0104642	0 029562	0 0096282	0 0121518	0 0173561	0 0391361	0 519323	0 411481	0 288084	0 383279
677	476 459	0.0286434	0.0190061	0 00687677	-0 0104623	0 0295806	0 00963782	0 0121522	0.0173588	0.0391488	0 518798	0 411461	0 288039	0 383154
678	475 663	0.0287094	0 0191067	0 00688955	-0 0104711	0 029636	0.00964705	0.0121614	0.0173727	0 0391812	0 518307	0 411152	0 287809	0.382838
679	475 31	0.0287719	0 0191469	0 00690941	-0.0104841	0.0296985	0.00967286	0 0121462	0.0173943	0 0392134	0 516942	0.411684	0.287452	0 382523
680	475 221	0 028796	0.0190951	0 00693564	-0 0104883	0 0297178	0.00972086	0 0120863	0.0174178	0 0392249	0 514411	0.413765	0 287064	0.382411
681	474 773	0.0287828	0 0189931	0 00698141	-0.0104677	0 0296766	0 00978399	0.0119849	0.0174367	0 0392056	0.511102	0.417304	0.286753	0.3826
682	474.309	0.0287545	0.0188905	0.00704783	-0.0104196	0 0296117	0.00984997	0.0118649	0.0174446	0 0391595	0.507672	0 421529	0.286622	0.383051
683	473 867	0 0287247	0 0188004	0.00710321	-0 010363	0 0295685	0 00990811	0 0117558	0.0174365	0.0391004	0.504676	0 425408	0.286757	0.383631
684	473 425	0.0286957	0 0187188	0 00711126	-0.0103239	0 0295524	0.00995027	0 0116815	0.0174105	0 0390422	0.502521	0.42807	0 287187	0.384201
685	473 071	0 0286711	0 0186591	0 0070716	-0 0103085	0 0295401	0.00996886	0.0116534	0 0173701	0.0389923	0 501577	0 42908	0.287857	0 384692
686	473.071	0 0286551	0 0186469	0 00701901	-0 0102968	0 0295151	0.00995711	0 0116695	0.0173241	0.0389507	0.502182	0 428489	0 288621	0.385103
687	472 983	0.0286436	0.0186876	0 00698729	-0 010271	0.0294776	0 00991202	0 01172	0 017284	0.038916	0.504503	0 42666	0 289289	0.385447
688	472.535	0 0286279	0.0187622	0.00698295	-0 0102407	0 0294365	0 00983704	0.0117941	0.0172598	0.0388909	0.508395	0.423997	0.289692	0.385695
689	472 159	0.0286071	0.0188558	0.0069918	-0.0102333	0 0294028	0 00974194	0 0118852	0 0172553	0 0388825	0.513389	0.420763	0.289767	0 385778
690	472 071	0 0285931	0 0189659	0 00699581	-0 0102651	0 0293843	0.00964029	0 011989	0 0172652	0 0388945	0.518802	0.417135	0.289602	0.38566
691	471 717	0.0285967	0 0190806	0 00697897	-0 0103238	0 0293829	0 00954584	0.0120975	0.0172774	0.0389207	0 523905	0 413395	0.289397	0.3854
692	471 717	0 0286079	0 0191722	0.00693486	-0.0103782	0 0293959	0 00946956	0.0121953	0.0172804	0.0389452	0.52808	0.410059	0.289346	0.385157
693	471 629	0 0285996	0.019216	0.00687887	-0 0104038	0 0294163	0 00941879	0.0122628	0.0172711	0.0389527	0 530889	0.407773	0.289502	0.385083
694	471 275	0 0285601	0 019206	0 0068407	-0 0104	0.0294319	0 00939814	0 0122848	0 0172557	0.0389386	0.532039	0.40703	0 28976	0.385222
695	471 275	0 0285125	0 0191519	0 00683719	-0 0103835	0.0294307	0.00940895	0.012259	0.0172436	0 0389116	0.531435	0 407892	0.289963	0 38549
696	471 275	0 0284879	0 01907	0 006858	-0 0103711	0.0294116	0.00944533	0 0121993	0 0172396	0 0388843	0.529405	0 409899	0.290029	0 38576
697	471.275	0.028489	0 018978	0.00687914	-0 0103681	0.0293817	0.0094903	0 012131	0.0172415	0.0388628	0 526898	0 412205	0 289998	0.385973
698	471.275	0 028491	0 0189013	0.00688541	-0 0103695	0.0293463	0 00951881	0.0120814	0.0172435	0.0388438	0.525316	0.413883	0.289964	0.386163
699	471 275	0 0284714	0 0188758	0 00687946	-0 0103686	0.0293087	0 00950944	0 0120701	0.0172416	0 0388212	0.525854	0.414266	0.289996	0.386388
700	471 275	0 0284287	0 0189218	0 0068718	-0 0103646	0 0292774	0.00945801	0 0121024	0.0172349	0.0387953	0.528754	0.413173	0.29011	0.386645
701	471 275	0 0283798	0 0190144	0.00686308	-0 0103649	0.029264	0.009382	0.0121695	0.0172235	0 038775	0.533053	0 410913	0 290302	0 386848
702	471 364	0 0283495	0 0191025	0 00684122	-0 0103771	0.029273	0.00931123	0.0122539	0.0172065	0.0387716	0 537071	0 408089	0.290589	0 386881
703	471 629	0 0283597	0 0191597	0.00679962	-0 0103966	0 0292997	0.00927148	0 0123359	0 0171827	0 0387901	0.539333	0.405365	0.290992	0.386698
704	471.364	0.028415	0 0191931	0 0067491	-0 0104097	0 0293326	0 00927255	0 0123971	0.0171524	0.038822	0.53926	0.403347	0 291508	0 38638
705	471.717	0.0284872	0.0192001	0.00670555	-0.0104098	0 0293506	0.00930697	0.0124225	0.0171187	0.0388482	0.537277	0 402512	0 292082	0 38612
706	471 629	0 0285207	0.0191512	0 0066764	-0 0103997	0.0293316	0.00935681	0.0124063	0.0170869	0.0388499	0 534417	0 403046	0 292625	0.386102
707	471 452	0 0284775	0 0190403	0 00666455	-0.0103808	0.0292767	0 00940304	0.0123585	0.0170618	0.0388234	0.531775	0.40461	0 293054	0.386367
708	472 253	0 0283884	0 0189219	0.00667005	-0.010361	0.029215	0.00943286	0 0123055	0.0170453	0 0387836	0 530076	0 406351	0 293337	0 386763
709	472.629	0.0283302	0.0188668	0 00667816	-0.0103577	0 0291735	0.00944272	0.0122759	0.0170359	0 0387545	0 529514	0 40732	0.293499	0 387053
710	472.718	0 0283384	0 018892	0 00666331	-0.0103739	0.0291533	0 00943683	0 012282	0.0170318	0.0387507	0 529843	0.407115	0 293568	0 387091
711	473 071	0.0283776	0.0189555	0.00662451	-0.0103924	0 029143	0.00942378	0.0123103	0.0170362	0 0387702	0 530577	0 406182	0 293494	0.386895
712	473.16	0.028405	0 01901	0.00660346	-0.0104044	0 0291383	0.00941367	0.0123309	0 0170564	0 038801	0 531147	0 405501	0.293149	0.386589
713	473 513	0 0284186	0.0190346	0.00664103	-0.0104184	0 0291306	0 00941506	0 0123196	0.0170964	0.0388311	0.531071	0.405878	0 292467	0.386289
714	473 602	0 0284304	0 0190229	0 00672244	-0 0104382	0.029102	0.00943093	0.012273	0.0171485	0.0388524	0.530183	0.407433	0 291579	0.386077
715	474.044	0.0284345	0.0189742	0 00678987	-0.0104562	0 0290581	0.00945574	0 0122074	0.0171957	0 0388589	0 528793	0.409624	0 290776	0 386013
716	474 492	0 0284176	0.018908	0.00680555	-0.0104631	0 0290447	0.00947804	0 0121444	0.017224	0.0388464	0.527545	0 411738	0.290296	0 386136
717	474 956	0.0283805	0 0188604	0 00678713	-0.0104527	0.0290927	0 00948849	0 012095	0 0172333	0 0388168	0.52696	0 413408	0 290137	0 386431
718	475 398	0 0283421	0 0188512	0 00678311	-0 0104257	0.0291692	0 00948718	0 012055	0.0172367	0 0387789	0.527031	0.414778	0 290079	0 386809
719	475.752	0 0283238	0 0188648	0 0068215	-0 0103926	0.0292192	0 00948303	0 0120123	0 0172495	0 0387448	0.527261	0 41626	0.289866	0.38715
720	475.928	0 0283295	0.0188696	0.00688896	-0 0103681	0.0292292	0.00948517	0.0119588	0.0172782	0.0387221	0.527143	0.418132	0.289386	0.387376
721	476.73	0.028342	0.0188485	0 00695565	-0 0103641	0.0292195	0.00949397	0.0118972	0.0173171	0.0387083	0.526655	0.420298	0.288737	0 387514
722	477.105	0.0283413	0 0188114	0.00700242	-0.0103808	0.0292018	0.00949937	0.0118392	0.0173516	0 0386902	0.52636	0.422352	0.288161	0.387696
723	477 282	0.028316	0 0187807	0.00702326	-0 010396	0.0291749	0.0094877	0.0117972	0.017366	0.0386509	0.527021	0.423844	0.287922	0.388093
724	478.078	0.0282569	0.0187659	0.00702002	-0.0103805	0.029148	0.00945153	0.011778	0.0173509	0.0385805	0.529062	0.424527	0 288174	0 388804
725	478 52	0 0281624	0 0187574	0 00699632	-0 0103338	0 0291407	0 0093958	0 0117798	0 0173093	0 038485	0 532219	0 424458	0 28887	0 38977

Point	MTSP.y	A.y	B.y	C.y	D.y	EE.y	ThickA.y	ThickB.y	ThickC.y	SheetThick.y	DenA.y	DenB.y	DenC.y	SheetDen.y
726	478.968	0.0280542	0.0187457	0.00695313	-0.0102874	0.0291553	0.00933656	0.011794	0.0172555	0.0383861	0.535588	0.423949	0.289771	0.390774
727	479.52	0.0279688	0.0187293	0.00690015	-0.0102674	0.029162	0.0092934	0.0118086	0.0172087	0.0383107	0.538052	0.423423	0.290556	0.391539
728	480.316	0.0279332	0.0187081	0.0068643	-0.0102713	0.0291262	0.00927956	0.0118144	0.017184	0.0382779	0.53884	0.423216	0.290971	0.391873
729	480.758	0.0279506	0.0186842	0.00686369	-0.0102892	0.0290491	0.00929524	0.01181	0.0171851	0.0382903	0.537934	0.423374	0.290951	0.391746
730	481.206	0.0280018	0.0186657	0.0068831	-0.0103205	0.0289701	0.00932771	0.0118041	0.0172033	0.0383351	0.536064	0.423586	0.290643	0.391289
731	481.67	0.0280578	0.0186632	0.0068956	-0.0103581	0.0289308	0.00935823	0.0118109	0.0172217	0.0383908	0.534308	0.423349	0.290333	0.390721
732	482.201	0.0280954	0.0186821	0.00688693	-0.0103834	0.0289384	0.00937183	0.0118409	0.0172238	0.0384366	0.533525	0.422286	0.290298	0.390255
733	482.996	0.0281059	0.0187175	0.00684696	-0.0103914	0.0289625	0.00936403	0.0118938	0.0172015	0.0384593	0.53397	0.42042	0.290677	0.390023
734	483.444	0.0280923	0.0187512	0.00677594	-0.0103938	0.0289731	0.00934106	0.0119569	0.0171579	0.0384559	0.535285	0.418201	0.291418	0.390058
735	483.997	0.0280627	0.0187642	0.00670531	-0.0103887	0.0289722	0.00931454	0.012013	0.0171046	0.0384321	0.536807	0.416238	0.292328	0.3903
736	484.792	0.028029	0.0187552	0.00667033	-0.0103617	0.0289805	0.0092947	0.0120511	0.0170547	0.0384006	0.537947	0.414908	0.293179	0.39062
737	485.235	0.0280104	0.0187413	0.00666716	-0.0103228	0.0290056	0.00928632	0.0120729	0.0170181	0.0383774	0.538429	0.414153	0.293807	0.390856
738	485.771	0.0280215	0.0187398	0.00666887	-0.0103057	0.0290348	0.0092886	0.0120889	0.0169973	0.0383748	0.538296	0.413605	0.294166	0.390882
739	486.588	0.0280534	0.0187543	0.00666268	-0.0103238	0.0290526	0.00929838	0.0121094	0.0169873	0.0383951	0.537731	0.412909	0.294338	0.390676
740	487.031	0.0280812	0.0187736	0.00664388	-0.010356	0.02905	0.00931395	0.0121372	0.0169793	0.0384304	0.536836	0.411964	0.294477	0.390317
741	487.473	0.0280975	0.01878	0.00660316	-0.0103801	0.0290192	0.00933594	0.0121678	0.0169668	0.0384705	0.535576	0.410929	0.294693	0.38991
742	488.009	0.0281199	0.0187679	0.00655078	-0.010391	0.0289511	0.00936375	0.0121933	0.0169515	0.0385085	0.53399	0.410067	0.294961	0.389525
743	488.827	0.0281619	0.0187544	0.00652573	-0.0103872	0.0288577	0.00939087	0.012209	0.016941	0.0385408	0.532447	0.409537	0.295143	0.389198
744	489.269	0.0282108	0.0187623	0.0065477	-0.0103705	0.0287881	0.00940527	0.0122163	0.0169427	0.0385642	0.531631	0.409292	0.295114	0.388962
745	489.711	0.0282355	0.0187908	0.00658344	-0.0103633	0.0287915	0.00939628	0.0122198	0.016957	0.0385731	0.532149	0.409171	0.294864	0.388872
746	490.247	0.0282048	0.0188138	0.00658916	-0.0103946	0.0288595	0.00936342	0.0122216	0.0169773	0.0385623	0.534032	0.409113	0.294512	0.388981
747	491.065	0.0281082	0.0188039	0.00656041	-0.0104569	0.0289286	0.0093201	0.012218	0.0169934	0.0385314	0.536517	0.409235	0.294234	0.389294
748	491.507	0.027977	0.0187494	0.00651962	-0.0105065	0.0289394	0.00928814	0.0122049	0.0169971	0.0384901	0.538353	0.409676	0.294169	0.389712
749	492.037	0.0278818	0.0186649	0.00648326	-0.0105174	0.0288798	0.00928466	0.0121846	0.0169867	0.0384559	0.538552	0.41036	0.294349	0.390058
750	492.839	0.0278808	0.0185932	0.00645709	-0.0105066	0.0287849	0.00931014	0.0121661	0.0169662	0.0384424	0.537086	0.410983	0.294706	0.390195
751	493.214	0.0279564	0.0185738	0.00644345	-0.0104949	0.0287127	0.00934772	0.012158	0.0169417	0.0384475	0.534923	0.411253	0.295131	0.390143
752	493.48	0.0280282	0.0186006	0.00644254	-0.0104749	0.0287073	0.00937569	0.0121613	0.0169188	0.0384558	0.533314	0.41114	0.295531	0.390059
753	494.629	0.0280464	0.0186364	0.00645357	-0.0104351	0.0287646	0.00938175	0.012169	0.0169026	0.0384534	0.532961	0.41088	0.295814	0.390083
754	495.077	0.0280379	0.0186652	0.00647668	-0.0103908	0.0288402	0.00936679	0.0121717	0.0168993	0.0384378	0.533814	0.410791	0.295872	0.390242
755	495.541	0.0280397	0.0186949	0.00651213	-0.0103684	0.0288894	0.00933833	0.0121623	0.0169138	0.0384144	0.535446	0.41111	0.295619	0.390479
756	496.071	0.0280312	0.0187188	0.0065568	-0.0103732	0.0288938	0.00930413	0.0121375	0.016946	0.0383876	0.537417	0.411956	0.29506	0.390752
757	496.867	0.0279779	0.0187177	0.00660192	-0.0103902	0.0288636	0.00927218	0.0120971	0.0169898	0.0383591	0.539265	0.413338	0.2943	0.391042
758	497.315	0.0279034	0.0186918	0.00663883	-0.0104067	0.0288297	0.00925164	0.0120438	0.0170377	0.0383331	0.540456	0.415176	0.293474	0.391307
759	497.779	0.0278646	0.0186532	0.00666717	-0.0104205	0.0288181	0.00924858	0.0119817	0.0170847	0.038315	0.540632	0.417334	0.292665	0.391492
760	498.221	0.0278678	0.0186071	0.00669176	-0.010436	0.0288257	0.00926034	0.0119144	0.0171307	0.0383054	0.539946	0.419696	0.29188	0.39156
761	498.752	0.0278628	0.0185604	0.00671455	-0.0104575	0.0288327	0.00927739	0.0118432	0.0171778	0.0382984	0.538952	0.422223	0.291079	0.391661
762	499.553	0.0278172	0.0185172	0.00673653	-0.0104842	0.0288275	0.00929203	0.0117677	0.0172282	0.038288	0.5381	0.42494	0.290228	0.391768
763	500.017	0.0277518	0.0184634	0.0067632	-0.0105133	0.028808	0.00930343	0.0116899	0.0172809	0.0382742	0.537439	0.427771	0.289344	0.391909
764	500.459	0.0277019	0.0183929	0.00680075	-0.0105427	0.0287735	0.00931344	0.0116205	0.0173292	0.0382631	0.536861	0.430317	0.288536	0.392023
765	500.99	0.0276802	0.0183391	0.0068417	-0.0105653	0.0287275	0.0093205	0.0115794	0.0173612	0.0382611	0.536455	0.431833	0.288003	0.392043
766	501.791	0.0276863	0.018344	0.006858	-0.0105693	0.0286754	0.00932054	0.0115864	0.0173642	0.0382712	0.536453	0.431584	0.287953	0.39194
767	502.255	0.0277219	0.0184071	0.00682499	-0.0105544	0.0286166	0.00931219	0.0116472	0.0173323	0.0382917	0.536934	0.429368	0.288489	0.391731
768	502.697	0.02778	0.0184876	0.00674878	-0.0105391	0.0285498	0.00929811	0.0117471	0.0172697	0.038315	0.537748	0.425744	0.289539	0.391492
769	503.139	0.0278275	0.0185427	0.00664901	-0.0105427	0.0284866	0.00928159	0.0118566	0.017189	0.0383272	0.538706	0.421804	0.290902	0.391368
770	503.582	0.0278198	0.0185481	0.00653331	-0.0105621	0.0284458	0.009265	0.0119428	0.0171056	0.0383135	0.539671	0.41872	0.292319	0.391509
771	504.029	0.0277419	0.0185003	0.00642302	-0.0105725	0.0284286	0.00925263	0.0119817	0.0170355	0.0382698	0.540393	0.417338	0.293516	0.391957
772	504.493	0.0276347	0.0184202	0.00637463	-0.0105542	0.028418	0.00925236	0.0119661	0.0169916	0.03821	0.540414	0.417884	0.29427	0.392571
773	504.935	0.027575	0.0183474	0.0064241	-0.0105118	0.0284115	0.00927033	0.0119112	0.0169774	0.0381589	0.539378	0.419821	0.294512	0.393095
774	505.378	0.0276101	0.0183134	0.00652624	-0.0104655	0.0284288	0.00930203	0.0118477	0.016984	0.0381337	0.537547	0.422063	0.294396	0.393354
775	505.82	0.0277069	0.0183257	0.0065973	-0.0104296	0.0284718	0.00933042	0.011804	0.016996	0.0381304	0.535909	0.423605	0.294188	0.393388
776	506.267	0.0277826	0.0183759	0.00661185	-0.010402	0.0285042	0.00933626	0.0117882	0.0170032	0.0381276	0.535574	0.424162	0.294064	0.393417
777	506.732	0.0277879	0.0184429	0.00661849	-0.0103708	0.0284933	0.00931267	0.0117864	0.0170063	0.0381054	0.536941	0.424222	0.294009	0.393646
778	507.174	0.0277389	0.0184861	0.00666069	-0.0103337	0.0284504	0.00926908	0.0117808	0.0170106	0.0380605	0.539472	0.424425	0.293935	0.394112
779	507.616	0.0276724	0.0184752	0.00671645	-0.0103083	0.0284111	0.00922114	0.0117688	0.0170162	0.0380061	0.54227	0.424861	0.293839	0.394676
780	508.058	0.0276061	0.0184302	0.00672879	-0.0103157	0.0283928	0.00917808	0.0117658	0.0170168	0.0379606	0.544803	0.424973	0.293829	0.395147
781	508.505	0.0275467	0.0183993	0.0066756	-0.0103543	0.0283915	0.00914045	0.0117903	0.0170059	0.0379367	0.547041	0.424104	0.294017	0.395396
782	508.97	0.0275082	0.0184086	0.0065884	-0.0104014	0.0284067	0.00910705	0.0118469	0.0169834	0.0379374	0.549043	0.422097	0.294407	0.395389
783	509.412	0.0275072	0.0184473	0.00651327	-0.0104337	0.0284482	0.00908077	0.0119228	0.0169559	0.0379595	0.550626	0.419415	0.294885	0.395159
784	509.854	0.027549	0.0185103	0.00647715	-0.0104374	0.0285172	0.00906713	0.0119976	0.0169324	0.0379972	0.551449	0.416789	0.295293	0.394768
785	510.296	0.0276244	0.018579	0.00648344	-0.0104133	0.0285921	0.00906873	0.0120548	0.0169203	0.0380438	0.551351	0.414794	0.295504	0.394284
786	510.744	0.0277113	0.0186323	0.00651472	-0.0103863	0.0286416	0.00908147	0.0120874	0.0169216	0.0380905	0.550579	0.413662	0.295481	0.393801
787	511.119	0.0277766	0.0186604	0.00654394	-0.0103858	0.0286469	0.00909654	0.0120962	0.0169322	0.0381249	0.549665	0.413356	0.295297	0.393444
788	511.208	0.0277914	0.0186651	0.006559	-0.0104045	0.0286108	0.00910724	0.0120852	0.0169429	0.0381353	0.549018	0.413735	0.295109	0.393337
789	511.65	0.0277552	0.0186472	0.00656977	-0.0104037	0.0285497	0.00911539	0.0120587	0.016945	0.0381191	0.548529	0.414649	0.295072	0.393505
790	512.092	0.0277025	0.0186091	0.00658314	-0.0103661	0.0284904	0.00913098	0.0120216	0.0169364	0.0380889	0.547605	0.415932	0.295223	0.393816
791	512.446	0.0276814	0.0185612	0.00658847	-0.0103198	0.0284635	0.00916369	0.0119793	0.0169238	0.0380668	0.545672	0.417399	0.295443	0.394045

Point	MTSP.y	A.y	B.y	C.y	D.y	EE.y	ThickA.y	ThickB.y	ThickC.y	SheetThick.y	DenA.y	DenB.y	DenC.y	SheetDen.y
792	512.628	0.0277145	0.0185142	0.00658016	-0.0103039	0.0284788	0.00921263	0.0119359	0.0169181	0.0380666	0.54279	0.418919	0.295542	0.394047
793	513.357	0.0277716	0.0184724	0.00657445	-0.010327	0.02851	0.00926389	0.0118925	0.0169255	0.0380819	0.539779	0.420447	0.295413	0.393889
794	513.446	0.0277939	0.0184367	0.006586	-0.0103631	0.0285199	0.00929907	0.0118499	0.0169423	0.0380912	0.537716	0.42196	0.29512	0.393792
795	513.799	0.0277509	0 018404	0.00660495	-0.0103811	0.0284963	0.00930779	0.0118112	0.0169584	0.0380774	0.5372	0.423337	0.29484	0.393936
796	513.888	0.0276684	0.0183692	0.0066124	-0.0103728	0.0284553	0.0092931	0.0117833	0.0169661	0.0380425	0.538048	0.424338	0.294706	0.394298
797	514.33	0.0275965	0.0183381	0.0066016	-0.0103606	0.0284202	0.00926654	0.0117722	0.0169656	0.0380044	0.53959	0.424733	0.294713	0.394692
798	514.772	0.0275593	0.0183273	0.00657308	-0.0103769	0.0284067	0.00923992	0.011778	0.0169631	0.037981	0.541141	0.424523	0.294758	0.394935
799	515 22	0.0275437	0.0183379	0.00653172	-0.0104253	0 02842	0.00922186	0.0117903	0.0169647	0.0379768	0.542197	0.424084	0.29473	0.394978
800	515.596	0.0275326	0.0183455	0.00649966	-0.0104662	0.0284537	0.00921839	0.0117917	0.0169752	0.0379853	0.542402	0.424035	0.294548	0.394889
801	515.684	0.0275337	0.0183322	0.00651009	-0.0104616	0.0284899	0.00923205	0.0117696	0.0169984	0.038	0.541606	0.424842	0.294149	0.394737
802	516.126	0.0275648	0.0183112	0.00657507	-0.0104286	0.0285045	0.00925903	0.0117255	0.0170358	0.0380203	0.540033	0.426447	0.293506	0.394526
803	516.48	0.0276166	0.0183053	0.00666478	-0.0104175	0.0284825	0.0092894	0.0116758	0.0170812	0.0380464	0.538264	0.428258	0.292727	0.394256
804	516.568	0.0276496	0.0183111	0.006723	-0.0104471	0.0284335	0.00931253	0.0116407	0.0171188	0.0380721	0.53692	0.42954	0.292082	0.39399
805	517.01	0.0276415	0.0183058	0.00671321	-0.0104861	0.0283853	0.00932227	0.0116319	0.0171315	0.0380857	0.536355	0.429862	0.291864	0.39385
806	517.364	0.0276175	0.0182879	0.00665607	-0.0104935	0.0283574	0.00931626	0.011648	0.0171134	0.0380776	0.536705	0.429267	0.292175	0.393933
807	517.364	0.0276122	0.0182872	0.00660832	-0.010457	0.0283441	0.00929181	0.0116793	0.0170742	0.0380453	0.538138	0.428117	0.292846	0.394268
808	517.458	0.0276177	0.0183277	0.00660382	-0.0103968	0.0283246	0.00924602	0.0117141	0.0170317	0.0379918	0.540836	0.426846	0.293576	0.394825
809	517.834	0.0275944	0.0183932	0.00663121	-0.0103437	0.0282895	0.00918201	0.0117433	0.016998	0.0379232	0.544634	0.425783	0.294155	0.39554
810	517.922	0.0275248	0 01844	0.00665872	-0.0103166	0.0282503	0.00911328	0.011763	0.0169728	0.0378491	0.548735	0.425065	0.29459	0.396315
811	518.276	0.0274353	0.0184354	0.00665833	-0.0103147	0.0282251	0.00905855	0.0117757	0.0169465	0.0377808	0.552017	0.424604	0.295049	0.39703
812	518.384	0 027369	0.0183857	0.00661642	-0.0103237	0.0282247	0.00902934	0.0117885	0.0169094	0.0377273	0.553772	0.424146	0.295699	0.397592
813	518.718	0.0273478	0.0183297	0.00654355	-0.0103274	0.0282489	0.00902185	0.0118075	0.0168602	0.0376895	0.554218	0.423464	0.296565	0.397989
814	518.806	0.0273573	0.0183056	0.00647366	-0.0103153	0.0282852	0.00902112	0.0118325	0.0168072	0.0376609	0.554261	0.42257	0.297499	0.398292
815	519.16	0.0273632	0.0183206	0.00644057	-0.010287	0.028318	0.00901444	0.0118557	0.016764	0.0376341	0.554674	0.421743	0.298264	0.398575
816	519.16	0.0273418	0.0183475	0.00644733	-0.0102561	0.0283385	0.00900234	0.0118671	0.0167412	0.0376106	0.555422	0.421335	0.298668	0.398824
817	519.16	0.0273015	0.0183498	0.00646467	-0.0102481	0.0283369	0.00899796	0.0118619	0.0167423	0.0376022	0.555699	0.42152	0.298647	0.398914
818	519.16	0.0272759	0.0183157	0.0064671	-0.0102806	0.0282963	0.00901553	0.0118436	0.0167627	0.0376219	0.554636	0.422173	0.298284	0.398706
819	519.248	0.027297	0.0182666	0.00645856	-0.0103401	0.0282196	0.00905706	0.0118221	0.0167925	0.0376717	0.552114	0.42294	0.297755	0.398181
820	519.602	0.0273693	0.0182359	0.00645572	-0.0103877	0.0281448	0.00910745	0.0118088	0.0168201	0.0377364	0.54906	0.423415	0.297266	0.397498
821	519.602	0.0274602	0.0182467	0.00646575	-0.0103945	0.0281036	0.00914228	0.0118112	0.0168375	0.0377909	0.546952	0.423332	0.296958	0.396923
822	519.696	0.0275148	0.0182994	0.00648545	-0.0103674	0.028079	0.00914366	0.0118292	0.0168429	0.0378157	0.546867	0.422691	0.296862	0.39666
823	520.072	0.0274966	0.0183628	0.00650046	-0.0103401	0.0280348	0.00911262	0.0118553	0.0168406	0.0378085	0.54874	0.421759	0.296902	0.396737
824	519.978	0.0274234	0.018392	0.00648924	-0.0103402	0.0279688	0.00906713	0.0118789	0.016838	0.0377839	0.55149	0.420921	0.296948	0.396995
825	519.696	0.0273519	0.0183688	0.00645111	-0.0103693	0.027918	0.00902615	0.0118927	0.0168421	0.0377609	0.553978	0.42043	0.296875	0.397236
826	520.072	0.0273167	0.0183192	0.00641849	-0.0104151	0.0279216	0.00899344	0.0118988	0.0168554	0.0377476	0.555987	0.420214	0.296643	0.397377
827	520.072	0.0272983	0.0182887	0.00641492	-0.0104678	0.0279867	0.00895711	0.0119075	0.0168711	0.0377357	0.558264	0.419909	0.296367	0.397502
828	520.072	0.0272536	0.0183023	0.00641523	-0.0105138	0.0280839	0.00890584	0.0119281	0.0168755	0.0377094	0.561512	0.419187	0.296291	0.39778
829	520.072	0.0271676	0.0183397	0.006379	-0.0105311	0.0281709	0.00884615	0.0119579	0.0168577	0.0376618	0.565311	0.418147	0.296605	0.398285
830	520.072	0.0270723	0.0183536	0.00631486	-0.0105083	0.0282211	0.00880416	0.0119798	0.0168213	0.0376052	0.567999	0.417383	0.297249	0.398884
831	520.072	0.0270229	0.0183228	0.00627614	-0.0104601	0.0282324	0.00881065	0.0119736	0.0167839	0.0375681	0.56763	0.417607	0.297911	0.399278
832	520.072	0.0270527	0.0182654	0.00629022	-0.0104196	0.0282185	0.00888236	0.0119304	0.0167649	0.0375777	0.563199	0.419137	0.298245	0.399177
833	520.072	0.0271516	0.0181925	0.00632479	-0.0104185	0.0281976	0.00901137	0.0118586	0.0167724	0.0376423	0.555292	0.421692	0.298112	0.398496
834	520.072	0.0272805	0.0180921	0.00633542	-0.0104641	0.0281799	0.00916538	0.011778	0.0168	0.0377434	0.545978	0.424574	0.297622	0.397431
835	520.072	0.0273909	0.017981	0.00631943	-0.0105287	0.0281627	0.00929811	0.0117101	0.0168353	0.0378435	0.538048	0.427015	0.296999	0.396377
836	519.978	0.0274404	0.0179214	0.00630754	-0.0105715	0.0281409	0.00936849	0.0116692	0.0168688	0.0379065	0.533867	0.428494	0.296408	0.395715
837	519.602	0.0274162	0.0179521	0.0063238	-0.0105745	0.0281233	0.00936086	0.0116571	0.0168973	0.0379153	0.534274	0.428928	0.295907	0.395621
838	519.602	0.0273456	0.0180379	0.00636868	-0.010553	0.0281277	0.00929194	0.0116657	0.01692	0.0378777	0.53827	0.428612	0.295509	0.396015
839	519.602	0.0272708	0.0181135	0.00642354	-0.0105303	0.0281538	0.00919789	0.0116844	0.0169338	0.0378161	0.543768	0.427925	0.295269	0.39666
840	519.602	0.0272155	0.018151	0.00645701	-0.0105137	0.028177	0.00911267	0.0117074	0.016933	0.0377531	0.548796	0.427086	0.295283	0.397321
841	519.602	0.0271778	0.0181619	0.00644099	-0.0105018	0.0281786	0.00905512	0.0117315	0.0169158	0.0377024	0.552223	0.42621	0.295585	0.397855
842	519.602	0.0271447	0.0181535	0.00637744	-0.0105017	0.0281635	0.00903021	0.0117497	0.016889	0.0376689	0.553717	0.42555	0.296053	0.398207
843	519.514	0.0271116	0.018115	0.00630772	-0.0105197	0.0281415	0.00903519	0.0117509	0.0168667	0.0376528	0.55341	0.42551	0.296444	0.398377
844	519.16	0.0270965	0.0180532	0.00628505	-0.0105387	0.0281107	0.0090618	0.011729	0.0168606	0.0376513	0.551794	0.426311	0.296551	0.398392
845	519.16	0.0271257	0.0180117	0.00633045	-0.0105296	0.0280697	0.00909579	0.0116911	0.0168723	0.0376592	0.549731	0.427693	0.296345	0.398309
846	519.16	0.0271932	0.0180269	0.00641496	-0.0104884	0.0280325	0.00912023	0.0116542	0.0168941	0.0376685	0.54825	0.429041	0.295964	0.39821
847	519.16	0.0272493	0.0180831	0.00648656	-0.0104453	0.0280174	0.00912376	0.0116327	0.0169152	0.0376717	0.548034	0.429829	0.295593	0.398177
848	519.16	0.0272514	0.0181331	0.0065144	-0.0104283	0.0280255	0.00910717	0.0116293	0.0169289	0.0376654	0.549034	0.429953	0.295353	0.398244
849	519.16	0.0272141	0.0181514	0.00650775	-0.0104338	0.0280377	0.00908184	0.0116368	0.0169335	0.0376522	0.550564	0.429671	0.295272	0.398383
850	519.16	0.0271858	0.0181509	0.00649602	-0.0104397	0.0280321	0.00906112	0.0116463	0.01693	0.0376375	0.551817	0.429322	0.295333	0.398539
851	519.16	0.0271889	0.0181527	0.00649525	-0.0104336	0.027998	0.00905267	0.0116518	0.0169196	0.037624	0.552327	0.42912	0.295516	0.398681
852	519.072	0.0272055	0.0181571	0.00649785	-0.0104164	0.0279392	0.00905722	0.0116503	0.0169033	0.0376109	0.55205	0.429173	0.295801	0.398821
853	518.718	0.0272118	0.0181492	0.00649239	-0.0103919	0.0278769	0.00907231	0.0116397	0.0168847	0.0375966	0.551135	0.429569	0.296128	0.398972
854	518.718	0.0272067	0.0181228	0.00648396	-0.0103644	0.0278389	0.00909507	0.0116174	0.0168715	0.037584	0.54976	0.430395	0.296359	0.399106
855	518.718	0.027209	0.0180896	0.00649092	-0.0103418	0.0278346	0.00912092	0.0115844	0.0168735	0.0375788	0.548204	0.431628	0.296325	0.399161
856	518.718	0.0272333	0.0180688	0.00652776	-0.0103326	0.0278504	0.00914111	0.0115473	0.0168949	0.0375834	0.546992	0.433014	0.295951	0.399113
857	518.718	0.0272663	0.0180744	0.00659102	-0.0103401	0.0278668	0.00914434	0.0115193	0.0169282	0.0375919	0.546803	0.434064	0.29537	0.399023

Point	MTSP.y	A.y	B.y	C.y	D.y	EE.y	ThickA.y	ThickB.y	ThickC.y	SheetThick.y	DenA.y	DenB.y	DenC.y	SheetDen.y
858	518.718	0.0272757	0.0181087	0.00665155	-0.0103558	0.0278713	0.00912313	0.0115146	0.0169547	0.0375924	0.548091	0.434244	0.294909	0.399017
859	518.629	0.0272486	0.0181562	0.00666481	-0.0103619	0.0278634	0.00907978	0.0115405	0.0169559	0.0375761	0.550727	0.433281	0.294888	0.39919
860	518.276	0.0272043	0.018193	0.00661334	-0.0103469	0.0278511	0.00902558	0.0115918	0.0169273	0.0375447	0.554037	0.431373	0.295388	0.399525
861	518.364	0.0271656	0.0182121	0.00653606	-0.0103204	0.0278435	0.00897429	0.0116534	0.016882	0.0375096	0.55719	0.429093	0.296182	0.399898
862	518.629	0.0271384	0.0182256	0.00648542	-0.0103089	0.0278481	0.00893609	0.011709	0.0168392	0.0374842	0.559551	0.427045	0.296932	0.400169
863	518.276	0.0271226	0.0182355	0.0064647	-0.0103291	0.0278738	0.00891594	0.0117492	0.0168089	0.037474	0.560803	0.425571	0.297464	0.400277
864	518.276	0.0271179	0.0182278	0.00644137	-0.0103653	0.0279203	0.00891408	0.0117727	0.016787	0.0374737	0.560916	0.424715	0.297852	0.40028
865	518.276	0.0271204	0.0182017	0.00640579	-0.0103796	0.027969	0.00892682	0.0117814	0.0167647	0.0374729	0.560118	0.424399	0.298248	0.40029
866	518.276	0.0271272	0.0181768	0.00638149	-0.0103509	0.0279976	0.0089483	0.0117769	0.0167401	0.0374652	0.558776	0.424564	0.298687	0.400371
867	518.276	0.0271382	0.0181648	0.00638718	-0.0103016	0.0280006	0.00897341	0.0117602	0.0167196	0.0374532	0.557214	0.425169	0.299051	0.4005
868	518.276	0.0271487	0.0181528	0.00641139	-0.0102746	0.0279956	0.00899909	0.0117347	0.01671	0.0374438	0.555623	0.426095	0.299223	0.400601
869	518.276	0.0271474	0.0181204	0.00642462	-0.0102873	0.0280069	0.00902277	0.0117078	0.016711	0.0374415	0.554163	0.427072	0.299205	0.400625
870	518.276	0.0271294	0.0180705	0.00641099	-0.0103181	0.0280406	0.00904107	0.0116892	0.0167167	0.037447	0.553038	0.427748	0.299103	0.400566
871	518.276	0.0271079	0.0180376	0.00638347	-0.0103402	0.0280788	0.00905211	0.0116856	0.0167225	0.0374602	0.552361	0.427879	0.298998	0.400425
872	518.276	0.0271064	0.0180523	0.00636633	-0.0103515	0.0281015	0.00905946	0.0116955	0.016728	0.037483	0.551914	0.427517	0.298901	0.400183
873	518.276	0.0271396	0.0181009	0.00637047	-0.0103604	0.0281041	0.00907139	0.0117093	0.0167338	0.0375145	0.551194	0.427015	0.298797	0.399847
874	518.276	0.0272019	0.0181361	0.00638806	-0.0103625	0.0280917	0.00909277	0.011715	0.0167387	0.0375464	0.549906	0.426806	0.29871	0.399506
875	518.187	0.0272632	0.0181267	0.00640037	-0.0103525	0.0280727	0.00911638	0.0117066	0.0167404	0.0375634	0.548486	0.427114	0.298679	0.399326
876	517.74	0.0272722	0.0180792	0.00639249	-0.0103435	0.0280626	0.00912471	0.0116865	0.0167403	0.0375515	0.547992	0.427848	0.298681	0.399453
877	517.458	0.0271933	0.0180248	0.00637202	-0.0103508	0.0280743	0.00910395	0.0116626	0.0167436	0.0375102	0.549263	0.428724	0.298621	0.399894
878	517.922	0.0270596	0.0179956	0.00636558	-0.0103687	0.0280982	0.00905796	0.0116419	0.016756	0.0374558	0.552069	0.429486	0.298403	0.400475
879	518.187	0.0269603	0.0180049	0.00638657	-0.0103843	0.0281043	0.00900816	0.0116271	0.0167774	0.0374127	0.555109	0.430032	0.298022	0.400936
880	517.834	0.0269515	0.0180375	0.00642053	-0.0103937	0.0280722	0.00897844	0.0116166	0.0168021	0.0373972	0.556922	0.430418	0.297584	0.401101
881	517.834	0.0270066	0.0180633	0.00644815	-0.0103943	0.0280123	0.00897947	0.0116071	0.0168218	0.0374083	0.556849	0.430773	0.297235	0.400981
882	517.834	0.0270642	0.0180633	0.00646297	-0.0103853	0.0279579	0.00900503	0.0115961	0.0168309	0.037432	0.555272	0.431181	0.297074	0.400727
883	517.834	0.0270967	0.0180434	0.00646421	-0.0103753	0.0279403	0.00903997	0.0115839	0.0168289	0.0374527	0.553123	0.431636	0.297109	0.400505
884	517.834	0.0271129	0.0180215	0.00645396	-0.0103685	0.0279694	0.00907033	0.0115718	0.0168194	0.0374615	0.551263	0.432087	0.297276	0.400411
885	517.834	0.0271195	0.0180075	0.00644462	-0.0103562	0.0280261	0.0090892	0.0115601	0.0168081	0.0374574	0.55011	0.432522	0.297476	0.400455
886	517.834	0.027109	0.0180021	0.00644968	-0.0103368	0.0280694	0.00909862	0.0115477	0.0167992	0.0374455	0.549538	0.43299	0.297634	0.400583
887	517.834	0.027084	0.018	0.00646292	-0.0103275	0.0280629	0.00910771	0.011533	0.0167928	0.0374335	0.548993	0.433542	0.297747	0.400711
888	517.834	0.0270679	0.0179813	0.00646136	-0.0103408	0.0280004	0.00912512	0.0115168	0.0167834	0.0374253	0.547954	0.434152	0.297914	0.400798
889	517.834	0.0270759	0.0179273	0.00643306	-0.0103618	0.0279082	0.00914846	0.0115033	0.0167638	0.0374156	0.546564	0.43466	0.298264	0.400903
890	517.834	0.0270871	0.0178609	0.00639125	-0.0103601	0.0278273	0.00916127	0.0114998	0.016731	0.0373921	0.545809	0.434793	0.298852	0.401156
891	517.834	0.0270653	0.0178376	0.00636009	-0.0103228	0.0277902	0.00914482	0.0115128	0.0166908	0.0373484	0.546816	0.434308	0.299572	0.401627
892	517.834	0.0270061	0.0178808	0.00635425	-0.0102679	0.0277978	0.00909595	0.011543	0.0166557	0.0372946	0.549785	0.433178	0.300201	0.402206
893	517.834	0.0269512	0.017959	0.00637022	-0.0102276	0.0278168	0.00903243	0.011584	0.0166376	0.0372541	0.553649	0.431645	0.300526	0.402643
894	517.834	0.0269494	0.0180327	0.00639255	-0.0102219	0.0278121	0.00897948	0.0116263	0.0166403	0.037246	0.556878	0.430075	0.300477	0.402729
895	517.834	0.0270041	0.0180866	0.00640857	-0.0102479	0.0277798	0.00895078	0.0116616	0.0166574	0.0372697	0.55863	0.428767	0.300169	0.402473
896	517.834	0.0270623	0.0181141	0.00641204	-0.0102869	0.0277319	0.00894231	0.011686	0.0166764	0.0373047	0.559145	0.427866	0.299826	0.402095
897	517.834	0.0270636	0.0181051	0.00639383	-0.0103224	0.0276679	0.00894167	0.0116987	0.0166866	0.037327	0.559181	0.427398	0.299642	0.401854
898	517.74	0.0270017	0.0180609	0.00634868	-0.0103488	0.0275954	0.00894055	0.0117004	0.0166855	0.0373265	0.559251	0.427335	0.299663	0.40186
899	517.458	0.0269299	0.0180041	0.00629761	-0.0103656	0.0275557	0.00893744	0.0116923	0.0166795	0.0373092	0.559446	0.427636	0.29977	0.402046
900	517.74	0.0269026	0.0179668	0.0062819	-0.0103687	0.0275792	0.00893161	0.0116767	0.0166776	0.0372858	0.559813	0.428207	0.299804	0.402298
901	517.364	0.0269191	0.0179701	0.00631981	-0.0103556	0.0276337	0.00891893	0.0116584	0.0166823	0.0372596	0.560616	0.42888	0.29972	0.402582
902	517.364	0.0269297	0.0180072	0.00638092	-0.0103314	0.0276606	0.00889657	0.0116424	0.016687	0.037226	0.562033	0.429466	0.299635	0.402945
903	517.364	0.0268956	0.018041	0.00641527	-0.0103027	0.0276507	0.00887087	0.0116309	0.0166829	0.0371846	0.563665	0.429892	0.29971	0.403394
904	517.364	0.0268346	0.0180339	0.00640243	-0.0102734	0.0276502	0.00885717	0.0116213	0.016669	0.0371475	0.564537	0.430246	0.29996	0.403798
905	517.364	0.0268009	0.0179876	0.00636647	-0.0102539	0.027696	0.00886936	0.0116103	0.0166555	0.0371351	0.563776	0.430655	0.300203	0.403932
906	517.364	0.0268309	0.0179432	0.00634847	-0.0102604	0.0277746	0.00890885	0.0115982	0.0166543	0.0371614	0.561298	0.431102	0.300224	0.403648
907	517.276	0.026915	0.0179374	0.00636745	-0.0102912	0.027849	0.00896377	0.0115909	0.0166668	0.0372215	0.557865	0.431374	0.3	0.402998
908	516.922	0.0270131	0.0179686	0.00640282	-0.0103181	0.0279013	0.00901774	0.0115956	0.0166801	0.0372934	0.55451	0.431203	0.299761	0.40222
909	516.922	0.0270908	0.0180091	0.00641569	-0.0103156	0.0279285	0.00905873	0.0116149	0.0166779	0.0373515	0.551979	0.430489	0.299802	0.401593
910	516.922	0.0271398	0.0180368	0.00639077	-0.0102866	0.0279203	0.00908084	0.0116438	0.0166546	0.0373792	0.550622	0.429421	0.300223	0.401294
911	516.922	0.0271594	0.0180456	0.0063492	-0.0102522	0.0278661	0.0090809	0.0116715	0.0166204	0.0373728	0.550621	0.428402	0.300839	0.401362
912	516.922	0.0271345	0.0180374	0.00631901	-0.0102303	0.027774	0.0090565	0.0116871	0.0165946	0.0373381	0.552127	0.427828	0.301307	0.401736
913	516.833	0.0270572	0.0180191	0.00631062	-0.010232	0.0276745	0.00900822	0.011685	0.0165924	0.0372856	0.555119	0.427902	0.301347	0.402303
914	516.568	0.0269524	0.0180025	0.00632277	-0.0102623	0.0276048	0.00894329	0.0116682	0.0166172	0.0372267	0.559171	0.428597	0.300898	0.402939
915	516.922	0.0268498	0.0179933	0.00635052	-0.0103111	0.0275899	0.00887663	0.0116349	0.0166594	0.0371709	0.563361	0.429751	0.300138	0.403543
916	516.833	0.0267588	0.0179841	0.00638378	-0.0103513	0.0276298	0.00882794	0.0115965	0.0167016	0.037126	0.56644	0.431176	0.299379	0.40403
917	516.568	0.0266997	0.0179638	0.0064101	-0.0103604	0.0276957	0.00881454	0.0115556	0.0167283	0.0370984	0.567293	0.432703	0.298898	0.40433
918	516.833	0.0267085	0.0179271	0.00641927	-0.0103427	0.0277442	0.00884145	0.0115164	0.0167331	0.0370909	0.56559	0.434175	0.298811	0.404412
919	516.48	0.0267759	0.0178763	0.00640581	-0.0103212	0.0277497	0.00889496	0.0114822	0.0167205	0.0370977	0.562203	0.435463	0.299035	0.404338
920	516.48	0.0268298	0.0178196	0.00637405	-0.010314	0.0277268	0.00894741	0.0114552	0.016702	0.0371046	0.558888	0.436486	0.299367	0.404263
921	516.391	0.0268137	0.0177683	0.00634034	-0.0103242	0.0277098	0.00897227	0.0114363	0.0166897	0.0370982	0.557316	0.437206	0.299588	0.404332
922	516.126	0.0267441	0.0177379	0.00632468	-0.0103418	0.0277115	0.00895835	0.0114261	0.0166917	0.0370762	0.558188	0.437597	0.299551	0.404574
923	516.48	0.0266728	0.0177452	0.0063358	-0.0103543	0.0277138	0.00891283	0.0114245	0.0167112	0.0370485	0.561059	0.437656	0.299204	0.404875

Point	MTSP.y	A.y	B.y	C.y	D.y	EE.y	ThickA.y	ThickB.y	ThickC.y	SheetThick.y	DenA.y	DenB.y	DenC.y	SheetDen.y
924	516 48	0 0266283	0 0177891	0 0063647	-0 0103646	0.027695	0 00885405	0.0114295	0 0167464	0.03703	0 564785	0.437464	0.298577	0.405078
925	516 48	0 0266102	0.017844	0.00639686	-0 0103875	0 0276573	0.00880164	0.0114361	0 0167918	0.0370296	0 568125	0.437212	0.29777	0.405082
926	516.48	0 0266106	0.0178825	0.00642675	-0.0104252	0.027621	0.00876974	0 0114386	0.0168377	0.037046	0 570166	0.437119	0.296959	0.404903
927	516 48	0 0266248	0.0178961	0 00645291	-0 0104578	0 0276009	0 00876444	0.011434	0.016871	0.0370694	0.570504	0.437293	0.296371	0.404647
928	516.48	0.0266468	0 0178876	0 00646518	-0.0104658	0 0275983	0 00878431	0.0114243	0.0168801	0 0370887	0 569223	0.437664	0.29621	0.404436
929	516 48	0.0266652	0 0178552	0.0064484	-0.0104507	0 0276086	0 00882237	0.0114146	0.0168605	0 0370975	0.566781	0 438038	0.296556	0.40434
930	516.48	0.0266707	0.0177977	0 00640015	-0.0104293	0 0276218	0.00886778	0.0114109	0.0168176	0.0370963	0.563881	0.438179	0.297315	0.404353
931	516 48	0 0266697	0 0177349	0.00633969	-0 0104134	0.0276301	0.0089076	0.0114192	0.016763	0.0370898	0.561348	0.437864	0.298285	0.404424
932	516 48	0.0266794	0 0177065	0 0062937	-0.0104006	0 0276405	0 00893006	0.0114431	0.016708	0.0370812	0 559923	0.436954	0.299266	0.404518
933	516 391	0.0267042	0 0177376	0.00627234	-0.0103788	0.0276651	0.00892987	0.0114803	0.0166599	0 03707	0 559932	0.435548	0.300128	0.40464
934	516.038	0 0267289	0.0178097	0.00626818	-0.0103402	0 0276963	0.00891226	0.0115195	0.0166228	0.0370546	0.561041	0.434061	0.300794	0.404808
935	516 038	0.026741	0.0178774	0 00627961	-0.0102907	0.0277082	0.00889161	0.0115452	0.0166007	0.0370375	0 562343	0 433091	0.301194	0.404995
936	516 038	0.0267508	0.0179114	0 00631719	-0.0102467	0 0276834	0.00888361	0.0115465	0.0165953	0.0370253	0.562848	0.433042	0.301292	0.405128
937	516 038	0.0267786	0.0179143	0 00637752	-0 0102201	0 0276283	0.0088954	0.0115262	0 0166023	0.037024	0.562107	0 433805	0.301163	0.405143
938	516 038	0.0268216	0.0178976	0 00642743	-0 0102107	0 0275706	0.00892067	0.0115012	0 0166109	0.0370328	0 560518	0.43475	0.301007	0.405047
939	516 038	0 0268482	0.017867	0.00643072	-0 0102129	0.0275438	0.008943	0.0114935	0.0166093	0.0370457	0.559116	0.435045	0.301038	0.404905
940	516 038	0.0268395	0.0178414	0.00638525	-0 0102238	0.0275574	0.00894554	0.0115198	0.0165925	0.0370579	0.558961	0.434068	0.301343	0 404772
941	516.038	0.0268162	0.0178557	0.00632013	-0.0102416	0.0275826	0.00892079	0 0115843	0.016565	0.03707	0 560531	0.431686	0.301844	0.40464
942	516 038	0.0268067	0.0179241	0 00625971	-0 0102637	0.027581	0.00887493	0.0116755	0.0165354	0.0370858	0.563443	0.428332	0.302384	0.404468
943	516 038	0.026814	0.0180167	0 00620913	-0 0102881	0 0275492	0.00882465	0.0117706	0.0165112	0.0371064	0.566647	0.424861	0.302827	0.404244
944	516 038	0 0268277	0.0180874	0 0061721	-0.0103112	0.0275203	0 00878886	0.0118432	0 0164956	0.0371277	0.568934	0.422225	0.303112	0.404011
945	516.038	0 0268379	0.0181053	0 00615424	-0.0103268	0 0275218	0 00878008	0.0118744	0.0164889	0.0371434	0.569493	0.421096	0.303234	0.40384
946	516.038	0.0268309	0.0180606	0.00614827	-0.0103343	0.0275457	0.0088003	0.0118595	0.0164903	0.0371502	0.568196	0.421627	0.303208	0.403767
947	516 038	0.026803	0.0179705	0.00614292	-0.0103443	0.0275631	0.00884241	0.0118084	0.0164988	0.0371495	0 565507	0.423466	0.303054	0.403774
948	516 038	0.0267743	0.0178758	0.0061432	-0 010363	0.0275555	0.00889489	0.0117385	0.0165119	0.0371454	0 562176	0.425993	0 302812	0.403819
949	515.855	0 0267644	0.0178048	0.00615667	-0.0103804	0 0275281	0.00894535	0.0116676	0.0165255	0.0371384	0 558994	0.428574	0.302564	0.403894
950	515.308	0.0267643	0.0177501	0.00616967	-0.0103846	0.0275023	0.00898155	0.0116092	0.0165347	0.0371254	0.556724	0.430719	0.302395	0.404036
951	515.949	0.0267464	0.0176998	0.00616461	-0.010378	0.0275015	0.00899294	0.0115712	0.0165395	0.0371036	0.556015	0.432119	0.302308	0.404274
952	515 684	0.0266961	0.0176725	0.00614954	-0.0103739	0.0275348	0.00897592	0.0115557	0.0165456	0.0370772	0.55708	0.432692	0.302196	0.404562
953	516.126	0 0266333	0.017693	0.00614628	-0.0103854	0.0275835	0.00893949	0.0115575	0.0165602	0.0370573	0.559359	0 43262	0.30193	0.40478
954	516.391	0.0266006	0.0177475	0.00616374	-0.0104131	0.0276122	0.00890279	0.0115667	0.0165836	0.037053	0 561656	0.432279	0.301506	0.404826
955	516 038	0.0266237	0 0177924	0.00619821	-0.0104352	0.027603	0.00888248	0.0115745	0.0166065	0.0370635	0 562924	0.431985	0.30109	0.404712
956	516 038	0.0266825	0.0178072	0.00623627	-0.0104247	0.0275721	0.00888024	0.0115804	0.0166161	0.0370767	0 563058	0.431766	0.300915	0.404567
957	516.038	0.0267307	0.0178111	0 00625199	-0.0103843	0.0275479	0.00888321	0.0115895	0 0166066	0.0370793	0 562868	0.431427	0.301088	0.404538
958	516.038	0 0267409	0.0178288	0 0062335	-0 010343	0 0275462	0.00887773	0.0116038	0.0165843	0 0370658	0.563218	0.430897	0.301493	0.404686
959	516 038	0.0267193	0.0178579	0.00620923	-0.010319	0.0275629	0.00886302	0.0116153	0.0165637	0.037042	0 564157	0.430474	0.301867	0.404947
960	516.038	0.0266855	0.0178749	0.00621352	-0.0103106	0.0275796	0.00885265	0.01161	0.0165574	0.03702	0.564821	0.430675	0.301982	0.405187
961	516.038	0.0266589	0.0178556	0.00623779	-0.0103164	0.0275817	0 0088634	0.0115785	0.0165698	0.0370117	0.564154	0.431858	0 301757	0.405278
962	516 038	0.026654	0.017791	0.00625001	-0 0103395	0.0275832	0 00890089	0.0115225	0.0165984	0.0370218	0.561803	0.433972	0.301237	0.405167
963	516.038	0.0266676	0.0176978	0.00624748	-0.0103761	0 0276105	0.00895352	0.0114532	0.0166391	0.0370458	0.558507	0 436605	0.300503	0.404904
964	516 038	0.0266768	0.0176184	0.00625854	-0 0104174	0 027653	0.00899959	0.0113861	0.0166868	0.0370725	0.555626	0.439168	0.299645	0.404613
965	516 038	0.0266656	0.0175911	0.00629823	-0.0104522	0.0276615	0.00902261	0.0113356	0.0167324	0 0370906	0.554185	0 44111	0.298827	0.404416
966	516 038	0.0266436	0.0176132	0.0063444	-0 0104688	0.0276081	0.00902179	0.0113103	0.0167623	0.0370944	0.554225	0.442084	0.298293	0.404374
967	516.038	0.0266329	0.0176452	0.00636098	-0.0104611	0.0275183	0.00900864	0.0113111	0.016764	0.0370838	0.55503	0.442049	0.298262	0.40449
968	516.038	0.0266391	0.0176558	0 00633539	-0.0104341	0.0274384	0.00899434	0.0113319	0.0167348	0.0370611	0.55591	0.44124	0.298786	0.404738
969	516.038	0 026644	0.0176496	0.00628604	-0.0103995	0.0273991	0.0089813	0.0113622	0.0166842	0.0370277	0.556717	0.440064	0.299694	0.405103
970	516.038	0 0266306	0.0176479	0 00623947	-0.0103657	0.027405	0.0089659	0.01139	0.0166291	0.036985	0.557676	0.43899	0.300686	0 405572
971	516.038	0 026601	0.0176534	0.00621197	-0.0103374	0.0274322	0.00894622	0.0114041	0.016585	0.0369353	0.558905	0.438445	0.301482	0.406117
972	516 038	0.0265596	0.0176451	0.00620922	-0 0103201	0.0274334	0.0089256	0.0113992	0.0165586	0 0368834	0 560195	0.438634	0.301961	0.40669
973	516.038	0.0265058	0.0176106	0.00622677	-0.0103166	0.0273748	0.00890985	0.0113807	0.0165448	0.0368353	0.561181	0.43935	0.302212	0.40722
974	516 038	0.0264544	0.0175666	0.00624355	-0.0103191	0.0272771	0.00890301	0.011364	0.0165306	0 0367976	0 56161	0.439996	0.302471	0.407636
975	516.038	0.0264332	0.0175384	0.00622879	-0.0103145	0 0272038	0.00890534	0.0113656	0.0165045	0.0367754	0.561463	0.439937	0.302952	0.407882
976	516 038	0.0264485	0.0175345	0.00617272	-0.0103008	0.0272009	0.00891379	0.0113911	0.0164657	0.0367706	0.560931	0.438956	0.303669	0.407935
977	516 038	0.0264782	0.017548	0.00610324	-0.01029	0.0272597	0.00892384	0.0114311	0.0164262	0.0367812	0 560299	0.437422	0.304397	0.407818
978	516 038	0.0265025	0.0175654	0.00605713	-0.0102937	0.0273336	0.0089311	0.0114681	0.0164038	0.036803	0.559843	0.436007	0.304812	0.407577
979	516.038	0.0265157	0.0175731	0.00604817	-0 0103128	0.0273757	0.00893164	0.0114897	0.01641	0.0368313	0.559811	0.435179	0.304697	0.407263
980	516.038	0.0265161	0.0175725	0.00607181	-0.0103462	0.0273606	0.00892188	0 0114972	0.0164427	0.0368618	0.560428	0.434893	0.304093	0.406926
981	516.038	0.0265057	0.0175833	0.00611265	-0.0103929	0.02729	0.0089004	0.0115023	0.0164862	0.036889	0.561789	0.434698	0.303291	0.406626
982	515.949	0 026493	0.0176203	0.00613871	-0.010438	0.0271942	0.00887123	0.0115151	0.0165195	0.0369058	0.56364	0.434219	0.302678	0.40644
983	515.684	0.026484	0.0176669	0.00612208	-0.0104574	0.0271203	0.00884452	0.0115315	0.0165287	0 0369047	0.565338	0.433605	0.302507	0.406452
984	516.038	0.0264725	0.0176813	0.00607684	-0.0104441	0.0271032	0.00883145	0.0115338	0.0165158	0.0368811	0.56617	0.433526	0.302743	0.406714
985	516.038	0.0264431	0.0176312	0.00604997	-0.0104146	0.027137	0.00883653	0.0115059	0.0164946	0.036837	0.565844	0.434593	0.303132	0.407201
986	516.038	0.0263862	0.0175273	0.00606431	-0.0103903	0.0271786	0.00885408	0.0114512	0.0164777	0.0367829	0.564723	0.436684	0.303442	0.4078
987	516.038	0.026313	0.017417	0.00608937	-0.0103855	0.0271857	0.00887249	0.0113955	0.0164673	0.0367353	0.563548	0.438812	0.303632	0.408328
988	515.949	0.026254	0.017349	0.00607916	-0.0104016	0.0271531	0.00888264	0.0113706	0.016458	0.0367113	0.5629	0.439762	0.303804	0.408595
989	515.684	0.0262412	0.0173525	0.00602689	-0.0104233	0.0271066	0.00888371	0.0113909	0.016447	0.0367216	0.56283	0.438986	0.304007	0.408481

Point	MTSP.y	A.y	B.y	C.y	D.y	EE.y	ThickA.y	ThickB.y	ThickC.y	SheetThick.y	DenA.y	DenB.y	DenC.y	SheetDen.y
990	515.949	0.0262914	0.0174261	0.00597313	-0.0104352	0.0270717	0.00888172	0.0114432	0.0164405	0.0367654	0.562956	0.436984	0.304128	0.407995
991	515.596	0.0263926	0.017528	0.00596612	-0.0104391	0.0270641	0.00888166	0.011499	0.0164473	0.0368279	0.562961	0.434854	0.304004	0.407304
992	515.596	0.0264991	0.0176033	0.00601703	-0.0104409	0.0270905	0.00888018	0.0115359	0.0164684	0.0368845	0.563061	0.433443	0.303615	0.406678
993	515.596	0.0265559	0.0176387	0.00608885	-0.0104344	0.0271381	0.00886668	0.0115513	0.0164937	0.0369117	0.563934	0.432657	0.303148	0.406377
994	515.596	0.0265403	0.0176648	0.00613271	-0.010414	0.027179	0.00883407	0.0115553	0.0165104	0.0368998	0.566038	0.432704	0.30284	0.406508
995	515.596	0.0264747	0.0176982	0.00613669	-0.0103886	0.0271968	0.00878905	0.0115553	0.016513	0.0368574	0.568945	0.432703	0.302792	0.406976
996	515.596	0.0264033	0.0177118	0.00612633	-0.0103713	0.0271984	0.00874933	0.0115496	0.0165059	0.0368049	0.571511	0.432919	0.302922	0.407557
997	515.596	0.0263612	0.0176781	0.00612272	-0.0103647	0.0271995	0.00872869	0.0115353	0.0164971	0.0367611	0.572843	0.433456	0.303085	0.408042
998	515.596	0.0263519	0.0176188	0.00612441	-0.0103632	0.0272058	0.00872528	0.0115183	0.0164913	0.0367349	0.573057	0.434097	0.30319	0.408332
999	515.596	0.0263535	0.0175892	0.00612534	-0.010363	0.0272099	0.00872653	0.0115106	0.0164895	0.0367266	0.572973	0.434389	0.303223	0.408424

APPENDIX V

Data Reduction and Plotting Procedure used in *Igor*™.

```
Window Targets() : Graph
	PauseUpdate; Silent 1		| building window...
	Display /W=(3,41,509,339) EE,D,C,B,A vs xTime
	Append /R MTSP vs xTime
	Modify lStyle(D)=4,lStyle(C)=3,lStyle(B)=2,lStyle(A)=1
	Modify nticks(left)=20,nticks(bottom)=10
	Modify minor=1
	Modify fSize=12
	Modify lowTrip(left)=0.01,lowTrip(bottom)=0.001
	Label left "\Z12Target Height (mm)"
	Label bottom "\Z12Time (sec)"
	Label right "\Z12Pressure (MPa)"
	SetAxis left -0.1,1.3
	SetAxis right -0.05,6
	Textbox /F=0/A=MC/X=37.5321/Y=41.7004
"\Z12T4690G\rSoftwood\r694 CSF"
	Tag /F=0/X=0/Y=10.9312 A, 100, "\Z12A"
	Tag /F=0/X=0/Y=7.05394 B, 100, "\Z12B"
	Tag /F=0/X=0/Y=8.40336 C, 100, "\Z12C"
	Tag /F=0/X=0.496278/Y=9.31174 D, 100, "\Z12D"
	Tag /F=0/X=13.3663/Y=-0.414938 MTSP, 650, "\Z12Pressure"
	Tag /F=0/X=-8.41584/Y=-0.414938 EE, 330, "\Z12Head"
EndMacro

Window Thick() : Graph
	PauseUpdate; Silent 1		| building window...
	Display /W=(3,41,509,339) ThickC,ThickB,ThickA vs xTime
	Append /R MTSP vs xTime
	Modify lStyle(ThickC)=3,lStyle(ThickB)=2,lStyle(ThickA)=1
	Modify nticks(left)=20,nticks(bottom)=10
	Modify minor=1
	Modify fSize=12
	Modify lowTrip(left)=0.001,lowTrip(bottom)=0.001
	Label left "\Z12Zonal Thickness (mm)"
	Label bottom "\Z12Time (sec)"
	Label right "\Z12Pressure (MPa)"
	SetAxis left 0.05,0.45
	SetAxis right -0.05,6
	Textbox /F=0/A=MC/X=38.9333/Y=40.8907
"\Z12T4690G\rSoftwood\r694 CSF"
```

```
	Tag /F=0/X=15.3465/Y=0 MTSP, 650, "\Z12Pressure"
	Tag /F=0/X=0/Y=-10.3734 ThickC, 200, "\Z12SPZ"
	Tag /F=0/X=0.247525/Y=9.12863 ThickB, 200, "\Z12MZ"
	Tag /F=0/X=0.247525/Y=8.71369 ThickA, 200, "\Z12FEZ"
EndMacro

Window Density() : Graph
	PauseUpdate; Silent 1		| building window...
	Display /W=(3,41,509,339) DenC,DenB,DenA vs xTime
	Append /R MTSP vs xTime
	Modify lStyle(DenC)=3,lStyle(DenB)=2,lStyle(DenA)=1
	Modify nticks(left)=20,nticks(bottom)=10
	Modify minor=1
	Modify fSize=12
	Modify lowTrip(left)=0.001,lowTrip(bottom)=0.001
	Label left "\Z12Apparent Zonal Density (g/cm\S3\M)"
	Label bottom "\Z12Time (sec)"
	Label right "\Z12Pressure (MPa)"
	SetAxis left 0.1,0.65
	SetAxis right -0.05,6
	Textbox /F=0/A=MC/X=-38.8889/Y=41.7004
"\Z12T4690G\rSoftwood\r694 CSF"
	Tag /F=0/X=-0.247525/Y=9.12863 DenC, 800, "\Z12SPZ"
	Tag /F=0/X=0/Y=10.7884 DenA, 800, "\Z12FEZ"
	Tag /F=0/X=0.495049/Y=-9.95851 DenB, 800, "\Z12MZ"
	Tag /F=0/X=-12.9187/Y=-0.404858 MTSP, 530, "\Z12Pressure"
EndMacro
```

APPENDIX VI

List of Problems Encountered

1. The two-shaft type of falling weight wet press simulator produced an uneven application of pressure to the surface of the sheet. The head fell unevenly due to uneven friction in the two sets of slider bearings.

2. The extension shaft used to attach the upper press head to the MTS hydraulic ram provided insufficient rigidity and should be eliminated in future applications of the equipment.

3. Operation of the proximity detector calibration micrometer in both directions to calibrate the proximity detectors resulted in a backlash error that was unacceptable. Calibration of the proximity detectors should be done in a consistent manner in one direction only.

4. Handsheets in which a target was dislodged from either surface of the sheet produced erratic results. Any handsheet in which a target is dislodged should be discarded.

5. The original technique of putting a few fibers down on the surface of the forming wire before placing the first target should not be used. These fibers made it difficult to reproduce the positions of this target.

APPENDIX VII

List of Datafiles on Diskettes Presented in Appendix VIII.

These data were saved on 3.5 inch diskettes compatible with the Apple Macintosh and the program *Igor*™.

Run	Basis Weight (g/m^2)	Ingoing Moisture Ratio	Furnish/ Freeness SWD/HWD (CSF)	Initial 3.75" Handsheet Weight (g)	Final 3.75" Handsheet Weight (g)	Water Removal (g)
T122989A	150.0	3.30	SWD/605	4.655	3.860	0.795
T21990C	150.0	3.57	SWD/694	5.191	4.946	0.245
T21990F	150.0	3.72	SWD/353	5.345	4.947	0.398
T22790D	157.0	2.66	SWD/353	3.960	3.402	0.558
T22790E	157.0	2.46	SWD/353	3.933	3.400	0.533
T22790K	157.0	1.32	SWD/353	2.721	2.660	0.061
T22790L	157.0	1.31	SWD/353	2.743	2.680	0.063
T32690A	150.0	4.04	HWD/480	5.737	3.080	2.657
T4690A	150.0	4.59	SWD/694	6.426	-------	
T4690D	150.0	4.24	SWD/694	6.088	-------	
T4690E	150.0	4.62	SWD/694	6.500	-------	
T4690F	150.0	5.43	SWD/694	7.630	3.387	4.243
T4690M	150.0	3.32	HWD/480	5.060	2.985	2.075
T4690P	150.0	4.26	SWD/353	6.052	3.584	2.468
T4690R	150.0	3.57	SWD/353	6.425	-------	
T4690S	150.0	3.89	SWD/353	5.657	3.490	2.167

APPENDIX VIII

Remaining Data Not Presented in Thesis Body

The results obtained are divided into two categories based on the extent of retraction of the press head and release of the compressing force. The first category includes all handsheets in which the applied load was not relieved completely during the expansion of the handsheet. This resulted in a residual load on the handsheet at the end of the cycle and allowed examination of the effects of asymmetric loads on the handsheet. The second category includes handsheets in which the applied load had a symmetric haversine shape. In these handsheets the expansion cycle was completed with full retraction of the falling press head. In both cases all of the target positions were recorded along with the force applied to the sheet.

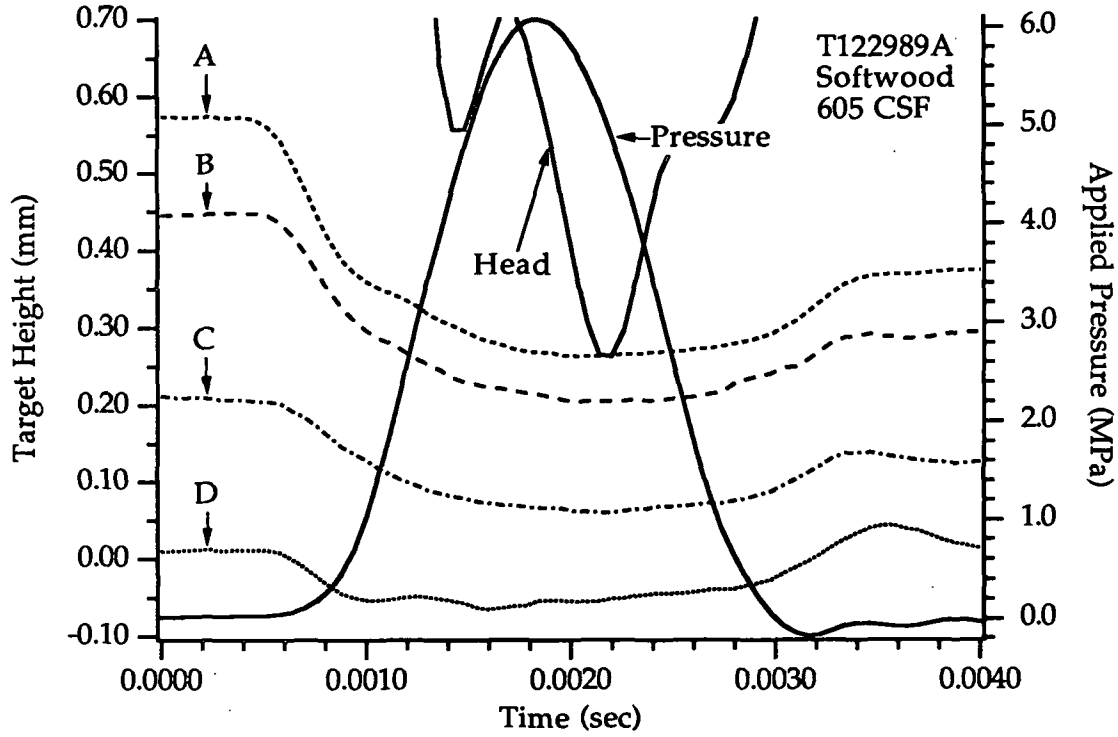

Figure 86. Target displacements for handsheet T122989A.

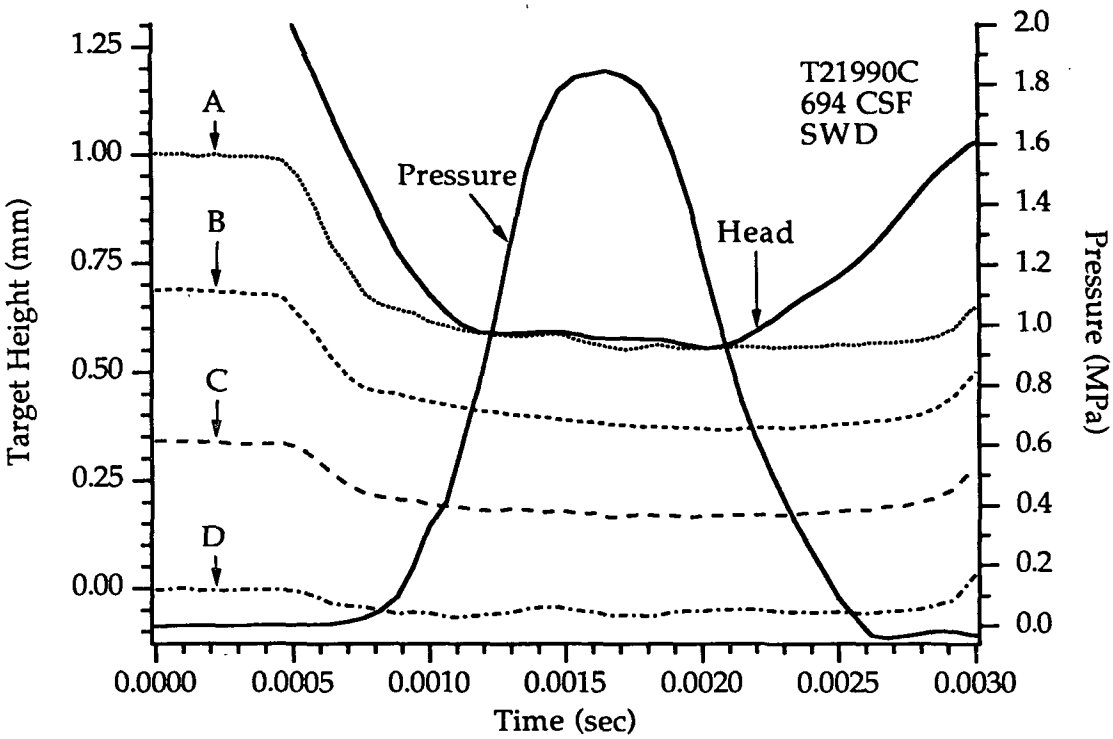

Figure 87. Target displacements for handsheet T21990C.

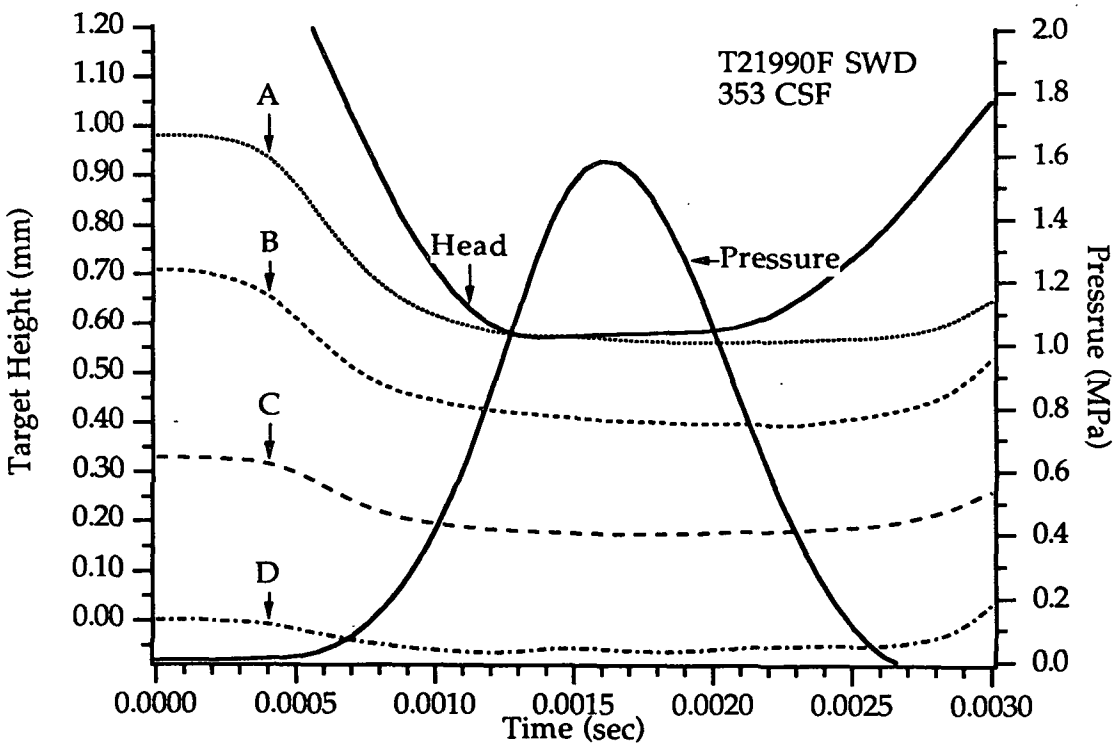

Figure 88. Target displacements for handsheet T21990F.

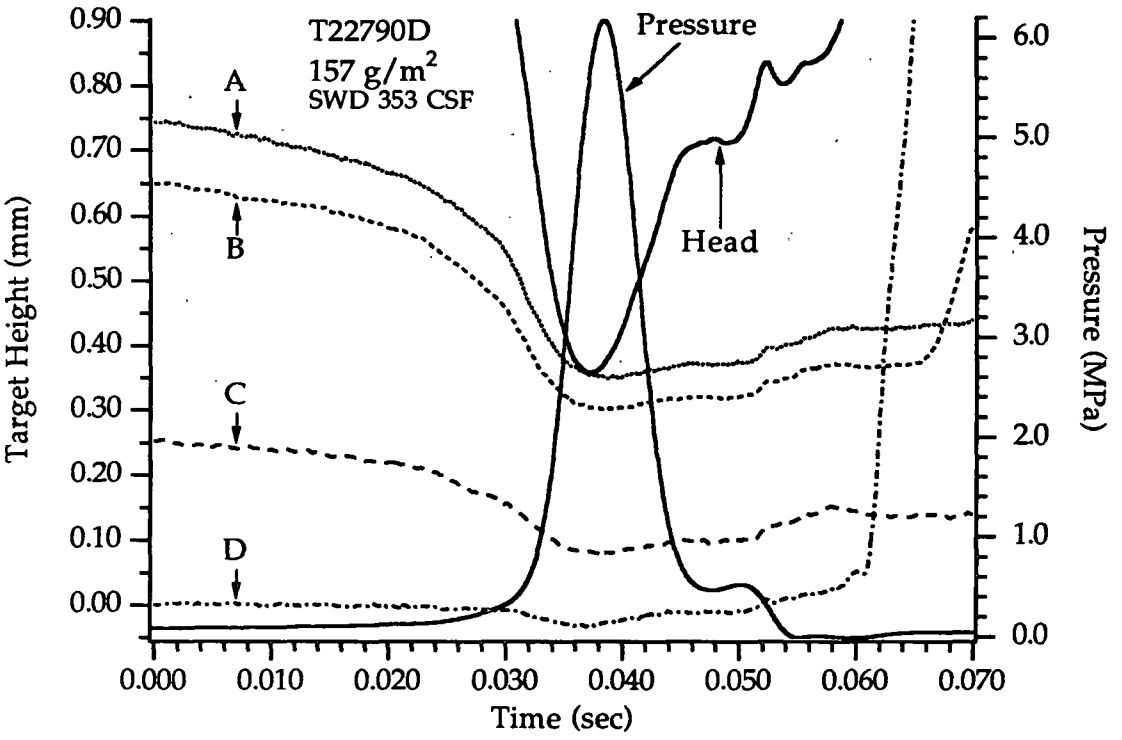

Figure 89. Target displacements for handsheet T22790D.

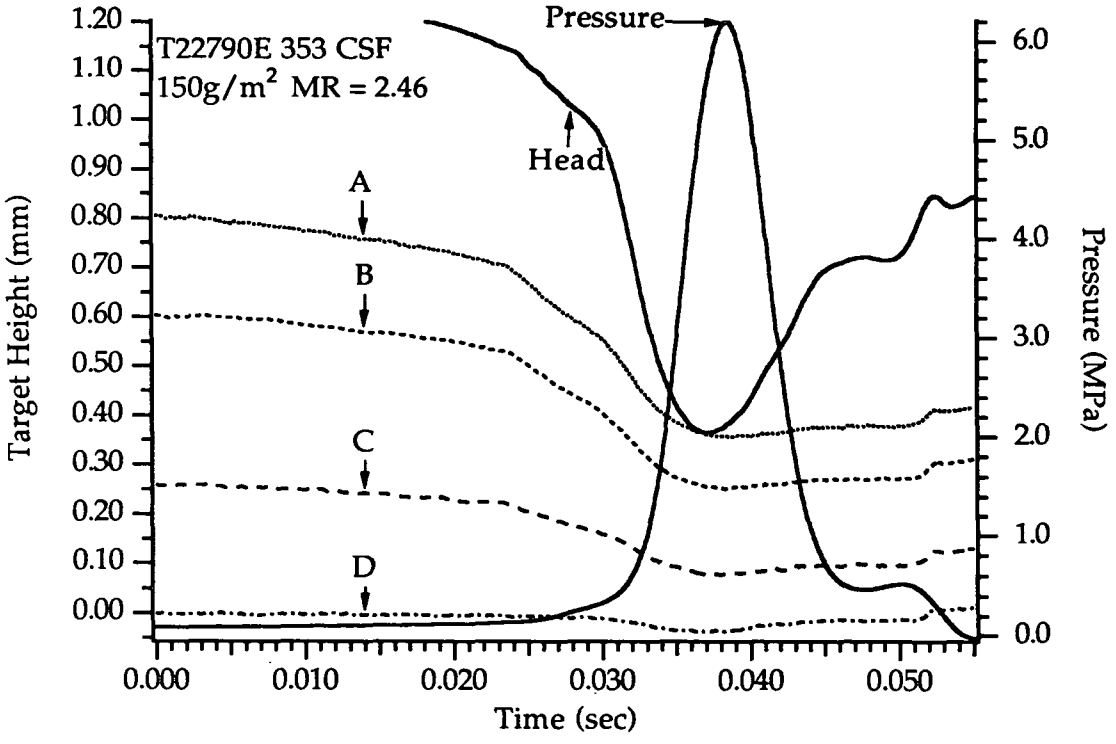

Figure 90. Target displacements for handsheet T22790E.

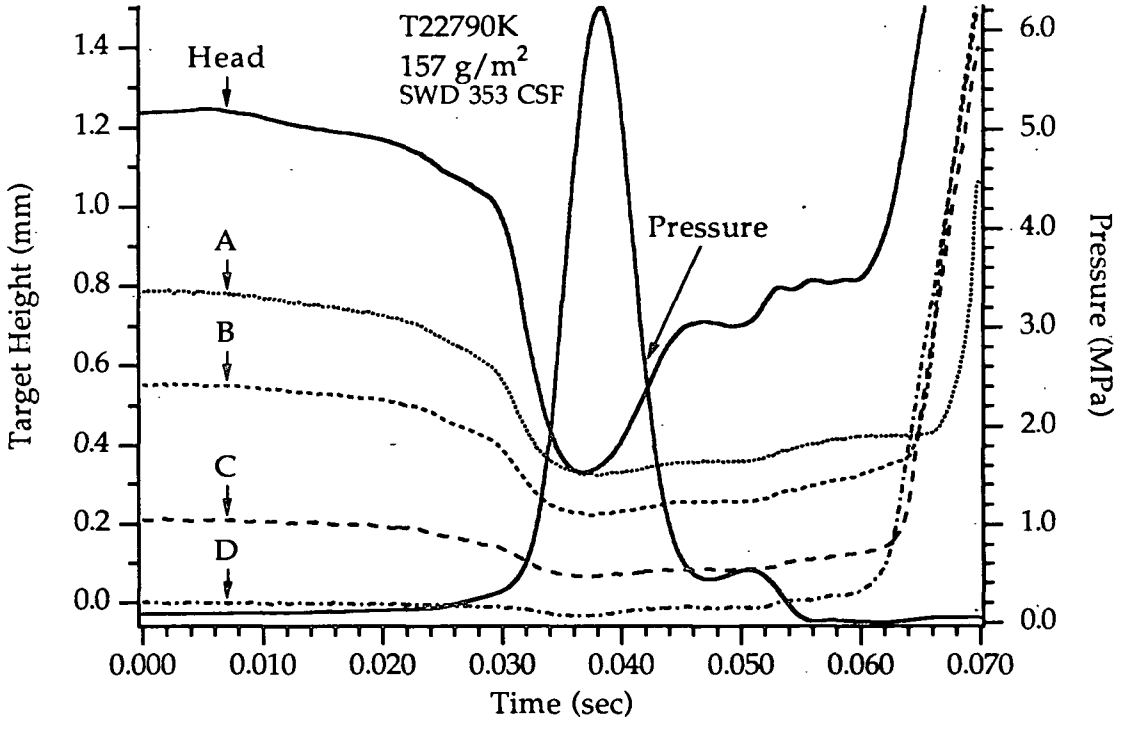

Figure 91. Target displacements for handsheet T22790K.

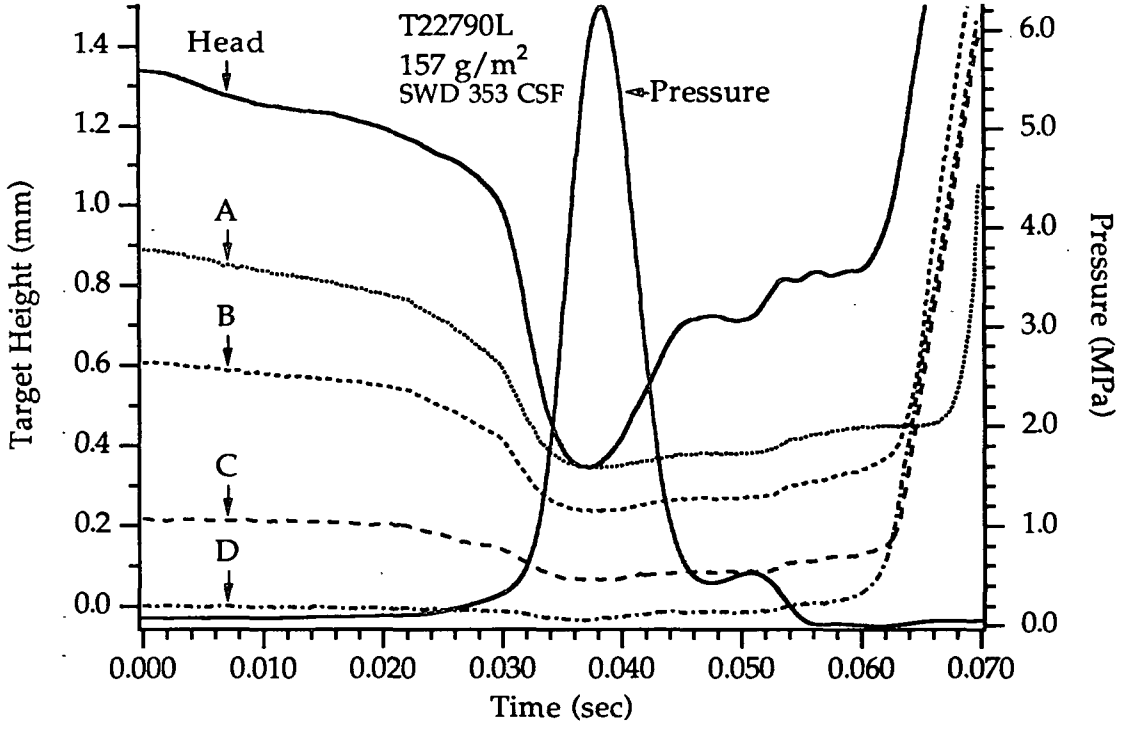

Figure 92. Target displacements for handsheet T22790L.

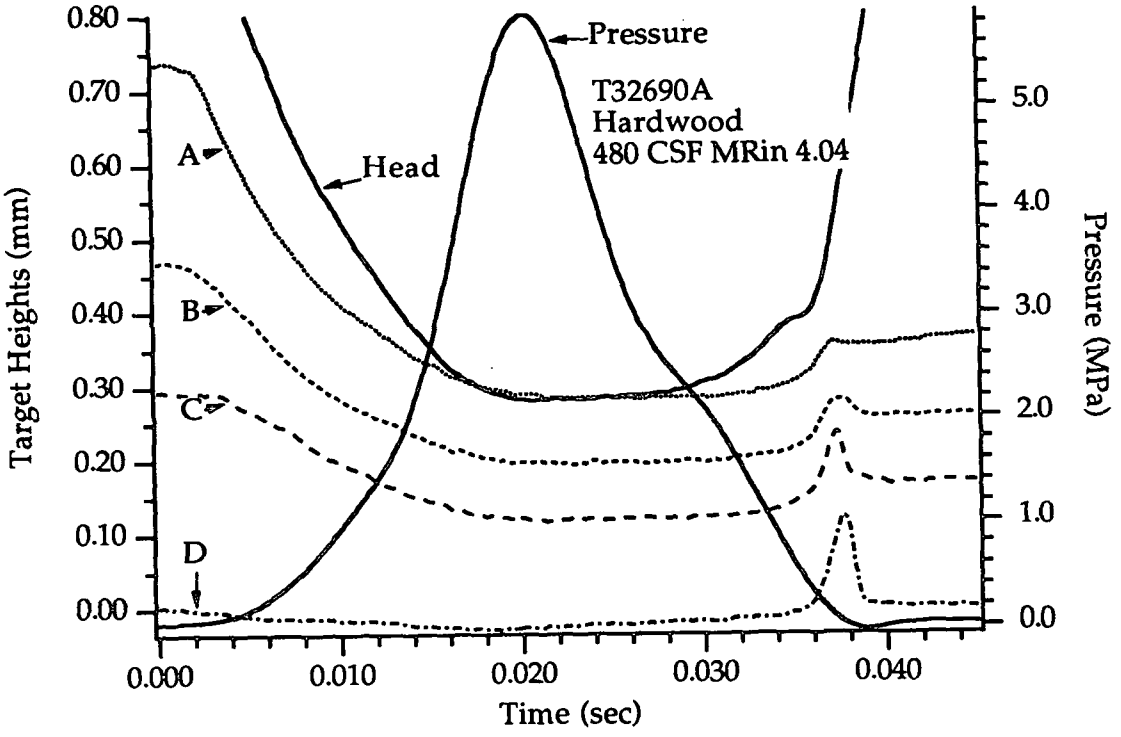

Figure 93. Target displacements for handsheet T32690A.

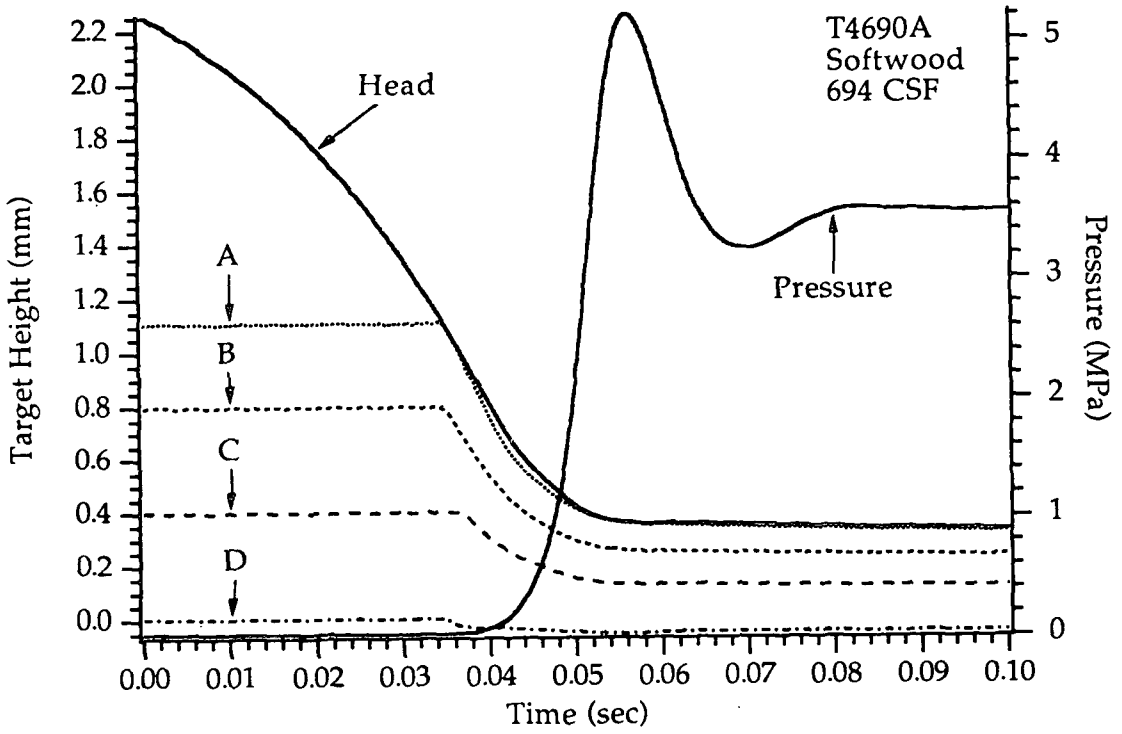

Figure 94. Target displacements for handsheet T4690A.

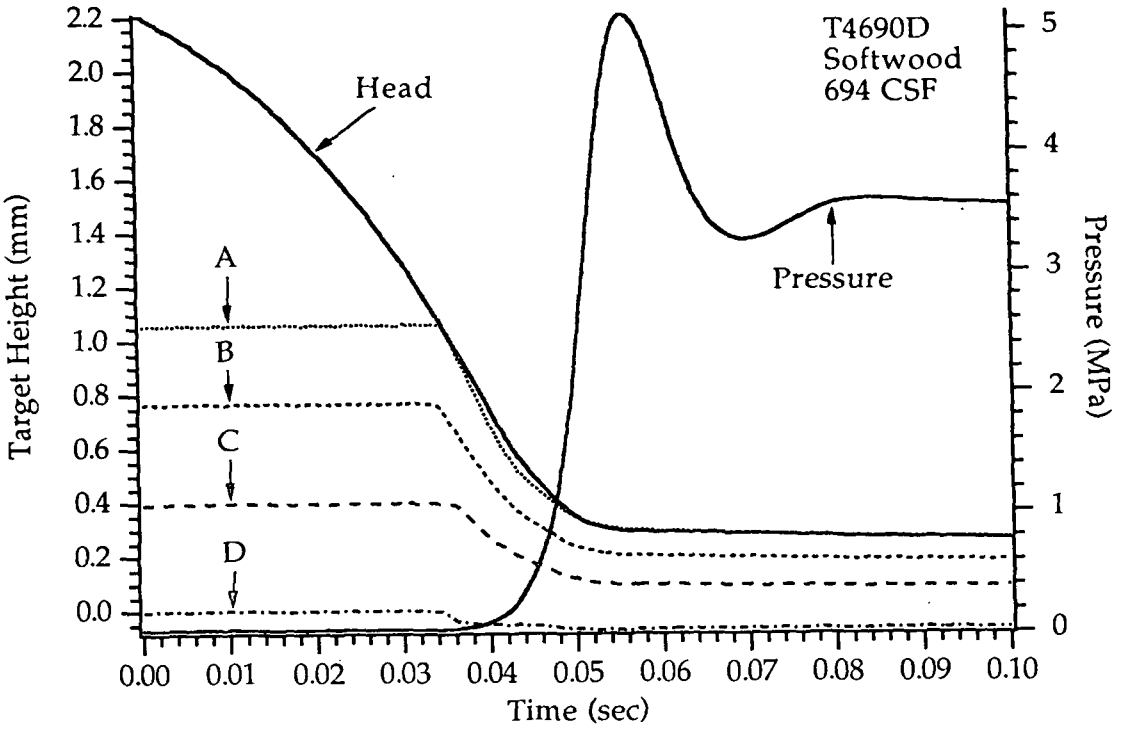

Figure 95. Target displacements for handsheet T4690D.

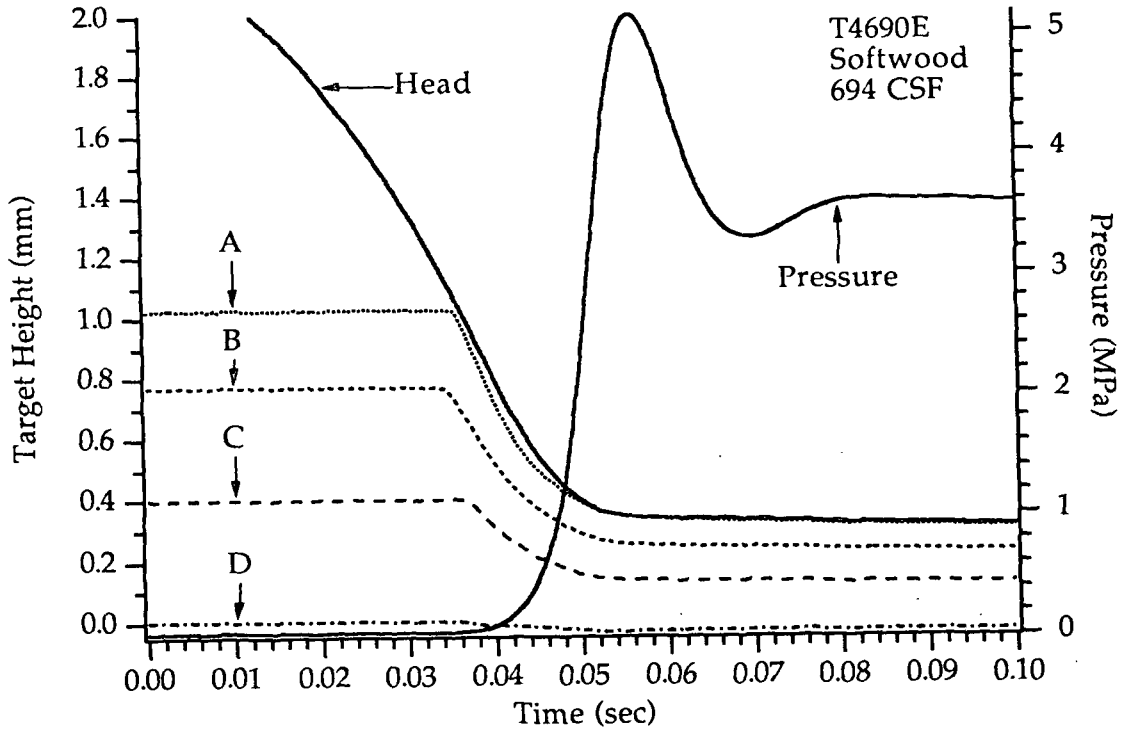

Figure 96. Target displacements for handsheet T4690E.

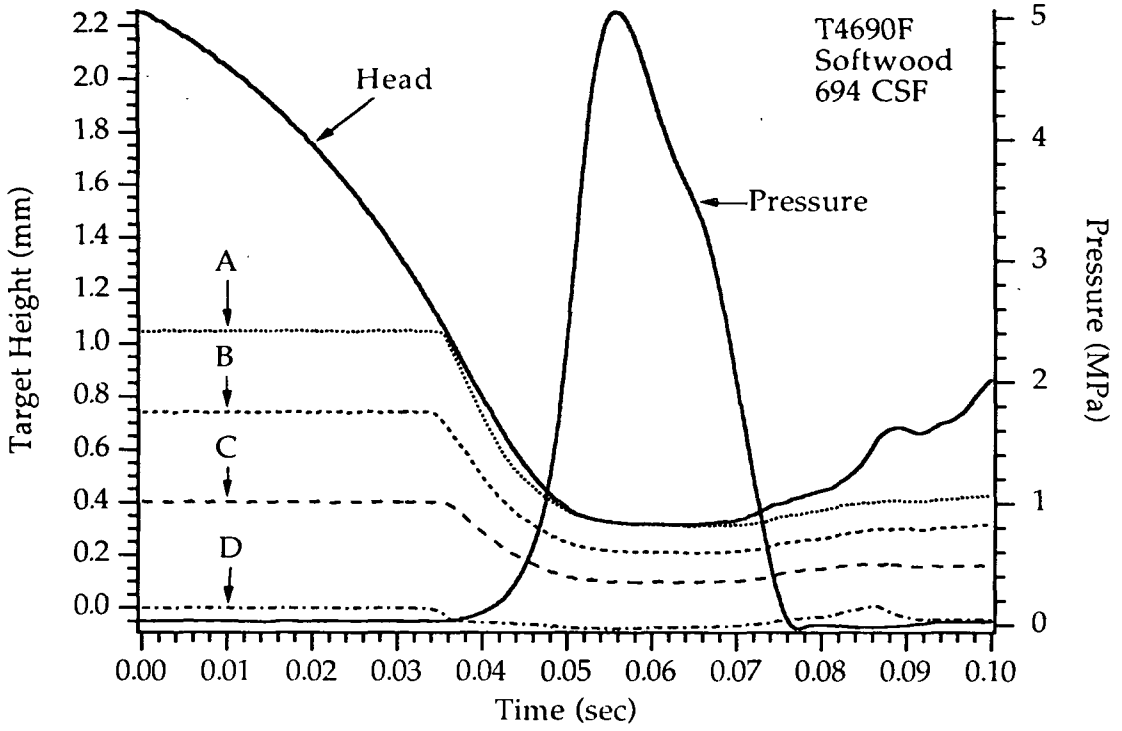

Figure 97. Target displacements for handsheet T4690F.

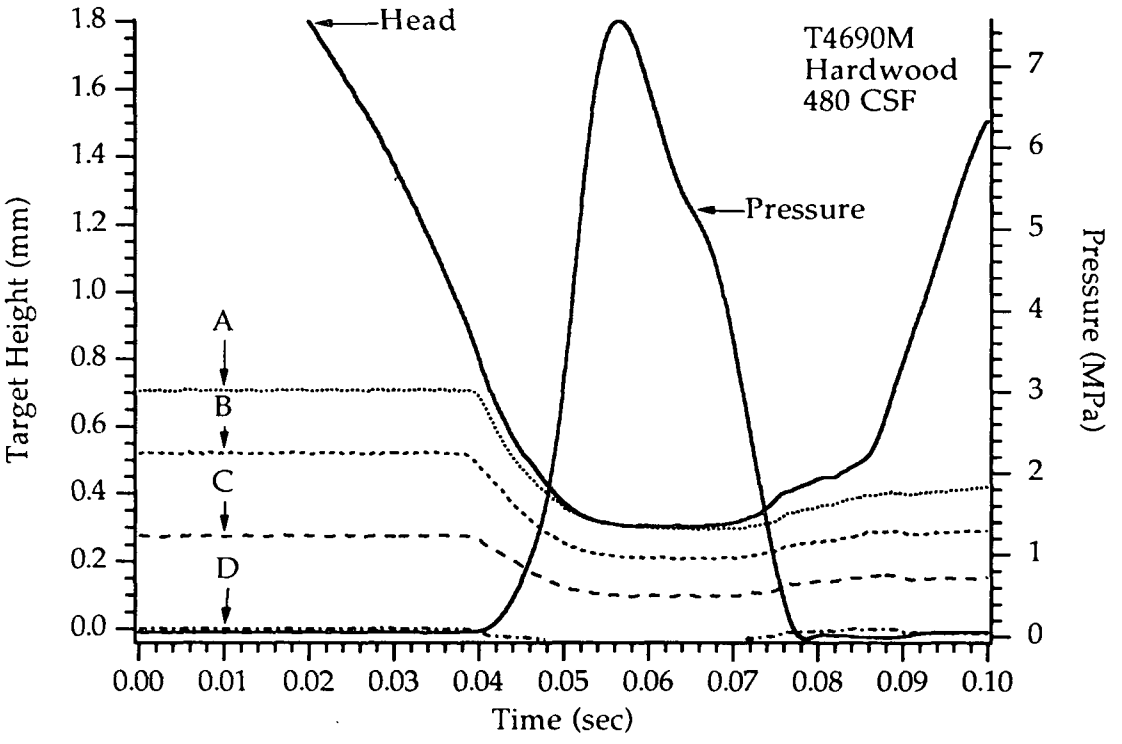

Figure 98. Target displacements for handsheet T4690M.

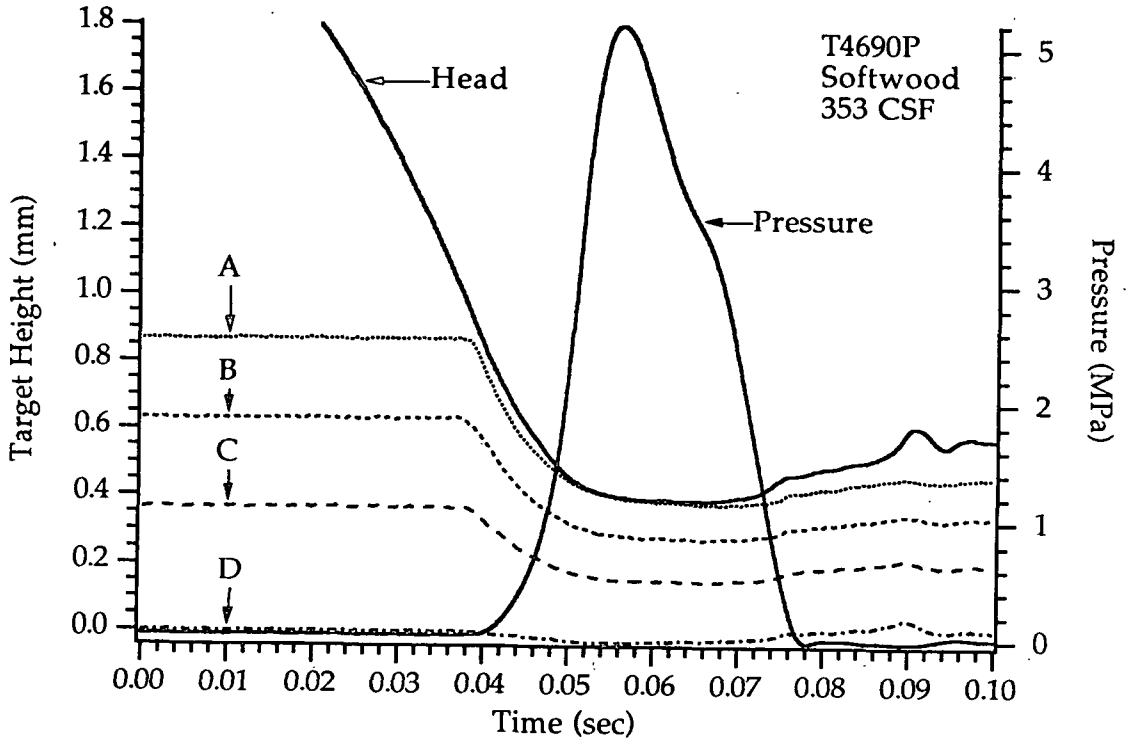

Figure 99. Target displacements for handsheet T4690P.

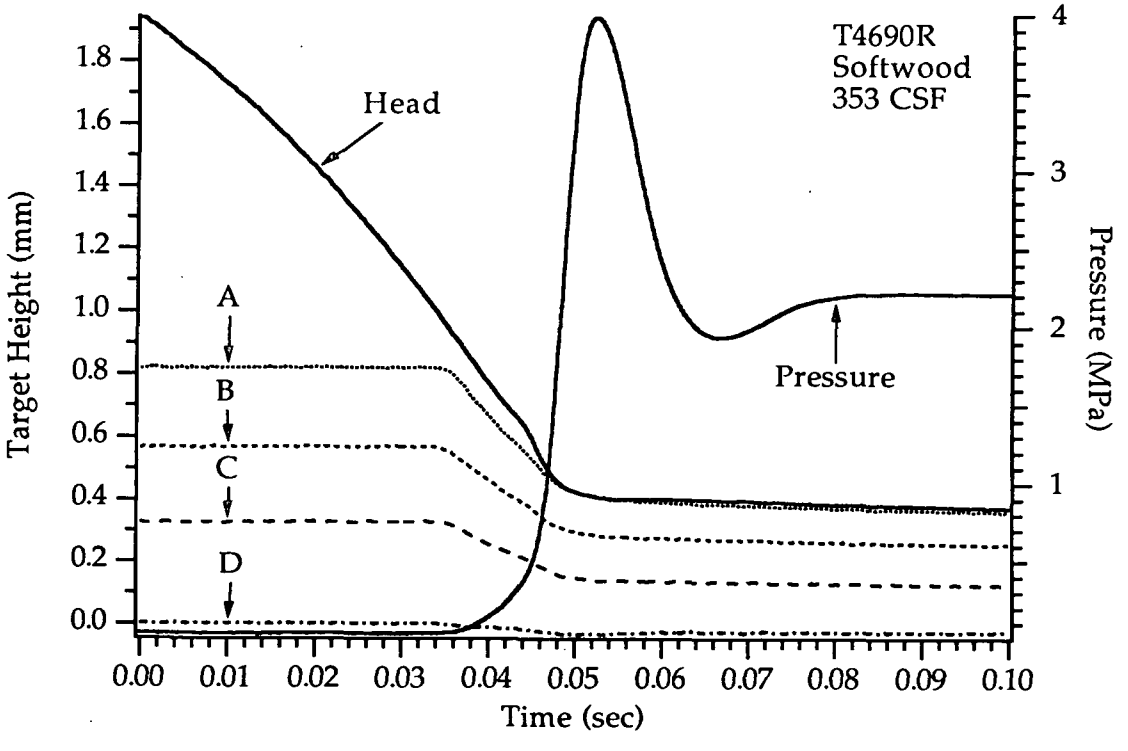

Figure 100. Target displacements for handsheet T4690R.

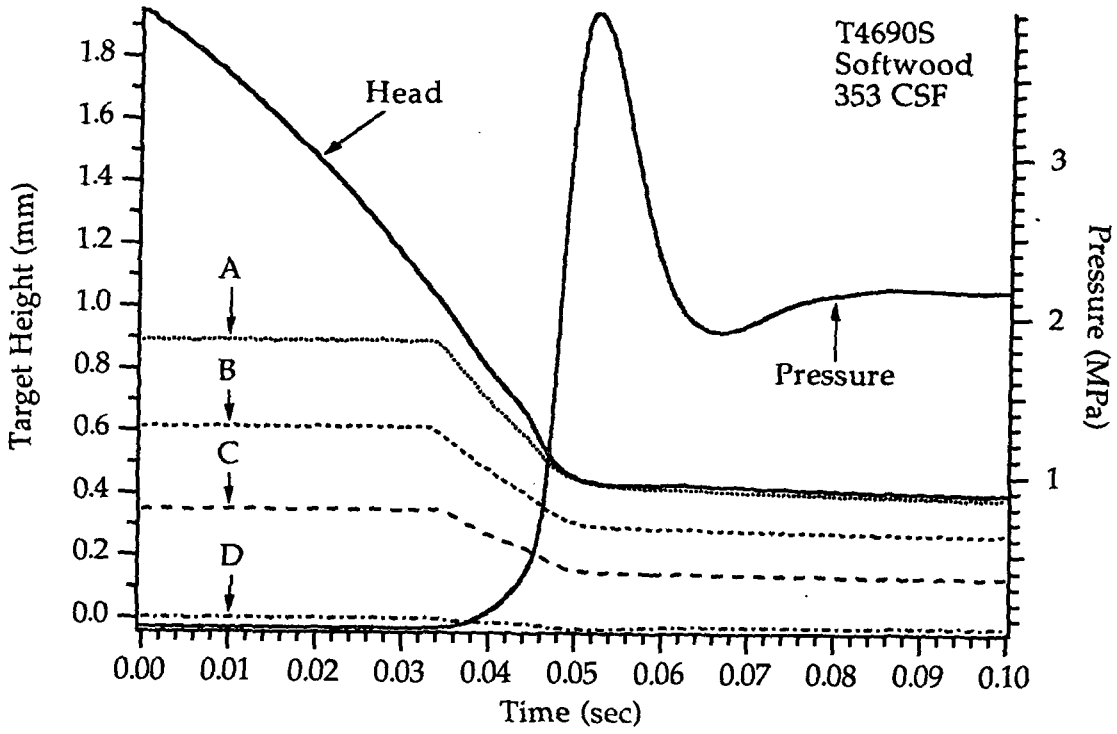

Figure 101. Target displacements for handsheet T4690S.

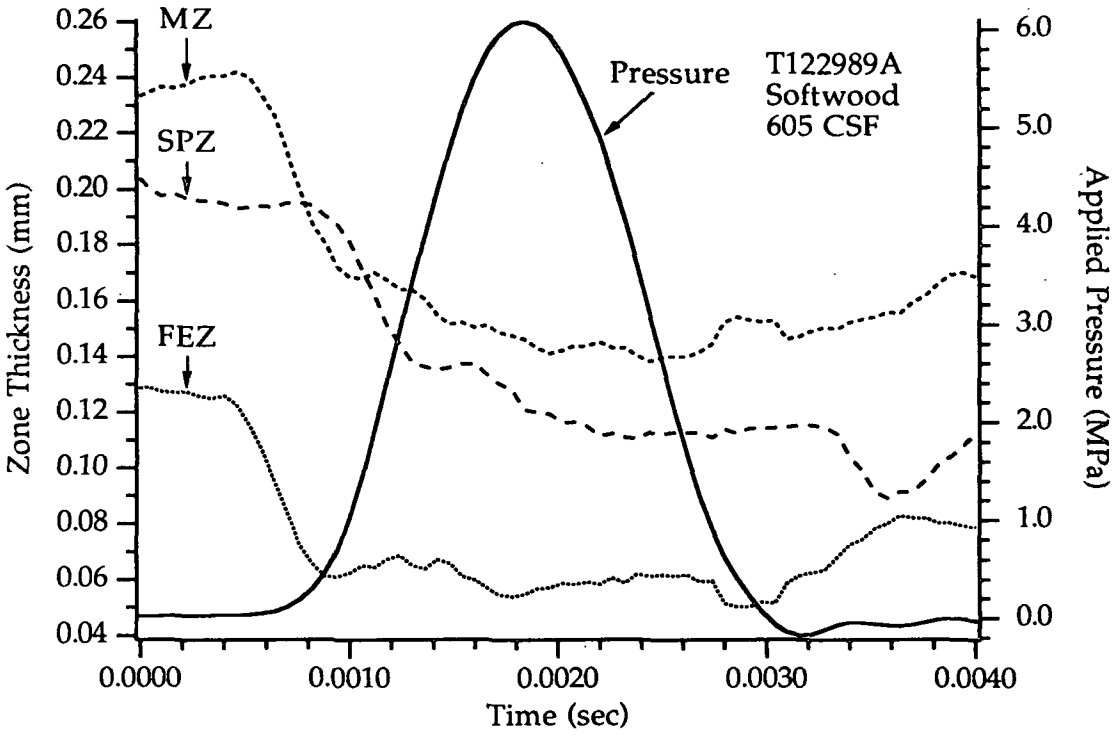

Figure 102. Zonal thickness change in handsheet T122989A.

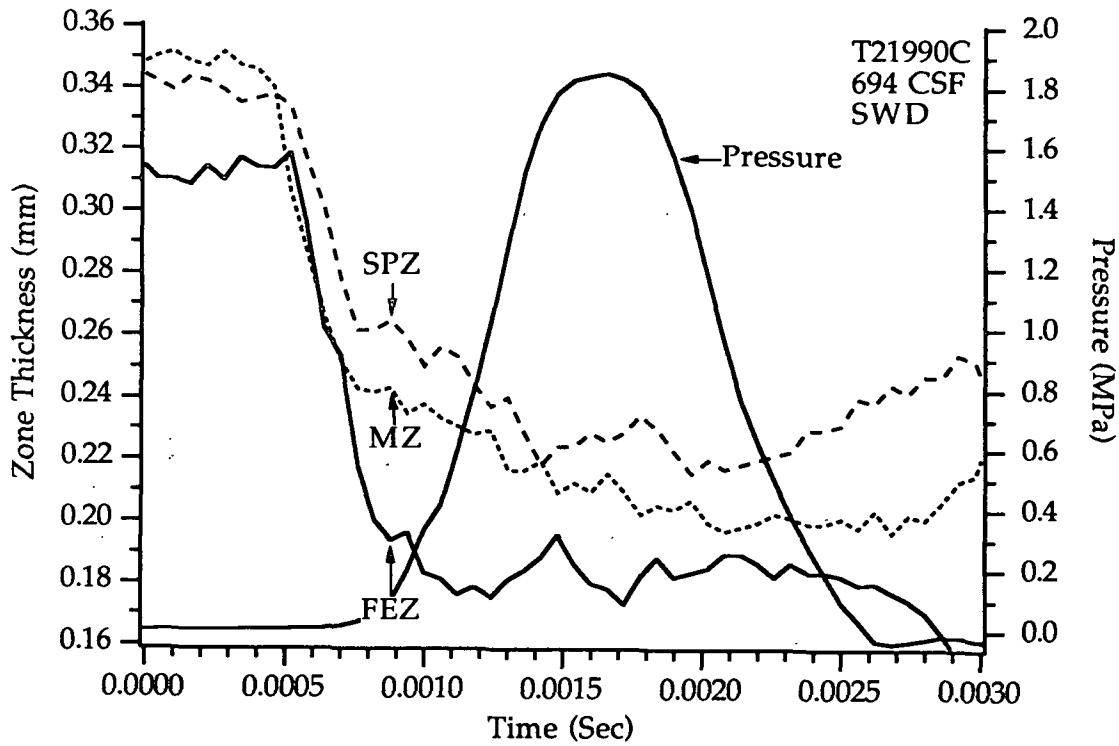

Figure 103. Zonal thickness change in handsheet T21990C.

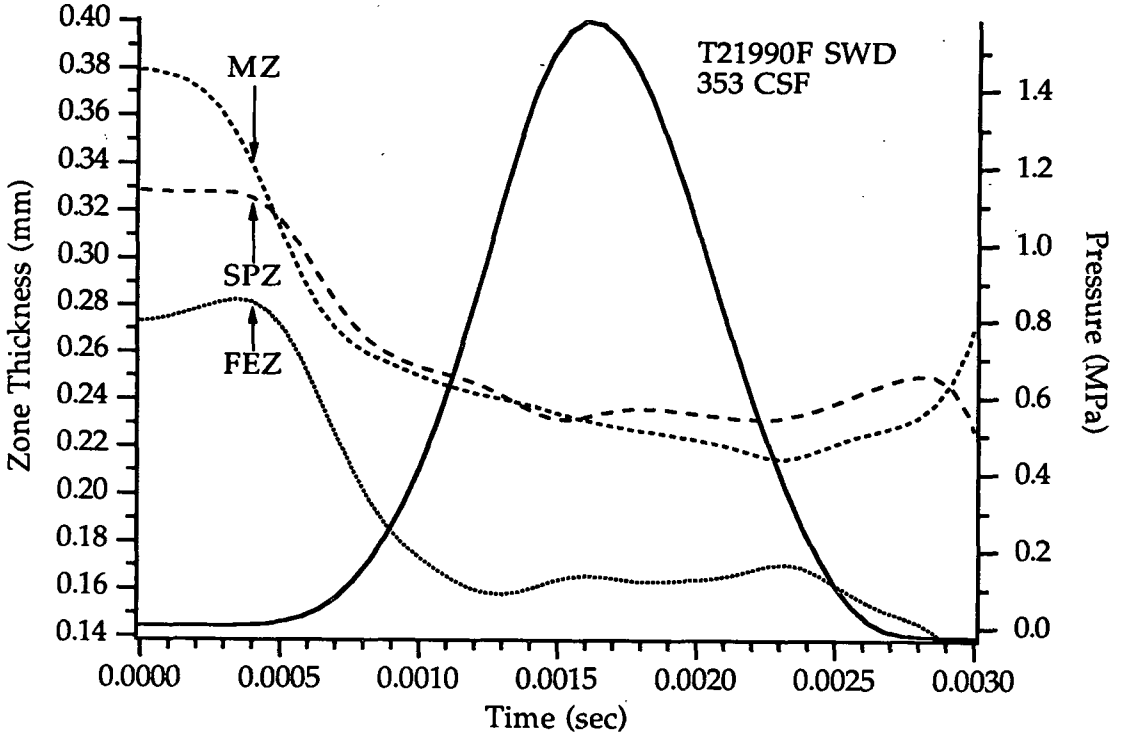

Figure 104. Zonal thickness change in handsheet T21990F.

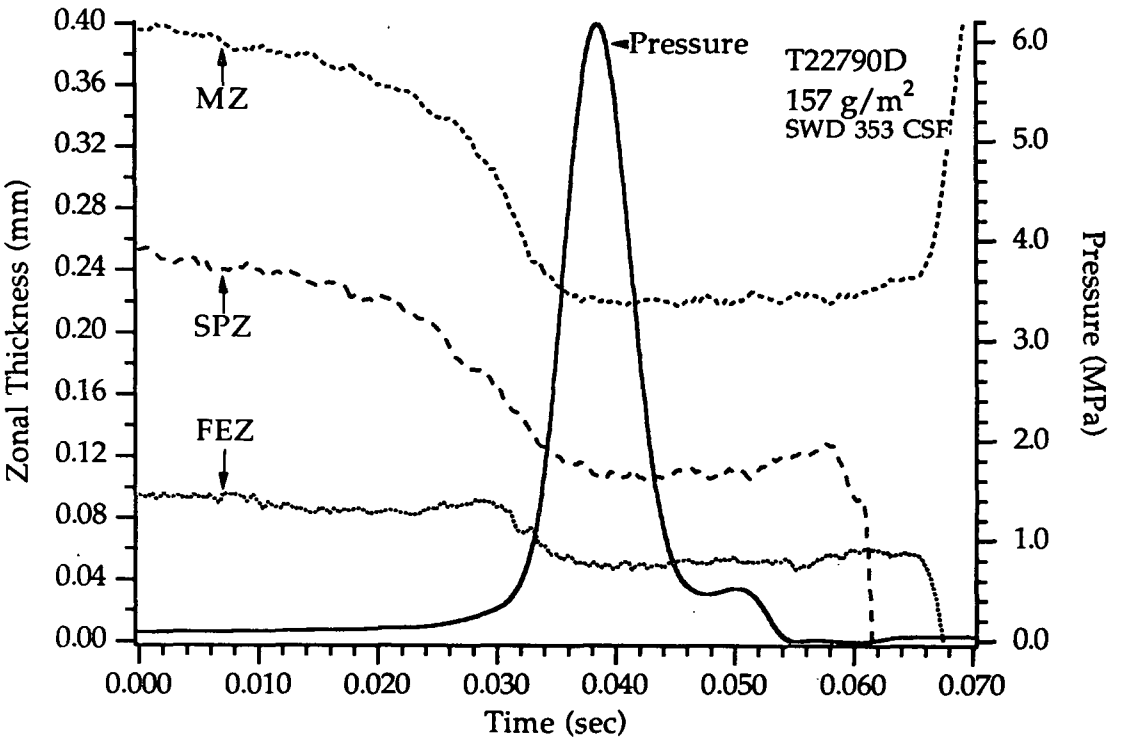

Figure 105. Zonal thickness change in handsheet T22790D.

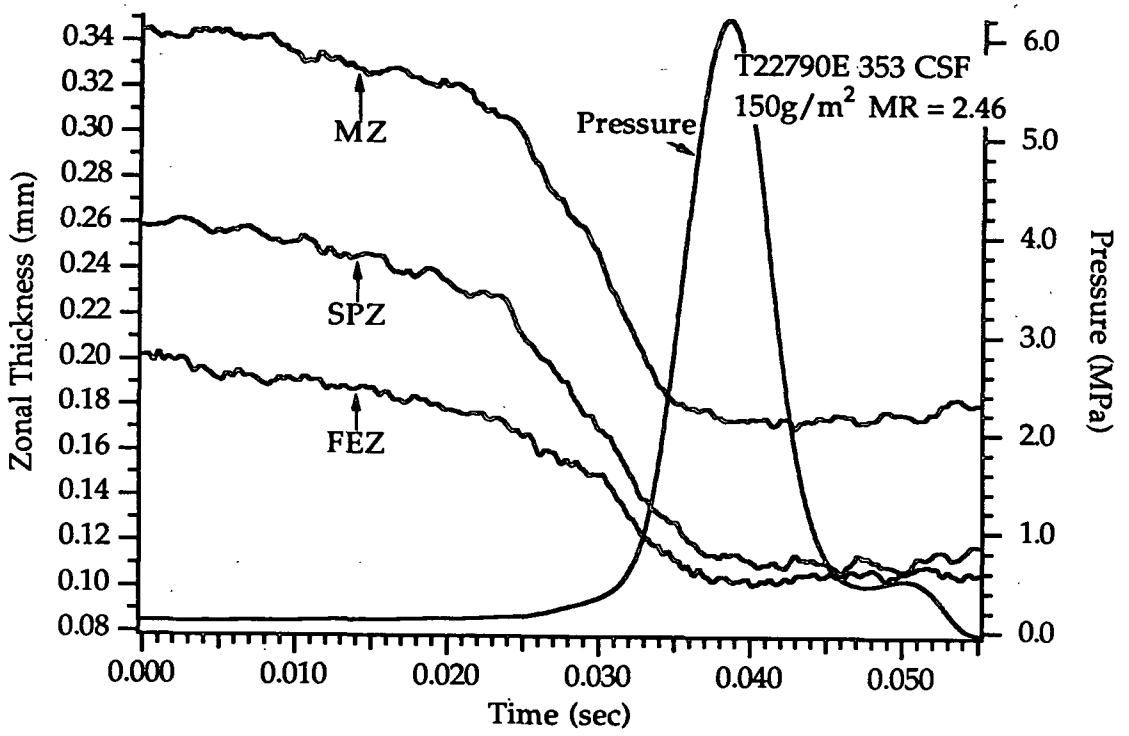

Figure 106. Zonal thickness change in handsheet T22790E.

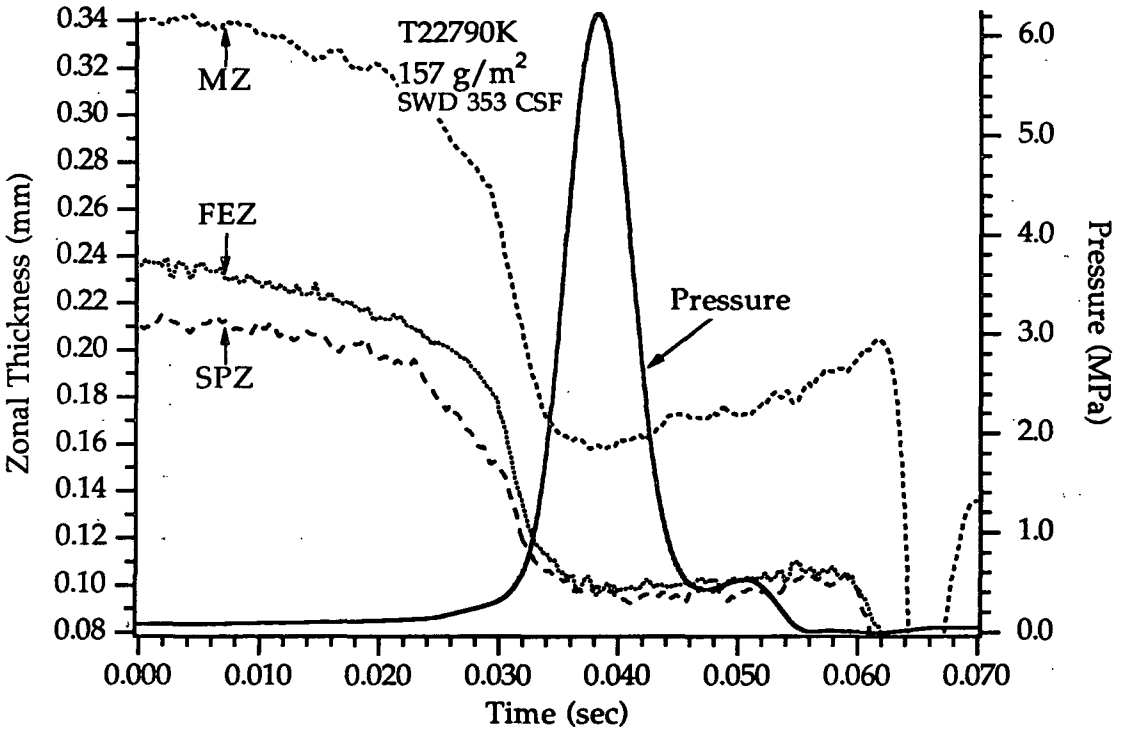

Figure 107. Zonal thickness change in handsheet T22790K.

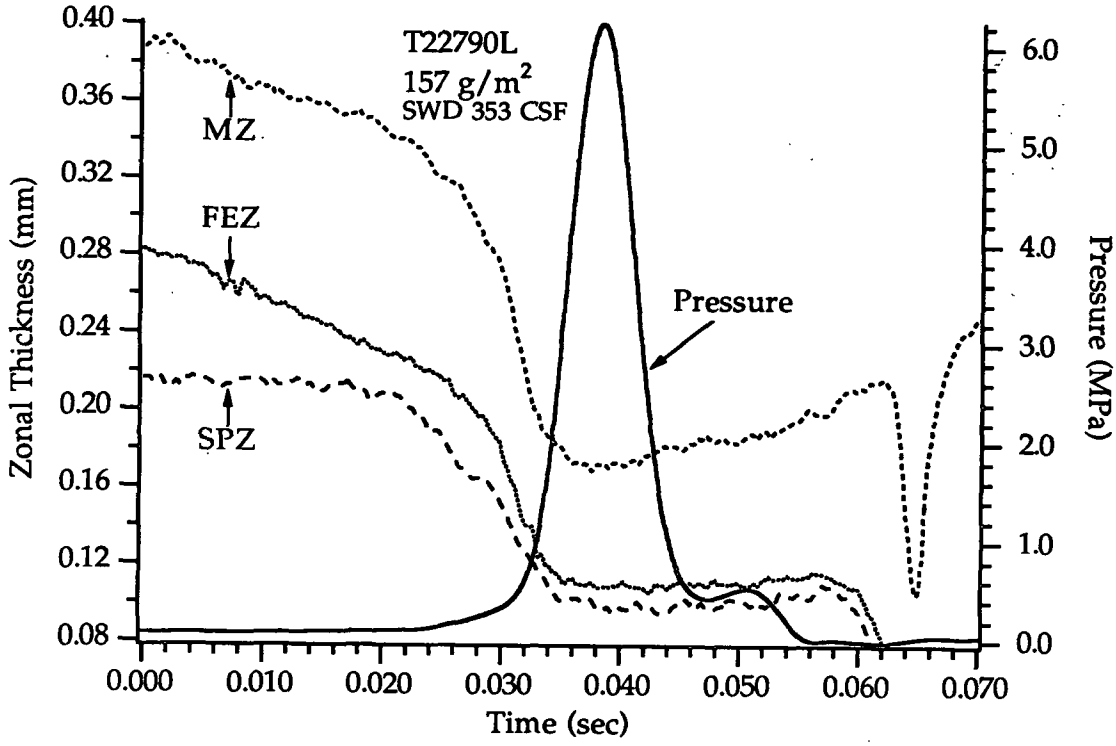

Figure 108. Zonal thickness change in handsheet T22790L.

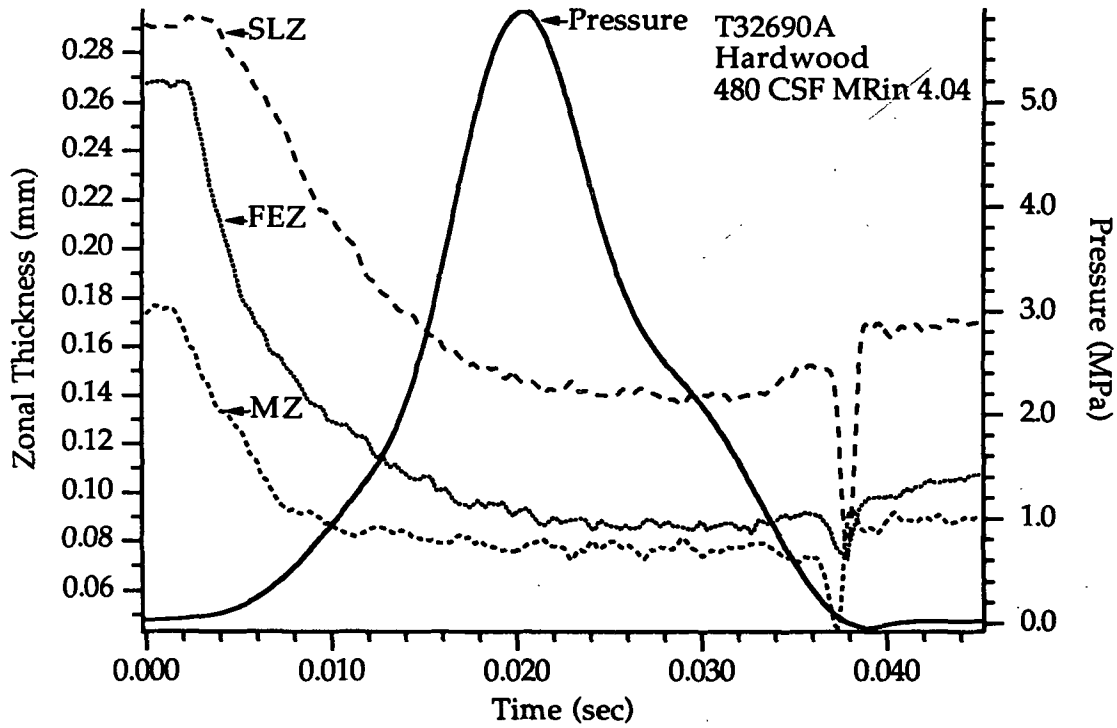

Figure 109. Zonal thickness change in handsheet T32690A.

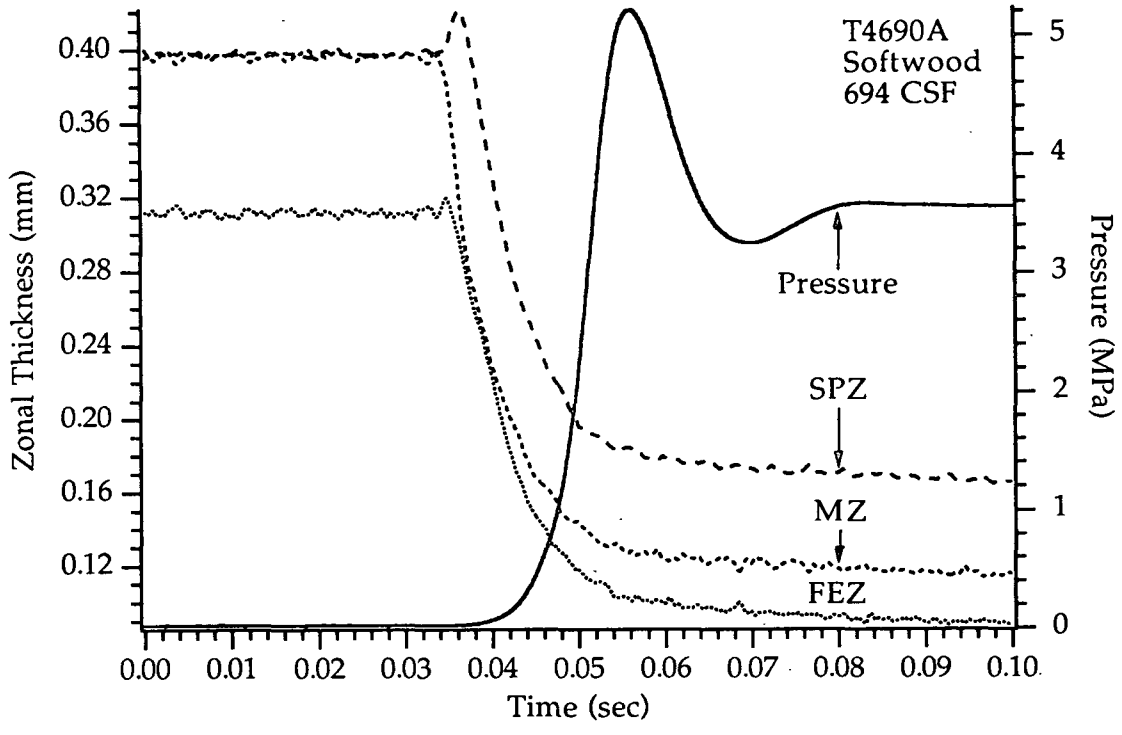

Figure 110. Zonal thickness change in handsheet T4690A.

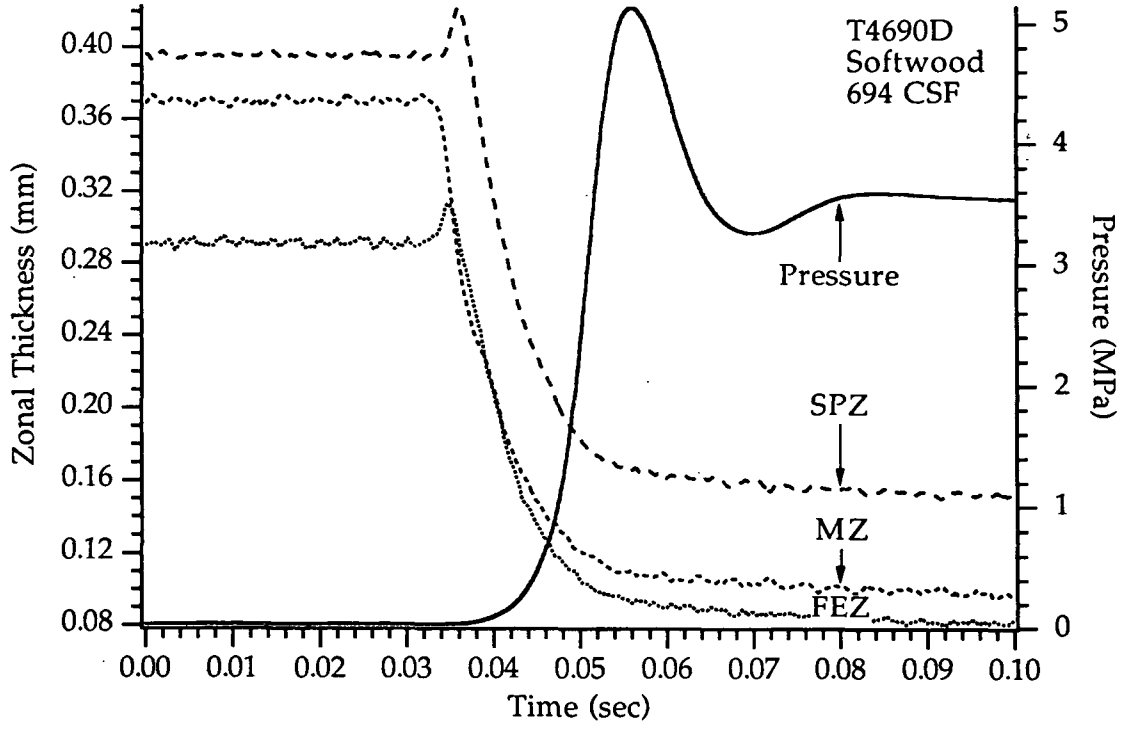

Figure 111. Zonal thickness change in handsheet T4690D.

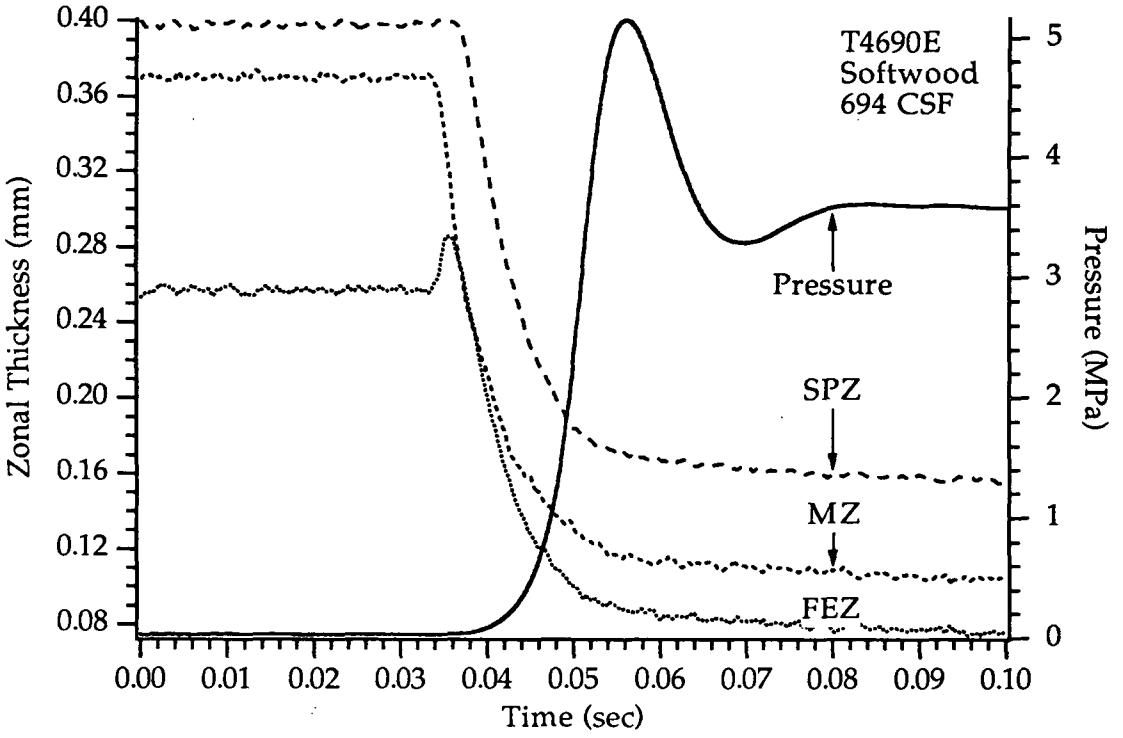

Figure 112. Zonal thickness change in handsheet T4690E.

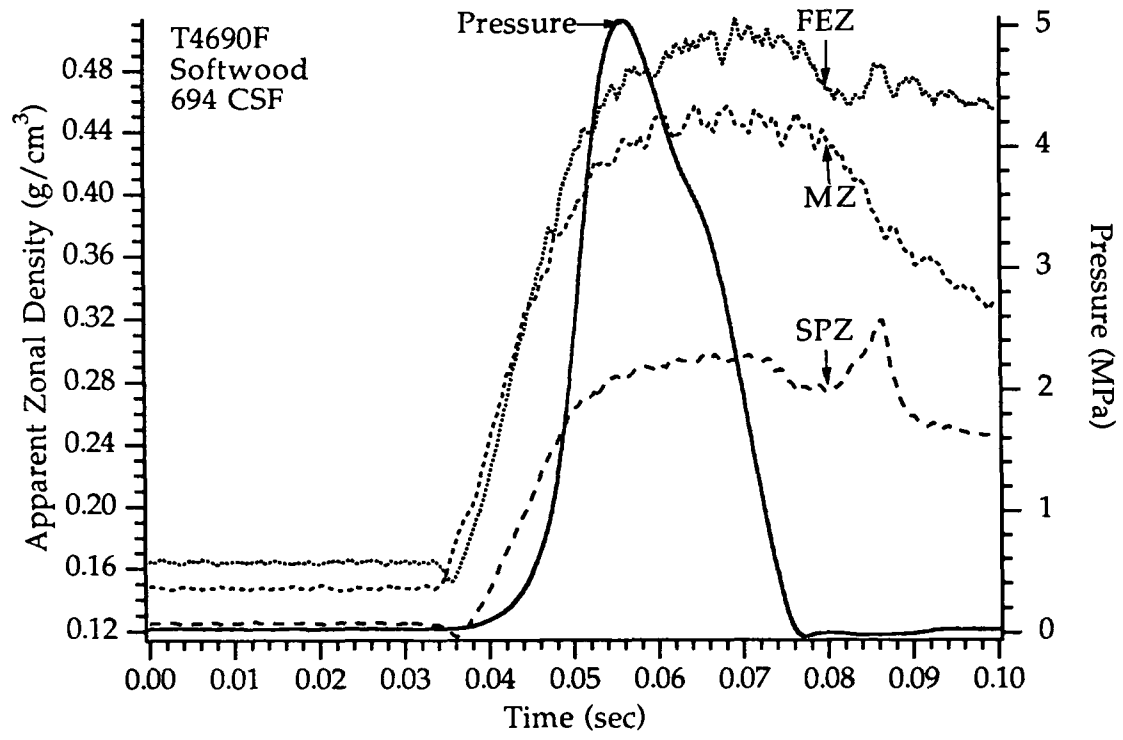

Figure 113. Zonal thickness change in handsheet T4690F.

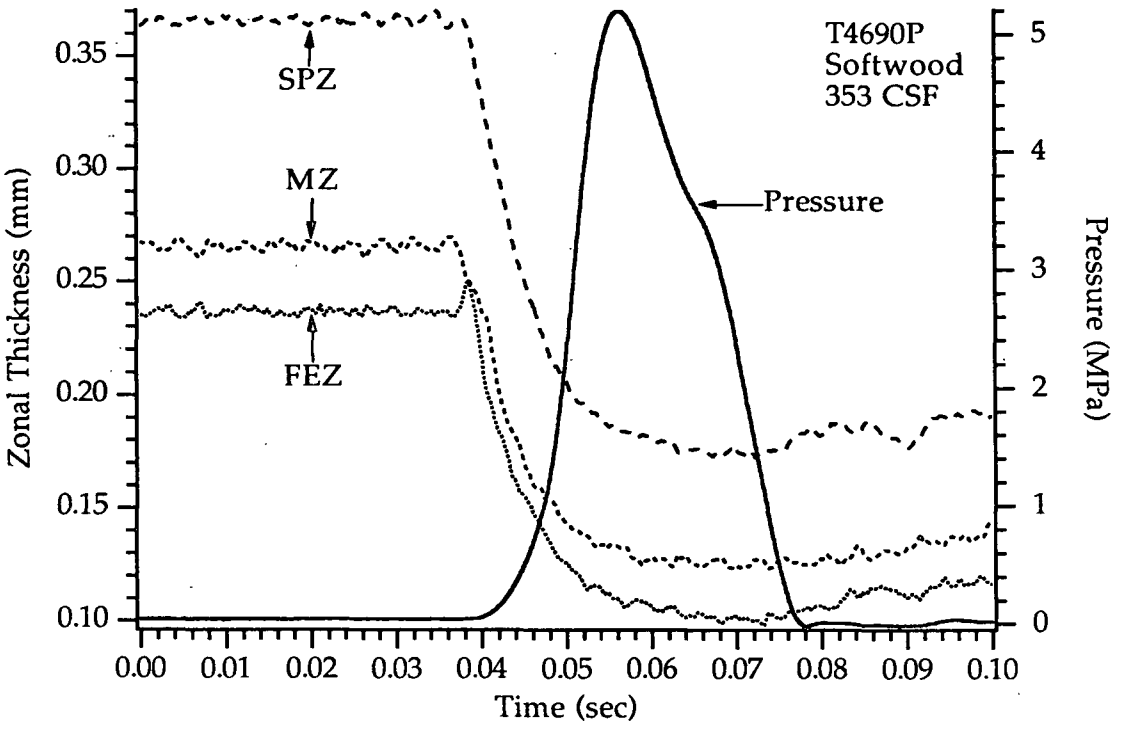

Figure 114. Zonal thickness change in handsheet T4690M.

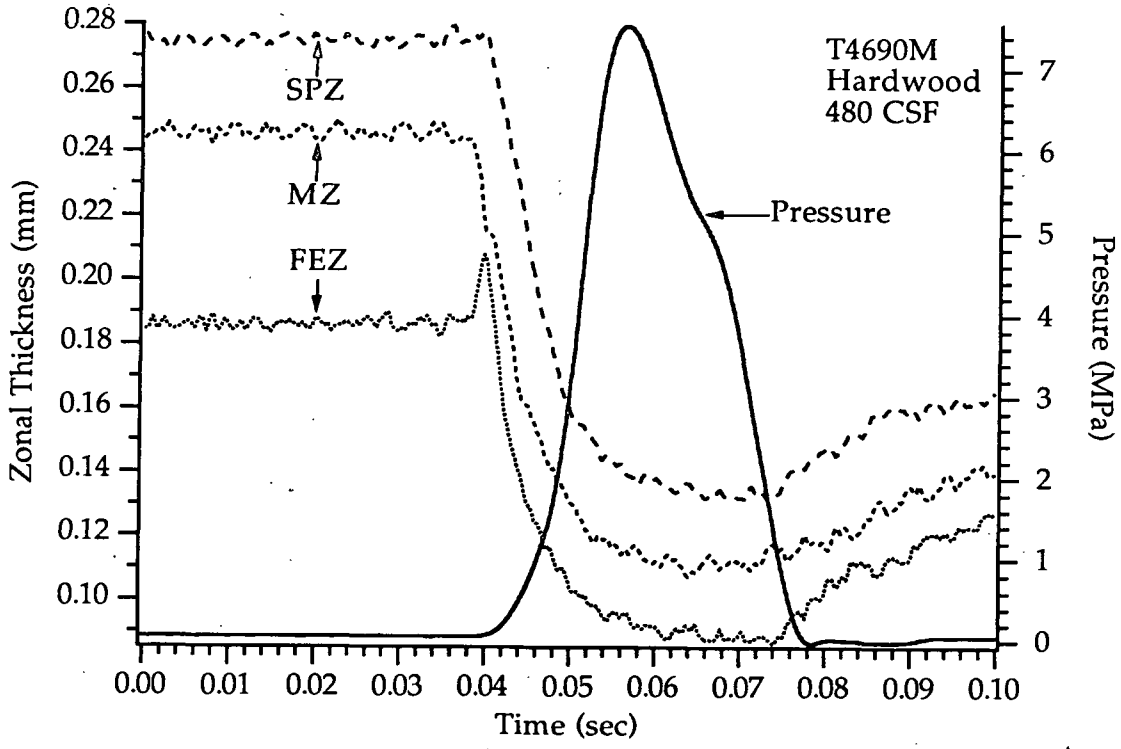

Figure 115. Zonal thickness change in handsheet T4690P.

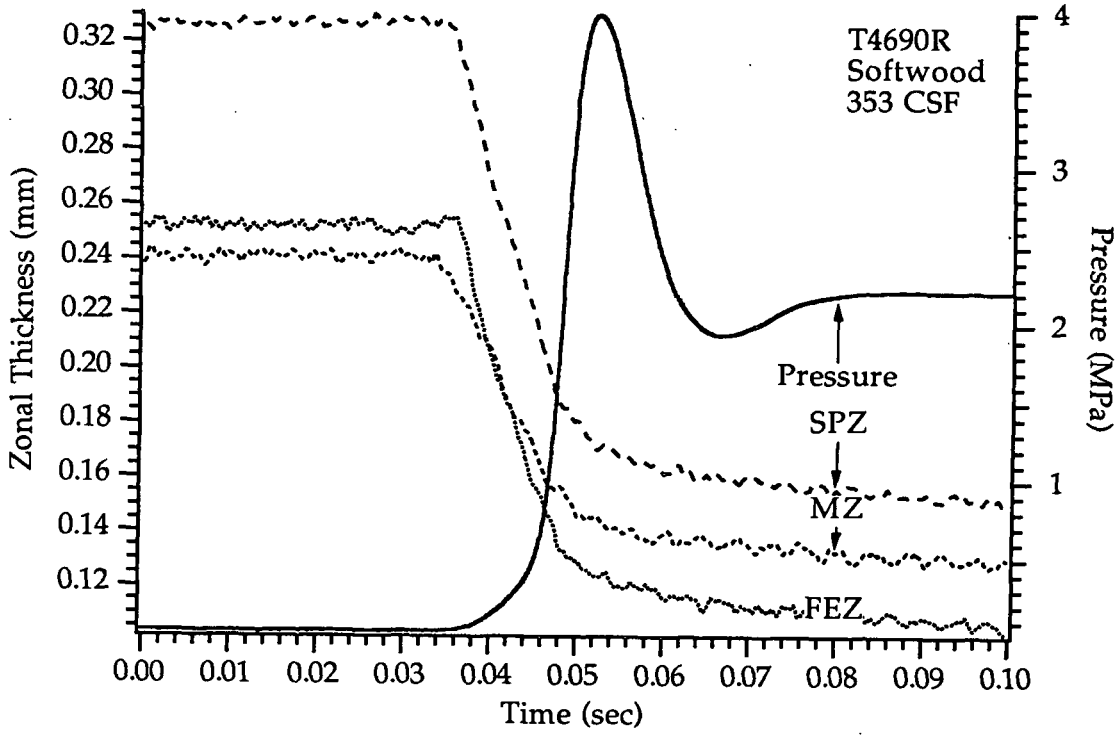

Figure 116. Zonal thickness change in handsheet T4690R.

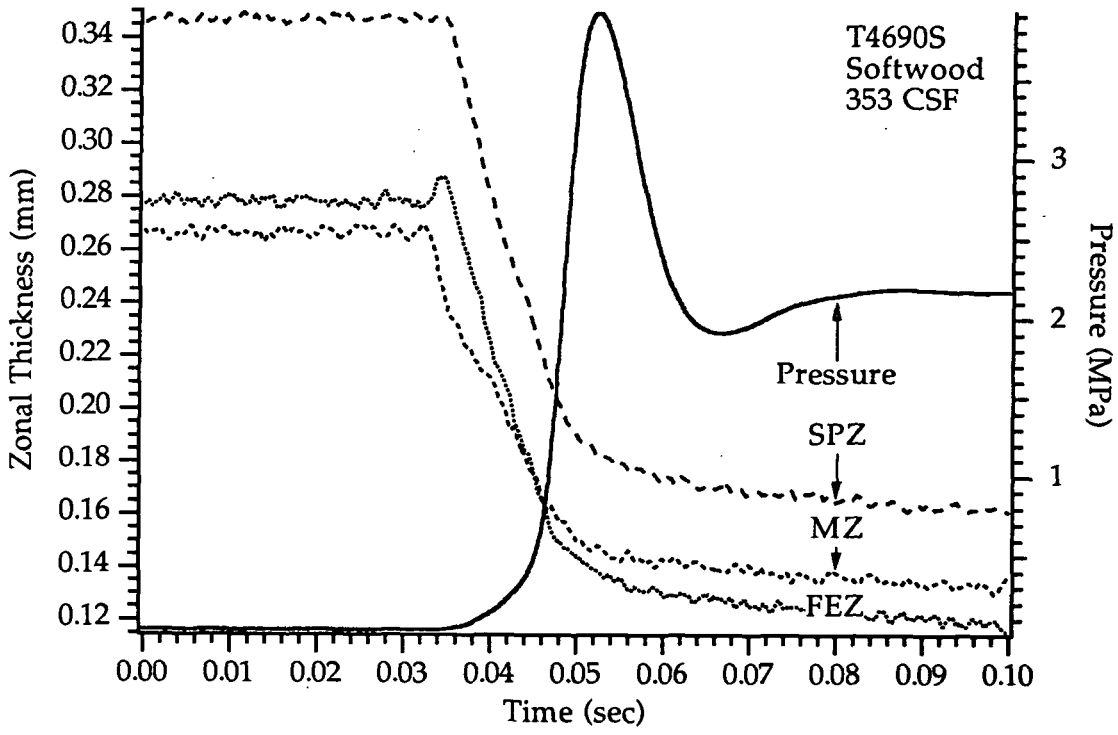

Figure 117. Zonal thickness change in handsheet T4690S.

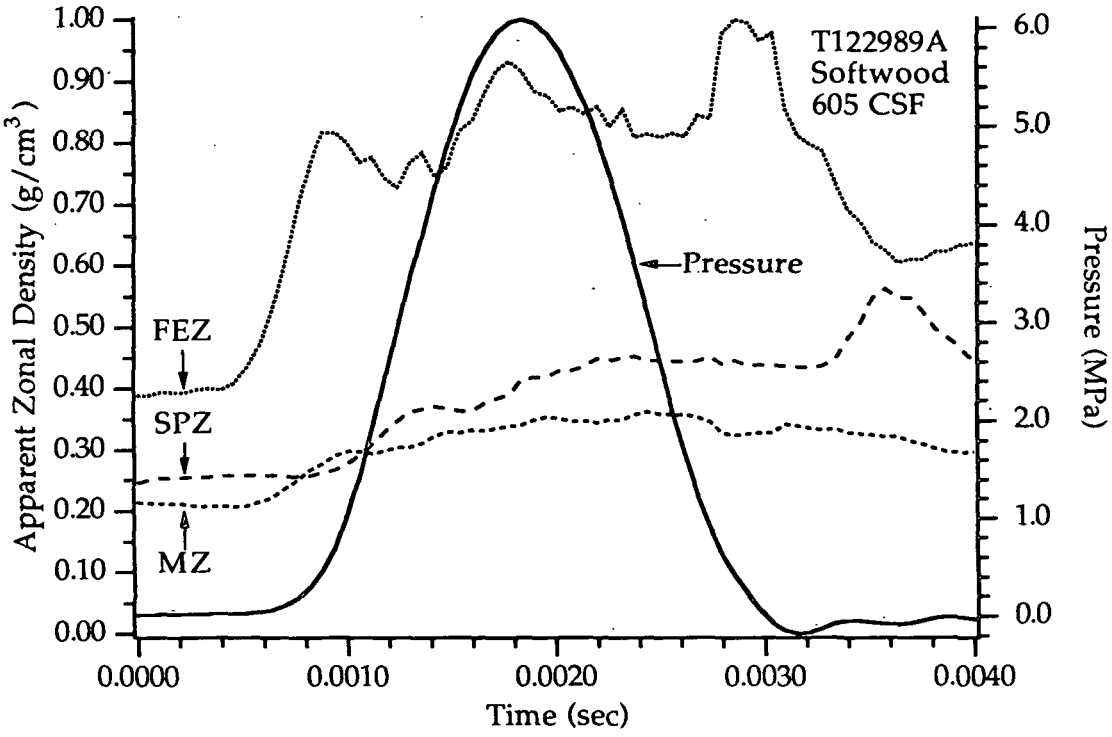

Figure 118. Zonal density-time histories in handsheet T122989A.

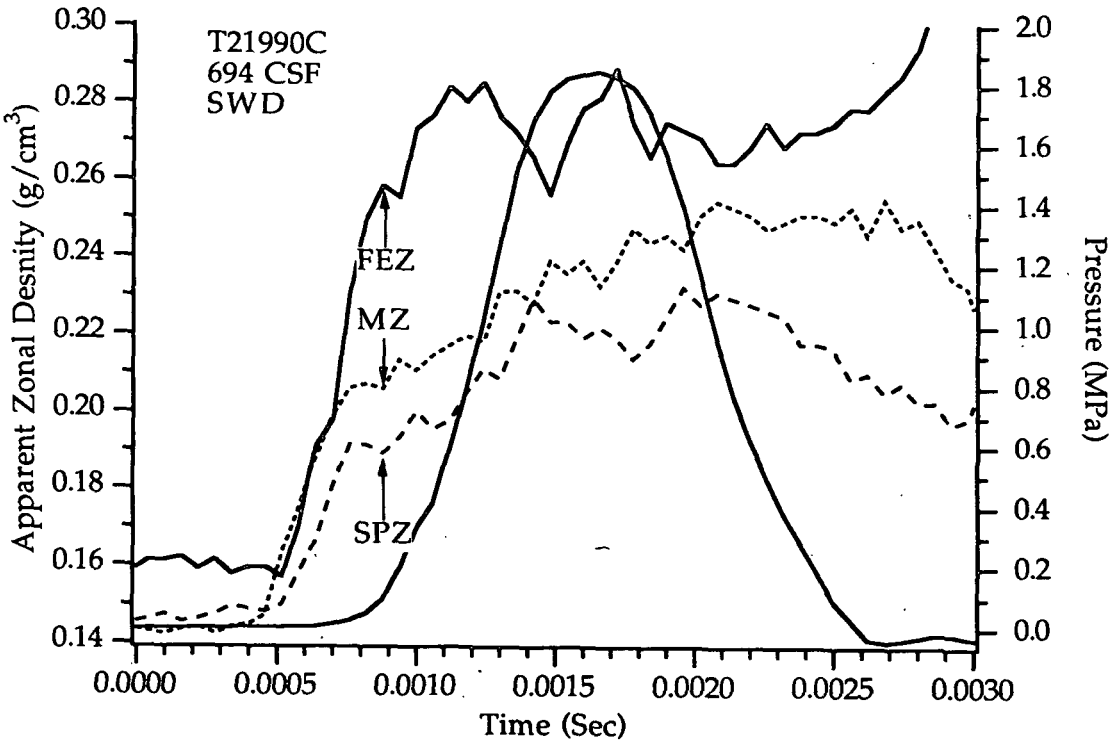

Figure 119. Zonal density-time histories in handsheet T21990C.

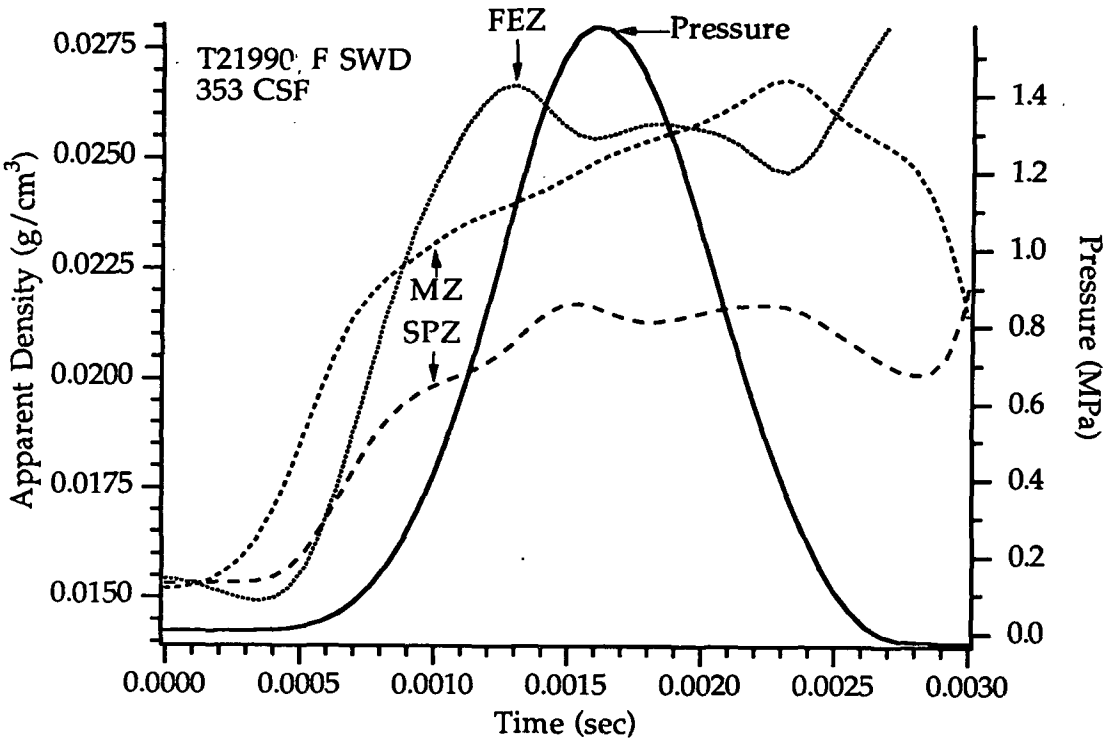

Figure 120. Zonal density-time histories in handsheet T21990F.

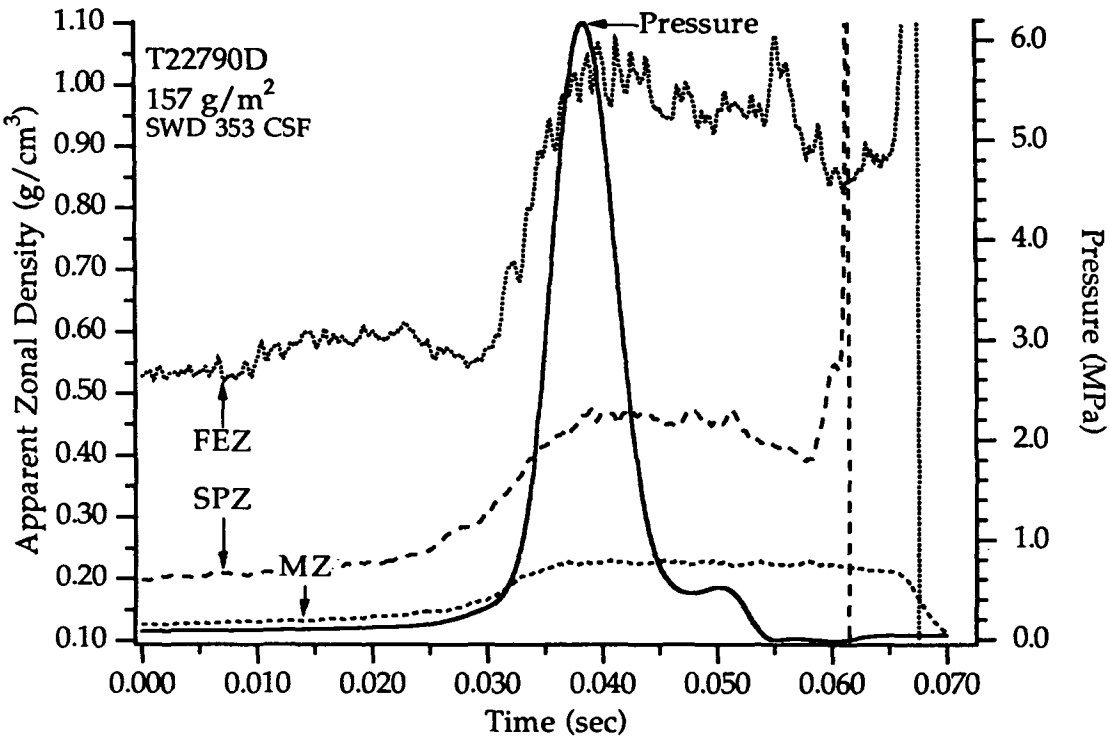

Figure 121. Zonal density-time histories in handsheet T22790D.

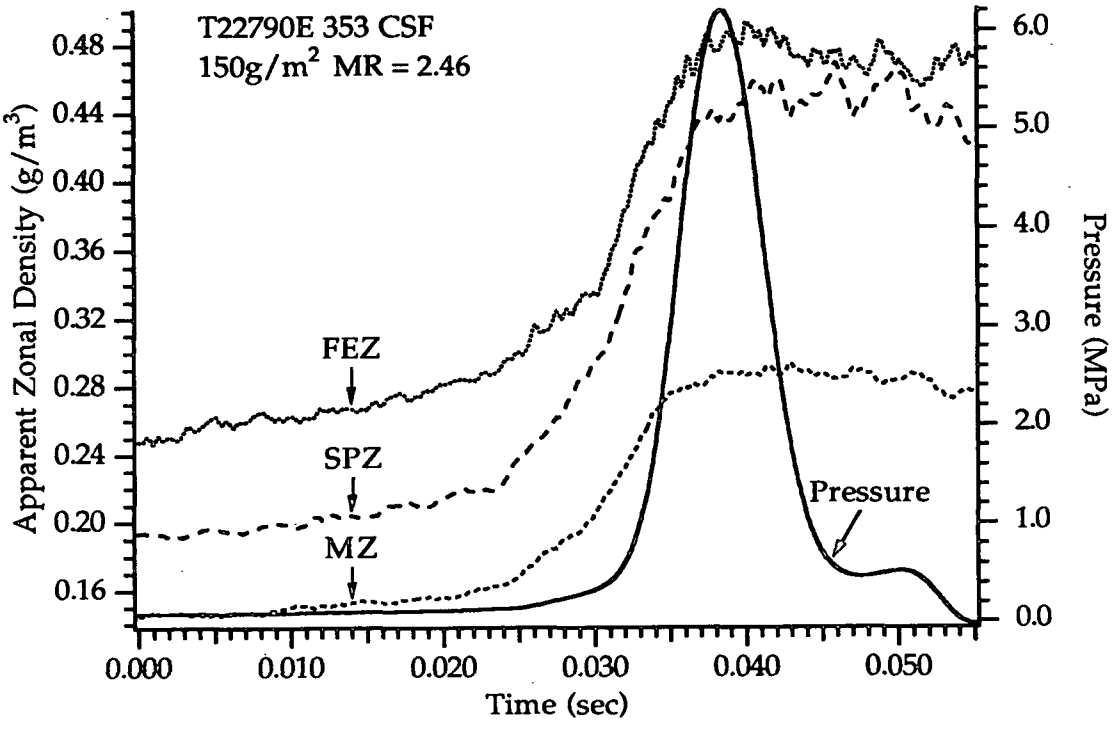

Figure 122. Zonal density-time histories in handsheet T22790E.

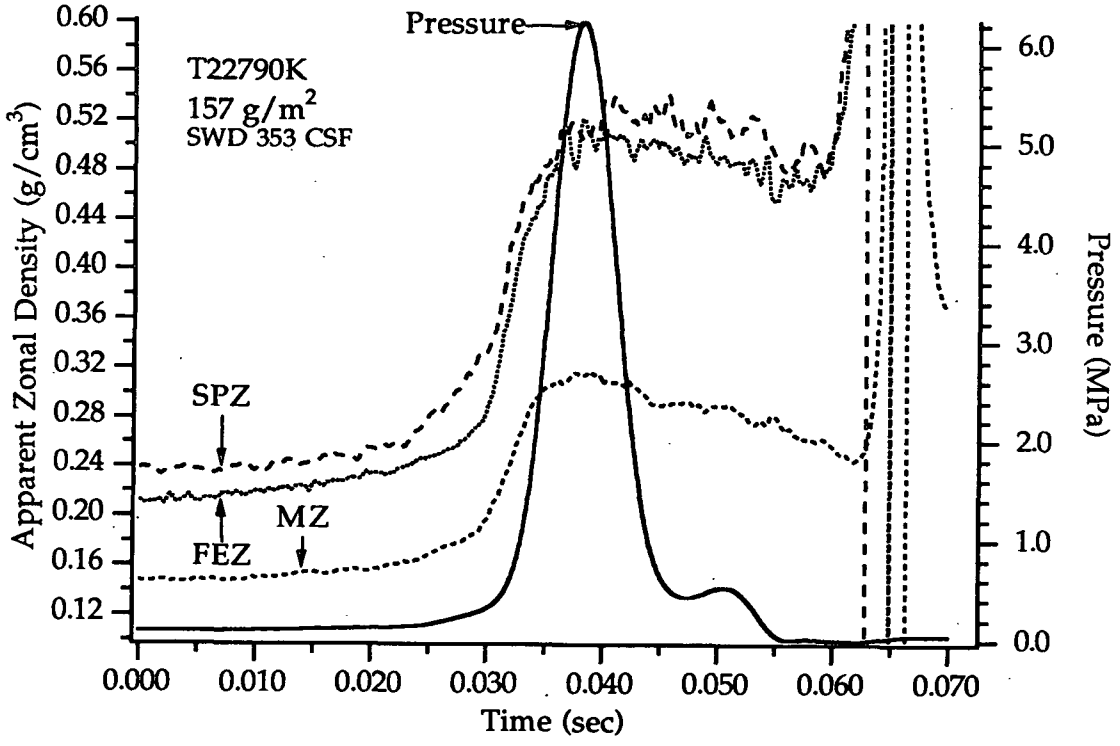

Figure 123. Zonal density-time histories in handsheet T22790K.

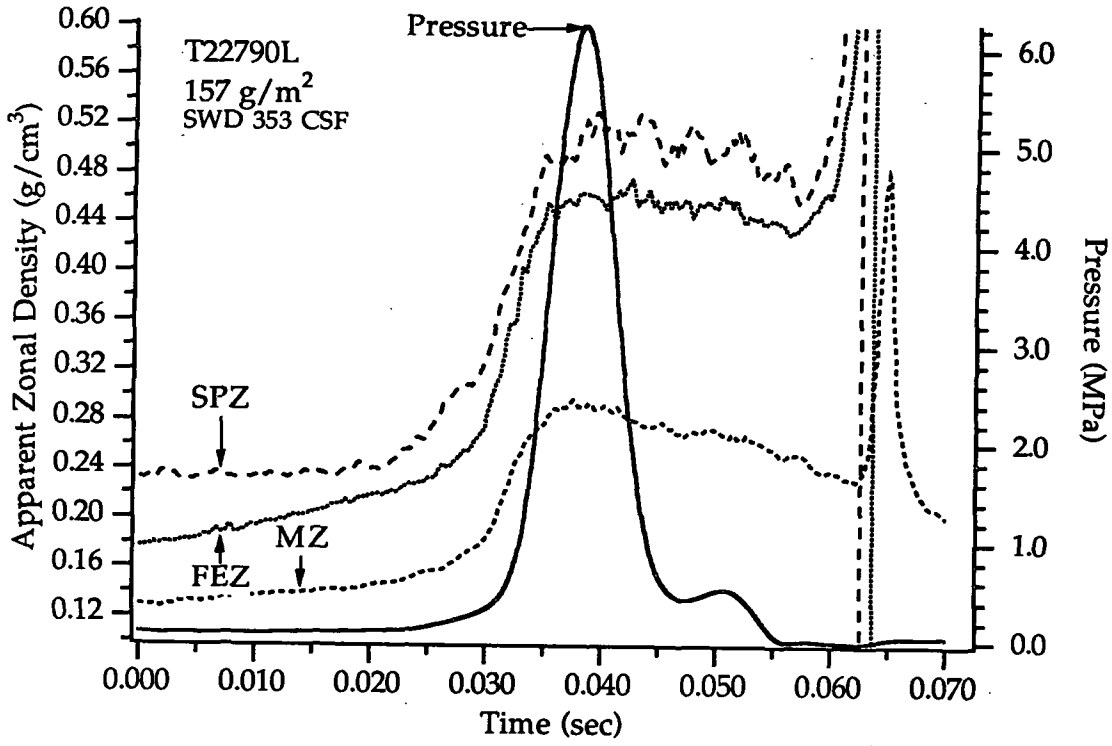

Figure 124. Zonal density-time histories in handsheet T22790L.

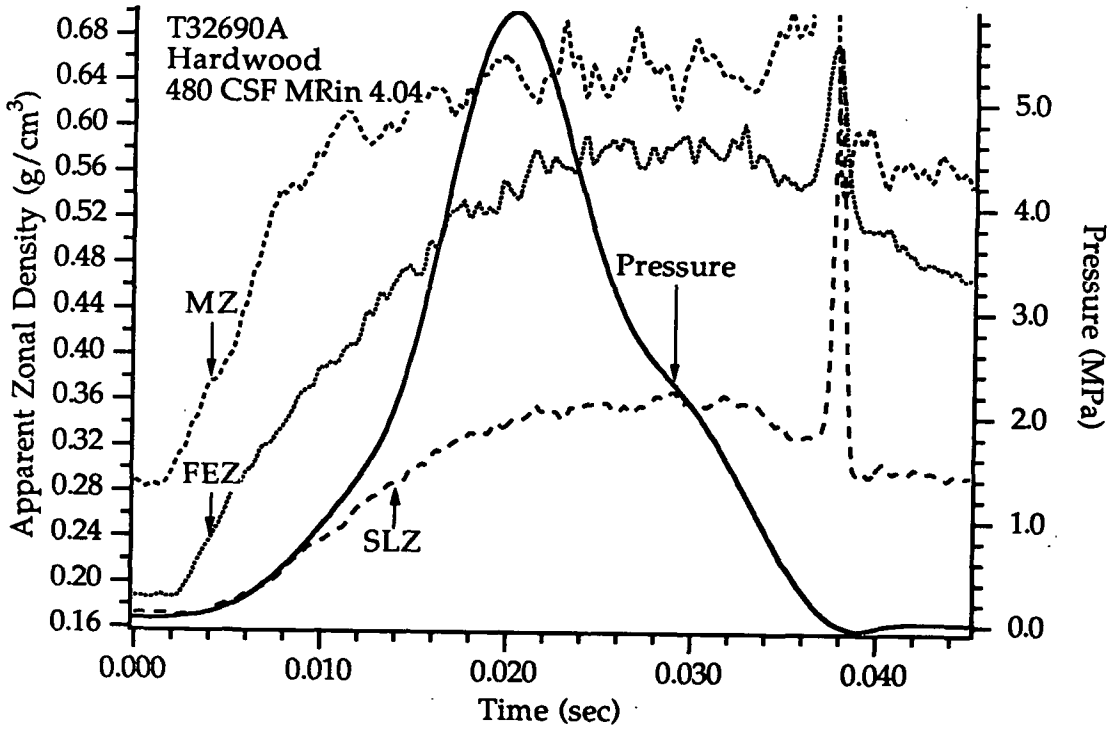

Figure 125. Zonal density-time histories in handsheet T32690A.

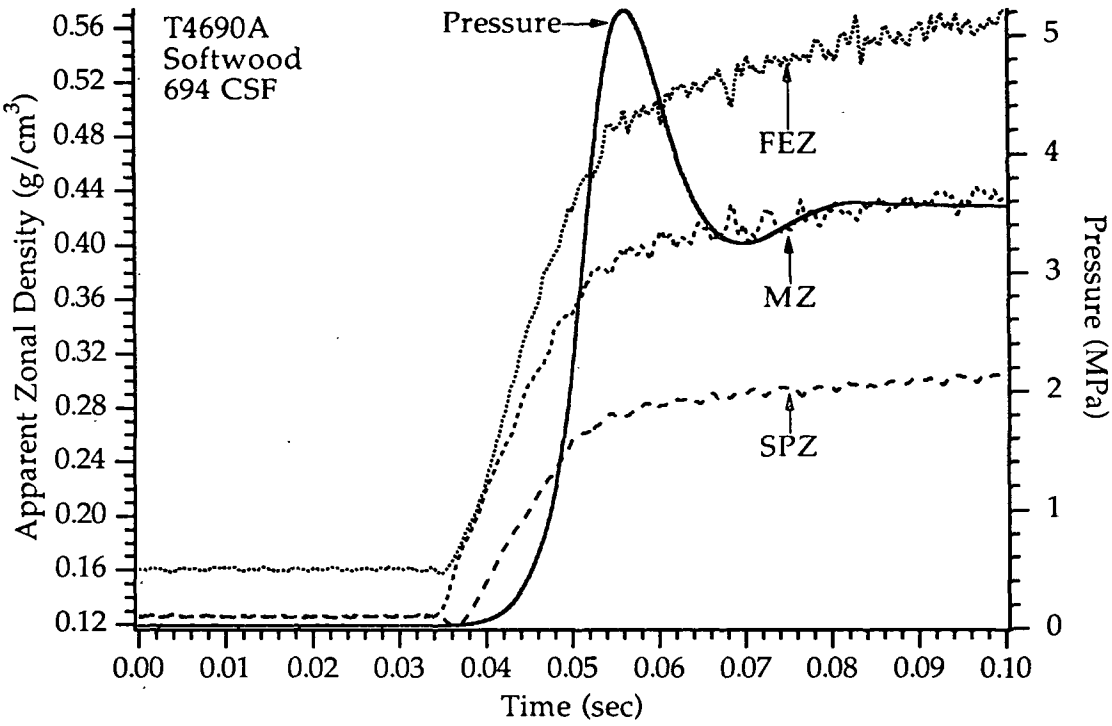

Figure 126. Zonal density-time histories in handsheet T4690A.

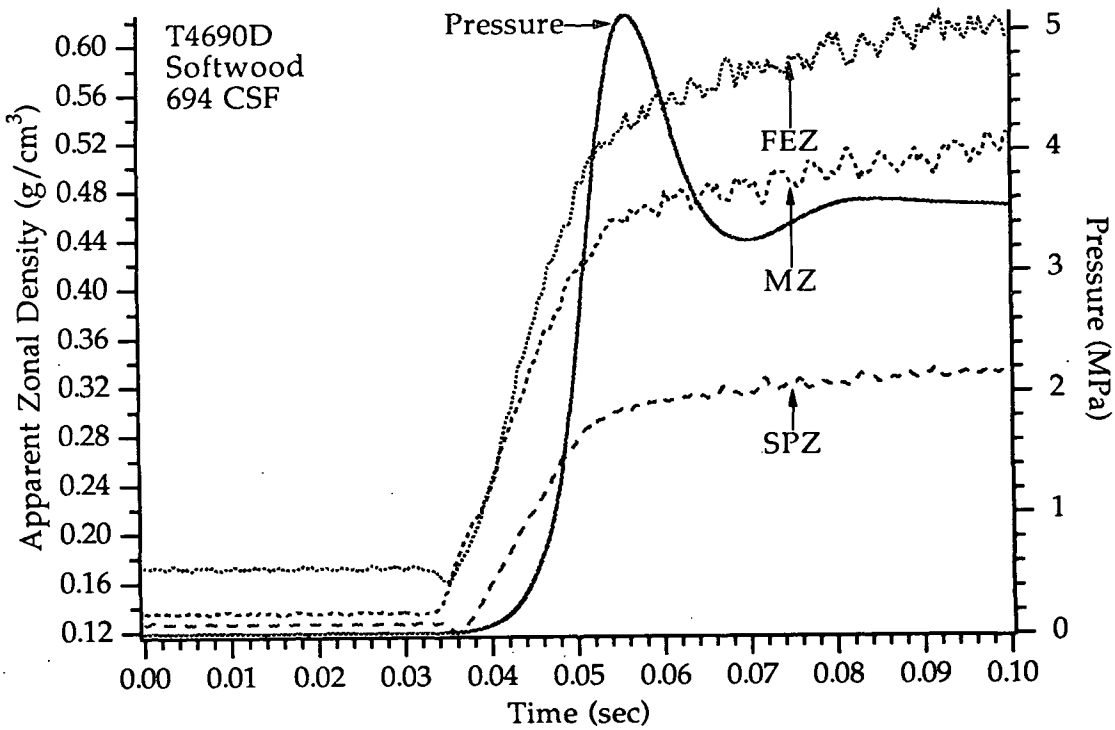

Figure 127. Zonal density-time histories in handsheet T4690D.

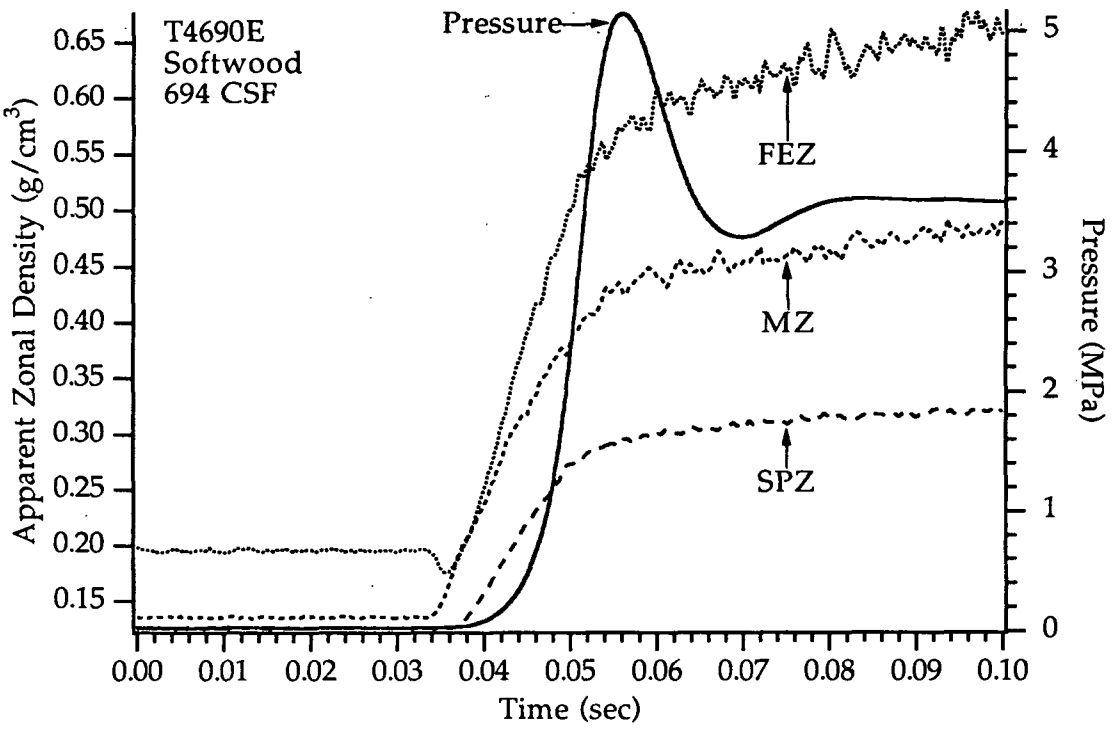

Figure 128. Zonal density-time histories in handsheet T4690E.

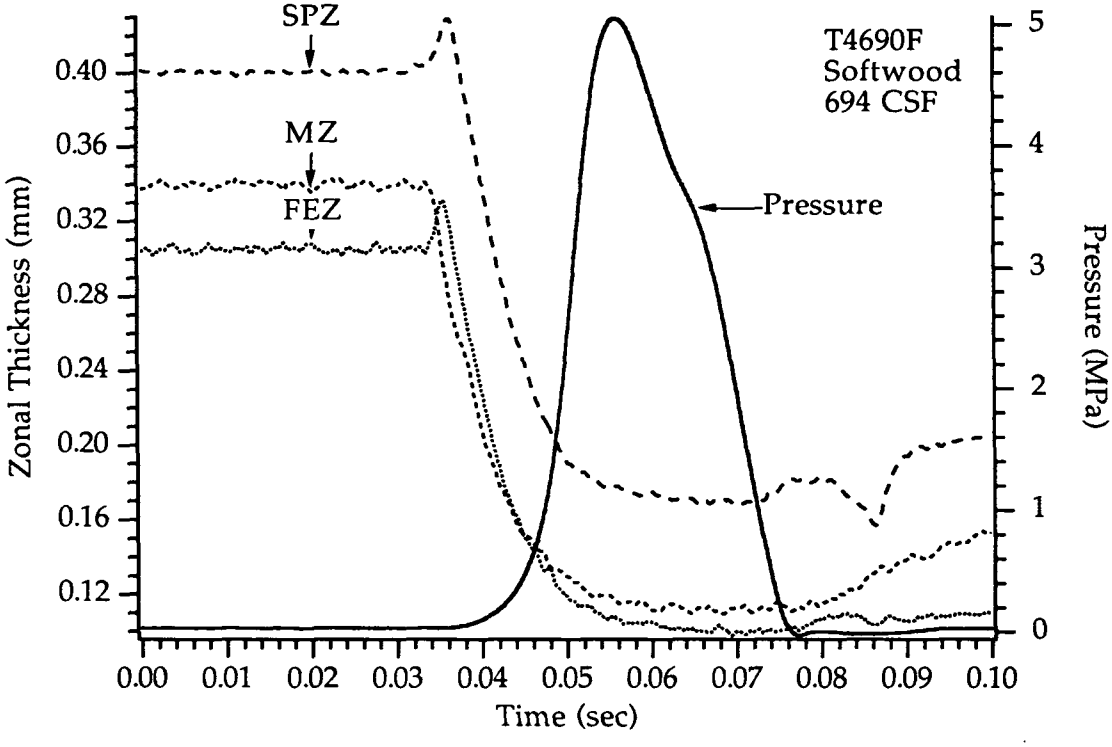

Figure 129. Zonal density-time histories in handsheet T4690F.

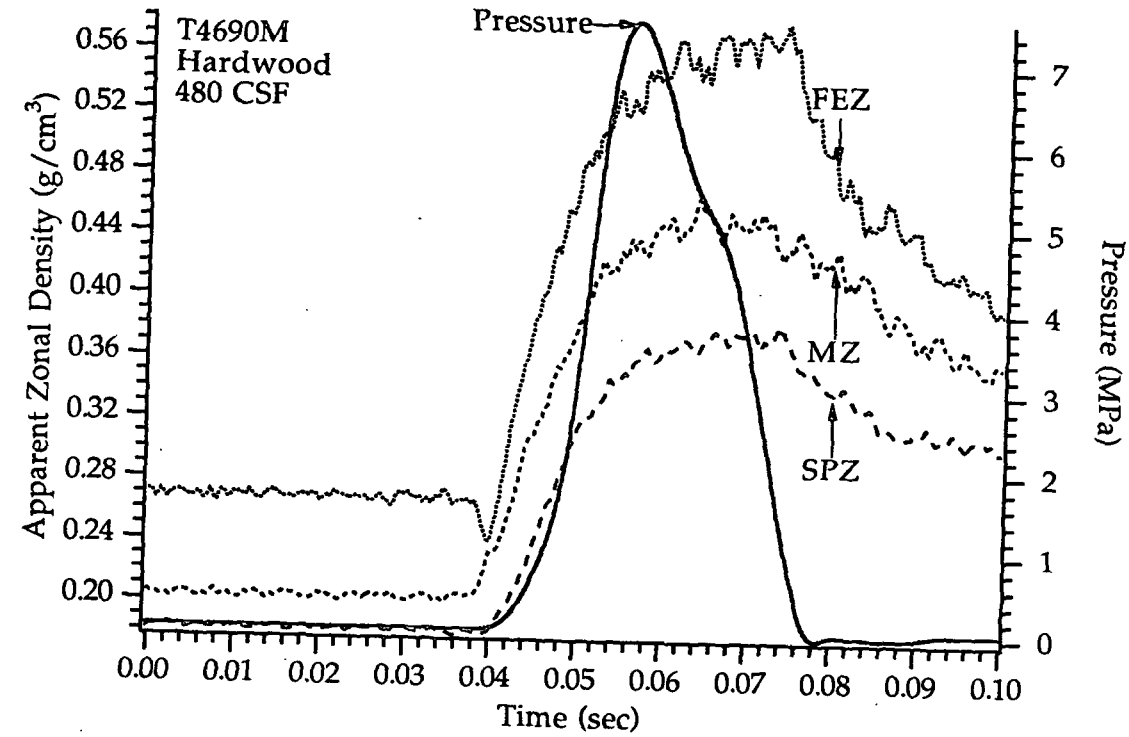

Figure 130. Zonal density-time histories in handsheet T4690M.

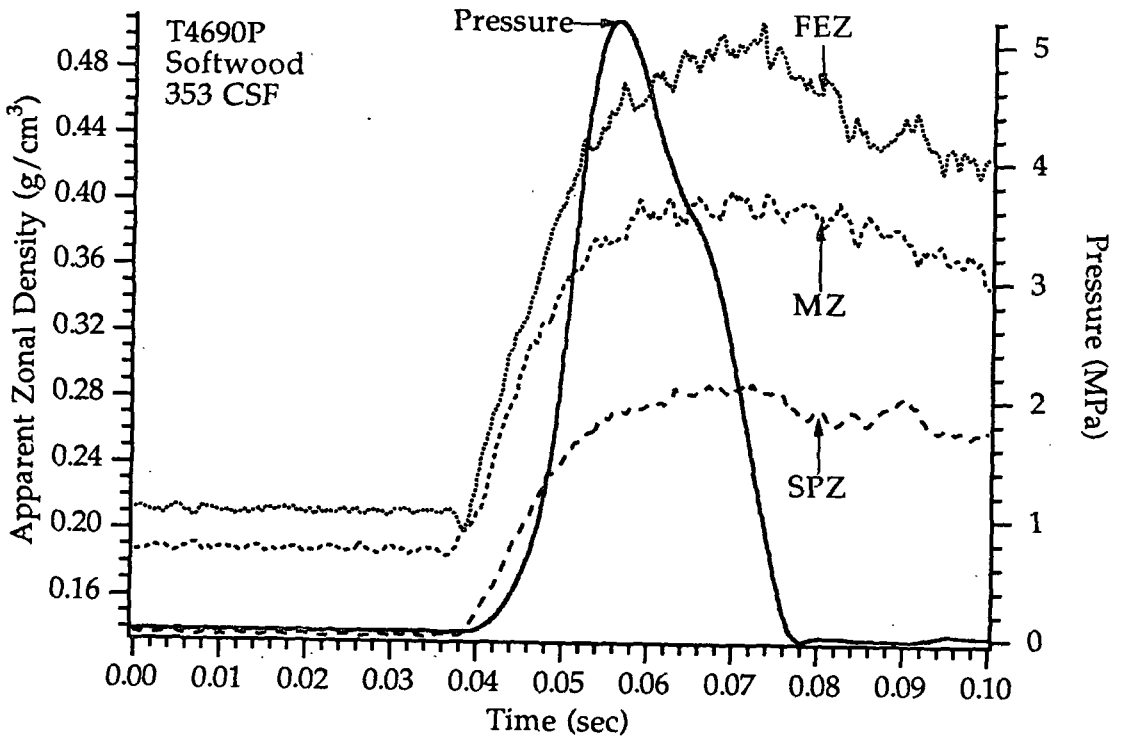

Figure 131. Zonal density-time histories in handsheet T4690P.

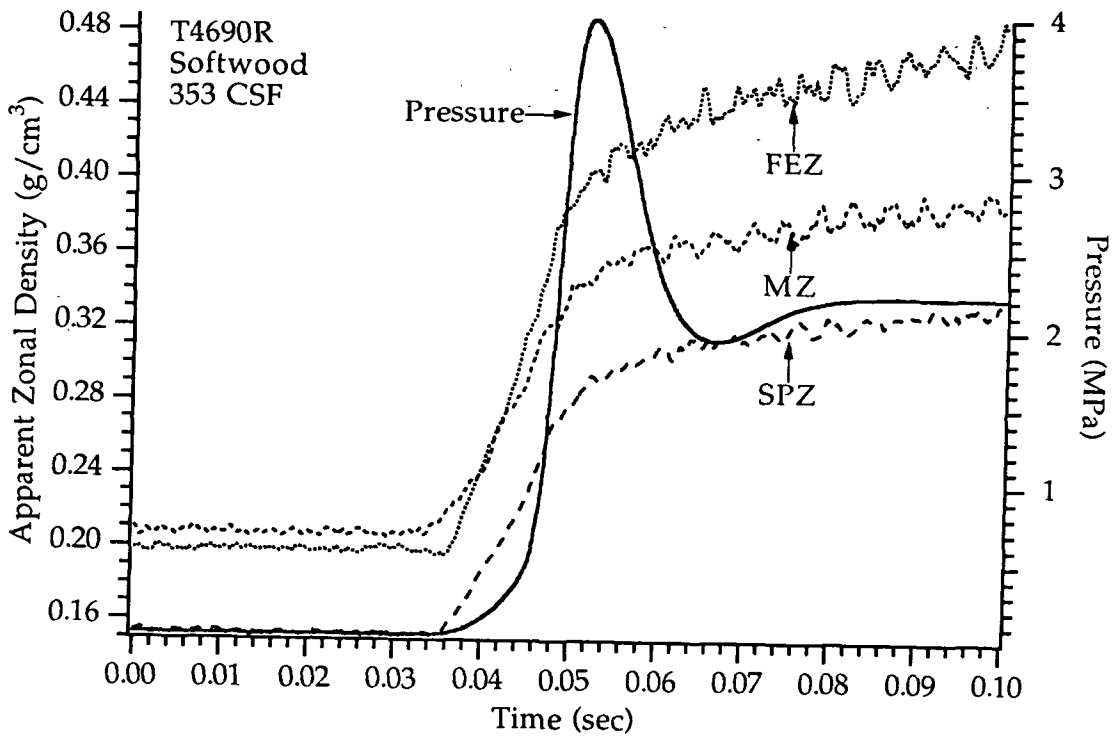

Figure 132. Zonal density-time histories in handsheet T4690R.

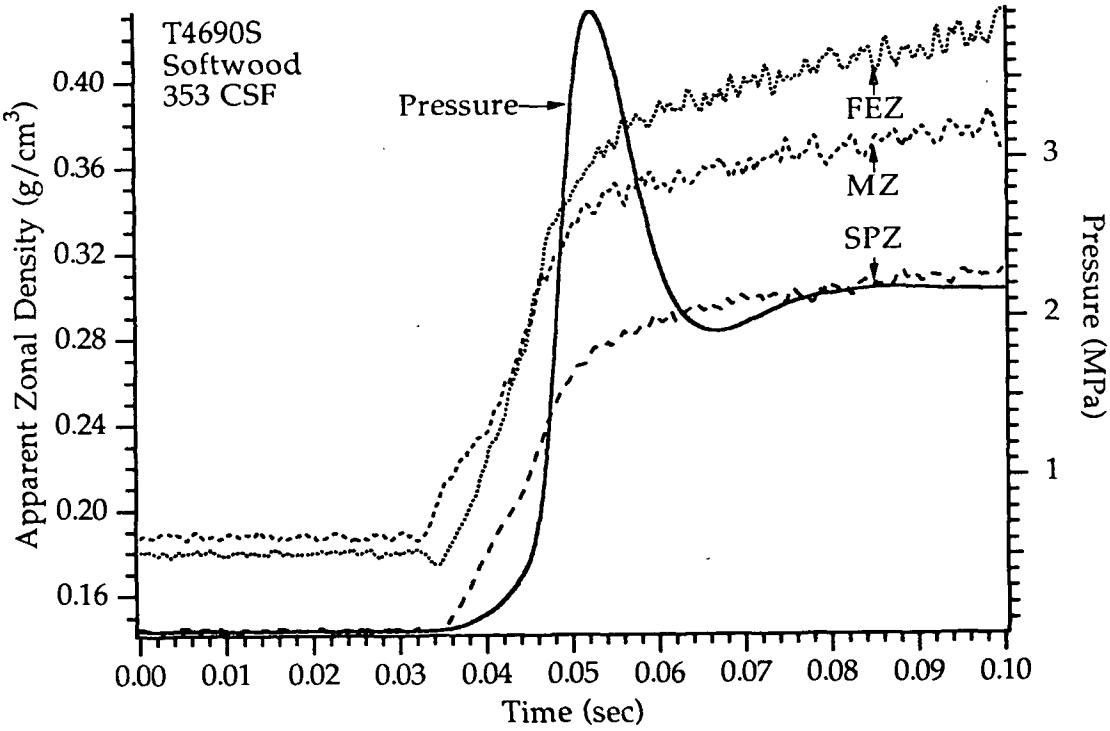

Figure 133. Zonal density-time histories in handsheet T4690S.

APPENDIX IX

This section contains details on the sources of uncertainty and the precision associated with the experiments in this thesis and discusses the methods used to determine this uncertainty. The procedure implemented for determining the uncertainty in these experiments was suggested by Kline (1985) for a zeroth-order estimate.

The value of a variable or parameter in science and engineering is subject to a level of uncertainty due to our inability to measure it with perfect accuracy. The level of inaccuracy is comprised of two components: a fixed or systematic error and a random component. The fixed or systematic error expresses the difference between the true value and the recorded value and is often referred to as the bias error. This error is typically constant within a certain procedure or piece of equipment and cannot be measured; therefore, it must be estimated. Calibration against a "known" standard helps to reduce the potential magnitude of this error. The random component of uncertainty is a statistical quantity which can be estimated by repetitious measurement of a variable and is quantified for a certain confidence level through a standard deviation procedure.

Moffat (1982) has described three different kinds of uncertainty associated with experiments: interpolation uncertainty, unsteadiness, and instrument calibration. Interpolation uncertainty arises from the inability of an observer to ascribe a certain numerical value to a phenomenon with absolute certainty. An example of this type of error can be seen when reading the calibration micrometer. It is impossible to say with absolute certainty the position of the cross hairs. Unsteadiness describes the variation due to

unsteadiness in an instrument or apparatus (drift) observed when a measurement is repeated over a prolonged period of time. An example pertinent to this thesis is the drift in the proximity detector output voltage over prolonged periods of time (days). Instrument calibration uncertainty represents the variability obtained over long periods of time when an apparatus is cycled on and off. Repeated cycling of the proximity detectors was avoided to prevent this error from becoming significant. In addition a standardized calibration procedure was adopted for calibration of each proximity detector before use.

Table 7 contains a summary of the estimated uncertainties for measured and calculated data. Unfortunately, repeated measurements were not obtained for the different pieces of equipment in order to estimate the uncertainty of the measurements. However, the uncertainty in the measurement is estimated using a zeroth-order method. Application of this method requires that the smallest interval between scale markings on the instrument must be determined. In such an estimate, the contribution of the bias and precision cannot be distinguished. Therefore, the best available estimate is for the total uncertainty interval, and it is based on experience gained with repeated use of the equipment and the previously determined least count for the instrument. At this point a rough estimate of the uncertainty is made by assigning a value of twice the least count as shown in Table 7.

In these experiments there are four parameters of interest. These parameters are 1) the target heights, 2) the pressure generated in the nip, 3) the sheet basis weight, and 4) the zonal basis weights. The target heights, zonal, and sheet basis weights are further combined to yield the zonal

thicknesses, the zonal densities, and the sheet density. The uncertainty is taken as the sum of the uncertainties of the individual measurements in the absence of a rigorous method of combining the individual uncertainties. The uncertainty in the target displacements and the zonal thickness measurements is on the order of ±40.1 μm. The uncertainty in the zonal densities is a combination of the uncertainties in the zonal thickness and the zonal basis weights. Therefore, linearly combining these uncertainties gives an uncertainty of ±4.3% for the zonal density and and an uncertainty of ±5% for the sheet density.

Table 7. Uncertainty of measured and calculated data.

Parameter	Instrument	Bias (B_{P_X})	Precision (S_{P_X})	Uncertainty
	DAS/ECT		5.08 μm	±2.04 μm
	Micrometer		(±25.4 μm)	±0.0005 inch (±12.7 μm)
Target Height				±27.44 μm
Pressure(Load Cell)		0.0	8.77 kPa	±8.77 kPa
	Large Graduated Cylinder	0.0	1%	±1%
	Small Graduated Cylinder	0.0	.1%	±.1%
	Balance		0.0003%	±0.0003%
Sheet Basis Weight				±1.53 g/m^2(1%)
Zonal Basis Weight				±0.153 g/m^2(0.3%)

Note: DAS = data acquisition system, and ECT = eddy current transducer.